

Department Biologie II
Anthropologie und Humangenetik
Ludwig-Maximilians-Universität München

Histone lysine methylation in the context of nuclear architecture



Roman Zinner

Dissertation an der Fakultät für Biologie
der Ludwig-Maximilians-Universität München
Eingereicht am 21.03.2007

Histone lysine methylation in the context of nuclear architecture

Dissertation an der Fakultät für Biologie, Department II
Der Ludwig-Maximilians-Universität München (LMU)

Vorgelegt von
Dipl.Biol. Roman Zinner

Gutachter:
Erstgutachter: Prof. Dr. Thomas Cremer
Zweitgutachter: (PD) Dr. Angelika Böttger

Tag der mündlichen Prüfung:
25.06.2007

Stufen

Wie jede Blüte welkt und jede Jugend
dem Alter weicht, blüht jede Lebensstufe
blüht jede Weisheit auch und jede Tugend
zu ihrer Zeit und darf nicht ewig dauern
es muß das Herz bei jedem Lebensrufe
bereit zum Abschied sein und Neubeginne
um sich in Tapferkeit und ohne Trauern
in andre, neue Bindungen zu geben
und jedem Anfang wohnt ein Zauber inne
der uns beschützt und der uns hilft zu leben
wir wollen heiter Raum um Raum durchschreiten
an keinem wie an einer Heimat hängen
der Weltgeist will nicht fesseln uns und engen
er will Stuf' um Stuf' uns heben, weiten
kaum sind wir heimisch einem Lebenskreise
und traulich eingewohnt, so droht Erschlaffen
nur wer bereit zu Aufbruch ist und Reise
mag lähmender Gewöhnung sich entrafen
Es wird vielleicht auch noch die Todesstunde
uns neuen Räumen jung entgegenschicken
des Lebens Ruf an uns wird niemals enden
Wohlan denn, Herz, nimm Abschied und gesunde.

Hermann Hesse, Das Glasperlenspiel

1	Summary	
2	Introduction	1
2.1	Goals of the study	1
2.2	A higher order functional nuclear topology	3
2.3	Chromatin	5
2.4	Euchromatin versus (facultative) heterochromatin	6
2.5	Epigenetics and the histone code	8
2.6	The nucleosome core particle	11
2.7	Histone lysine methylation	12
2.7.1	H3K4	15
2.7.2	H3K9 (and interaction with HP1)	16
2.7.3	H3K27 (and X-inactivation)	19
2.7.4	H4K20	21
2.8	Chaetocin, inhibitor of the HMT SUV39H1	22
2.9	RNA interference and heterochromatin formation	22
2.10	DNA methylation	23
2.11	Commonly used techniques in the field	24
2.12	Outlook	26
3	Methods and Protocols	27
3.1	Cell culture	27
3.1.1	Procedure for cell cultivation	27
3.1.2	Thawing and freezing of cells	28
3.1.3	Slide preparation	29
3.1.4	Seeding cells on coverslips	29
3.2	Replication labeling with BrdU	30
3.3	Scratch transcription labeling with BrUTP	31
3.4	Polymerase chain reaction (PCR)	32
3.4.1	DOP-PCR	32
3.4.2	Label-PCR	35
3.5	Metaphase preparation	37
3.6	2D-FISH	39

3.7	Peptide competition assay	42
3.8	Immunostaining	45
3.9	Sequential antibody labeling	46
3.10	3D-Immuno-FISH	47
3.11	Chaetocin treatment	51
3.11.1	Calculation of the molarity out of the Chaetocin concentration	51
3.11.2	Experimental Chaetocin setup	52
3.12	Microscopy	52
3.12.1	Transmitted light microscopy	52
3.12.2	Epifluorescence microscopy	53
3.12.3	Confocal-laser-scanning microscopy	53
3.13	Deconvolution	54
3.13.1	Deconvolution in general	54
3.13.2	Deconvolution setup	55
3.13.3	The impact of deconvolution on image restoration	59
3.13.4	The consistency of evaluation results at different thresholds	61
3.14	Image processing	63
3.14.1	Documentation and shift correction	63
3.14.2	Photoshop and Image J	63
3.14.3	Co-localization analysis	63
3.14.4	Amira 3D reconstruction	67
3.14.5	Radial autocorrelation (RAC) function analysis	68
3.14.6	Evaluation procedure in Chaetocin experiments	68
4	Results	70
4.1	Nuclear patterns of distinct histone methylation sites	70
4.1.1	Methylation sites and their arrangement in regard to centromeres	70
4.1.2	Overlap assessment between centromeres and histone modifications	73
4.1.3	Relation between different histone modifications and nascent RNA	75
4.1.4	Pattern formation in cycling and quiescent nuclei	76
4.1.5	Interrelationship of different lysine methylation sites	78
4.1.6	The formation of distinct nuclear zones by lysine methylation sites	82
4.2	Changes in nuclear 3D topology after Chaetocin treatment	83
4.2.1	Test for the assessment of an appropriate Chaetocin dilution	83
4.2.2	Test for cells in S-phase	84
4.2.3	Investigation of cell morphology in a test for Chaetocin cytotoxicity	85
4.2.4	Changes in nuclear topology after Chaetocin treatment	86
4.2.5	Investigation of HP1-alpha distribution after Chaetocin treatment	89

4.2.6	No reorganization of chromatin occurs after Chaetocin rescue _____	92
4.2.7	Evaluation of H3K9me3 pattern size in Chaetocin experiments _____	94
4.3	Lysine methylation sites and specific chromatin segments _____	97
4.3.1	Modifications correlate with gene density on the chromosomal level _____	98
4.3.2	“Holes” in chromosome paints are filled with heterochromatin _____	101
4.3.3	Distinct lysine methylations correlate with expression levels _____	102
5	Discussion _____	108
5.1	Lysine methylation patterns are arranged in nuclear zones _____	108
5.2	Changes in nuclear 3D topology after Chaetocin treatment _____	114
5.3	Analysis of lysine sites with regard to chromatin segments _____	118
5.4	The methodological approach _____	121
6	References _____	125
7	Appendix _____	138
7.1	Material and technical equipment _____	138
7.1.1	Cells _____	138
7.1.2	Chemicals, enzymes and reagents _____	138
7.1.3	Media, buffers and solutions _____	141
7.1.4	Equipment and instrumentation _____	142
7.1.5	BACs used in the experiments _____	146
8	Abbreviations _____	151
9	Table of Figures _____	152
10	Publications _____	154
11	Curriculum Vitae _____	156
12	Acknowledgement _____	158

1 Summary

Uncovering the organization of a higher order nuclear architecture and its implications on nuclear function has become a topic of major interest in the recent past. There is growing evidence that beyond the DNA sequence information, gene expression is organized on different epigenetic levels, comprising modifications of histones and DNA and higher order chromatin arrangement.

The present work focuses on histone lysine methylations which are known to represent an essential epigenetic mechanism of gene regulation both for gene repression and gene activation. Immunofluorescence together with confocal microscopy and quantitative image analysis was used to reveal the nuclear topology and spatial relations of lysine methylation sites (H3K4me3, H3K9me1, H3K9me3, H3K27me3, H4K20me1 and H4K20me3) with centromeres, nascent RNA or with each other in various human cell types. Pattern formation varied in the investigated cell types. An apparent association with centromeres was found only for lysine methylation sites linked to constitutive heterochromatin. Nascent-RNA was found associated, though to a different degree, with all histone methylation sites. A difference in pattern formation in relation to the cell cycle stage was observed for methylation sites which are assigned to constitutive heterochromatin. Simultaneous visualization of different histone lysine methylation sites and their pattern formation, compared to general chromatin density visualized by DAPI-counterstaining, revealed, that methylation patterns are organized in distinct nuclear zones with little apparent intermingling.

Experiments performed with the fungal toxin Chaetocin an inhibitor of the histone methyltransferase SUV39H1 (responsible for H3K9me3) altered the overall chromatin organization in human fibroblasts but not in cancer cell-lines DLD-1 and MCF-7. Surprisingly, H3K9me3 intensity was not found decreased after Chaetocin treatment but a distinct clustering occurred as detected by H3K9me3 antibody signals and DAPI-counterstaining. The comparison of distinct cellular targets in Chaetocin treated and untreated control cells by IF could help to ensure that the observed rearrangements caused by the drug were not due to cytotoxic effects. A rescue assay after Chaetocin application could not reestablish the former chromatin state thereby indicating a long term irreversible epigenetic change of higher order chromatin.

To investigate whether distinct histone methylation sites (H3K4me3, H3K9me3 and H3K27me3) co-localize with defined chromatin segments an elaborate multicolor immunofluorescence protocol was established. In an experimental setup entire chromosome territories of human chromosomes HSA #18, #19 and X as well as chromosomal subdomains with different regional gene densities or highly transcribed and repressed genes from HSA #12 and X were compared to the respective lysine methylation sites. Co-localization analysis

(using Manders co-localization coefficients) revealed distinct differences in the level of H3K4me3 between the chromosome territories of the gene-poor HSA #18 and the gene-dense HSA #19, but no differences were detectable for H3K9me3 and H3K27me3. Data from five color immuno-FISH experiments were supportive that H3K27me3 known to be essential for gene-repression on Xi can also be assigned to gene repression on the active X-chromosome, since repressed genes showed higher levels of co-localization with H3K27me3 staining foci compared to the entire chromosome or highly expressed genes on the active X. For H3K4me3 similar high co-localization values were found for gene-dense chromatin segments as well as for highly expressed genes on HSA #12. This supports the idea that H3K4me3 is not only a marker for ongoing transcription but reflects a rather “poised” state for transcription.

2 Introduction

2.1 Goals of the study

The main purpose of the present thesis was to investigate histone lysine methylation in the light of nuclear architecture. By a collaboration with A.Peters (Friedrich Miescher Institute for Biomedical Research, Basel) highly specific antibodies to discriminate different lysine methylation sites and even distinct methylation states were available.

The first goal pursued in this work was to investigate the 3D nuclear topology and spatial interrelationships of different lysine methylation sites (tri-H3K4, mono-H3K9, tri-H3K9, tri-H3K27, mono-H4K20 and tri-H4K20) in different cell types and in relation to the cell cycle. Immunofluorescent experiments and confocal microscopy together with quantitative evaluation of 3D image stacks should be used to investigate spatial relations of distinct methylation sites with each other, centromeres and nascent RNA. Another task was to explore whether histone lysine methylation patterns are arranged in distinct three-dimensional nuclear zones and would thus represent nuclear subcompartments. To check for cell type dependent variations in pattern formation, histone lysine methylation sites should be analysed and compared in three different human cell-lines.

Co-localization analysis (Manders et al., 1993) should provide information on the degree of overlap between histone lysine methylation sites with regard to each other and to defined nuclear targets such as centromeres and nascent RNA. Differences of lysine methylation patterns between cycling and non cycling cells were evaluated with a radial autocorrelation function (RAC) program.

A manipulative approach to assess histone lysine methylation features was the application of Chaetocin, a fungal toxin, that specifically inhibits the histone methyl transferase (HMT) SUV39H1, responsible for trimethylation of H3K9. Since experiments with inhibitors require tests concerning the proper concentration for a given cell type, analysis of the drug impact over time should be performed and information about cytotoxic bystander effects collected, which can blur results significantly. Chaetocin application was expected to lead to changes in H3K9me3 pattern formation and also chromatin reorganization on a higher level. To receive information about Chaetocin's cytotoxicity, ongoing cell division should be analysed by BrdU incorporation and IF be performed with antibodies against microtubules, nucleoli and speckles. Interaction of H3K9me3 with HP1 alpha was a target of interest and analysed before and after Chaetocin application to get further information about their role in heterochromatin formation.

The methods to investigate cells after drug treatment remain comprised immunofluorescence, confocal microscopy and sophisticated 3D image computer analysis.

In the third part of this work the question was addressed, to what extent defined chromatin segments (whole chromosome territories, gene poor/gene rich regions or differently expressed genes) can be attributed to distinct lysine methylation states. Therefore co-localization analysis of histone lysine methylation patterns and selected chromosomal targets should be performed. The problem which emerges by application of immunofluorescence (IF) together with Fluorescence In Situ Hybridisation (FISH) is that both methods aim at rather opponent goals: The maintenance of the antibody-epitopes is required as good as possible, whereas a successful FISH experiment necessitates harsh treatment (especially HCl and denaturation) of cells which is harmful to lysine epitopes. To combine IF (lysine methylation) and FISH an Immuno-FISH protocol optimized for the epitope structure of interest has to be established. FISH probes comprised chromosome paints for whole chromosomes and BAC probes for chromosomal subdomains of HSA 12 and X.

The **inactive** X-chromosome can be detected and visualized by H3K27me3 antibody-staining. The hypothesis tested in this work was if this histone modification can also be correlated to a distinct expression status on the **active** X-chromosome and (if there is rather a noticeable correlation of H3K27me3 to the active X-chromosome than compared to the inactive X-chromosome) autosomes (e.g. HSA #12). This question was addressed in five color immuno-FISH experiments with BACs containing genes with different expression levels and H3K27me3 antibody-staining have to be performed, confocal images recorded and the spatial relationship of the targets investigated by co-localization analysis.

In the following chapters, I want to introduce thematically the main topics that were central for this work. First I will give a short overview of different aspects of nuclear architecture. Next I try to summarize the rather new and complex topic of epigenetics in general and histone lysine methylation in particular. Current knowledge of the respective lysine methylation sites investigated in this thesis is outlined as well as other common epigenetic modifications and the SUV39H1 inhibitor Chaetocin.

2.2 A higher order functional nuclear topology

When the 50th anniversary of the double helix' discovery was celebrated in 2003, James Watson gave the following comment concerning where genetics is heading for: "You can inherit something beyond the DNA sequence. That's where the real excitement in genetics is now" (Watson, 2003).

Many mechanisms that regulate gene expression on the DNA level have been revealed in the last decades but now also growing evidence emerges that gene expression is controlled by nuclear architecture in a superordinate way. The cell nucleus is not just a simple spherical organell that harbours DNA, but it is also specifically compartmentalized within itself (reviewed by (Cremer and Cremer, 2001; Misteli, 2004; Misteli, 2005; Parada et al., 2004) (Spector, 2001). This compartmentalization is closely related to genome function and processes like transcription, splicing and replication are integrated therein (Belmont et al., 1999; Dundr and Misteli, 2001). The nucleus however has no membrane bound subcompartments like the Golgi apparatus or Endoplasmatic Reticulum (ER). This means that localized substructures must be created by the interaction of nuclear components (the cellular organization of genome function was recently reviewed (Misteli, 2007)).

Transcription by RNA polymerase II (Pol II) is not associated with the large scale organization that is observed for polymerase I transcription in the nucleolus (Raska et al., 2004), but there is growing evidence that Pol II is organized into smaller structures termed transcription factories reviewed by Martin et al. (Martin and Pombo, 2003). Regulation of transcription includes a number of different organization levels in the cell nucleus. Control of gene expression can occur on the DNA-level by regulatory sequences e.g. promotores, silencer and enhancers (Alberts, 2002), but the control of accessibility of the transcription machinery on a more global level, is influenced by higher order chromatin structures that impede or permit access of factors to the genes (Li et al., 2007).

Basic principles of the higher order arrangement of chromatin in interphase nuclei have become clearly apparent, including the distinctly different, spatial arrangement of early and mid to late replicating chromatin (Dimitrova and Berezney, 2002) and the non-random, radial arrangement of gene dense and gene poor chromatin (Boyle et al., 2001; Cremer et al., 2001) (Kupper et al., 2007).

The idea that chromatin forms higher order structures in the interphase nucleus which consist of subchromosomal domains with variable density, has led to the formulation of a topological model of gene expression termed the chromosome-territory-interchromatin compartment (CT-IC) model (figure 1) (Cremer and Cremer, 2001; Cremer et al., 1993).

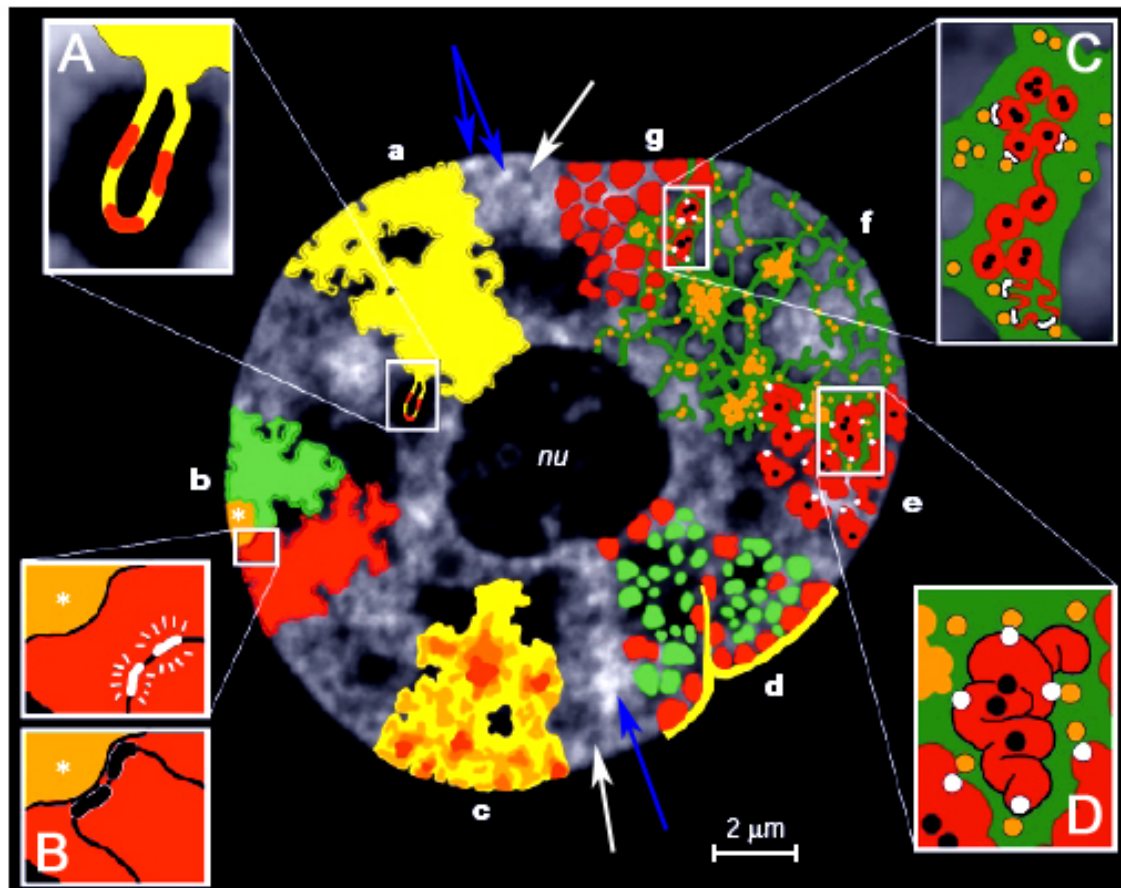


Figure 1

Scheme taken from Cremer and Cremer 2001 (Cremer and Cremer, 2001)

Structural features of the CT-IC model in an optical section of a nucleus in a HeLa histone H2B-GFP expressing cell. Insets show topological models of gene regulation. **(a)** CTs have complex folded surfaces. **A** A giant chromatin loop with active genes expands into the IC space **(b)** CTs contain distinct arm domains for the short (p) and long (q) chromosome arms, and a centromeric domain (Volpi et al., 2000) (Williams et al., 2002) which represents constitutive heterochromatin and consists mainly of repetitive sequences of tandem DNA. **B** Top: actively transcribed genes (white) are located on a chromatin loop that is remote from centromeric heterochromatin. Bottom: Recruitment of the same genes in the proximity of centromeric heterochromatin leads to their silencing (Brown et al., 1997; Fischer et al., 2006). **(c)** CTs have variable chromatin densities. Lax chromatin at least partly expands to the IC, whereas the condensed chromatin (especially constitutive heterochromatin corresponding to H3K9me3 and H4K20me3) is remote from the IC. **(d)** Shown are early replicating chromatin domains which comprises predominantly active and gene-rich regions (green). These regions would correspond to H3K4me3 patterns. The mid replicating chromatin (red) is preferentially located at the periphery and in close contact with the nuclear lamina and around the nucleolus (similar to H3K27me3 staining (Zinner et al., 2006)). **(e)** Higher order chromatin structures built up from a hierarchy of chromatin fibers (Belmont and Bruce, 1994; Felsenfeld and Groudine, 2003; Lesne and Victor, 2006). **D** Active genes (white dots) may be at the surface of convoluted chromatin domains while silenced genes (black dots) may be retreated towards the interior of the chromatin structure. **(f)** The CT-IC model predicts that the IC (green) contains complexes (orange dots) and factors for transcription, splicing, DNA-replication and repair. **(g)** CT with 1-Mb domains (red) and IC (green) expanding between these domains. **C** Topological relationship between the IC, and active/inactive genes. The

finest branches of the IC end between 100-kb chromatin domains. Active genes (white dots) are located at the surfaces of these domains, whereas silent genes (black dots) are located in the interior.

Actively transcribed chromatin (white arrows) is located between the gene poor compartments. This chromatin can be visualized by H3K4me3 antibody staining (Sims et al., 2003; Zinner et al., 2006). The white clusters (blue arrows) represent regions of highly condensed chromatin probably repetitive sequences at and around centromeres. These distinct constitutive heterochromatic regions are late-replicating and can be marked by H3K9me3 and H4K20me3 antibodies (Schotta et al., 2004b; Zinner et al., 2006).

2.3 Chromatin

In eukaryotic cells, the genetic material is organized into a complex structure that is known as chromatin (from the Greek "*khroma*" meaning coloured), which was first detected with basic dyes at the end of the nineteenth century (Flemming, 1882).

Chromatin is built up of DNA wrapped around histones. Each nucleosome consists of a histone octamer containing the proteins histone H2A, H2B, H3 and H4 each present twice in the octamer and 146 bp of DNA wrapped around it. The nucleosomes are linked by histone H1, which was found to significantly stabilize DNA within the nucleosomal particle (Simpson, 1978). H2A and H2B form a stable dimer, whereas H3 and H4 form a tetramer in the absence of DNA (Kornberg, 1974). All core histones are evolutionary highly conserved in length and amino acid sequence (calf and pea histone H4 differ at only two sites in 102 residues (DeLange, 1969a; DeLange, 1969b). The four histones contain an extended histone fold domain at the C-terminus through which interactions with other histones or DNA occur and a charged tail at the N-terminal end which contain the bulk of lysine residues that can be epigenetically modified (figure 3) (Arents et al., 1991). Early biochemical analyses have indicated that methylatable N-terminal lysine positions in histones H3 and H4 can exist in mono-, di-, and trimethylated states (Paik and Kim, 1971). The N-terminal tails of the core histones also provide contact surfaces with other, non histone proteins, that organize higher order chromatin structures (Edmondson et al., 1996; Hecht et al., 1995).

Electron microscopy analysis provided evidence for an ordered structure of chromatin organisation. The "beads on a string" images were compelling evidence for a regular and repeating form of chromatin assembly (Olins and Olins, 1974).

The next level of higher chromatin organization in the nucleus which has also been investigated in detail is the 30nm or solenoid structure where nucleosomes are packed leading to a compaction of about 6-fold compared to the beads on a string conformation. (figure 2). But less is known about the arrangement of chromatin between the 30nm structure and the highest degree of condensation which is achieved at the beginning of mitosis. Here compared to interphase chromatin a 250-fold compaction of chromatin occurs (Belmont et al., 1999; Earnshaw and Bernat, 1991).

Two principal models have been proposed to explain how such a high and reversible degree of compaction can occur. On the one hand there is the idea of an organization of the fibre into loops that are radially arranged along the axis of the chromosome (Gasser and Laemmli, 1986; Paulson and Laemmli, 1977) and on the other hand a helical folding of the 30nm chromatin fibre is suggested (Sedat and Manuelidis, 1978).

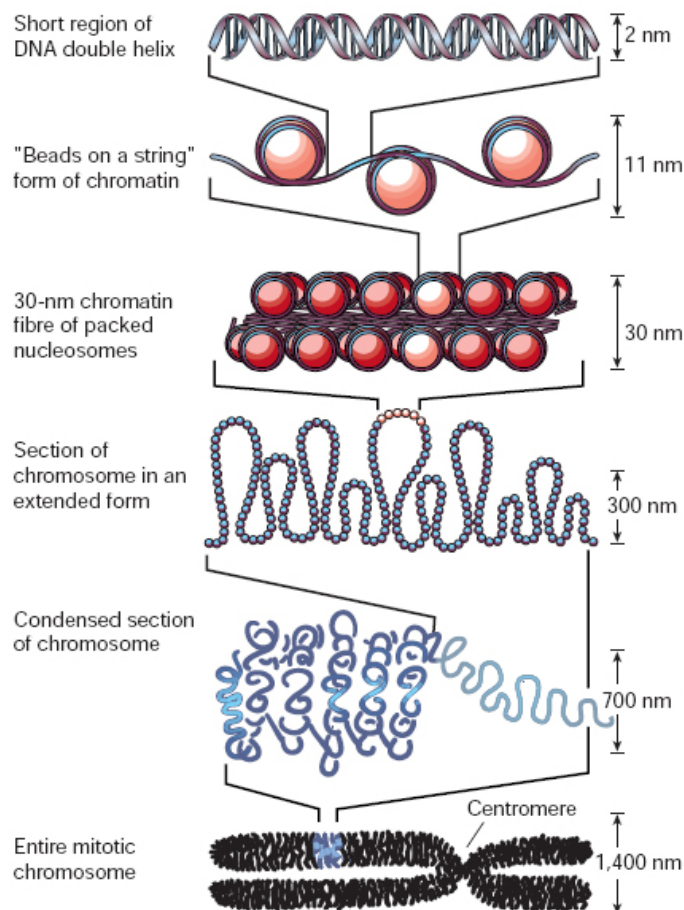


Figure 2

Felsenfeld Nature 2003 (Felsenfeld and Groudine, 2003)

From the double helix to the mitotic chromosome.

The images show how the folding of higher order chromatin might occur. The view of the double helix up to the 30nm fibre is regarded as fact. The shown pictures of the 300nm and 700nm organization are very speculative.

2.4 Euchromatin versus (facultative) heterochromatin

In the following section I want to give a short sketch of the concepts of eu- and (facultative) heterochromatin embracing early definitions from the 1920s to today's molecular aspects.

Exclusively based on histological observations, in 1928 Heitz described his concept of heterochromatin (Heitz, 1928). He defined heterochromatin (HC) as the chromosomal segments which remain condensed throughout the interphase, whereas the rest of the nucleus is occupied by euchromatin, which appears diffuse and relatively light in colour.

Only two years later Hans Muller already described the phenomenon of position effect variegation (PEV) in *Drosophila*, meaning that genes that were placed near heterochromatin are silenced (Muller, 1930). These studies were continued by Schultz, 1939 (Schultz, 1939)

who provided data that genes more proximal to heterochromatin were silenced first compared to distal genes.

In 1966 almost 40 years later the term “facultative” heterochromatin was introduced by Brown (Brown, 1966). He established the idea that all chromatin regions are potentially capable of becoming heterochromatic. Today another 40 years later a lot of information has been collected about heterochromatin, especially on the molecular level.

Modification of histones by chemical groups and their impact are already known since 1964 when Allfrey et al. demonstrated that histone acetylation influences transcriptional activity in vitro (Allfrey, 1964). The highly dynamic process of modifications with acetyl groups by HATs and its removal by histone deacetylases (HDACs) is known since the mid 1990s (Taunton et al., 1996; Wolffe, 1996).

The different types of chromatin can be subdivided into three distinct classes: euchromatin, facultative heterochromatin and constitutive heterochromatin (the properties of the chromatin types are summarized in table 1).

	Euchromatin	Facultative Heterochromatin	Constitutive Heterochromatin
Character	dynamic	reversible	stable
State	dispersed	condensed	highly condensed
Nucleosome array	irregular	regular	regular
Nuclease sensitive sites (HS)	+	-	-
Replication timing	early	mid	late*
Banding pattern (metaphase)	R	G	C (subset of G)
Base content	GC-rich	relatively AT-rich	mostly AT-rich
Genes	gene dense housekeeping genes tissue specific genes	gene poor tissue specific genes inactive X	almost devoid of genes
Characteristic sequences	Single copy, SINES	LINES	Repetitive sequences, (satellite -DNA) transposons,
CpG islands	frequent	rare	absent
Epigenetic marks	H3/4 hyperacetylation H3K4me2 and	variable	H3/4 hypoacetylation H3K9me3** H4K20me3

H3K4me3 methylation, H3K36 methylation R-methylation hypomethylated DNA	methylated DNA RNAi
---	------------------------

Table 1 Different classes of chromatin * exceptions (Kim et al., 2003) are possible

** all histone lysine methylations are named according to the Brno nomenclature (Turner, 2005)

Constitutive heterochromatin in animals is mainly found at and around centromeres. It is permanently heterochromatic and consists of repetitive sequences (Martens et al., 2005; Myster et al., 2004).

There are various types of satellite DNA in human which can be separated by gradient density centrifugation. The so called alpha-satellite DNA is rich in A-T and is located in the centromeric region of the chromosomes. DNA satellite I, which is also A-T rich, is located more specifically at the centromeres of chromosomes 3 and 4, the short arm of the acrocentric chromosomes and the long arm of the y-chromosome. The DNA satellites II and III are both A-T rich. DNA satellite II is primarily located at the secondary constriction of chromosome 9, the short arms of the acrocentrics and the y chromosome (Grady et al., 1992; Therkelsen et al., 1997; Waye and Willard, 1989).

2.5 Epigenetics and the histone code

Epigenetic phenomena (from the Greek prefix “epi” meaning “in addition to”) do not change the actual, primary sequence of nuclear DNA but act on different cellular processes like transcription, DNA repair mechanisms and replication. Several posttranslational modifications like acetylation, histone methylation, DNA-methylation, phosphorylation, ADP-ribosylation, ubiquitination and SUMOylation are involved in controlling the epigenetic output (Kouzarides, 2007). Chromatin can respond to intrinsic and external signals. Not only the already mentioned modifications can influence chromatin structure but also ATP consuming nucleosome remodeling systems (Mellor, 2005; Varga-Weisz and Becker, 2006), histone variant incorporation and non-coding RNAs (Matzke and Birchler, 2005). These alterations altogether determine epigenetic transitions that bias gene expression patterns in many ways. If one thinks about that roughly 30000 human genes can give rise to about 200 distinct cell types (Lander et al., 2001; Waterston et al., 2002) it is clear that complex mechanisms are required to conduct all factors that define the heritable state of a cell type, establish gene sets and maintain a specific cellular phenotype.

Lately, a “histone code” hypothesis has been suggested (Jenuwein and Allis, 2001; Strahl and Allis, 2000; Turner, 2000). Different modifications (e.g. acetylation and methylation) of histone N-termini represent an evolutionarily conserved mechanism that can induce and stabilize functionally distinct chromosomal subdomains (Jenuwein and Allis, 2001).

The enzymes responsible for these histone tail modifications are highly specific for particular amino acid positions, thereby extending the information content of the genome beyond the genetic code (Turner, 2000).

The histone code hypothesis predicts that:

1. Distinct modifications of the histone tails induce interaction affinities for chromatin-associated proteins.
2. Modifications on the same or different histone tails may be interdependent and generate various combinations on any one nucleosome, thereby creating unique biological outcomes.
3. Distinct qualities of higher order chromatin, such as euchromatic or heterochromatic domains, are largely dependent on the local concentration and combination of differentially modified nucleosomes.

Jenuwein and Allis envision that this “nucleosome code” then permits the assembly of different epigenetic states, leading to distinct “readouts” of the genetic information, such as gene activation versus gene silencing, or more globally, cell proliferation and cell differentiation (Jenuwein and Allis, 2001). Data presented by Sun and Allis were the first demonstration that the histone code on one tail can control that of another on a different histone tail (Sun and Allis, 2002). Other examples of crosstalk as predicted in the histone code hypothesis have been reported in the last years (Mateescu et al., 2004; Zhang et al., 2005).

Expression of genes in higher organisms is highly dependent on DNA accessibility (Khorasanizadeh, 2004; Langst and Becker, 2004). DNA packaging has inherent consequences regarding the accessibility of factors to DNA.

Histone acetylation (Daujat et al., 2002; Grant et al., 1999; Schiltz et al., 1999) and arginine methylation (Bauer et al., 2002; Strahl et al., 2001; Wang et al., 2001) have been linked mainly with transcriptional activation (Clarke et al., 1999; Mathis and Althaus, 1990; Parthun et al., 1996; Smith et al., 2005; Turner, 2000). This is because histone acetylation decreases internucleosome interaction and the interaction of nucleosome tails with linker DNA (Gorisch et al., 2005). Acetylation delivers its epigenetic power by “opening” chromatin via neutralization of the positive charged lysines and arginines and by repulsion of the negatively

charged acetyl groups and the negatively charged phosphate group of the DNA backbone. Negative acetyl groups can be easily added to the positive charged amino acids. Thereby each added acetyl-group reduces the net positive charge of the histone by 1. On the higher chromatin level the enhancement of negative charged groups leads to a repulsion with the negatively charged DNA backbone (electrostatic mechanism).

Hyper- and hypoacetylation of individual lysines are associated with transcriptional regulation, generating distinct patterns of acetylation, resulting in an environment either permissive or not permissive transcriptional state. Many transcriptional activators have histone acetyltransferase (HATs) activities (Brownell et al., 1996) and quite some repressors are histone deacetylases (HDACs) (Taunton et al., 1996). Certain acetylation patterns may be used as surfaces for specific protein-histone interactions, providing one mechanism for coordinate regulation of chromatin processes that are biologically related (Kurdistani et al., 2004). Arginines are substrates for members of the protein arginine methyl-transferase (PRMT) family (Bedford and Richard, 2005) which can mono or dimethylate this amino acid (Bannister et al., 2002). However, this classical view has been re-evaluated in light of accumulating data that histone deacetylases also function as activators of transcription in yeast (Kurdistani and Grunstein, 2003).

Phosphorylation is thought to act similarly to acetylation by adding negative charges which repulse from the DNA-phosphate groups resulting in a more open configuration. It is involved in transcriptional activation of developmental early genes (Cheung et al., 2000; Clayton et al., 2000) and a necessary marker for mitotic chromosome condensation (Wei et al., 1999b).

By mid of the 1990s a lot of information about posttranslational modifications was collected but none of the enzymes responsible for these modifications was identified. In 1996 the first histone acetyltransferase was identified which demarcated a new era in histone research (Brownell et al., 1996). It was known that histone acetylation serves as a binding site for bromo-domain proteins found in HAT-complexes thereby functioning as a self reinforcing system (Dhalluin et al., 1999).

Recently many enzymes involved in histone methylation have been disclosed (figure 4) with SUV39H1 being the first histone methyltransferase that was discovered (Rea et al., 2000). SUV39H1 was demonstrated to be a highly specific histone lysine methyltransferase (HMT) on H3 peptides (Microsequencing revealed strong incorporation of a radioactive methyl group at the H3 lysine 9 residue). The fact that H3K9 was known as a site for acetylation (Nicolas et al., 2003) together with the observation that H3K9 methylation prevents phosphorylation of H3S10 (Aagaard et al., 1999) gave rise to the assumption that these modification underlies highly specific regulation.

Investigation of SUV39H1 revealed also a special sequence motif the catalytically active set-domain and a chromo-domain which was already indentified in chromatin associated proteins like heterochromatin protein 1 (HP1) and polycomb proteins (Paro and Hogness, 1991).

Trans-histone tail interactions, meaning that two epigenetic modifications can result in a totally different biological output, different from one of these modifications alone, seem to play an important role in epigenetic events. At the moment three examples of trans-tail histone codes have been described involving H2B ubiquitination and H3K4 methylation (Sun and Allis, 2002) or H3K79 methylation (Briggs et al., 2001) in yeast and H3K9 and H4K20me3 in mammals (Schotta et al., 2004b). They could show that in Suv39h dn female MEFs, H4K20 mono- and dimethylation are unaltered, but H4K20me3 is entirely lost from pericentric heterochromatin, concluding that the presence of the Suv39h enzymes can direct pericentric H4K20me3, or in other words this data suggest that H4K20me3 is highly dependent from a preceding H3K9me3 (Kourmouli et al., 2004). In this publication H4K20me3 staining of an immortalized embryonic fibroblast cell line which lacks any functional Suv39h HMTase was compared to a WT cell line. In the immortalized cells no antibody staining was detectable at centromeric regions while in wt-cells H4K20me3 staining was found to be associated with centromeric heterochromatin clusters, which led to the conclusion that there has to be some kind of “cross-talk” between both histone methylation sites (the mammalian epigenome was recently reviewed by (Bernstein et al., 2007)). The large field of epigenetics was recently reviewed in a comprehensive textbook (Allis, 2007).

2.6 The nucleosome core particle

The structured globular domain of the nucleosome core particle is also extensively modified adding a new dimension to the histone-code hypothesis. The finding that the nucleosome core particle plays a key role in regulating chromatin dynamic makes a interpretation of histone modifications even more complex. Early indications of the importance of the structured histone globular domain came from genetic screens in yeast, which identified numerous globular-domain amino-acid residues important for gene expression (Kruger et al., 1995; Park et al., 2002). Core histone phosphorylation is thought to have important structural consequences for nucleosome assembly and integrity. Histone H3 is rapidly phosphorylated on serine residues when extracellular signals like growth factors stimulate cells to proliferate (Mahadevan et al., 1991). Phosphorylation of H4 and H2A occurs in the cytoplasm shortly after histone synthesis (Dimitrov et al., 1994).

The recent application of mass spectrometry to histone biology has led to the startling discovery that many of the same residues are targeted for post-translational modifications (Cocklin and Wang, 2003; Freitas et al., 2004; Ng et al., 2003; van Leeuwen et al., 2002;

Zhang et al., 2003). A new model implementing previously published data was recently proposed (Cosgrove et al., 2004).

2.7 Histone lysine methylation

The characterization of histone methylation is lagging behind that of histone acetylation and phosphorylation in its characterization, but it is rapidly catching up, as can be perceived from the high number of published reviews in recent years (Dillon, 2004; Fischle et al., 2003b; Huisinga et al., 2006; Lachner et al., 2003; Lesne, 2006; Martin and Zhang, 2005; Nightingale et al., 2006; Sims et al., 2003). Unlike histone acetylation, histone methylation does not alter the overall charge of the nucleosome. Both modifications can act by recruiting proteins that regulate processes that require DNA access like transcription, mRNA splicing and DNA repair (Sims et al., 2003). Whereas acetylation functions at least partly by changing the charge of the histone protein, methylation exerts its effect via many different adaptor and effector proteins. A unique feature of histone lysine methylation is that its functional impact depends on the modification site and the modification state (mono-, di- and tri-methylated states can be distinguished). H3K4me3 is associated with active genes (Santos-Rosa et al., 2002) whereas H3K9me3 is found at silent loci (Lachner and Jenuwein, 2002). Trimethylation of H3K4, H3K9, H3K27 and H4K20 are especially stable and can persist through mitosis and over several cell generations (Lachner et al., 2004; Reinberg et al., 2004).

The stability of histone methylation marks renders them particularly suited for the propagation and inheritance of epigenetic states. The homeobox-containing proteins (HOX), a highly conserved class of transcriptional regulators determine the positions of structures along the anterior-posterior axis of the embryo and mutations in HOX genes transform one body segment into another one. The expression-status of this family of genes depends on two groups of antagonistic proteins. The Polycomb group (PcG) genes encode proteins that maintain the HOX genes silent in tissues where they should not be expressed while the Trithorax group (TrxG) genes are required for expression of HOX genes in proper cells (Ringrose and Paro, 2004). Several mechanisms have been suggested to explain the fate of histone lysine methylation marks during transitions between epigenetic states. For instance, the respective modification could be diluted through replication cycles by inhibition of the corresponding HMT. Another possible mechanism could be the replication dependent histone exchange. This process disrupts and ejects histones from the DNA template (Janicki et al., 2004; Schwabish and Struhl, 2004; Schwartz and Ahmad, 2005). Histone methylation could also be eliminated by cleavage of the histone tails (Bannister et al., 2002). Finally modifications might persist but no longer be able to perform their function, due to removal of

their interaction partners or changes of neighboring modifications (Bannister et al., 2002; Fischle et al., 2003a).

The mystery of histone demethylation was partly solved in 2004 with the discovery of a lysine specific demethylase (LSD1) which was described as an amine oxidase able to remove methyl groups from lysine 4 of histone 3 (Shi et al., 2004). However it should be noted that the mechanism by which LSD1 demethylates is not a “true” demethylation because the enzyme acts specific on H3K4me₂ by FAD-dependent oxidative destabilization of the amino-methyl bond (Shi et al., 2004) and, furthermore, that mechanisms to remove trimethyl groups were discovered only recently (Trewick et al., 2005; Tsukada et al., 2006; Whetstine et al., 2006). For an up to date review of histone lysine demethylation by demethylases read (Shi and Whetstine, 2007).

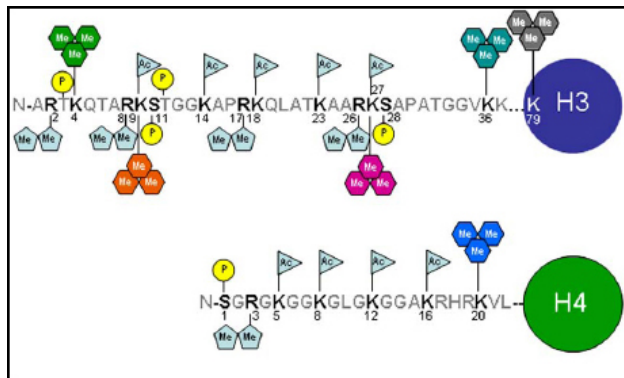


Figure 3

Histone modifications and where they occur

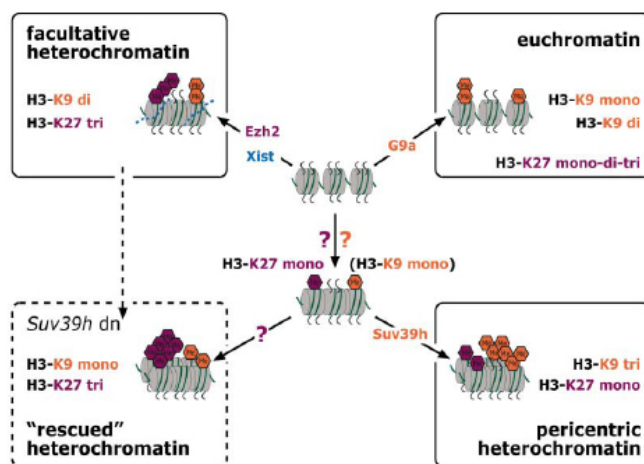
Substrate	Histone lysine methyltransferases
H3K4	SET9, SET1, MLL, ASH1L, SMYD3, PRDM9, SETMAR
H3K9	SUV39H1, SUV39H2, EHMT1, EHMT2, SETDB1, PRDM2, ASH1L
H3K27	EZH2, EHMT2
H3K36	NSD1, SETD2/HYPB, SETMAR
H3K79	DOT1L
H4K20	SET8, SUV420H1, SUV420H2, NSD1, ASH1L

Figure 4

The enzymes responsible for the methylation of human histone lysine sites

For more information on the different HMT families classified according to sequence similarities within their SET domain and within adjacent sequences, see the review by Völkel and Angrand, 2006 (Volkel and Angrand, 2006).

There are about 50 SET domain gene sequences in the mammalian genomes (Kouzarides, 2002), five lysines that can be methylated in the histone N-termini, and three distinct methylation states at each position. These numbers would account for 15 methylation systems which are present in several multigene families. There are also more than one enzyme observed to finally create one methylation state (figure 4). For example H3K9 has to be monomethylated before it can be trimethylated. In addition new methylation sites have been found (H3K18, H3K56, H3K64, H3K122) although these are only methylated at low frequency (Peters et al., 2003 online supplementary files) (Peters et al., 2003). Taken together, these modifications allow a high combinatorial diversity for potential interaction mechanisms (figure 5).

**Figure 5**

Partitioning of chromatin by histone lysine methylation

From Peters et al., 2003 Mol Cell

(Peters et al., 2003)

As was demonstrated by Mass Spectrometry (MS) analysis, up to 40-70% of a given histone lysine residue at each of the six methylation sites H3K4, H3K9, H3K27, H3K36, H3K79 and H4K20 are actually methylated in one form or another (Fodor et al., 2006). The relative abundance of the three distinct methylation states showed that di-methylation is the most frequent, followed by mono-methylation and tri-methylation (Fodor et al., 2006).

The availability of highly specific antibodies for a given modification site (Perez-Burgos et al., 2004; Schotta et al., 2004a) has opened up the way for investigations of the functional and spatial arrangements of distinct methylation sites. The most critical step to raise these highly specific antibodies was an appropriate peptide (antigen) design. Peptide antigens differed in length (6 to 20 amino acids), configuration (linear versus branched peptide) and methylation state of the lysine of interest (mono-, di-, or tri-). Three types of quality controls were used to assess antibody specificity: Enzyme-linked immunosorbent assays (Elisas), peptide spotting analyses (dot blots) and protein blots with recombinant and nuclear histones. Finally as the most stringent test for antibody specificity was performed by comparing signals in a wild type (wt) and mutant background (dn for the HMT responsible for the modification the antibody should detect). Although slight discrepancy of antibody specificity was observed all antibodies recognized the appropriate lysine residue and methylation state with high specificity (Perez-Burgos et al., 2004).

In the following I want to give an overview about recent research results about the meaning and interactions of the histone methylation sites that were investigated in this thesis.

2.7.1 H3K4

Epigenome-wide investigation of H3K4me3 was performed in mouse and other higher eukaryotic organisms by chromatin immuno precipitation (ChIP) techniques (Bernstein et al., 2005; Martens et al., 2005; Schneider et al., 2004; Schubeler et al., 2004).

H3K4me3 is an epigenetic mark associated with active genes in yeast and *Tetrahymena* (Dehe and Geli, 2006; Strahl et al., 1999). But similar to many other histone lysine methylation sites also for H3K4me3 contradictory data are available (Shi et al., 2006). The authors identified a new class of H3K4me3 effector proteins and describe a new mechanism, in response to DNA damage, by which H3K4me3 functions in active gene repression.

The function of di and monomethylated H3K4 seems to be at least partially unclear. It was suggested that dimethylation correlates with a permissive state of chromatin, marking actively transcribed or potentially active genes. **Dimethylation** of H3K4 occurs on both inactive and active euchromatic genes, whereas trimethylation is present exclusively at active genes (Santos-Rosa et al., 2002). Detailed investigation of the global distribution of histone acetylation and H3K4 methylation revealed that H3K4me2 in coding regions correlates with transcriptional activity and that the HMTase Set1 (the enzyme for H3K4me3) protects active coding regions from deacetylation (Bernstein et al., 2002). The apparently ubiquitous presence of H3K4me2 is consistent with previously reported findings at the β -globin locus, where H3K4me2 is detected on large euchromatic regions encompassing both active and inactive genes (Litt et al., 2001). Briggs et al., 2001 show in a rescue assay that H3K4 methylation is important for cell growth and transcriptional silencing of rDNA (Briggs et al., 2001). In recent years several binding proteins like complex proteins associated with Set 1 (COMPASS) (Krogan et al., 2002) and inhibitor of growth 2 (ING2) (Shi et al., 2006) that target this epigenetic mark have been identified. At different time points in development a marked enrichment of H3K4me3 was found in the transcribed regions of actively transcribed genes. More precisely H3K4me3 persists to mark recently active genes after a transcriptional response has ended (Ng et al., 2003) but the trimethylated state changes during heterochromatin formation. This process is gradual and requires multiple cell division cycles and leads finally to a H3K4me1 state (Katan-Khaykovich and Struhl, 2005). Interestingly dimethylation as well as trimethylation of H3K4 was detectable on inactive globuline genes (Schneider et al., 2004). In this paper the first time a strongly and preferentially association of H3K4me3 with the transcribed regions of active genes was demonstrated for eukaryotes. Plasticity across evolution, as analyzed for various species, in the association of histone lysine methylation with functionally distinct chromatin domains was shown for H3K4me3 (Spada et al., 2005).

In *Chlamydomonas* it was shown that functional differences between H3K4me2 and H3K4me1 exist, with the latter operating as an epigenetic mark for repressed euchromatin

while dimethylated H3K4 can be attributed to a transcriptionally permissive state (Dijk, 2005). The intricacy of writing and reading a single epigenetic mark and the mechanisms involved in histone lysine methylation were recently exemplified for H3K4 (Ruthenburg et al., 2007).

2.7.2 H3K9 (and interaction with HP1)

In mouse as well as in humans, constitutive heterochromatin is marked by **H3K9me3** (Lehnertz et al., 2003; Martens et al., 2005; Rea et al., 2000; Rice et al., 2003). H3K9 methylation is largely, although not abundantly, conserved from *S.pombe* to mammals (Lachner et al., 2004).

Suv39H1 the first HMT to be identified and meanwhile the best characterized one is responsible for H3K9me3 (Nakayama et al., 2001; Peters et al., 2001; Rea et al., 2000; Schotta et al., 2002). A role for SUV39H1 and its associated H3K9 methyltransferase activity in heterochromatin function was first indicated in *Drosophila* experiments by showing its association with the heterochromatin protein 1 (HP1) (Aagaard et al., 1999). Subsequent studies showed that H3K9me3 serves as a binding site for the chromodomain of HP1 proteins. Suv 39h double null (dn) cells do not show pericentric heterochromatin accumulation of HP1. This phenotype could be rescued by heterologous expression of a catalytically active Suv39h1 demonstrating that Suv39h1 mediated H3K9 trimethylation is a binding site for HP1 (Bannister et al., 2001; Lachner et al., 2001). Unlike the H3K9me3-HP1 system which is necessary for the formation of constitutive heterochromatin, the formation of facultative heterochromatin can occur in the absence of HP1 (Gilbert et al., 2003).

HP 1 was initially identified in *Drosophila melanogaster* in a screen for nuclear proteins that show a predominant localization to the chromocentre of polytene chromosomes (James and Elgin, 1986). Shortly after the protein was reported to play an essential role in position effect variegation (PEV) (Eissenberg et al., 1990). Homologous proteins have been found in several organisms and three isoforms HP1 α , HP1 β and HP1 γ have been identified in *Drosophila* (Singh et al., 1991). While HP1 α is only localized at centromeric heterochromatin, HP1 β and particularly HP1 γ also localize to euchromatic sites (Nielsen et al., 2001). HP1 proteins act via their chromodomain (Bannister et al., 2001; Lachner et al., 2001) which is connected by a hinge region to a chromoshadow domain (figure 6). These domains are found in many proteins that contribute to chromatin organization and regulation of gene expression like the Polycomb group proteins or SUV39H1 itself (Jones et al., 2000).

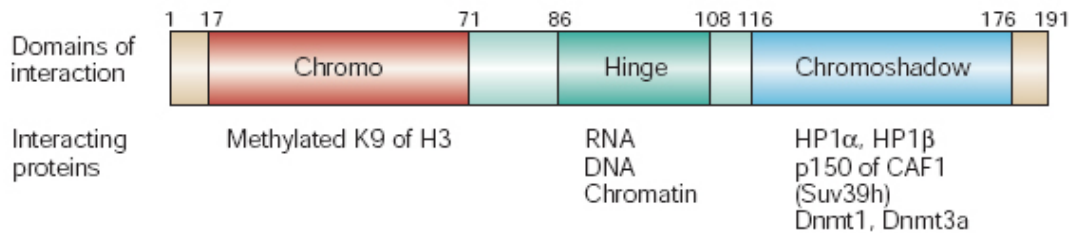


Figure 6

This scheme depicts HP1-alpha domains of interaction with selected partners that are potentially important for the stability of heterochromatin domains. From Maison and Almouzni Nature reviews 2004 (Maison and Almouzni, 2004).

The chromoshadow domain functions as a homodimerization module for all isoforms of the HP1 proteins. Self-association might contribute to heterochromatin compaction and clustering. H3K9me3 alone is not sufficient to recruit HP1 specifically but an RNA component is also required, as was shown in the mouse model (Maison et al., 2002). Heterochromatin is often described as static but recent work on heterochromatic domains revealed that HP1 proteins are highly dynamic (Cheutin et al., 2003; Festenstein et al., 2003). A role for the retinoblastoma protein in heterochromatin formation and regulation of HP1-alpha dynamics was lately suggested (Siddiqui et al., 2007). The mechanism of HP1 for heterochromatin formation is more complex than it seems at a first glance. Indeed as was shown recently H3K9 methylation alone is not sufficient to recruit HP1 to chromatin but it can suppress transcription via a mechanism involving histone deacetylation by recruiting HDACs. Additionally a secondary direct protein-protein interaction with SUV39H1 (Stewart et al., 2005) was reported for stable binding of HP1 to methylated H3K9me3. For further information about HP1 function in heterochromatin formation and maintenance read the review of Maison and Almouzni (2004) (Maison and Almouzni, 2004).

Structure-function relationships and intercellular dynamics as well as hypothetical models describing how HP1 can organize peripheral heterochromatin acting as a crosslinker is described by Singh and Georgatos (Singh and Georgatos, 2002). To make the hole think even more complex, recently evidence for the existence of an HP1-mediated subcode was provided (Lomberk et al., 2006). The authors report that all three HP1 isoforms can be extensively modified, similar to histones, suggesting that the silencing of gene expression may be further regulated beyond the histone code.

In 2000 O'Carroll and colleagues could show the existence of Suv39h2, a second mouse HMTase specifically expressed in testis, where it organizes meiotic heterochromatin. Based on their results, these authors suggested a redundant enzymatic role for Suv39h1 and Suv39h2 during mouse development and a function for Suv39h2 in organizing meiotic heterochromatin (O'Carroll et al., 2001). H3K9 methylation by Suv39h1 and Suv39h2 occurs

at mammalian telomeres and is important for telomere length regulation (Garcia-Cao et al., 2004). These findings imply that epigenetic errors could alter telomere length thereby providing a connection between the transcriptional silencing of genes near the telomeres and the regulation of telomere length. In addition the viability of mice with inactivated Suv39h1 and Suv39h2 genes was impaired and chromosomal instabilities that are associated with greater tumor risk and overall altered methylations patterns were observed (Peters et al., 2001).

Apart from heterochromatin organization, H3K9me3 is important for chromosome segregation and mitotic progression (Melcher et al., 2000). Furthermore there are several reports demonstrating silencing effects correlated with, or resulting from H3K9me3 including the inactive X chromosome (Xi) (Boggs et al., 2002; Heard et al., 2001; Mermoud et al., 2002), and developmentally regulated genes (Litt et al., 2001).

The subnuclear localization of all three H3K9 methylation states and their replication timing was investigated in mammalian cells (Wu et al., 2005). H3K9me1 was found in replicating punctate domains of early replicating chromatin in the nuclear interior whereas the pattern of H3K9me2 was similar to the DNA replication pattern in mid S-phase i.e. localized at the nuclear and nucleolar periphery. H3K9me3 decorated late replicating DAPI-dense heterochromatic regions.

The H3K9me3-SUV39H1-HP1 system is not only involved in local gene repression (Firestein et al., 2000) but also has a role in repressing euchromatic genes through interaction with the retinoblastoma protein (Rb) and other corepressor proteins (Nielsen et al., 2001). The interaction with the Rb tumor-suppressor-protein shows that epigenetic modifications and their associated proteins do not represent an isolated system, but probably work as interaction partners in networks of many pathways.

In contrast to H3K9me3, **H3K9me1** and **H3K9me2**, are excluded from pericentromeric regions and enriched within silent domains of euchromatin. In mouse the enzyme G9a was found to be responsible for H3K9me1 and H3K9me2 (Rice et al., 2003). G9a HMT activity has no effect on H3K9me3 patterns but only on H3K9me1 and H3K9me2 patterns, as was shown in the absence of G9a (Peters et al., 2003). H3K9me1 is predicted to function as a substrate for the Suv39h HMTases that change the monomethylated state into a trimethylated state (Peters et al., 2003). In mouse embryonic stem cells (ES) that are double null (dn) for both SUV39h1 HMTs, pericentric heterochromatin becomes enriched for H3K27me3 and H3K9me1, thereby illustrating an unexpected plasticity between the H3K9 and H3K27 methylation systems. These results however, could not be reproduced by Rice and colleagues (Rice et al., 2003). Surprisingly H3K9me2 was also established as an epigenetic imprint of facultative heterochromatin e.g. the inactive X-chromosome in female

mammals (Boggs et al., 2002; Peters et al., 2001). H3K9me3 is retained throughout mitosis, suggesting that it might act as an epigenetic imprint to maintain the inactive state.

In double null mouse cells for both Suv39h HMTases, H3K9me3 disappears from constitutive heterochromatin but is still found on Xi. Hence a Suv39h-HP1 independent pathway for the establishment of H3K9me3 at facultative heterochromatin seems to exist (Peters et al., 2001). Recent findings demonstrate that specific HMTs direct H3K9me1 and H3K9me2 to silent domains within euchromatin, whereas the bulk of H3K9me3 occurs in pericentric regions which represent the archaetype of constitutive heterochromatin (Dillon and Festenstein, 2002). H3K9me2 is found to be associated with facultative heterochromatin, while H3K9me1 is found in non-heterochromatic regions, referred to as euchromatin (Peters et al., 2003; Rice et al., 2003).

2.7.3 H3K27 (and X-inactivation)

H3K27me3 became famous through its correlation with facultative heterochromatin most notably the inactivated X-chromosome (Xi) (Okamoto et al., 2004; Plath et al., 2003; Silva et al., 2003). In female mammals facultative heterochromatinization of one X-chromosome occurs during development, silencing more than 1000 genes and gives rise to an inactive X-chromosome (Lyon, 1999). X-linked gene products can thus be dosage-compensated between males (XY) and females (XX). The key-locus underlying the initial differential treatment of two X chromosomes is the X inactivation centre (Xic). Xic ensures that only a single X chromosome remains active in a cell with a diploid autosomal set (counting) and it provides a signal that triggers silencing: the non coding XIST transcript (Avner and Heard, 2001). The 19kb long untranslated XIST transcript coats the X-chromosome in "cis". This is followed by gene silencing across the chromosome (during embryonic stem cell differentiation) (Okamoto et al., 2004; Panning et al., 1997; Sheardown et al., 1997). X-inactivation can be subdivided into two consecutive processes: imprinted and random X-inactivation. In development, mouse imprinted X-inactivation takes place and the paternal X chromosome becomes silent in all the cells of the embryo (Okamoto et al., 2004). The paternal X remains inactive in cells that contribute to extraembryonic tissues, but X-inactivation is reversed in cells that create the embryo proper. In these cells X-inactivation is re-established and both X-chromosomes paternal and maternal can then be inactivated randomly.

Among the earliest chromatin changes that occur during the inactivation process are the loss of euchromatin-associated histone modifications (H3K9 acetylation, H3K9me1 and H3K9me2) just after XIST RNA coating (Chaumeil et al., 2002; Heard et al., 2001). Global histone hypoacetylation occurs shortly afterwards (Keohane et al., 1996). After these

changes several new histone modifications appear on the Xist-RNA coated chromosome. Several recent studies have implicated Polycomb group proteins in promoting some of these marks (Brinkman et al., 2006; Plath et al., 2003; Rougeulle et al., 2004). To date modifications involved in the process of X-inactivation: H4K20me1, H3K9me2 and H3K27me3 (Heard et al., 2001; Kohlmaier et al., 2004; Rougeulle et al., 2004; Silva et al., 2003).

The Xi presents many epigenetic hallmarks like a mosaic of cells with Xi (depending on inactivation of either the paternal or maternal X-chromosome), mitotic heritability but also a developmental reversibility of the inactive state and a replication pattern that is asynchronous with the rest of the genome (Heard, 2005). X-inactivation has certain similarities to constitutive heterochromatin: Xi is replicated later in S-phase than Xa (Xiong et al., 1998), retains a condensed heterochromatic morphology during interphase (Barr body) (Barr and Bertram, 1949), and is depleted in both H3K4 and H4 acetylated histones (Boggs et al., 2002).

H3K27 methylation occurs predominantly by the enzyme enhancer of zeste (EZH2) (Czermin et al., 2002; Kuzmichev et al., 2002). Moreover interrelations between Su(var) and Polycomb pathways have been described (Sewalt et al., 2002). E.g. **H3K27me1** was reported to be associated with pericentric heterochromatin (Peters et al., 2003; Rice et al., 2003).

New investigations revealed that intergenic, coding and promoter regions are segregated into differentially marked chromatin. The presence of H3K27me3 at unexpressed autosomal genes suggests that this mark may be a more global heterochromatic mark rather than an X-specific mark (Brinkman et al., 2006).

H3K27 methylation also plays a role in laminopathies, e.g. in cells of Hutchinson-Gilford progeria Syndrome (HGPS) patients. There are currently only 30 to 40 known cases worldwide. Physical features of Progeria children include dwarfism, wrinkled/aged-looking skin, baldness, and a pinched nose. Their mental growth is equivalent to other children of the same age. This disease is caused by a mutant lamin A and recently attracted a lot of attention in the media.

Shumaker and colleagues demonstrated that there are significant changes in the epigenetic control of both facultative and constitutive heterochromatin. These changes are a direct consequence of the expression of the lamin A mutant which alters the state of histone methylation. In early passages of cultured female HGPS cells a loss of H3K27me3 was observed especially at the Xi (Shumaker et al., 2006).

H3K27 methylation could indicate the emergence of multicellularity and cell-type differentiation, as it is absent in both budding and fission yeast. The presence of H3K27 methylation signals appears tightly coupled to the existence of the Polycomb system, which

is involved in lineage commitment and in coregulating the stability of gene expression programs (Lachner et al., 2004).

2.7.4 H4K20

H4K20 was the first described methylated lysine residue (Murray, 1964). It is highly conserved and most abundant across epigenetic model organisms ranging from *S.pombe* to mammals (Lachner et al., 2004). **H4K20me1** is catalyzed by the HMT SET8/PR-Set7 (Fang et al., 2002; Nishioka et al., 2002; Xiao et al., 2005). In this work it was noted that levels of H4K20me1 fluctuate during cell cycle. This suggests that this modification is somehow involved in cell cycle regulation. Indeed loss of the *Drosophila* homologue leads to cell cycle arrest (Karachentsev et al., 2005). It has also been described to contribute to chromosome segregation during mitosis (Julien and Herr, 2004). H4K20me1 is furthermore reported to be involved in DNA repair mechanisms in yeast (Nakamura et al., 2004; Sanders et al., 2004) and initiation of X-inactivation in mouse (Kohlmaier et al., 2004).

Pericentric regions representing constitutive heterochromatin are enriched in **H4K20me3** (Kourmouli et al., 2004; Martens et al., 2005; Schotta et al., 2004b). A similar, but not totally identical pattern formation to H3K9me3 was observed very recently for H4K20me3 (Zinner et al., 2006).

In a present work a role for the Rb-family not only in global chromatin modifications, but also in the assembly of constitutive heterochromatin was suggested (Gonzalo et al., 2005). Suv4-20h1 and Suv4-20h2 the HMTs responsible for H4K20me3 surprisingly interact directly with the famous tumor suppressor protein Rb, as was also shown for the trimethyl H3K9-Suv39H1-HP1 system.

Recently a close interrelationship involving H4K20 and H3K9 methylation was reported (Sims et al., 2006). Their findings indicate that the corresponding methylated states of H4K20 and H3K9 tend to localize to the same silent compartments in the nucleus and within the same genomic regions on chromatin fibers. H4K20me3 and H3K9me3 were both selectively enriched within pericentric heterochromatin. Analysis on the nucleosomal level revealed that H4K20me1 and H3K9me1 were preferentially and selectively enriched on the same nucleosome core particle in vivo.

In a work by Talasz et al., H4K20me1 was shown to be associated with active chromatin (Talasz et al., 2005). On the contrary several independent reports showed that H4K20me1 correlates with silent chromatin in higher eukaryotes (Karachentsev et al., 2005; Kohlmaier et al., 2004; Nishioka et al., 2002; Vaquero et al., 2004). Sims et al., (Sims et al., 2006) observed H4K20me1 enriched within silent regions of chromosome arms and within the inactive-X chromosome which implies that this modification marks facultative heterochromatin. H4K20me2 is independent of H4K20me1 and H4K20me3 and therefore

facultative and constitutive heterochromatin, so they conceive that H4K20me2 may define an entirely unique type of heterochromatin that has not yet been described. Schotta and colleagues observed already a few years earlier that H4K20me2 is also broadly distributed over euchromatic regions but shows a more speckled pattern compared to monomethylation (Schotta et al., 2004a). Both, H4K20me1 and H4K20me2 appear as uniformly distributed foci throughout the nucleus, excluding nucleoli and the nuclear periphery. The findings that loss of H4K20me3 is a common hallmark of human tumor cells (Fraga et al., 2005) linked also histone lysine methylation to the already complex field of cancer biology.

2.8 Chaetocin, inhibitor of the HMT SUV39H1

Inhibitors have been very popular in biological experiments concerning transcription and epigenetics. Actinomycin D (Frey et al., 1996; Galun et al., 1964), alpha-Amanitin (Gong et al., 2004) or DRB (Clement and Wilkinson, 2000; Hensold et al., 1996) for example are common inhibitors of RNA polymerase II activity. Changes in epigenetic mechanisms have been mainly investigated by the application of 5-aza-cytidine which sequesters DNA methyltransferases (Doiron et al., 1999; Lu and Randerath, 1980), short-chain fatty acids (e.g. sodium butyrate) (Bell and Jones, 1982; Hague et al., 1993) and hydroxamic acids (trichostatin A) (Yoshida et al., 1990), the last two acting as inhibitors of histone deacetylases.

Lysine methylation was shown to be catalyzed by enzymes using S-adenosyl-methionine (SAM) as the methyl-group donor (Kim and Paik, 1965; Paik and Kim, 1971). But it was not until the year 2000 that the molecular identity of the first histone methyltransferase was discovered. The trimethylation of H3K9, a marker for constitutive heterochromatin is catalyzed by the HMT SU(VAR)H1 (Rea et al., 2000). Inhibitors of histone methyltransferases were not known until recently when the SUV39H1 inhibitor Chaetocin was discovered (Greiner et al., 2005). This fungal toxin acts as a competitive inhibitor for S-Adenosyl-Methionin (SAM) the most important donor of methyl groups in a cell. Despite Chaetocin has structural similarities to HDAC inhibitors it yet does not alter cellular levels of acetylated histone H3 at cytotoxic concentrations (Isham et al., 2006). The discovery that Chaetocin affects enzymes responsible for methylations at other lysine sites to a much lower extent than H3K9me3 (Greiner et al., 2005), highlights the inhibitory specificity of Chaetocin.

2.9 RNA interference and heterochromatin formation

Nuclear RNA-interference (RNAi) functions as a surveillance mechanism against foreign nucleic acids, e.g., retroelements and transposons (Buchon and Vaury, 2006). Recent

studies have revealed that components of the RNAi machinery are associated not only with the impairment of RNA translation but also involved in DNA-methylation and the formation of heterochromatin (Matzke and Birchler, 2005; Zaratiegui et al., 2007). The detailed events involved in RNAi in mammals and plants are described in detail in a review by Wassenegger et. al (Wassenegger, 2005).

The initiation of heterochromatin formation of specific chromosomal regions such as centromeric regions is thought to result from the bidirectional transcription of repetitive sequences by Pol II (Sarraf and Stancheva, 2004). The enzyme dicer then cuts the double stranded RNA into small interfering RNAs (siRNAs). After being loaded to the RITS-complex (RNA-induced initiation of transcriptional gene silencing), siRNA targets RITS to sites of heterochromatin. RITS recruits on the one hand SUV39H1, on the other hand it recruits the RDRC-complex (RNA-directed RNA polymerase) which functions in the production of additional double-stranded RNA. With this mechanism RITS reinforces its own recruitment to heterogenic regions (Martin and Zhang, 2005).

2.10 DNA methylation

DNA-methylation can be found in several different organisms like many prokaryotes, mammals, fungi and plants (Hendrich and Tweedie, 2003). DNA methylation in mammals is a post replicational modification that is found in cytosines of the dinucleotide sequence CpG. In the 1960s scientists suggested that DNA methylation might protect cells against the integration of foreign DNA or making host DNA resistant to DNases directed against foreign DNA (Srinivasan, 1964). It was proposed in 1975 that DNA methylation might be responsible for the stable maintenance of a particular gene expression pattern through mitotic cell division (Riggs, 1975). Proteins that specifically recognize methyl-CpG were identified more than a decade ago (Lewis et al., 1992; Meehan et al., 1989).

Nowadays its widely accepted that DNA-methylation is a key-player in establishing silent domains by collaborating with proteins that modify nucleosomes. For a comprehensive coverage of the topic DNA-methylation the following reviews are recommended (Bender, 2004; Bird, 2002; Freitag and Selker, 2005; Li, 2002).

DNA methylation affects gene expression mainly in two ways: First, the modification of cytosines prevents DNA binding factors from associating to their specific DNA sequence by blocking them (Watt, 1988). Second, distinct proteins that recognize methyl-CpG can enhance the repressive potential of methylated DNA by recruiting enzymes responsible for epigenetic modifications which leads to a change in chromatin density, e.g. HDACs and HMTs (Hendrich and Bird, 1998; Nan et al., 1998; Sarraf and Stancheva, 2004). Epigenetic “cross-talk” in mammals was reported for the Suv39h-HP1 histone methylation system and

DNA methyltransferase 3b (Dnmt3b) (Lehnertz et al., 2003). Methyl-binding proteins (MBPs) use transcriptional co-repressor molecules to silence transcription and modify surrounding chromatin by recruiting HDACs and chromatin remodelling factors (Wade et al., 1999).

These mechanisms are never isolated events but act as a bridge between two global epigenetic modifications, DNA-methylation and histone modifications (Fuks, 2005; Fuks et al., 2003).

In mammals four catalytically active DNA methyltransferases (DNMTs) have been described (Robertson et al., 2000). Whereas DNMT3a and DNMT3b have been shown to be required for de novo DNA methylation (Okano et al., 1999), DNMT1, as a component of the multiprotein DNA replication complex (Vertino et al., 2002), is propagating heritable DNA methylation patterns following DNA replication (Li et al., 1992). DNMT2 shows only weak DNA methyltransferase activity in vitro (Hermann et al., 2003). Global de novo methylation has been documented during germ-cell development and early embryogenesis, when many DNA methylation marks are re-established after phases of genome demethylation (Reik et al., 2001). For de novo methylation mediated by DNMT3a and DNMT3b several models for DNA targeting have been suggested (Klose and Bird, 2006):

1. DNMTs themselves might recognize the DNA or chromatin template
2. DNMTs are recruited by protein-protein interactions with transcription factors
3. The RNA interference system (RNAi) targets de novo methylation to specific DNA sequences

DNA-methylation is not only involved in many cellular processes but plays a role in several diseases (Robertson, 2005). Of outstanding interest is the role of DNA-methylation in cancer which is still one of the most common disease in the western world (Jones and Baylin, 2002).

2.11 Commonly used techniques in the field

The analysis of the modification status has been traditionally performed using specialized gel systems or the incorporation of radioactive precursor molecules followed by a complete protein hydrolysis and the analysis of the resulting amino acid (Allfrey, 1964; Waterborg et al., 1983).

Many of the data which contributed to linking histone lysine methylations to a gene expression state, either active (H3K4, H3K36, H3K79) (Krogan et al., 2002; Santos-Rosa et al., 2002; Schubeler et al., 2004) or repressed (H3K9, H3K27, H4K20) (Cao et al., 2002; Rice et al., 2003; Schotta et al., 2004b) were raised by chromatin-immunoprecipitation (ChIP) experiments. By ChIP analysis certain DNA sequences can be identified which are

precipitated by an antibody against a certain protein (modification) (Bernstein et al., 2004; Bernstein et al., 2005). Traditional methods for analyzing gene expression provide only a partial glimpse into gene regulation, but transcription is a complex process that requires multiple interactions and the orchestrated binding of numerous components. A method that raised scientists interest in recent years is chromatin immunoprecipitation-on-chip (ChIP-on-chip) (Boyer et al., 2006; Cam et al., 2005; Pokholok et al., 2005). ChIP-on-chip, also known as location analysis (LA), provides insight into key mechanisms of methylation, histone modification, as well as DNA replication, modification, and repair. It has been used to understand diseases such as diabetes, leukemia, and breast cancer, and has already provided important insight to vital processes like cell proliferation, cell fate determination, oncogenesis, cell cycle, apoptosis, and neurogenesis. ChIP-on-chip pairs chromatin immunoprecipitation (ChIP) with glass slide microarrays (chip) to analyze how regulatory proteins interact with the genome of living cells. For further information describing ChIP-on-chip technology read Blais and Dynlacht, 2005 (Blais and Dynlacht, 2005). A very direct technique to study histone modifications is mass spectrometry. Every modification adds a distinct mass to the molecule studied and thanks to the high resolution of modern mass spectrometers and the development of “soft” ionization techniques, the mapping of posttranslational modifications has been greatly facilitated during the last couple of years (Mann and Jensen, 2003; Sickmann et al., 2002).

RT-PCR techniques with gene-locus specific primers allow the analysis of the methylation status of a gene or a gene sub-region in correlation to its state of activity (Schneider et al., 2004; Su et al., 2004). A rather new method for the investigation of chromatin binding proteins is chromatin profiling which allows an *in vivo* assay and is based on a combination of targeted DNA methylation and microarray technology (Pickersgill et al., 2006; van Steensel et al., 2001). Another approach for getting information about the role of epigenetic modifications in common and for nuclear architecture in special, is the use of highly specific antibodies in immunofluorescence (IF) experiments. Although the antibodies developed in recent years are very sensitive, new problems arise from using them. It turned out that because of the similarity between different modification sites, many antibodies showed significant cross reactivity and were not as specific as researchers have initially hoped for (Perez-Burgos et al., 2004). Compared to immunofluorescence microscopy, ChIP-analysis provides a much higher resolution; however its information is restricted to the sequences associated with distinct proteins and does not provide any information about the three dimensional nuclear arrangement.

2.12 Outlook

The importance of epigenetic processes in the eukaryotic genome is reinforced by the growth of our knowledge about covalent modifications of histone proteins, and about the enzyme systems that transduce or remove these modifications. Enzymes involved in histone modifications use metabolic cofactors (e.g. nicotinamide adenine dinucleotide and SAM) to regulate other enzymes also involved in epigenetic mechanisms, thereby supposing that histone modifications may also act as a “sensor” for metabolic processes. (Imai et al., 2000). The secrets of epigenetics are just touched to a minor extent and it will take big efforts to gain better insights into the complex network of epigenetic mechanisms. The participating enzyme systems and mechanisms how they are recruited have to be identified in detail. Finally the interactions with partners downstream have to be clarified. Its still very difficult to link a specific modification to a distinct disease but stable markers like H3K9me3 and H4K20me3, can be correlated with diverse cell fates or with different proliferative potentials which can be of diagnostic importance. Senescent cells for example accumulate large clusters of “ectopic” heterochromatin (Narita et al., 2003). By contrast there is a general reduction in global H3K9me3 and H4K20me3 in cells that resemble an uncommitted fate (Baxter et al., 2004). A correlation of increased histone acetylation and reduced H4K20me3 has been recently reported for several types of human cancer (Fraga et al., 2005; Seligson et al., 2005). The fact that epigenetic modifications are often altered in cancer cells makes it a very interesting target for cancer therapies (Espino et al., 2005).

3 Methods and Protocols

3.1 Cell culture

Cell-lines used in the present work

Cell line	Medium	Split ratio	Split frequency
DLD-1	McCoy 5A+ 10% FCS+ 100U/100 µg/ml Penicillin/Streptomycin	1:2	every 3-4 days
MCF-7	RPMI+10% FCS+ 100U/100 µg/ml Penicillin/Streptomycin	1:6	every 3-4 days
Primary human fibroblasts	DMEM+20% FCS+ 100U/100 µg/ml Penicillin/Streptomycin	1:3	every 3-4 days
Mouse embryonic fibroblasts - W9	DMEM+20% FCS+ 100U/100 µg/ml Penicillin/Streptomycin	1:2	every 2-3 days

Cells are routinely cultivated in 25cm² tissue flasks with appropriate medium supplemented with 20% fetal calf serum (FCS) and antibiotics at 37°C and 5% CO₂ in an (humidified for HFb cells) incubator. After reaching confluency cells were split, i.e trypsinized and resuspended in fresh medium in an appropriate dilution. For the setup of an experiment cells were seeded on coverslips or cultivated onward.

3.1.1 Procedure for cell cultivation

Equipment and solutions:

- Serological pipettes (2ml, 5ml, 10ml, 25ml)
- Automatic pipette
- 25cm² tissue culture flasks
- 1xTrypsin-EDTA solution
- PBS (Mg²⁺ + Ca²⁺- free)
- Appropriate culture medium (prewarmed to 37°C)
- Waste container
- PBS (Mg²⁺ + Ca²⁺- free)

Procedure:

All steps are carried out in a sterile laminar airflow cabinet equipped with a Bunsen-burner, an automatic pipette aid and a waste container.

1. Decant medium to a waste container.
2. Wash cells with PBS to remove medium which could inactivate trypsin.
3. Add 1ml Trypsin/EDTA-solution. Discard the trypsin supernatant after a few seconds.
4. Incubate the flask about 5min at 37°C in the CO₂ incubator.
5. Tap the flask carefully against the palm of your hand until all cells are detached from the flask bottom. Control the procedure under the phase contrast microscope.
6. Resuspend cells in about 3-10ml appropriate medium (depending on cell concentration and the intended further proceeding, e.g. seeding on coverslips and splitting in several culture flasks for freezing of cells).
7. Incubate cells at 37°C and 5% CO₂ in a humidified incubator.

Note: Make sure to wear plastic gloves when working in the sterile airflow cabinet to avoid contamination.

3.1.2 Thawing and freezing of cells

Equipment and solutions

- 1xPBS (Mg²⁺ + Ca²⁺ - free)
- Cryo-tubes
- Culture flask (25cm²)
- Freezing medium (10% DMSO in appropriate complete medium, depending on the cell type)
- Liquid nitrogen tank with racks
- Centrifuge
- Sterile 50ml/15ml Falcon tubes
- Laminar airflow cabinet
- Waterbath
- Isopropanol box
- Trypsin/EDTA

Thawing:

1. Take a stock of frozen cells (10% DMSO in culture media) from the liquid nitrogen tank and let it thaw.
2. Mix cells with 8ml prewarmed medium in a 15ml Falcon tube.
3. Spin it down for 10min at 1000rpm (200g).
4. Discard supernatant and resuspend cells in prewarmed medium and transfer it to the culture flask. Now the rest of freezing medium containing DMSO is removed.

Freezing:

1. Grow cells in a 75 cm² tissue culture flask.
2. Use cells in the logarithmic phase of growth (70-80% confluency). After washing and trypsinizing (see protocol 3.1.1) uspend cells in 20ml full medium and transfer them to a 50ml Falcon tube.
3. Centrifuge for 10min at 1000rpm (200g).
4. Discard supernatant and resuspend pellet in 10ml freezing medium.
5. Aliquot cell suspension into 2ml cryotubes and place them immediately onto ice. Cool down cryotubes at -20°C for a few hours. Subsequently keep them at -80°C in an isopropanol box (up to 3 days possible). Thereafter the cells can be stored in liquid nitrogen.

3.1.3 Slide preparation

Coverslips (15x15mm/20x20mm square or 24x60mm) are washed thoroughly with dH₂O to remove dirt and then stored in 100% technical ethanol. Before use, each coverslip is flamed and then transferred to a dish or well plate respectively.

3.1.4 Seeding cells on coverslips

Equipment and solutions

- Fine tweezers
- Coverslips (15x15mm/20x20mm square or 24x60mm stored in 100% technical ethanol)
- Fixative: formaldehyde 3,7%
- 0,1% PBST
- Tissue culture dishes or 6 well plates
- 1xPBS
- Incubator, 37°C
- Appropriate cell culture medium
- Trypsin/EDTA solution

1. Trypsinize cells from a confluent culture flask under routine conditions and add 10ml medium.
2. Calculate volume of cell suspension needed.
3. Mix well and distribute cells on dishes prepared with cleaned coverslips.
4. Incubate in CO₂ incubator until the cells reached the desired density.
5. Fix cells for 10min in 3,7% formaldehyde.
6. Wash cells in 0,1% PBST. Cells can be stored in PBST for several weeks.

3.2 Replication labeling with BrdU

Labeling of replicating cells with the halogenated thymidine analogue BrdU has been a well-established technique since the early 1980s (Gratzner, 1982). The addition of this modified nucleotide analogue to a growing cell culture leads to an uptake and incorporation. The incubation time depends on the number of cells one wants to catch in S-phase. A minimum time of at least 10min is necessary for pulse labeling of cells during S-phase. Sites of BrdU incorporation are easily detectable by applying immunofluorescence.

The purpose of BrdU-incorporation for the present experiments was to distinguish between S-phase and non S-phase cells (therefore a pulse of 30-45min is sufficient).

Equipment and solutions

- Tweezers
- Coverslips (15x15mm/18x18mm)
- Fixative: formaldehyde 3,7%
- BrdU stock solution (10mM BrdU/PBS)
- 0.5% Triton-X-100 in PBST
- 0.1N HCl
- Blocking solution Bovine Serum Albumine (BSA) 2% and 4% in PBST
- Solution 3 (60mM Tris/ 0.6mM MgCl₂/ 1mM 2-mercaptoethanol) Nick translation buffer is also possible (MgCl₂ is essential)
- DNase I stock solution (2U/μl)
- Primary antibody: mouse anti BrdU (Roche)
- Secondary antibody : sheep anti mouse Cy3 or goat anti mouse alexa488
- Parafilm
- Shaker, Incubator, 37°C
- Slides
- Humidified chamber for incubation with antibodies
- PBST pre-warmed at 37°C
- Counterstain DAPI (0.02μg/ml in PBST) or TO-PRO-3 (1-2μM in PBST)
- Antifade mounting medium (Vectashield)
- Nail polish

Procedure:

1. Grow cells on coverslips (15x15mm/18x18mm) for about 24h until they reach > 50% confluency.
2. Add BrdU to the medium at a final concentration of 10-20μM, and incubate 45min in the CO₂ incubator.
3. Fix for 10min with 3,7% formaldehyde at room temperature (RT).
4. Wash coverslips 2min in 0,1%PBST.
5. Permeabilize 10min with 0,5% Triton in PBST.
6. Wash 2x5min in 0,1% PBST.
7. Incubate in 0,1 N HCl for 10min (check under the microscope if cells remain attached to the slide).
8. Block 10min in 4% BSA in PBST.
9. Prepare solution of primary antibodies together with DNase

incubation mix:

- 20µl Solution 3
- 77µl blocking solution (2% BSA in PBST)
- Histone lysine methylation antibody (final dilution 0,6:250)
- 2µl DNase I (final dilution 1:50)
- 0,5 µl mouse anti BrdU (final dilution 1:200)

10. Apply primary antibody solution: Add one drop mix (50µl for a 15x15mm coverslip) onto a piece of PARAFILM and place the coverslip cell-side down onto the drop. Incubate 1h at 37°C in a humidified chamber.
11. Wash 2x 5min with PBST.
12. Incubate with secondary antibodies 30-40min at 37°C.
Sheep anti-mouse Cy3 (1:500 in blocking solution) or
Goat anti-mouse Alexa488 (1:200 in blocking solution)
13. Wash 2x5min with PBST while shaking.
14. Counterstain and mount cells in antifade medium.

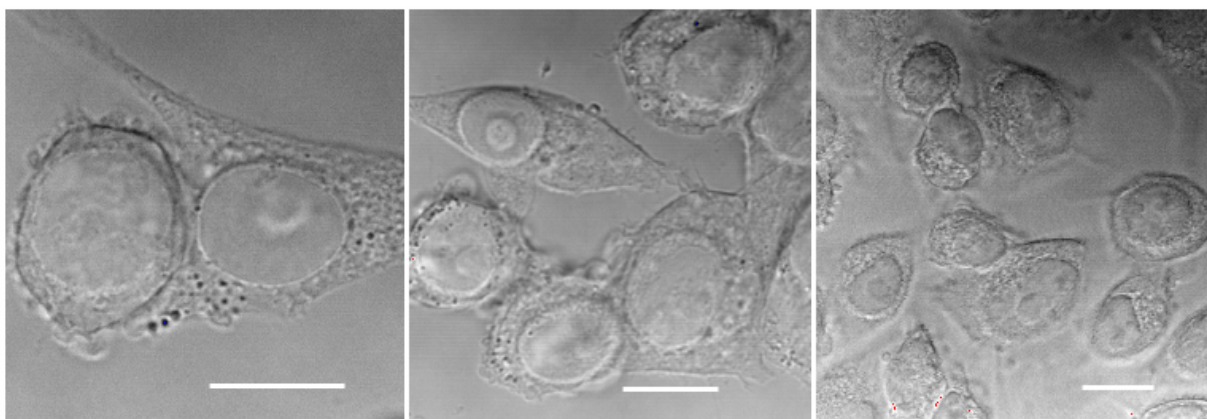


Figure 7

Transmission images of DLD-1 cells with different magnifications recorded at the confocal laser scanning microscope Zeiss LSM 410. Cells were seeded on a coverslip, fixed and embedded with anti-fade medium. These pictures should illustrate to the reader how the cells adhere to the coverslip. Fluorescent signals only provide abstract views of a cell nucleus but no information how the cell as a whole grows in flasks or on coverlips.

These pictures exemplify the nucleus embedded in the cytoplasm. Even nucleoli and cytoplasmatic substructures are visible. Bar indicates 10µm

3.3 Scratch transcription labeling with BrUTP

For the detection of nascent RNA, cells need to be labeled by BrUTP. The scratching procedure with a canula creates “transient holes” by damaging the cell membrane. In contrast to permeabilization with detergents like Triton-X 100, which kills cells within minutes, scratching allows a further cultivation of the cells. The fraction of BrUTP labeled cells

depends on the density of scratches applied on the cell layer. For further information read Schermelleh et al. (Schermelleh et al., 2001).

Equipment and solutions

- Tissue culture dish
- Canula
- Coverslips, Tweezers
- Appropriate cell culture medium, pre-warmed to 37°C
- Labeling solution: 20µM BrUTP (diluted in medium)
- Paper to wipe off
- Phase contrast microscope to control scratching procedure
- Fixative 3,7% formaldehyde

Procedure:

1. Seed cells on small coverslips (15x15mm) and let them grow until they reach 80-90% confluency.
2. Take the coverslip with fine tweezers, wipe off the excess medium and place it into an empty culture dish. Removal of fluid prevents sliding of the coverslip during the subsequent scratching procedure.
3. Add 10µl of the labeling solution onto the cells and distribute it by rotating the dish.
4. Make parallel scratches into the cell layer with the tip of the canula. For best surveillance scratching should be performed under phase contrast microscope. To avoid drying of cells handling should be carried out fast.
5. Add 5ml of pre-warmed medium and incubate further on.
6. After about 10min nascent RNA-should be detectable.
7. Fix cells with 3,7% formaldehyde.
8. Proceed with immunostaining as described in 3.8.

3.4 Polymerase chain reaction (PCR)

The purpose of PCR is to make a huge number of copies of a DNA-sequence. It is commonly used for a variety of tasks (e.g. genetic fingerprinting, in diagnostics and cloning). In this work the method was mainly used to label paint and BAC probes.

3.4.1 DOP-PCR

Chromosome painting probes are usually generated from flow sorted chromosomes and initially amplified by DOP PCR using the universal primer 6MW (Telenius et al., 1992). Primary amplification products can be increased if necessary by few further rounds of DOP-PCRs (up to four amplifications).

6 MW-primer:

Equipment and solutions

- PCR-tubes
- PCR-buffer
- 6 MW-primer (20µM) (sequence CGACTCGAGNNNNNNATGTGG)
- Polyoxyethylene ether W1 (1%)
- dNTPs
- H₂O
- Genomic DNA
- Taq-polymerase

Mastermix:

Concentration

- | | |
|---------------------------------------|-------|
| ➤ 200µl PCR buffer D 5x | 1x |
| ➤ 100µl 6MW-primer (20µM) | 2µM |
| ➤ 100µl Polyoxyethylene ether W1 (1%) | 0,1% |
| ➤ 80µl dNTP-mix (2,5mM each) | 200µM |
| ➤ 490µl H ₂ O | |

970µl (for 20 reactions)

For standard DOP-PCR amplification:

- 48,5µl Mastermix (MM)
- 1µl DNA (DOP amplified chromosome paint DNA)
- 0,5µl Taq-polymerase (5U/µl)

PCR-Program

		Primary	Secondary
Low Stringency (x8)	Initial denaturation	96°C → 3min	96°C → 3min
	Denaturation	94°C → 1min	
	Annealing	30°C → 1,5min	
	Extension	Time ramp 14°C/min 72°C → 2min	
High Stringency (x35)	Denaturation	94°C → 1min	94°C → 1min
	Annealing	56°C → 1min	56°C → 1min
	Extension	72°C → 2min	72°C → 2min
	Final extension	72°C → 5' min	72°C → 5min
	Approximate time	4h15min	3h

- The amplification success can be checked by gel electrophoresis on a 1% agarose gel using standard protocols.
- Probe length and amount can be estimated from the gel by comparing the PCR product with λ HindIII DNA molecular weight marker and by commercial C₀t1-DNA of known concentration.

DOP2, DOP3-PCR

For a primary amplification of BAC-DNA and subsequent label PCR for 3D-FISH experiments a modified DOP-PCR was used employing two different primers in separate amplification reactions described as DOP2 and DOP3 by Fiegler et al. (Fiegler et al., 2003).

The two different DOP2/DOP3 primer recognize different subsets of DNA and thus increase the probe complexity.

The amplification and labeling reactions were performed in separate PCR-setups for each DOP2 and DOP3 primer.

Equipment and solutions

- PCR-tubes
- PCR-buffer
- DOP2-primer sequence: CCGACTCGAGNNNNNNTAGGAG
- DOP3-primer sequence: CCGACTCGAGNNNNNNTTCTAG
- Polyoxyethylene ether W1 (1%)
- dNTPs
- H₂O
- Genomic DNA
- Taq-polymerase

Mastermix:	Concentration
➤ 200µl PCR buffer D 5x	1x
➤ 100µl DOP2 or DOP3-primer (20µM)	2µM
➤ 100µl Polyoxyethylene ether W1 (1%)	0,1%
➤ 80 µl dNTP-mix (2,5mM each)	200µM
➤ 180µl H ₂ O	
<hr/>	
640µl (for 20 reactions)	

For standard DOP-PCR amplification:

- 33 µl Mastermix (MM)
- 1 µl BAC-DNA (50-200ng)
- 15 µl H₂O (Bi-distilled)
- 0,5 µl Taq-polymerase (5U/µl)

PCR-Program

	Initial denaturation	96°C → 3min
Low stringency (only for primary amplification) (10 cycles)	Denaturation	94°C → 1,5min
	Annealing	30°C → 2,5min
	Time ramp 6°C/min extension	72°C → 3min
	Denaturation	94°C → 1min
High stringency (30 cycles)	Annealing	62°C → 1,5min
	Extension	72°C → 2min

	Final extension	94°C → 1min 62°C → 1,5min 72°C → 8min
	Approximate time	4h30min
<p>- The amplification success can be checked by gel electrophoresis on a 1% agarose gel using standard protocols.</p> <p>- Probe length and amount can be estimated from the gel by comparing the PCR product with λ Hind III DNA molecular weight marker and by commercial C₀t1-DNA of known concentration.</p>		

3.4.2 Label-PCR

For labeling of chromosome painting probes (first amplified by DOP-PCR), a label-PCR was used. Probes were generated using a slightly modified amplification program compared to DOP-PCR. One nucleotide is substituted by a labeled analogue and finally incorporated into the new created strand. The paint probe can either be directly labeled with fluorochrome tagged nucleotides (Tamra-dUTP or TexasRed-dUTP) or indirectly by the hapten Biotin or the glycosid Digoxigenin. In the present case Tamra and Texas-Red were used at a final concentration of 20 μ M while its unlabelled counterpart dTTP was present at a concentration of 80 μ M. The other three nucleotides were used at 100 μ M. This PCR based technique has the great advantage to increase the probe output while labeling from small amounts of starting material. This makes it preferably to e.g. nick translation which needs high amounts of DNA at the beginning and is only suitable for very special cases.

The amplification program differs from secondary DOP-PCR in that the number of cycles is reduced to 20 compared to 35, and that the elongation time is decreased to 30 seconds compared to 2 minutes.

DOP-Label-PCR

Nucleotide mix

2mM ACG mix	1mM T
10 μ l A (100mM)	10 μ l T (100mM)
10 μ l C (100mM)	
10 μ l G (100mM)	
Ad 500 μ l H ₂ O	Ad 990 μ l H ₂ O

Mastermix Label-PCR

Cetus II buffer	100 μ l
MgCl ₂ (25mM)	80 μ l
6MW Primer (17 μ M)	100 μ l
AGC-mix (2mM)	50 μ l
T (1mM)	80 μ l
H ₂ O bidest	490 μ l
	Σ 900 μ l

PCR-Program

20 cycles	Initial denaturation	94°C → 3min
	Denaturation	94°C → 1min
	Annealing	56°C → 1min
	Extension	72°C → 0,5min
	Final extension	72°C → 5min
	Approximate time	1h15min

For standard Labeling-PCR amplification:

- 45,5µl Mastermix (MM)
- 1µl paint or BAC-DNA (50-200ng)
- 3µl e.g. Tamra-dUTP
- 0,5µl Taq-polymerase (5U/µl)

DOP2/DOP3 labeling PCR

In my case DOP2/DOP3 labeling PCR was only used to create direct labeled BAC-probes. For directly labeled nucleotides the master-mix was set up first and the fluorescent labeled dUTP is added before starting up the reaction.

Mastermix DOP2/DOP3 Label-PCR

Cetus II buffer	100µl
MgCl ₂ (25mM)	80µl
DOP2 or DOP3-primer (20µM)	100µl
AGC-mix (2mM)	50µl
T (1mM)	80µl
H ₂ O bidest	490µl
	Σ900µl

PCR-Program

20 cycles	Initial denaturation	94°C → 3min
	Denaturation	94°C → 1min
	Annealing	56°C → 1min
	Extension	72°C → 0,5min
	Final extension	72°C → 5min
	Approximate time	1h15min

For standard Labeling-PCR amplification:

- 45,5µl Mastermix (MM)
- 1µl paint or BAC-DNA (50-200ng)
- 3µl e.g. Tamra-dUTP
- 0,5µl Taq-polymerase (5U/µl)

After completion of the DOP2/DOP3 Label-PCR the DOP2 and DOP3 amplification products targeting the same BAC-clone can be merged in one tube since they will be always used together as hybridization probes.

For some experimental approaches it is necessary to generate complex probe sets. In this case BAC-pools were used, consisting of eight single BAC-clones. Therefore a pre-pool of each primary DOP2 and DOP3 amplified BAC-DNA, containing an approximately equal amount of amplified DNA from each BAC, was mixed. For further information read Cremer et al. 2006 (epigenetics protocol database).

3.5 Metaphase preparation

To test the quality and specificity of FISH probes, mitotic chromosomes of human lymphocytes were prepared.

Therefore proliferating cells are required, the bulk of them ideally in mitosis. The lymphocytes extracted from peripheral blood were incubated for about 72h at 37°C and 5%CO₂ in the incubator to allow cells to run through the cell cycle. Application of Colcemid inhibits the spindle apparatus and leads to an arrest of cells in mitosis. The longer Colcemid is present in the medium the more condensed the chromosomes appear. To get a high amount of mitotic cells on the one hand and a satisfying condensation state of chromosomes on the other hand the Colcemid incubation time should not go beyond 40min. A hypotone treatment with 0,56M KCl leads to a swelling of cells which facilitates the bursting of cells when dropped on the slide. The addition of fixative leads to an extraction of chromosomal proteins and increases the accessibility of target DNA for FISH-probes.

Equipment and Solutions

- Centrifuge, incubator, 37°C, shaker
- Freezer -20°C
- Pasteur pipette, slides, metal box
- 15ml/50ml test tubes
- 1xPBS
- 0,01N HCl
- Colcemide (10µg/ml)
- Ethanol 70%, 90%, 100%
- Fixative : Methanol/glacial acetic acid (3:1), ice cold
- Hypotonic solution: 0,56% KCl, 37°C
- Pepsin (320-450u/µl)
- Silicagel with moisture indicator
- Coplin jars
- Trypsin/EDTA (0,02%/0,05%)
- Waterbath at 37°C
- Waterbath at 50°C
- Antifade medium (Vectashiled)

Procedure:

1. Cells are grown until 70%-80% confluency.
2. 8µl colcemide per ml medium is added.
3. Cells are placed back in the CO₂ incubator until mitotic (apoptotic bodies) cells appear. Longer incubation times result in shorter mitotic chromosomes.
4. Trypsinize cells as described in 3.1.1.
5. Cells are transferred to 50ml tubes and centrifuged at 1000rpm for 10min.
6. Supernatant is removed and a few ml of a 37°C 0.56% KCl solution are applied. Mix the suspension carefully with a pasteur pipette and fill up tube to 20ml with hypotonic solution.
7. Cell suspension is incubated for 15-20min at 37°C (Depending on the cell type duration of hypotonic treatment varies).
8. 1ml ice-cold fixative is added and the suspension is thoroughly mixed (Add fixative slowly to avoid agglutination).
9. Cells are centrifuged at 1000rpm for 10min.
10. Supernatant is removed until 10-15ml are left and after resuspending the cells, they are transferred to 15ml test tubes.
11. Cells are centrifuged at 1000rpm for 10min.
12. Supernatant is removed until the taper of the tube. 1ml of ice-cold fixative is slowly added and cells are resuspended very gently. Further 14ml of fixative are added.
13. Cell suspension is incubated 30min at -20°C.
14. For the washing procedure the following steps can be repeated up to 10 or times:
 - Cells are centrifuged for 10min.
 - Supernatant is removed.
 - 15ml ice-cold fixative is applied and cells are thoroughly resuspended.
15. Slides for dropping are incubated for ~30min in absolute ethanol, and cleaned using a dry lint-free cloth. Slides are stored at -20°C and should be completely cooled down before use.

The water bath water level is adjusted in order to obtain an appropriate surface/volume ratio (for further information read (Deng et al., 2003)).
16. Cell suspension (RT) is dropped (10µl/drop) from a height of about 10cm on slides, while the slide is slightly tilted. The slide is put immediately into the metal box for 1min which is fixed at the border of the water bath.
17. A few minutes later, the slide is dried and can be checked for quality of the metaphase spreads and cell concentration using a phase contrast microscope (if necessary, the concentration can be adjusted by either adding fixative or by centrifuging and then removing fixative). To remove residues of cytoplasm finally a pepsinization protocol can be applied.

18. Slides are aged by incubation ON at 37°C.
19. After drying, slides are put in storage boxes together with silica gel pearls, to prevent re-hydration. Slides are stored at -20°C.

Pepsinization (optional)

20. 0.01N HCl is warmed-up at 37°C and slides are placed in coplin jars.
21. Pepsin (320-450u/μl) is diluted 1/2000 in 0.01N HCl (37°C) to a final concentration of 0.2-0.25u/μl.
22. Slides are incubated in pepsin dilution for 10min at 37°C.
23. Slides are washed 3 times for 5min with 1xPBS using a shaker.
24. Preparations are dehydrated by successive incubation in 70% EtOH for 10min, 90% EtOH for 1min and 100% EtOH for 1min.

3.6 2D-FISH

Fluorescence in situ hybridization (FISH) is based on the property of single stranded nucleic acids to bind to their complementary counterparts after denaturation. Target-DNA is detected by labeled probes, predominantly extracted from genomic DNA.

To avoid unspecific binding of probes to highly repetitive sequences (LINEs, SINEs and satellite-DNA) human cot1 DNA is added to the reaction mix. Cot1-DNA contains the same repetitive sequences as the target DNA. These sequences were saturated by cot1-DNA and are no longer a target for the applied probes.

Paint-or BAC-probes were tested (figure 8) on metaphase slides, prepared as described in 3.5.

Labeled probe-DNA is precipitated with 100% pure ethanol and afterwards resuspended in formamide to bring down the denaturation temperature. Dextran sulfate increases the volume thereby retaining the DNA concentration.

Equipment and solutions

- Cot1-DNA
- Ethanol 100%, ice cold
- Formamide
- Mastermix
- Probe
- Speed Vac.
- 0.1x SSC 60°C, 2x SSC 37°C, 4x SSC 37°C
- Shaker, Parafilm
- 2% BSA in 4xSSC 37°C, 4% BSA in 4xSSC 37°C
- Coverslips (12x12mm for 2μl Hybmix, 15x15 for 5μl Hybmix, 24x32mm)
- Fixogum
- Hot Block 76 °C
- Hybridization mix
- Metal box

- Metaphase spreads
- Tweezers, coplin jar
- Fridge
- Water bath 37°C and 80°C
- Appropriate antibodies (if probe is not directly labeled)
- DAPI (0,05µg/ml)
- H₂O dest.
- Nail polish
- Anti-fade medium (Vectashield)

Procedure:

Precipitation of probes:

1. pro reaction mix:
 - probe (dependent on chromosome size or the final hybridization mix volume*)
 - approx. 10µl cot1 DNA
 - optional 2µl blue stain (to visualize the pellet)
 - add 2.5 x reaction-volume of ethanol
 2. Vortex for about 15sec.
 3. Store at -20°C for 30-60min.
 4. Centrifuge 20min at 13000rpm.
 5. Ethanol-supernatant is removed.
 6. Dry pellet in "speed vac" for 5min.
 7. Add ½ vol. formamide and ½ vol. mastermix (dextransulfate).
 8. Put the mix 1h or overnight on the shaker until solution is totally dissolved.
- * recommended final-concentration for paints is 20-30ng/µl (2D-FISH) and 40-60ng/µl (3D-FISH).

Hybridization:

9. Choose appropriate metaphase spreads and mark the area where hybridization is planned.
10. Coat the chosen area with 2µl hybridization mix and put a 12x12mm coverslip on it.
11. Seal the coverslip with fixogum and let it dry for about 20min (fixogum should be flat and totally transparent).
12. Denature preparation (target- and probe-DNA) on the heat block (76°C) for 2min.
13. Put the slides in a metal box and incubate it over night at 37°C in a water bath.

Post-hybridization washings:

14. Remove the fixogum very carefully.
15. Wash slide on the shaker 2x5min with 2xSSC 37°C.
16. Wash slide on the shaker 3x5min with 0.1xSSC 60°C.
17. Equilibrate at RT for a few minutes in 4xSSC.

Detection:

18. Block slide 10-15min in a coplin jar with 4%BSA/4xSSCT at 37°C.
19. Prepare appropriate dilution with (fluorochrome conjugated) antibody in 2%BSA in 4xSSC.
20. Bring about 100µl antibody dilution on the area with metaphases and cover with a 24x32mm coverslip. Incubate for approximately 40min.
21. If you use more than one layer of antibodies wash in-between 2x5min with 2xSSC.

Counterstaining:

22. Stain with DAPI for 5min.
23. Wash slide with distilled water and let it dry by air in the dark.
24. Cover the marked area with an appropriate coverslip and one drop of vectashield.
25. Seal slide with nail polish.

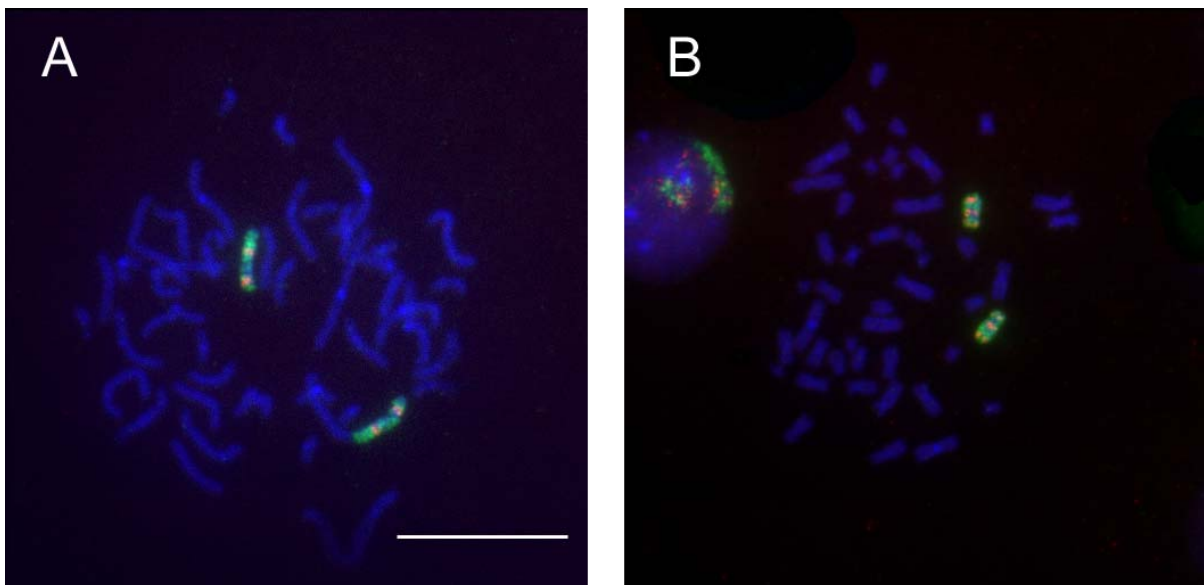


Figure 8

Gene poor (A, red spots) and gene-rich (B, red spots) BACs and a paint of #12 (green) were tested on metaphase spreads of human lymphocytes. Images were recorded by a CCD-camera on an epifluorescent microscope. Bar indicates 5µm

3.7 Peptide competition assay

For antibodies used in the experiments a peptide competition assay was performed to ensure their specificity. Such tests are essential especially in cases where the antibody recognition site is embedded within the same small surrounding amino acid sequence, e.g. the “ARKS” amino acid sequence identical for H3K9 and H3K27.

The respective antibody was diluted to the working solution (approximately 0.04 μ M in 1xPBS/0.01%Tween/2%PBS) and incubated for at least 45min at 37°C with a 100 fold molar excess of the peptide (length of 20 amino acids) carrying this specific histone lysine methylation site. After blocking the slide with nuclei in 4%BSA/1xPBS/0.01%Tween cells were incubated with the pre-incubated antibody for 1h at room temperature, followed by the incubation with the appropriate fluorochrome-labeled second antibodies as described in the chapter “immunostaining” (3.8). Images of staining patterns after the peptide competition assay were delineated in figures 9, 10 and 11.

As a negative control antibodies were incubated with unmodified peptides, similar modified and without peptides, while an antibody against centromeres on the same slide served as a positive control. Peptides for H3K9me3, H3K27me3, H4K20me1, H4K20me3 and unmodified peptides were kindly provided by A.Peters (Basel) at a concentration of 10mM.

Equipment and solutions

- Cells on coverslips (15x15mm)
- Fixative: formaldehyde 37% (dilution 1:10 in PBST)
- 0,5% Triton X-100
- 4% BSA in PBST
- Top cover of a 6 well plate
- Parafilm
- Metal box
- Water bath 37°C
- Antibodies
- Antibody specific and unspecific peptides
- DAPI
- Nail polish
- Tweezers
- Antifade medium (Vectashield)

Calculation of the dilution for the antibody and peptide solutions

General information:

Antibody concentration: 3mg/ml

Molarity Peptide: 10mM

1Mol antibody is equivalent to ~150kg (150kDa)

Calculate the working solution out of your Ab-concentration (dilution 1:500)

3mg/ml = 3000 μ g/ml \rightarrow 6 μ g/ml \rightarrow 6mg/l (molarity working solution)

1:500

$$150 \times 10^{-6} \text{ mg} = 1 \text{ Mol}$$

$$6 \text{ mg} = x \text{ Mol} \rightarrow x = 6 \text{ mg} \times 1 / 150 \times 10^{-6} \text{ mg} = 4 \times 10^{-8} \text{ M} = 0,04 \mu\text{M}$$

The antibody working solution is a 0,04 μM solution. The peptide should be in a 100 fold excess (100 molecules peptide for 1 molecule antibody) which means **4 μM** .

Molarity peptide: 10mM = 10000 μM \rightarrow 1:10 dilution in dest. water \rightarrow 1000 μM

1 μl of this dilution in 200 μl of a 1:500 antibody dilution (2% BSA in PBST) to achieve **5 μM** (to work exactly give 1 μl peptide to 240 μl of a 1:500 antibody dilution).

1. Disseminate cells and let them grow to a confluence of about 70%.
2. Fix cells with 3,7% FA for 10 min.
3. Permeabilize cells in 0,5% Triton for 10min.
4. Block cells in 4% BSA in PBST for 10min.
5. Make a mixture of the antibody and the peptide you want to test and incubate it in the water bath at 37°C for 45min.

Make sure that incubation time is up when the 10min blocking time (step 4.) are over.

6. After peptide/antibody incubation incubate first antibody 1h in the water bath at 37°C.
Add one drop mix (50 μl for a 15x15mm coverslip) onto a piece of PARAFILM and place the coverslip cell-side down onto the drop. Incubate 1h at 37°C in a humidified chamber.
7. Wash 2x10min in PBST.
8. Second antibody 40min in the water bath at 37°C.
9. Wash 2x10min in PBST.
10. Counterstain with DAPI and TO-PRO-3 for 5min.

Note:

If the antibody is specific for the applied peptide it will bind to the peptide and one won't get a signal in the nucleus. Make a positive control for example centromeres on the same slide using another color for detection. To extend the specificity test make cross-tests, for example a H4K20me3 ab. against a peptide for monomethylated H4K20. Last but not least test ab's against unmodified peptides.

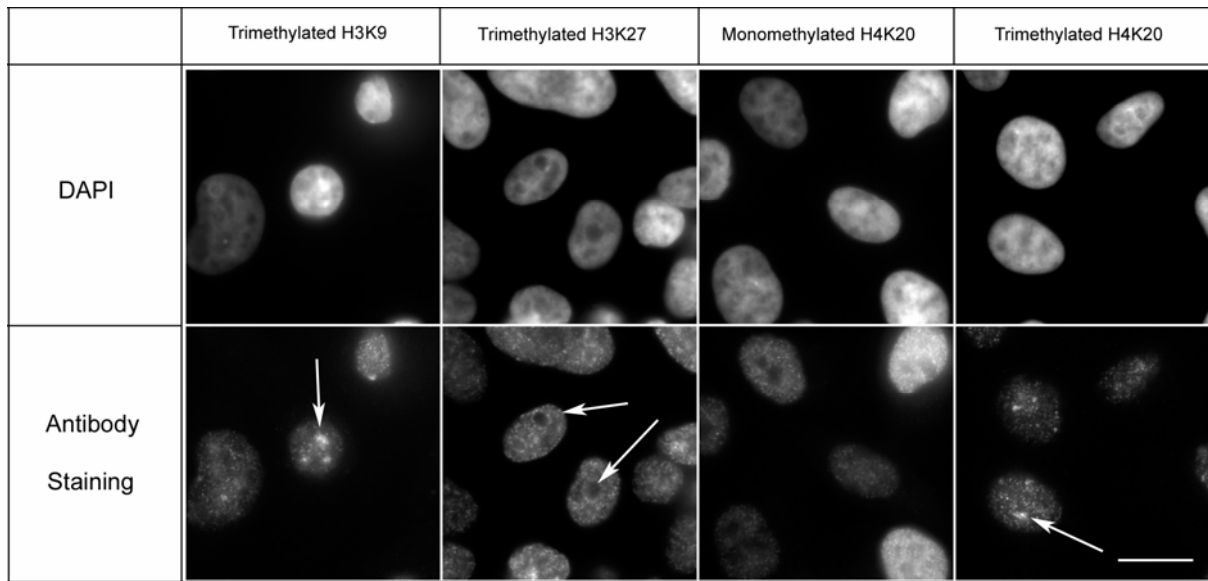


Figure 9

“Normal” antibody patterns without peptide pre-incubation in MCF-7 cells visualized by epifluorescence widefield microscopy. Bar indicates 10µm

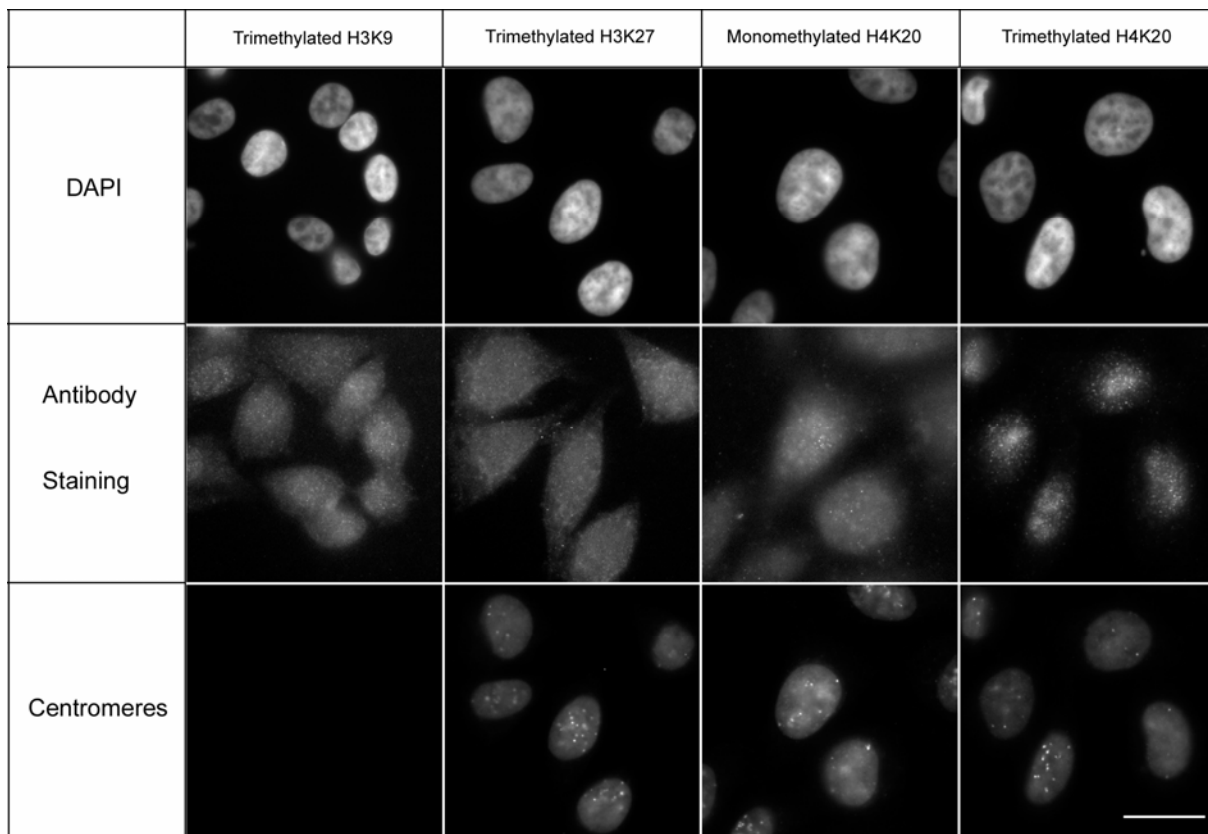


Figure 10

After incubation of antibodies with their specific peptides all antibody patterns disappear, thereby indicating their high specificity. Centromere staining was successfully used as positive control. Bar indicates 10µm

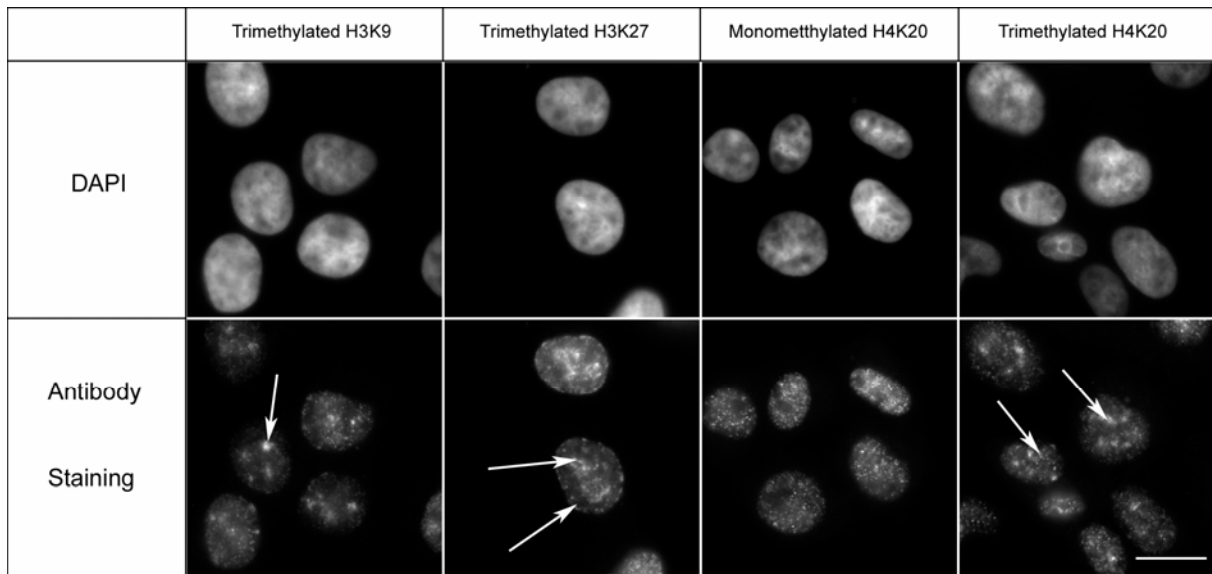


Figure 11

To test the high specificity of these anti-methylation antibodies emphatically, the antibodies were incubated with peptides that are different in only two methyl-groups (H3K9me3 was incubated with the H3K9me1 against which the monomethylated antibody was raised, H3K27me3 with an unmodified peptide, H4K20me1 with a H4K20me3 peptide and vice versa). As shown by white arrows typical antibody patterns (compare figure 9) can be found in all attempts. These findings demonstrate that the histone lysine antibodies can even distinguish between different methylation states. Bar indicates 10µm

3.8 Immunostaining

Immunostaining was performed in experiments when co-localization of histone lysine methylation sites, centromeres and nascent RNA was investigated. Detection schemes usually consisted of two layers, with a primary antigen-specific antibody as a first layer and a secondary antibody, which was specific for immunoglobulins from the species, the first antibody was generated in. The latter was conjugated with a fluorochrome allowing visualization by epifluorescence or confocal microscopy. Nuclei were counterstained with DAPI and additionally with the DNA binding dye TO-PRO®-3, since the utilized confocal microscopes were not equipped with an appropriate UV-laser. The latter can be excited by a 633nm laser line and emits light in the infrared spectrum.

Equipment and solutions

- Cells on coverslips
- Tweezers
- Fixative: formaldehyde 3,7%
- 0,5% Triton X-100
- 2% BSA in PBST, 4% BSA in PBST
- Primary antibodies, secondary antibodies
- 0.01% PBST
- Metal box
- Parafilm, slide
- Top-cover of a 6-well plate

- DAPI or TO-PRO-3
- Antifade medium (Vectashield)
- Nail polish

1. Seed cells on coverslips.
2. Let cells grow until they are about 60-70% confluent.
3. Fix cells with 3,7% FA 10min.
4. Permeabilize cells with 0.5% Triton for 15min.
5. Block with 4% BSA in PBST.
6. 1.Ab (rabbit anti lysine methylation dilution: 0.6:250) 1h at 37°C in the water bath. Add one drop mix (50µl for a 15x15mm coverslip) onto a piece of PARAFILM and place the coverslip cell-side down onto the drop. Incubate 1h at 37°C in a humidified chamber.
7. Wash 2x5min in PBST.
8. 2.Ab (e.g goat anti rabbit-cy3) 45min at 37°C in the water bath.
9. Wash 2x5min in PBST.
10. Counterstaining with DAPI (1:100 in PBS) for 3 min.
11. Put vectashield on your coverslip.
12. Seal coverslip with nail polish.

Note: The antibody incubation was made on the top of a 6-well plate which contained a stripe of parafilm. A drop of antibody solution (50µl for a 15x15mm coverslip) was pipetted on the parafilm and the coverslip placed on it.

3.9 Sequential antibody labeling

Sequential antibody labeling is required when two antibodies which are both raised in the same species (in this case rabbit) are combined in an experiment. For a complete blocking of the first antibody an incubation step with an unconjugated Fab-fragment is required.

Equipment and solutions

- Cells on coverslips (15x15mm)
- Fixative: formaldehyde 3,7%
- PBST 0,01 Tween
- 0,5% Triton X-100
- Tweezers
- 2% BSA in PBST, 4% BSA in PBST
- Metal box
- Parafilm, slide
- Top-cover of a 6-well platte
- Primary antibodies: rabbit anti-histone modification
- Secondary antibody: goat anti rabbit Cy3 Fab, goat anti human-FITC
- Goat anti rabbit Fab non-conjugated
- DAPI (stock solution 5µg/ml, final working solution 0,05µg/ml)
- Counterstain alternative: TO-PRO-3 (stock solution 1mM, final working solution 1µM)
- Nail polish
- Antifade medium (Vectashield)

1. Grow cells on coverslips (50-70% confluent).
2. Fix cells with 3,7% FA.
3. Permeabilize cells with 0.5% Triton X-100 for 10min.
4. Block with 4% BSA in PBST 10min.
5. 1.ab layer: rabbit anti histone methylation (dilution: 1:500)
1h at 37°C (if the result is not satisfying try over night). Add one drop mix (50µl for a 15x15mm coverslip) onto a piece of parafilm and place the coverslip cell-side down onto the drop. Incubate 1h at 37°C in a humidified chamber.
6. Wash 2x10min in PBST.
7. 2.ab. layer: goat anti rabbit Cy3 Fab (dilution 1:100) incubate 45min at 37°C.
8. Wash 2x10min in PBST.
9. 3. ab. layer: goat anti rabbit Fab non conjugated (to block the rest of the free binding sites, best dilution 1:500-1:800) 45min at 37°C.
10. Wash 2x10min in PBST.
11. 4. ab layer: rabbit anti histone (1:500) 45min at 37°C.
12. Wash 2x10min in PBST.
13. 5. ab layer: h.c.a. goat anti human FITC, dilute 1:200.
14. Wash 2x10min in PBST.
15. Counterstain with DAPI 5min.
16. Put coverslip on a slide with Vectashield and seal with nail polish.

3.10 3D-Immuno-FISH

The combination of FISH with the visualization of proteins by immunofluorescence is critical because antigenic or fluorescent epitopes can be destroyed by heat denaturation and HCl treatment required for FISH.

Since these essential steps of the FISH procedure are indispensable the focus had to be on the immuno-part of the protocol. One approach to achieve good immuno-FISH results was to change the order of single steps. Another option was to modify the antibody detection system. Different conceivable combinations and modifications, that were tested until a working protocol was found, are schematically listed in the flow chart (table2).

In the following, the most important steps of the finally used protocol are explained. First antibody detection was performed at the beginning of the experiment instead at the end of the experiment. However this change in the experimental order solely was not sufficient to achieve better immunostaining results. In the next step, instead of using a directly labeled secondary antibody for detection of histone lysine methylation sites, the Biotin/Avidin-system was used, since it is widely accepted as very stable due to its high binding affinity (Korpela,

1984). Furthermore it was reported to be thermal stable which is another advantage for immuno-FISH (Gonzalez et al., 1999; Wei and Wright, 1964). This approach yielded an improvement of signal quality at least by visual inspection but an optimal solution was not found until an additional fixation step with 1% formaldehyde was added to the protocol (post fixation step). This step probably enhances the stability of the primary (lysine methylation antibody)/secondary antibody (Biotin) complex and is a important feature of the protocol. It is essential for achieving the best results that the correct order as delineated in table 2 right column is abided.

<p>Pretreatment (Glycerol, HCl, Formamide, pepsinization)</p> <p>↓</p> <p>FISH (Hybridization of probes)</p> <p>↓</p> <p>Immunofluorescence (histone lysine antibodies) + FISH detection</p> <p>↓</p> <p>antibody pattern hardly to identify, bad signal</p>	<p>Primary histone lysine antibody</p> <p>↓</p> <p>(direct labelling or biotinylated Ab)</p> <p>↓</p> <p>Pretreatment (Glycerol, HCl, Formamide, pepsinization)</p> <p>↓</p> <p>FISH (Hybridization of probes)</p> <p>↓</p> <p>detection of FISH-probes and detection of biotinylated antibody with avidin</p> <p>↓</p> <p>good signal intensity, staining pattern seemed to be somehow affected by FISH treatment</p>	<p>Primary histone lysine antibody</p> <p>↓</p> <p>biotinylated Ab (important)</p> <p>↓</p> <p>post fixation 1% FA/PBST (essential step)</p> <p>↓</p> <p>Pretreatment (Glycerol, HCl, Formamide, pepsinization)</p> <p>↓</p> <p>FISH (Hybridization of probes)</p> <p>↓</p> <p>FISH detection and detection of biotinylated Ab</p> <p>↓</p> <p>best results, no difference to cells without denaturation and HCl treatment was observed by visual inspection</p>
--	--	--

Table 2

Flow chart of different approaches for a new immuno-FISH protocol. The protocol which turned out to perform best is delineated in the right column.

A comparison of morphology of nuclei and staining pattern after immuno-FISH could only be made with those achieved after IF. Incubation with the primary antibody at the beginning of the protocol and the detection of the biotinylated secondary antibody at the end makes it impossible to check whether changes occur during application of the immuno-FISH protocol.

Equipment and solutions

- Cells on coverslips
- Fixative: formaldehyde 3,7%
- Fixative: formaldehyde 1% for post-fixation
- 4% BSA in 0,01% PBST
- 2% BSA in 0,01% PBST
- 0,5% Triton X-100
- Antibodies:
 - rabbit anti histone lysine methylation
 - goat anti rabbit-Biotin
 - Streptavidin Cy5
 - sheep anti Dig-FITC
 - goat anti Streptavidin-Bio
- Glycerol
- Tweezers, slides
- Cot1-DNA
- Centrifuge (1300rpm)
- Coverslips (15x15mm)
- Vacuum centrifuge, metal box
- Ethanol
- Labeled DNA (40-60ng/μl)
- X-paint probes (Dig-labeled)
- Directly labeled BAC probes (Tamra and Texas Red)
- 0.1xSSC 60°C, 2xSSC 37°C, 4xSSC 37°C
- 50% formamide/2xSSC
- Liquid nitrogen
- 1N HCl
- Shaker, Water bath 37°C
- Heat block 76°C
- Pepsin (49,5ml H₂O + 0,5ml 1N HCl + 10μl Pepsin)
- PBS/MgCl₂ (95ml 1xPBS/5ml 1M MgCl₂)
- 2%BSA/4xSSC, 4%BSA/4xSSC
- Nail polish
- Antifade medium (Vectashield)
- DAPI (stock solution 5μg/ml, final working solution 0,05μg/ml)

Fixation

1. Cultivate cells on coverslips until they are about 50% confluent.
2. Fix cells in 3.7% FA for 10min.
3. Permeabilize cells in 0.5% Triton for 15min.
4. Block 10min in 4% BSA in PBST.
5. 1.Ab (rabbit anti histone methylation, dilution 0.6:250 in 2% BSA in PBST) 1h at 37°C in the water bath. Add one drop mix (50μl for a 15x15mm coverslip) onto a

piece of PARAFILM and place the coverslip cell-side down onto the drop. Incubate 1h at 37°C in a humidified chamber.

6. Wash 2x5min in PBST.
7. 2.Ab (goat anti rabbit-**Biotin**, dilution 1:100 in 2%BSA in PBST) 45min at 37°C in the water bath.
8. Wash 2x5min in PBST.
9. **Post-fixation 10min in 1% FA.**
10. Incubate with 0.1N HCl for 10min (depending on cell type: in cases it might be better to incubate 6-7min). Watch cells under the microscope to be sure that cells remain attached to the coverslip.
11. Permeabilize again with 0.5% Triton for 5min.
12. Incubate in 20% Glycerol for 45 min.
13. Nitrogen step:
Take coverslips out of the glycerol and freeze it for a few seconds in liquid nitrogen until you hear a snap. Let it thaw, dip it shortly in glycerol and freeze it again. Repeat these steps 4-5 times.
14. Wash in 2xSSC for 5min.
15. Store coverslips in 50% FA/2xSSC for at least 24h, better 48h.
16. Wash 8min in 2xSSC.
17. Change to PBST.

Pepsin treatment

18. Incubate 5min in pepsin (49,5ml H₂O + 0,5ml 1N HCl + 10µl Pepsin).
19. 2x5min in PBS/MgCl₂ (95ml 1xPBS/5ml 1M MgCl₂).
20. Post-fixation 3min in 1% FA.
21. Wash 3min in 1xPBS.
22. Wash 8min in 2xSSC.
23. Store 2h in 50% FA/2xSSC.

Hybridization

24. Put hybmix on your slide place the coverslip with cells on it and seal it with fixogum.
25. Wait about 20min until the fixogum is dried completely (flat and transparent).
26. Denaturation at 76°C on the hot block.
27. Incubation for 48h at 37°C in the water bath. Remove coverlips very carefully under fluid (2xSSC) to avoid cell damage.

Post hybridization washings and detection

28. Wash 3x3min in 2xSSC (from now on take care that coverslips are not exposed to any kind of light sources).
29. Wash 4x3min in 0.1xSSC.
30. 4xSSC for 1min.
31. Block 10min in 4% BSA/4xSSC
32. sheep anti Dig-FITC (dilution 1:100 in 2% BSA/4xSSC)
45min in a wet chamber at 37°C in the water bath.
33. Wash 2x5min in 4xSSC
34. Use additional Ab.layers for FISH-detection if necessary (to enhance signals).
35. Change to 1xPBS (because of the Streptavidin ab.).
36. Detection of immunostaining:
(**Strept**)avidin Cy5 (dilution 1:200 in 2%BSA in PBST).
45min in a wet chamber at 37°C in the water bath.
36. DAPI-counterstain in PBS (1:100).
37. Stain with DAPI for 3min.
38. Put vectashield on your slide and seal with nail polish.

Note:

- A test revealed that Streptavidin Cy5 worked perfectly together with the sheep anti Dig ab. in 2% BSA/2xSSC.
- To get a higher Cy5 signal intensity:
goat anti Streptavidin-Biotin (dilution 1:200) detect this ab. with Streptavidin Cy5 as described above.
- The Biotin-antibody detection should be always carried out at the end, otherwise the immunostaining gets clearly worse.

3.11 Chaetocin treatment

Chaetocin was recently described as a specific inhibitor of the histone methyltransferase Suv39h1 (Greiner et al., 2005). Treatment of cells with Chaetocin was performed to study its effect for spatial distribution of SUV39h1 mediated H3K9me3 methylation.

3.11.1 Calculation of the molarity out of the Chaetocin concentration

Concentration of the stock solution: 5mg/ml = 5g/l

MW (has to be known): 697

→ 1Mol = 697g

1Mol = 697g/l xMol = 5g/l xMol = 1Mol x 5g/l / 697g/l = 0,00717M = 7,17mM

Consider dilution factor! It might be appropriate to make an intermediate dilution step.

3.11.2 Experimental Chaetocin setup

Equipment and solutions

- Cells on coverslips
- Incubator, 37°C
- Fixative: formaldehyde 3,7%
- 6 or 12 well plate
- Appropriate medium
- Chaetocin (stock solution: 5mg/ml , working solution: 0,01µM)
- Medium (see appendix)
- All further equipment and solutions already listed under 3.9

1. Seed cells in a 6 or 12 well plate, on coverslips, with about 40-50% confluence.
2. Put cells in the incubator at 37°C.
2. Let cells attach to coverslip for about 2h.
3. Add Chaetocin in the appropriate dilution (Always think of a negative control e.g. let cells grow in DMSO. Use a high Chaetocin dilution as a positive control).
4. Fix cells after 3 days with 3,7% FA.
5. Proceed with immunostaining as described in 3.8.

Note: -The inhibition potency of Suv39H1 generated by Chaetocin treatment is negatively correlated to the density of the seeded cells.

-Dilute Chaetocin in the same medium as the cells grow.

3.12 Microscopy

3.12.1 Transmitted light microscopy

Transmitted light microscopy was used to

- a) monitor the status of cultured cells.
- b) control the procedure of scratch transcription labeling.

Transmitted light microscopy can provide valuable information about the state of cells and at higher magnification even of cellular substructures. The used microscope was the Axiovert 25C from Zeiss. It is very easy to handle and no special cell treatment of any kind (e.g. fluorescence staining) is necessary to assess cells. Due to its low light excitation the cells in culture flasks are not at risk of any damage.

3.12.2 Epifluorescence microscopy

Because of its selectivity (only objects of interest in an otherwise black background are visible), fluorescence imaging has become the mainstay of microscopy in many biological disciplines. For further information read the review by Lichtman and Conchello (Lichtman and Conchello, 2005).

Epifluorescent microscopy was used in this work to

- a) check success and quality of FISH and immunofluorescent experiments.
- b) take widefield pictures for documentation of experiments with a CCD-camera.

For all experiments a Zeiss Axiophot 2 microscope was used, equipped with a Coolview CCD camera with a spectral response of 400-900nm and a CCD chip resolution of 753x576 pixels.

3.12.3 Confocal-laser-scanning microscopy

Compared to conventional epifluorescence microscopy confocal microscopy shows a much better axial resolution. The reason is that instead of using widefield illumination, focused laser beams scan the specimen exciting only small areas at a time. In combination with using a pinhole in front of the detection device this step by step illumination excites and detects much less fluorescent entities that are not within the focus plane, resulting in highly decreased out of focus blur (for details on confocal microscopy and applications see (Conchello and Lichtman, 2005; Pawley, 2006).

In the present work, confocal-laser-scanning-microscopy was used for image recording concerning all quantitative evaluations.

Although confocal microscopy has a lot of advantages, it also suffers from limitations. A detraction is the high amount of excitation light required to produce a confocal image. So at least in some cases the excitation light which is necessary to obtain satisfactory 3D images bleaches the dye or fluorochrome. Although confocal images are affected to a much lesser extent by out-of-focus light than wide-field images they are still hindered by out-of-focus light. And it is very hard, especially for complex structures or patterns, to set the appropriate threshold. To facilitate this user based thresholding all 3D confocal data set were deconvolved before applying evaluation of any kind.

The following tables contain some typical parameters that were used for the Zeiss LSM 410 and the Leica SP2 microscopes (table 3 and 4).

Objective	63x plan-apochromat 1,4x oil
Voxel size (x,y,z)	66x66x200nm and 88x88x200nm
Image size	256x256

Average	4
Color depth	8 bit

Table 3 Parameters for Zeiss 410 LSM

Objective	HCX PL APO 63x1,4 oil
Voxel size (x,y,z)	60nmx60nmx160nm
Image size	512x512
Average	4
Color depth	8 bit
Pinhole	0,99

Table 4 Parameters for Leica SP2

3.13 Deconvolution

3.13.1 Deconvolution in general

The image formed by a conventional widefield fluorescence microscope contains light from throughout the specimen. This out-of-focus light confounds detection of what is actually present in the focal plane. Because this out-of-focus haze contributes significantly to background its removal is the task of 3D microscopy, thereby improving image contrast. This problem is partly solved in confocal microscopy by positioning a pinhole in front of the detector that most of the light passing through the pinhole derives from the focal plane but not from surrounding regions.

In this thesis the majority of pictures was produced by confocal microscopy. Stacks of single optical light sections comprising the complete 3D object per channel were recorded. Images are built up as a matrix of pixels in grey values from 0-255 in 8-bit pictures (indicating the depth of colour). All evaluation methods used required a threshold setting to separate true signal from background blur. Despite the fact that automated thresholding algorithms have been developed, in the case of complex staining patterns (e.g. lysine methylation) investigated in this work, setting of thresholds by the user was unavoidable. This means that the person who sets thresholds needs a lot of experience with the respective antibodies and their patterns to distinguish between true signals and disturbing background, especially if images exhibit a low signal to noise ratio.

In optics, the term “deconvolution” is used to refer to the process of reversing the optical distortion that takes place in a microscope to create clearer images. One gets the best picture by the assumption that a theoretical point source of light is in an optically perfect instrument, convolved with a point spread function (PSF), that is, a mathematical function that describes the distortion in terms of the pathway this point source takes through the

instrument. Usually each point source contributes to a small area of fuzziness to the final image. If the appropriate PSF can be determined, it is only a matter of computing its complementary function and convolving the acquired image with it, resulting in the original, undistorted image. With the introduction of deconvolution techniques (Shaw and Rawlins, 1991) and their incorporation into commercially available software modules a powerful tool for image restoration emerged.

But unfortunately this is only theory, in practice it is impossible to find the true PSF and even a good approximation to it is difficult. Real optics may have different PSFs at different focal and spatial locations. Finally the accuracy of the approximation of the PSF will dictate the result.

Deconvolution provides a similar exclusion of out of focus blur as confocal microscopy but the mechanism is not based on technical regulation (pinhole) but mathematical processing by a computer.

Using co-localization analysis, it was shown by different groups that deconvolution enhances the image quality also of confocal images (Landmann, 2002; McNally et al., 1999). The combination of confocal microscopy and deconvolution improves resolution beyond what is generally attainable by either technique alone. Thereby the benefit is a lower noise level and a higher contrast in confocal images which makes it for the user much easier to set thresholds.

3.13.2 Deconvolution setup

Artifacts in deconvolution analysis

The sources of image degradation can be divided into four independent phenomena: noise, scatter, glare and blur. The task of deconvolution is in principle to remove the out-of-focus blur from images.

After application of a chosen deconvolution algorithm (maximum likelihood estimation implemented in Huygens software), the restored images can show apparent aberrations such as striping and ringing. Artifacts can also occur when processing parameters (pinhole, quality criterion and number of iterations) are not configured correctly for the raw image.

The height of the background level crucially influences co-localization analysis often used in this thesis and impairs image quality in at least two respects. First it affects resolution, as the high frequency image components are generally of less intensity than the low frequency ones. Second low intensity signals are lost and image details appear obscure. This background noise is caused primarily by three components: electronic offset, stray light and blur from a specifically labelled part of the object (Sheppard and Török, 1997).

But often they are not caused by computation, but by histology, optical misalignment or electronic noise. To find the source of an artefact the first step should always be a comparison of the deconvolved and the raw image.

The point spread function

The concept of a three-dimensional PSF is of fundamental importance to understand the model of blur and finally pave a way to avoid imaging artifacts. It is based on an infinitely small point source of light originating in the specimen space. Because in the microscope only a fraction of the light emitted by this point is collected, it cannot focus the light into a perfect three-dimensional image of this point. Instead the point appears widened and spread into a three-dimensional diffraction pattern. Depending upon microscope system (transmitted light, widefield and confocal), the PSF has a different and unique shape and contour.

The point spread function can be defined either theoretically by utilizing a mathematical model of diffraction, or empirically by acquiring a three dimensional image of a fluorescent bead. The latter option was chosen for our approach. A theoretical point spread function generally has axial and radial symmetry. The PSF is symmetric above and below the x-y plane (axial symmetry) and rotationally about the z-axis (radial symmetry). But a PSF based on fluorescent bead measurement can deviate significantly from symmetry (figure 12). The deviation is in this case due to irregularities or misalignments in any components such as mirrors, beamsplitters, filters, tube lenses and apertures. That means the higher the quality of the optical components the closer the empirical PSF comes to ideal symmetrical shape.

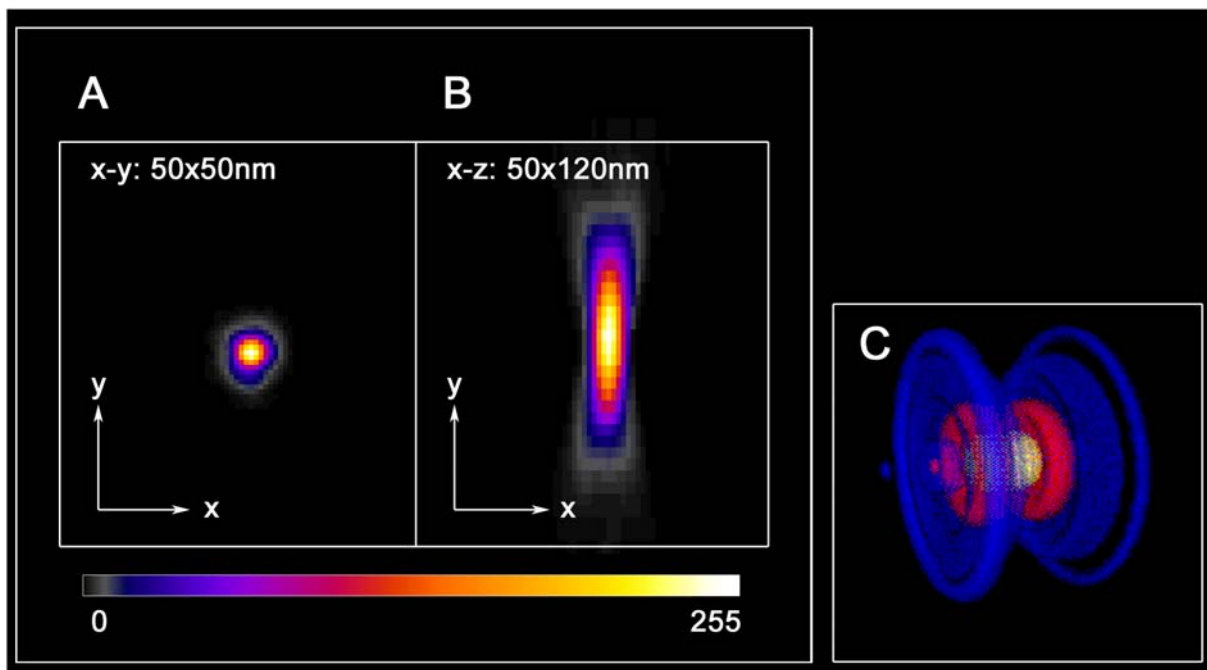


Figure 12 Pictures of PSFs by courtesy of Heiner Albiez
A and **B** PSFs of a fluorescent bead measured at our confocal Leica SP2 microscope. Diffraction rings (in **A**) are visible from top view, displayed by different gray values (different colours).

C Three dimensional contour of the point spread function of a high NA microscope objective (taken from wwwmc.bio.uva.nl/UploadImages)

Statistical Iterative Algorithms

The family of iterative algorithms uses probabilistic error criteria borrowed from statistical theory. The Huygens deconvolution software from SVI (<http://www.svi.nl/>) uses the maximum likelihood estimation (MLE). Statistical algorithms are more time consuming than classical methods and can take significantly longer to reach a solution. But they restore images to a higher degree and produce better results on noise images.

Despite many advantages of deconvolution mentioned in the text above, a not small number of experts still doubts the power of this method and the debate about artefacts and true restoration of images goes to the next round (Markham and Conchello, 2001).

Measuring PSFs

About 10 fluorescent nano-spheres (Huygens decides which beads can be used, so make sure to have enough beads for each colour) with 175nm (PS-speck Microscope Point-Source-Kit, Molecular Probes) were measured for each laser line. The voxel size xyz should be 50nmx50nmx120nm, at least less than xy-70nm and less than 150nm in z. Use average mode 4x and try to scan at least 40-50 sections to get all the diffraction rings. Therefore the beads were seeded on coverslips separately, dried and embedded in Vectashield. Directed by the “Huygens Essential User Guide” (<http://www.svi.nl/download/guides.php>) all parameters required for PSF distillation and for deconvolution procedure were adjusted (Table 5). For further information read Albiez et al. 2007 (in prep.) and (Wallace and Orr-Weaver, 2005).

General parameters for Huygens	
Numerical aperture of the used objectives (63xoil objective)	1.4
Lens medium (immersion oil) refractive index	1.518
Medium refractive index (Embedding medium-Vectashield)	1.457
Voxel size (x-y-z)	
Zeiss LSM 410	50x50x200nm
Leica SP2	60x60x150nm
Excitation wavelength of the used lasers	
Zeiss LSM 410	488nm, 543nm, 633nm
Leica SP2	405nm, 488nm, 561nm, 633nm
Emission wavelength	
According to the used fluorochromes	DAPI:461nm, FITC:519nm Alexa488:520nm, Cy3: 565nm,

According to the signatures of the used nano-spheres for PSF generation	Cy5:670nm, To-Pro-3: 661nm “blue”:440nm, “green”: 515nm, “orange”: 560nm, “far-red”: 660nm
Size of backprojekted pinhole according to used laser wavelength and microscope	
Zeiss LSM 410	315nm (for 488nm-, 543nm- and 633nm-laser line)
Leica SP2	176nm (for 405nm laser line), 213nm (for 488nm laser line), 244nm (for 561nm laser line) and 276nm (for 633nm laser line)
Excitation photon count	1
Bleaching correction	off
Iteration mode	High quality

Table 5 General parameters for Huygens

Important steps for application of deconvolution

Signal to noise ratio

This value is judged on the image quality and can adopt values from <10 (=noisy), 10<20 (=moderate noise) and >20 (=low noise). The data sets, investigated in this study were all set to 30.

Background estimation

Background values were always adopted by Huygens estimation on the input raw images with the recommended “lowest-value”-tool

Maximum iterations

Deconvolution by the iterative Maximum-Likelihood Estimation algorithm is a in principal endless precedure. A stopping criterion has to be assigned to stop the calculation and to avoid obvious artifacts by deconvolution. Based on experience and on comparison between raw data and deconvoluted images we did not apply more than 10 iterations. Ahigh number of iterations can produce artifacts. These are probably caused by over- or underestimations of some of the values of deconvolution parameters (Conchello and Lichtman, 2005; Markham and Conchello, 2001).

Quality threshold

Another quality characteristic is the quality level at which deconvolution is stopped. As soon as the quality between the previous image and the subsequent one is not more increasing as predetermined in this criterion, the whole procedure stops. The quality threshold was set in all cases at 0.1.

3.13.3 The impact of deconvolution on image restoration

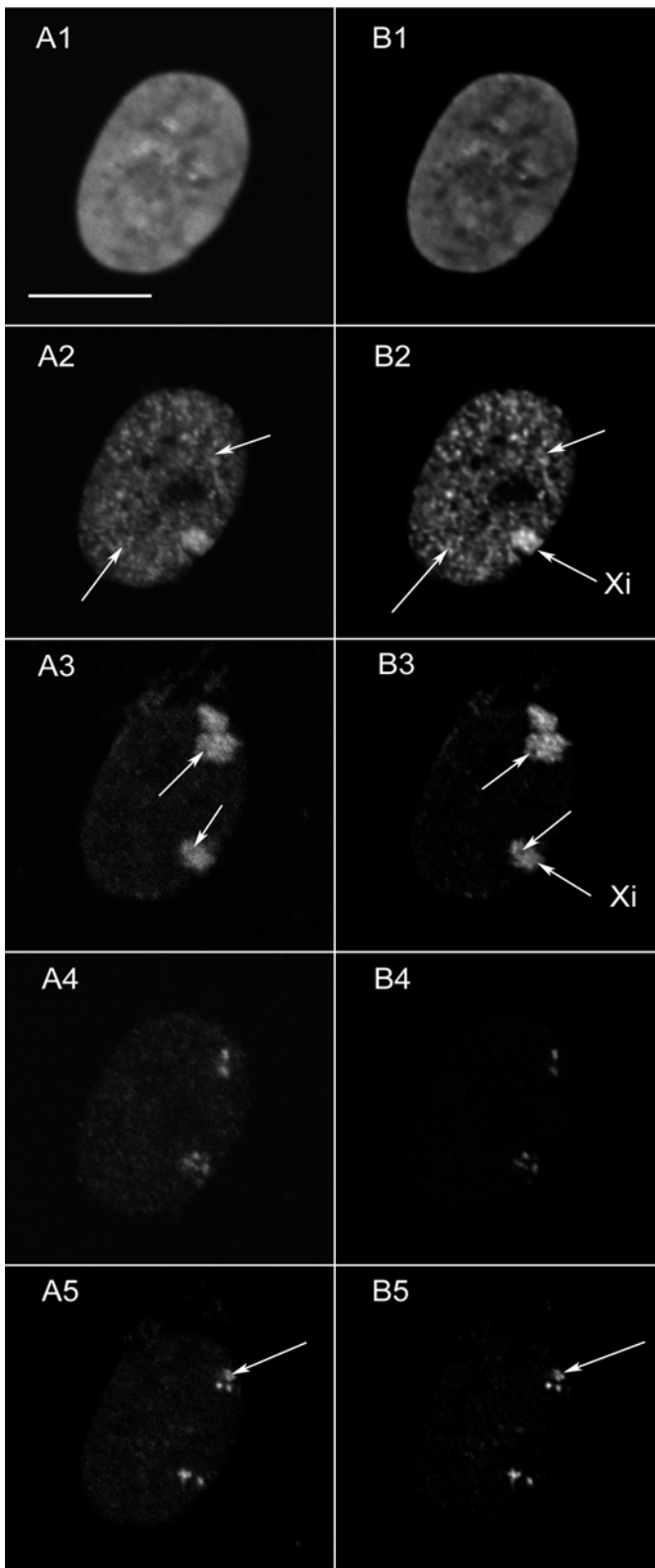


Figure 13

Single sections of a 5-colour immuno-FISH experiment before (column **A1-A5**) and after deconvolution (column **B1-B5**):

A1,B1 shows DAPI-counterstain,

A2,B2 H3K27me3 antibody staining, which marks the inactive X but displays also a foci like pattern throughout the nucleus.

A3,B3 shows X-chromosome paints

The active X-chromosome appears much more bigger and decondensed than the inactive X-chromosome.

Examples for distinct changes in the patterns after deconvolution are highlighted by white arrows.

After deconvolution sub-structures emerge (holes in the paints, arrows in **A3,B3**)

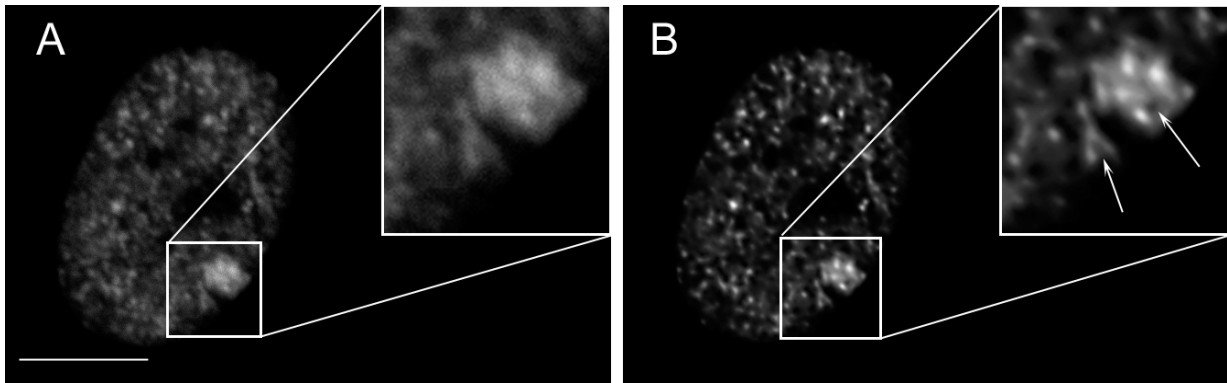
A4 and **B4** show BACs with weakly expressed genes

A5 and **B5** show BACs with mid-expressed genes

The impact of deconvolution is clearly visible in all channels. Background blur and noise are reduced to a minimum and contrast is enhanced thereby highlighting smaller structures that can be seen hardly in raw images.

Substructures which are hardly to identify in the raw images, emerge more clearly and with sharpened edges after deconvolution (figures 13 and 14). Examples are shown for a five-color immuno-FISH experiment in figures 13. In figure 14 a magnification of the inactive X-chromosome before and after deconvolution is delineated to exemplify the power of this tool. This makes it much more easy for the user to set thresholds which often turned out to be the most critical step in evaluation programs like co-localization analysis (figure 15).

The grainy signals shown for DAPI-counterstaining, H3K27me3 staining and chromosome paints (figure 15) make it difficult to set an appropriate threshold (figure 15, A1-A3). After application of deconvolution signals appear as well defined structures which facilitates significantly to distinguish between signals and background (figure 15, B1-B3). Through this clear separation it is much easier to determine thresholds.



Figur 14

The figure shows a typical H3K27me3 staining in a HFb-nucleus. The inactive X is magnified and structures that appear after deconvolution are marked by white arrows.

A H3K27me3 before deconvolution: in the raw image blur and higher background is obvious.

B H3K27me3 after deconvolution: blur and background noise are clearly reduced. In contrast to the raw image the consistency of substructures can be seen.

Both pictures are single confocal mid sections of a HFb-nucleus, bar indicates 5 μ m

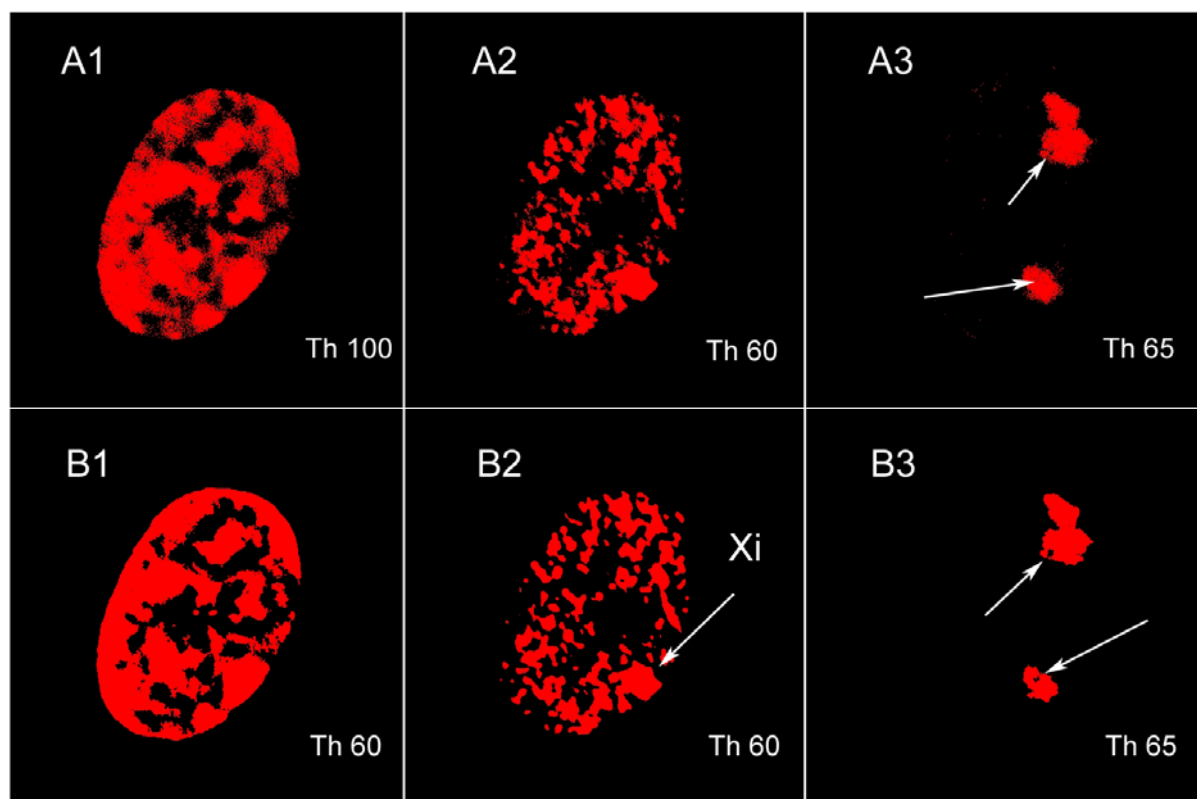
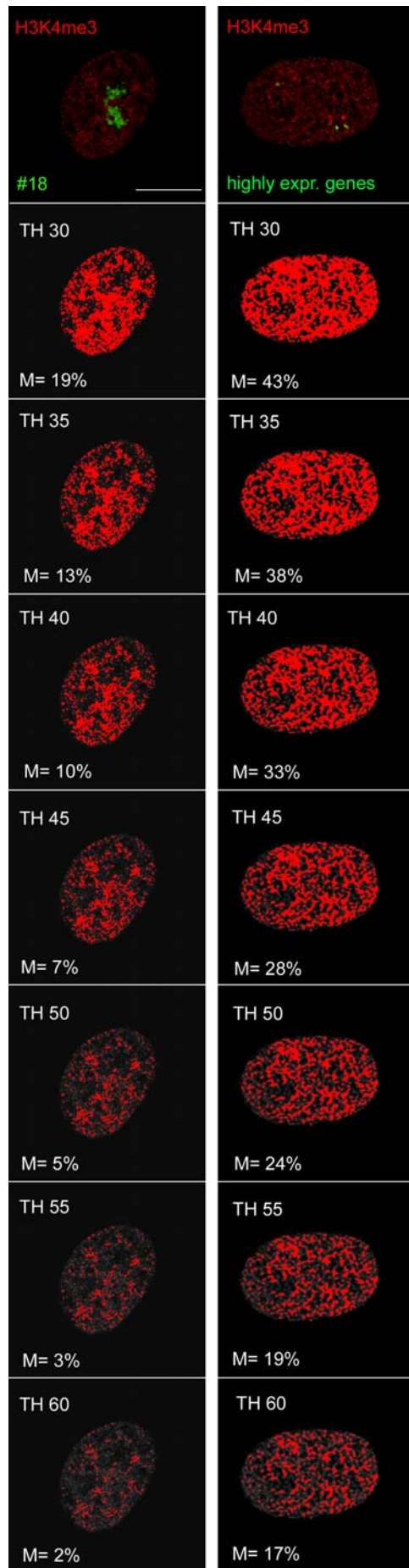


Figure 15

The upper row (A1-A3) shows raw data of mid sections of HFbs with thresholds which I would set to separate signals from background. Raw signals appear more grainy in all three channels compared to the deconvolved images (B1-B3). For the DAPI channel (A1) a threshold 40 grey values higher than for the deconvolved picture has to be set to achieve a similar signal indicating noise reduction after deconvolution. The raw pictures of H3K27me3 (A2) and X-chromosomal paints (A3) show clear graining. The same picture after deconvolution shows the chromosome territories more distinct and with sharpened edges.

3.13.4 The consistency of evaluation results at different thresholds

To test whether the results of the co-localization analysis were reliable co-localization analysis with deconvolved images was performed over a wide threshold range in steps of five (figure 16). The analysis was exemplified for H3K4me3 with paints (example for a big object) on the one hand and for BAC signals (small object) on the other hand. The applied thresholds were relatively low because deconvolution of images already took a considerable amount of signal intensity. The absolute co-localization values of H3K4me3 with #18 paints on the one hand and BACs containing highly expressed genes on the other hand deviated from each other because of their different properties (see chapter results figure 40 and 43). Despite co-localization values for thresholds 30 and 60 are very different for both CT#18 and BACs one should keep in mind that values divergate not too much from one threshold step to



the next (between 30 and 60 not more than 6% in all cases). Given that thresholds 30 and 60 are not appropriate it is convincing that if a threshold is not set totally wrong the achieved results are acceptable. However it is important for the user to get experience with histone methylation patterns to decide what is the appropriate threshold. Using a reasonable amount of nuclei a statistical error can be minimized.

To summarize the findings described above, taking the Manders coefficient for evaluation in co-localization analysis was an acceptable approach.

Figure 16

Test of the consistency of co-localization analysis results over a range of thresholds for BAC signals and chromosome 18 points with H3K4me3. The Manders coefficient M reflects the percentage of overlapping volume of the chromosome territories HSA #18 and highly expressed genes respectively with the H3K4me3 staining pattern. All images were deconvolved before co-localization analysis. Despite drastic changes concerning the amount of voxel in the H3K4me3 signal that contributes to co-localization analysis, the deviation in per cent from one threshold step to the next is reasonable and proves the choice of this evaluation method right for these kind of experiments.

Bar indicates 5µm

Note: The applied thresholds in the displayed images was 50 for CT #18 and 70 for highly expressed genes in all cases.

3.14 Image processing

3.14.1 Documentation and shift correction

For documentation purposes images were processed using Adobe Photoshop version 7.0 or Image J version 3.29 and 3.30. Usually in Image J only slight grey levels adjustments and false color assignments were performed on the raw images.

To measure the **axial shift**, image stacks of multi-fluorescent beads were collected using a very small z-step size (~50nm). Then the particular z-step position of the frame showing the biggest diameter of an individual bead within the stack was determined for each fluorescence channel and compared. The difference in this z-step position was then multiplied by the step size to give the z-shift in nm. This was repeated for several individual beads and the mean was calculated. **Lateral shift** was negligible.

3.14.2 Photoshop and Image J

Adobe photoshop is the world market leader for professional image manipulation. It shows a big number of options to edit and arrange pictures. In this thesis photoshop was used to arrange complex pictures and for the best presentation of signals, but never for any kind of evaluation.

The public Java imaging processing program **Image J** can display, edit, analyze, process and save pictures with different colour depths. The raw data from our microscopes have the TIFF image format which can be loaded in stacks as an image sequence. Now three dimensional measurements, analysis and processing functions, such as sharpening, smoothing, edge detection, and many more are possible. The program can measure distances and angles as well as line profile plots (line scans). In addition standard image processing functions as brightness/contrast, filtering, application of thresholding and grey value calibration are supported. With a huge number of plugins that are available the spectrum for image processing and analysis can be extended.

3.14.3 Co-localization analysis

Co-localization refers to *different data analysis methods* to characterize the degree of overlap between two signals and to investigate if two cellular targets (in this case nuclear targets) are located at least partly in the same spatial position.

Different approaches exist for co-localization analysis. Thus an appropriate method according to the type of analysis has to be chosen. A requirement, which a co-localization software should provide for our purposes is an intensity weighted voxel-by-voxel analysis. Another need is a certain statistical output, e.g. how many % of signal in channel A co-

localize with signal in channel B and vice versa. Practically this approach has to face the problem that two signals can have different sizes, can co-localize to a different extent (completely, partly or not at all) and vary in their intensity distribution.

Different coefficients are widely used in literature and should be explained exemplified by Paerson's and Manders' coefficients. Paerson's coefficient takes into account the signal intensities and integrates for each voxel both gray values (channel one and channel two). Values of the Paerson's coefficient range from -1 to +1 and can only be applied to a single population of signals which is not very common in biological problems. In this context interpretation of negative correlation is difficult.

The values used for quantitative evaluation of co-localization in this work were based on the Manders coefficients **M1** and **M2** (Manders et al., 1993). Calculation of Manders coefficients was performed using an Image J plugin (figure 18). The evaluation of the degree of co-localization of two channels was restricted to voxels that contributed to at least one of the channels after segmentation. These values measure the proportion of overlap between two channels relative to the total amount of signal contributing to each channel on a voxel based algorithm. The Manders co-localization coefficients M1 and M2 range from 0 to 1 (0%-100%) and can be treated as indicators of the percentage of the summed up intensities of co-localizing voxels in the two colour channels with regard to the summed up intensities of all voxels counted in the respective channel.

Manders coefficients M1 and M2

These coefficients are Mander's co-localization coefficients for channel 1 (M1) and channel 2 (M2).

Split-coefficients avoid issues relating to absolute intensities of the signal, since they are normalized against total pixel intensity. We also get information about how far channels overlap with each other. There might be cases where red may overlap significantly with green ("red" and "green" were just used to define two different channels), but most of the green may not overlap with the red or vice versa.

If the assumption is made that greyscale number equates to dye molecules (this is not necessarily correct) then these coefficients represent the percentage of red dye molecules that share their location with a green dye molecule.

These coefficients are very sensitive to poor background correction and do not take into account the intensity of the second channel, other than it is non-zero. For example, a bright red pixel colocalizing with a faint green pixel is considered equivalent to a bright red pixel

colocalizing with a bright green pixel. Intuitively, a red-green pixel-pair of similar intensities should be considered “more colocalised” than a pixel pair of widely differing intensities.

The plugins generate scatter plots plus correlation coefficients. In each scatter plot, the first (channel 1) image component is represented along the x-axis, the second image (channel 2) along the y-axis (figure 17). The intensity of a given pixel in the first image is used as the x-coordinate of the scatter-plot point and the intensity of the corresponding pixel in the second image as the y-coordinate.

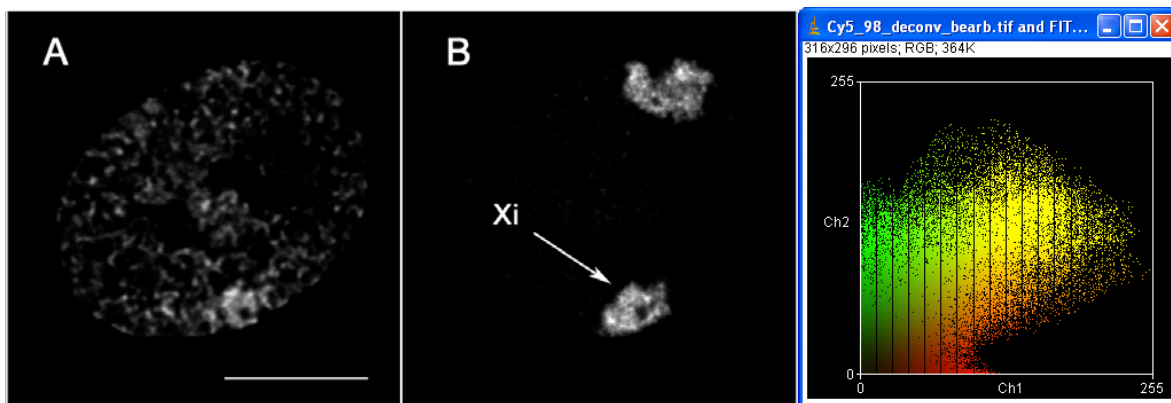


Figure 17

A shows a typical H3K27me3 staining pattern, **B** paint signals of the X-chromosomes. Co-localization analysis was performed for the Xi (visualized by paint probes and identified by conformity of paint and ab. staining) and the H3K27me3 pattern. The result is mirrored by the color scatterplot on the right. Yellow colour represents overlay of the channels 1 (red=H3K27me3) and 2 (green=Xi paint). The corresponding Manders coefficients are M1: 0.144 and M2: 0.887. The Manders values range from 0-1 this means in this case: all voxels above a distinct threshold in one channel colocalize with all voxels above a certain threshold in the other channel. In other words, 88,7% of the Xi-paint signal colocalize with the ab. staining and 14,4% of the antibody staining colocalize with the Xi-paint signal. Shown are single confocal mid sections after deconvolution of a HFb nucleus. Bar indicates 5µm

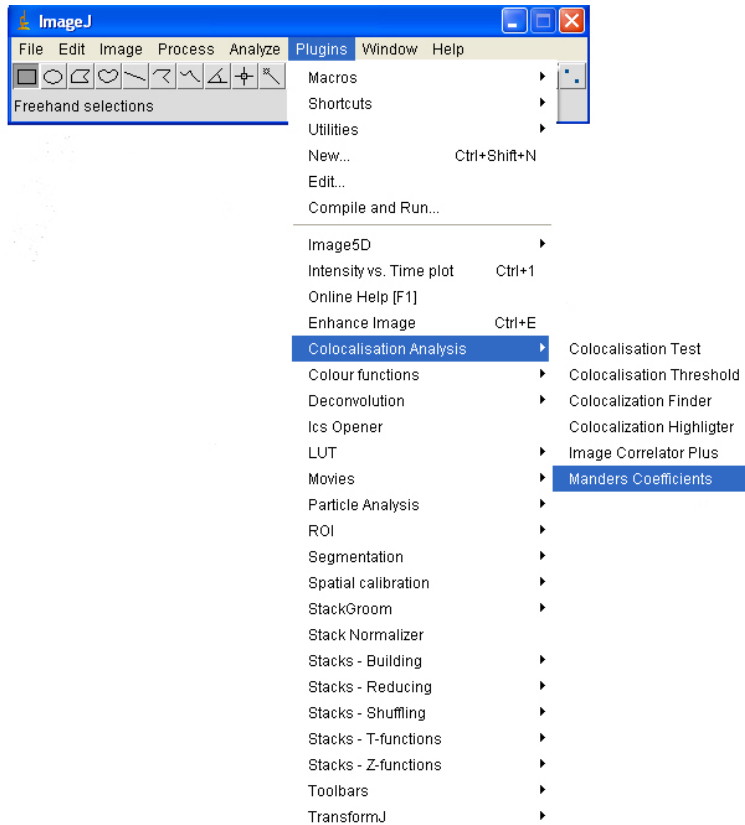


Figure 18

Path in Image J for calculating Manders coefficients out of two different image stacks. Before application stacks are shift corrected, deconvolved and a manual threshold was applied.

The intensities of each pixel in the “Correlation Plot” image represent the frequency of pixels that display those particular red/green values. Since most of the image will probably be background, the highest frequency of pixels will have low intensities so the darkest pixels in the scatter plot are in the bottom left hand corner – i.e. $x \sim \text{zero}$, $y \sim \text{zero}$ while the brighter pixels can be found in the upper right area of the scatter plot. The intensities in the “Red-Green correlation plot” image represent the actual colour of the pixels in the image.

Quantitative analysis removes user bias by analyzing all the pixels based on of their intensity (it must be noted that some authors consider this a drawback rather than an advantage due to the intrinsic uncertainty of pixel intensity; see Lachmanovich et al. (Lachmanovich et al., 2003). The path for calculating Manders coefficients in Image J is delineated in figure 18.

One key issue that can confound co-localization analysis is bleed through. Co-localization typically involves determining how much the green and red colours overlap. Therefore it is essential that the green emitting dye does not contribute to the red signal (typically, red dyes do not emit green fluorescence but this needs to be experimentally verified). One possible way to avoid bleed-through is to acquire the red and green images sequentially, rather than

simultaneously (as with normal dual channel confocal imaging) and the use of narrow band emission filters.

Qualitative analysis can be thought of as "highlighting overlapping pixels". Although this is often given as a number ("percentage overlap") suggesting quantification, the qualitative aspect arises when the user has to define what is considered "overlapping". The two channels have a threshold set and any areas where they overlap is considered "colocalised". Qualitative analysis has the benefit of being readily understood with little expert knowledge but suffers from the intrinsic user bias of "setting the threshold". There are algorithms available which will automate the thresholding without user intervention but these rely on analysis of the image's histogram which is subject to user intervention during acquisition.

The confocal image stacks had to be shift corrected first. After that they were deconvolved (described in 3.13) and processed to separate "true" signals from background signals.

The deconvolution of confocal images can have a profound impact on co-localization analysis (Sedarat et al., 2004). But in-depth investigations demonstrated that co-localization analysis shows clearly superior results after image restoration (Landmann and Marbet, 2004).

The deconvolution and processing of pictures makes it much easier for users to set the appropriate threshold.

3.14.4 Amira 3D reconstruction

3D reconstructions were generated using the software Amira (TGS) version 3.1.1, by surface rendering image stack data. The basic principle is that a surface is generated separating voxels beyond and above a certain subjectively set threshold. To improve the signal/noise ratio in order to facilitate threshold determination and to smooth signal boundaries, image stacks were modified using a 3D Gaussian filter, with a kernel size of 2. The threshold was chosen in a way that the generated surface would be aligned with the grey level images in the individual sections as close as possible, but without losing smaller, weaker signals.

It is important to mention, that Amira reconstructions were just used to illustrate the results, but never any kind of evaluation was performed with this program.

3.14.5 Radial autocorrelation (RAC) function analysis

To quantify the degree of clustering or spreading of the histone lysine immunofluorescence staining, an autocorrelation approach as described in Walter et al. (Walter et al., 2003) was applied. For each nucleus a maximum intensity projection of five central optical sections was generated. An intensity threshold value, which separates the signal from the background, was determined for each projection by visual inspection, and the threshold value was subtracted from all intensity values in the projection.

The relative distance between all possible pairs of pixels (i and j) was calculated as

$$d(i, j) = \frac{1}{l_{ref}} \sqrt{(\bar{x}_i - \bar{x}_j)^2}, \text{ with}$$

\bar{x}_i, \bar{x}_j : the positions of pixels i and j .

l_{ref} : reference length: the length of the long axis of the elliptically shaped nuclei

Using a plugin for Image J the radial autocorrelation function (RAC) of an image was calculated as

$$RAC(d) = \frac{1}{(\sum_i I_i)^2} \sum_{i, j; d \leq d(i, i) < d + 0.02} I_i \cdot I_j, \text{ with}$$

d : the starting value of a relative distance interval; $d = 0, 0.02, 0.04, \dots, 1$

I_i, I_j : fluorescence signal of pixels i and j (minus the threshold intensity)

The RAC is an intensity-weighted measure that reflects how many pairs of pixels fall into each relative distance interval.

3.14.6 Evaluation procedure in Chaetocin experiments

After Chaetocin treatment drastic changes in H3K9me3 pattern formation were observed in HFbs but not in the cancer cell-lines MCF-7 and DLD-1. To evaluate these changes in chromatin formation a good evaluation strategy was required. In HFbs H3K9me3 forms unspectacular small clusters which change to very big clumps after Chaetocin application. However MCF-7 cells show big clusters of constitutive heterochromatin in treated and untreated cells. The task was to find an evaluation method that allowed to investigate big staining signals (H3K9me3 clusters). The decision was made to take the volume of objects as a criteria for this evaluation. To eliminate the threshold problem as a major source of error, measurements in nuclei of HFbs was made threshold independently over a range from

0 to 100 in steps of five. All images were deconvolved in advance so a lot of background noise was already removed and therefore led to lower overall gray value intensities. The evaluation was performed with the freeware program Image J. The plug-in 3D objects counter provides amongst other things the volume of objects assessed by the number of voxels contributing to one object. To plot the results in a diagram and to get the best information out of the data, two groups of objects with different size were defined. The first group comprised objects >500 voxel while the second group consisted of objects >1000 voxel. These parameters served as criteria for the judgement of cluster formation in the respective cell-lines. A flow chart that describes how the evaluation was performed in detail is delineated in table 6.

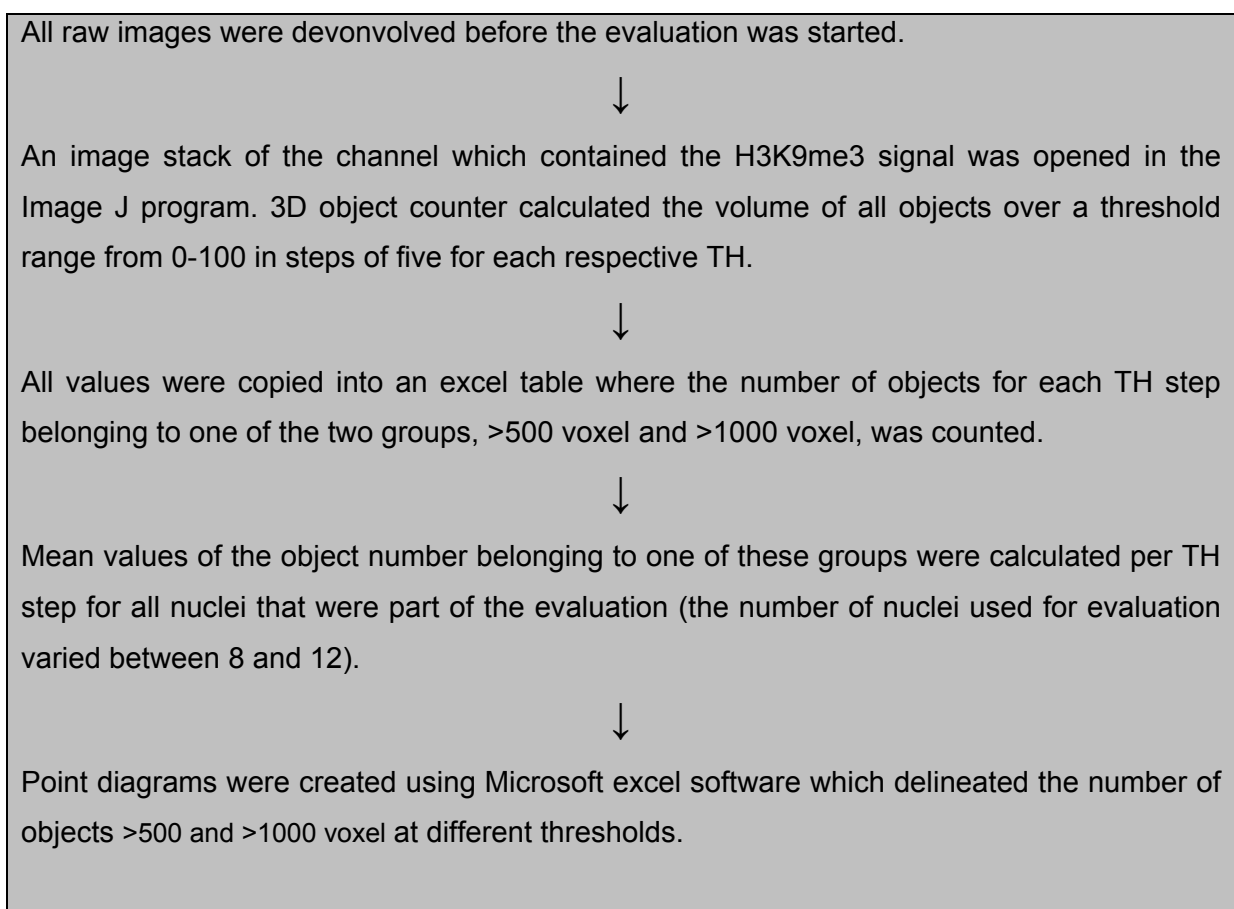


Table 6 Flow chart of the evaluation procedure after Chaetocin treatment

As deduced from the evaluation experience made with HFbs, evaluation for values at thresholds 25 and 35 were regarded as sufficient. These thresholds proofed to be representative in the case of HFbs to show that the pattern size in cells after drug application is different from untreated control cells.

On the one hand the diagrams provide information about potential differences of the cluster size in treated and untreated cells, on the other hand curve progression mirrors the integrity and intensity of heterochromatin clusters.

4 Results

4.1 Nuclear patterns of distinct histone methylation sites

4.1.1 Methylation sites and their arrangement in regard to centromeres

The staining patterns of various lysine methylation sites in three human cell types, diploid fibroblasts as well as two common cancer cell-lines (DLD-1 and MCF-7) was compared in its 3D context to DAPI-counterstaining on the one hand and centromere signals on the other hand. All nuclei shown in figures 19 and 20 show nuclei of cycling cells as identified by Ki-67 staining.

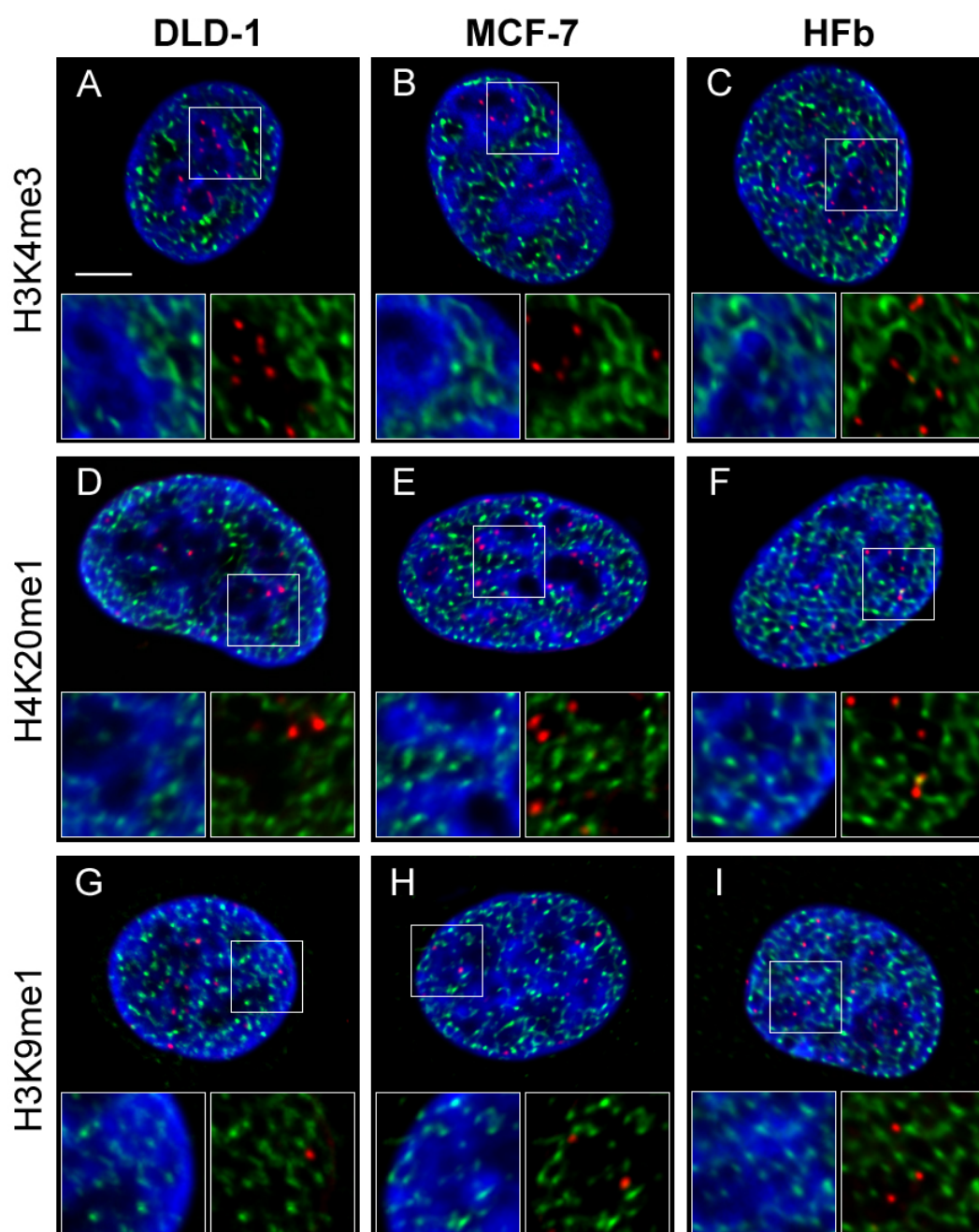


Figure 19

Histone lysine methylation patterns of H3K4me3, H4K20me1 and H3K9me1 (green) together with centromeres (red) after immunostaining and nuclear counterstain with TO-PRO-3 (blue) in DLD-1, MCF-7 and HFb cells. Insets show representative areas at a higher magnification (left panel antibody and DNA, right panel antibody and centromeres).

In most cases centromere signals are clearly separated from chromatin sites marked by the respective antibodies (**A,B,D,E,G-I**) in accordance with their functional assignment to active chromatin. Small overlapping sites can be seen in (**C**) and (**F**). H3K4me3 is predominantly located within chromatin areas of low staining intensity with TO-PRO-3 (**A-C**). A similar distribution within low compacted chromatin is observed for H4K20me1 (**D-F**), while a considerable fraction of H3K9me1 stained chromatin is found in TO-PRO-3 dense areas (**G-I**). All pictures display a projection of five confocal mid-sections (comprising a thickness of 1 μ m) of a nucleus. All images are deconvolved. Bar indicates 5 μ m

The specificity of all used antibodies (except H3K4me3 which was commercial and no peptides against this antibody was raised have been available) was tested accurately as described in 3.7. H3K4me3 which was allocated to actively transcribed chromatin (Santos-Rosa et al., 2002) forms a nuclear network in all cell types (A-C). The antibody signals were more (A, B) or less (C) found in areas of low TO-PRO-3 staining. In humans this counterstaining dye stains predominantly A-T-rich sequences and is concordant with DAPI. Accordingly very little staining was found in the proximity of centromeres, around nucleoli and at the nuclear rim.

A quite similar pattern was observed for H4K20me1 (D-F) which also expanded as a reticulation throughout the nucleus with very little overlapping to centromeres. But in comparison to H3K4me3 more overlap with TO-PRO-3 dense regions was observed. Unexpectedly about 25% of all cells had a distinctly higher staining intensity than the rest of the cells. This fraction likely represents nuclei between S and G2-phase as identified by Ki-67 staining and estimated by cell size (data not shown). Those differences within a cell population were not observed at any other antibody pattern.

Rice and colleagues assigned H3K9me1 to “silent domains of euchromatic regions” in mouse cells where it was found throughout the nucleus but excluded from DAPI-dense regions and nucleoli (Rice et al., 2003). Accordingly in the three human cell types examined here the antibody pattern appeared in small foci all over the nucleus (G-I) but in contrast to H3K4me3 and H3K9me1 the staining was predominantly found in TO-PRO-3 dense regions.

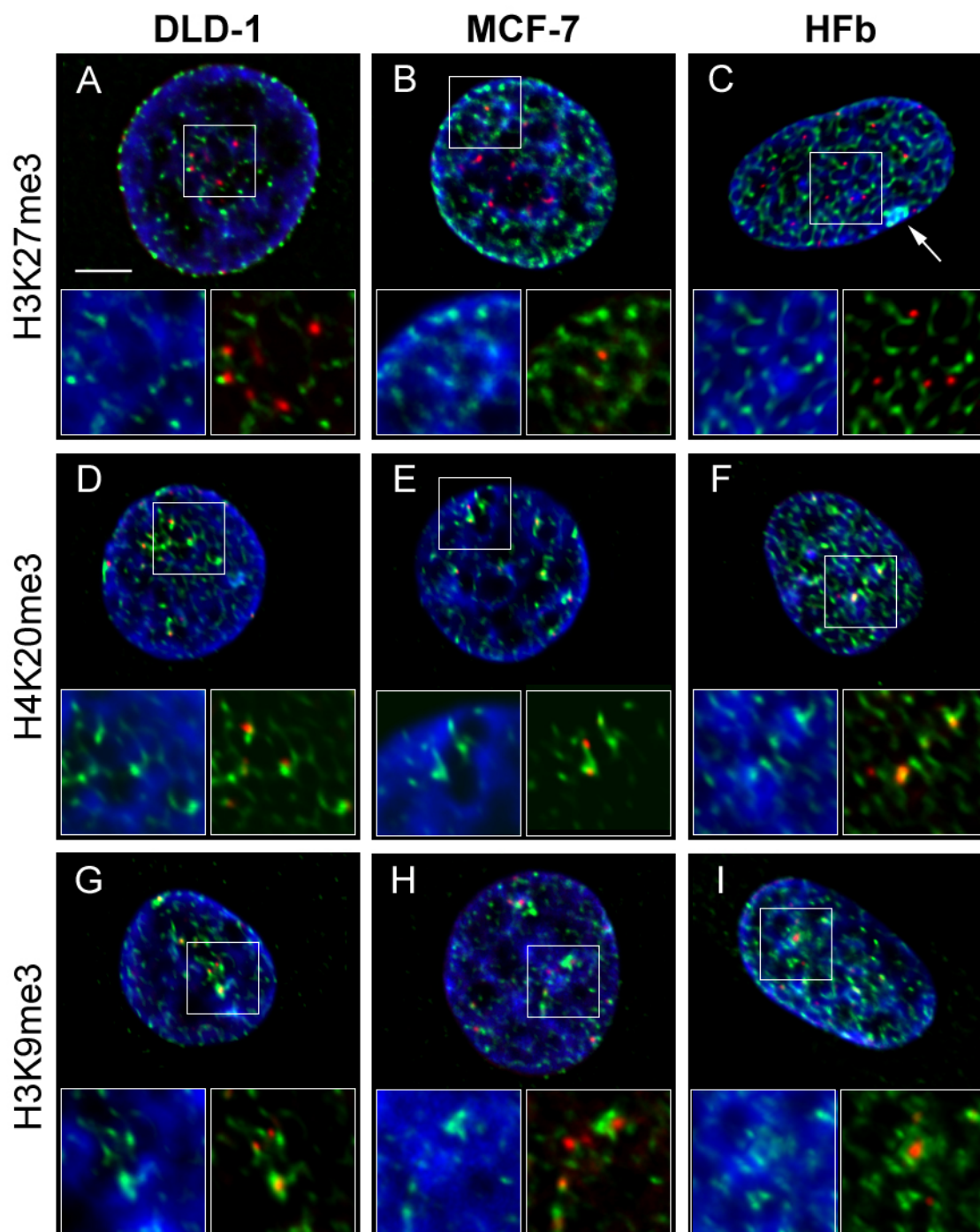


Figure 20

Histone lysine methylation patterns of H3K27me3, H4K20me3 and H3K9me3 (green) linked to repressed chromatin together with centromeres (red) after immunostaining in DLD-1, MCF-7 and HFb cells. Nuclei are counterstained by TO-PRO-3 (blue). Insets show representative areas at a higher magnification.

For H3K27me3 stained chromatin no overlapping with centromeres is visible in neither cell type (**A-C**). A distinct staining pattern at the nuclear periphery and around nucleoli is observed in DLD-1 and in MCF-7 cells (**A,B**). The staining of Xi in HFb is marked by an arrow (**C**). A strong association of centromeres with both H4K20me3 and H3K9me3 is shown for all cell-lines (**D-I**). Moreover the signals of these two antibodies co-localize mostly with DNA dense regions (TO-PRO-3, blue). All pictures display a projection of five confocal mid-sections (comprising a thickness 1 μm) of a nucleus. All images are deconvolved. Bar indicates 5 μm

The most prominent example of facultative heterochromatin is the inactive X-chromosome. Its association with H3K27me3 is demonstrated for female human fibroblasts (C, white arrow). Furthermore the foci like H3K27me3 pattern is distributed throughout the nucleus with an accentuation of the nuclear periphery and around nucleoli. It shows, if any only small overlap with centromeres. Staining of the inactive X-chromosome was lacking not only in male DLD-1 cells as expected but also in the female breast cancer cell line MCF-7 where X-chromosomes escape inactivation (Ganesan et al., 2002).

An interconnection of H3K9me3 and H4K20me3 as well as an assignment to constitutive heterochromatin has been shown for several species and cell types (Bannister and Kouzarides, 2004; Kourmouli et al., 2004; Lachner et al., 2003; Martens et al., 2005). In accordance to this we could show for all cell types a close spatial association of centromeres with both H3K9me3 and H4K20me3. Both modifications showed cluster formation around centromeres but there were also small foci uniformly distributed in the nucleus.

4.1.2 Overlap assessment between centromeres and histone modifications

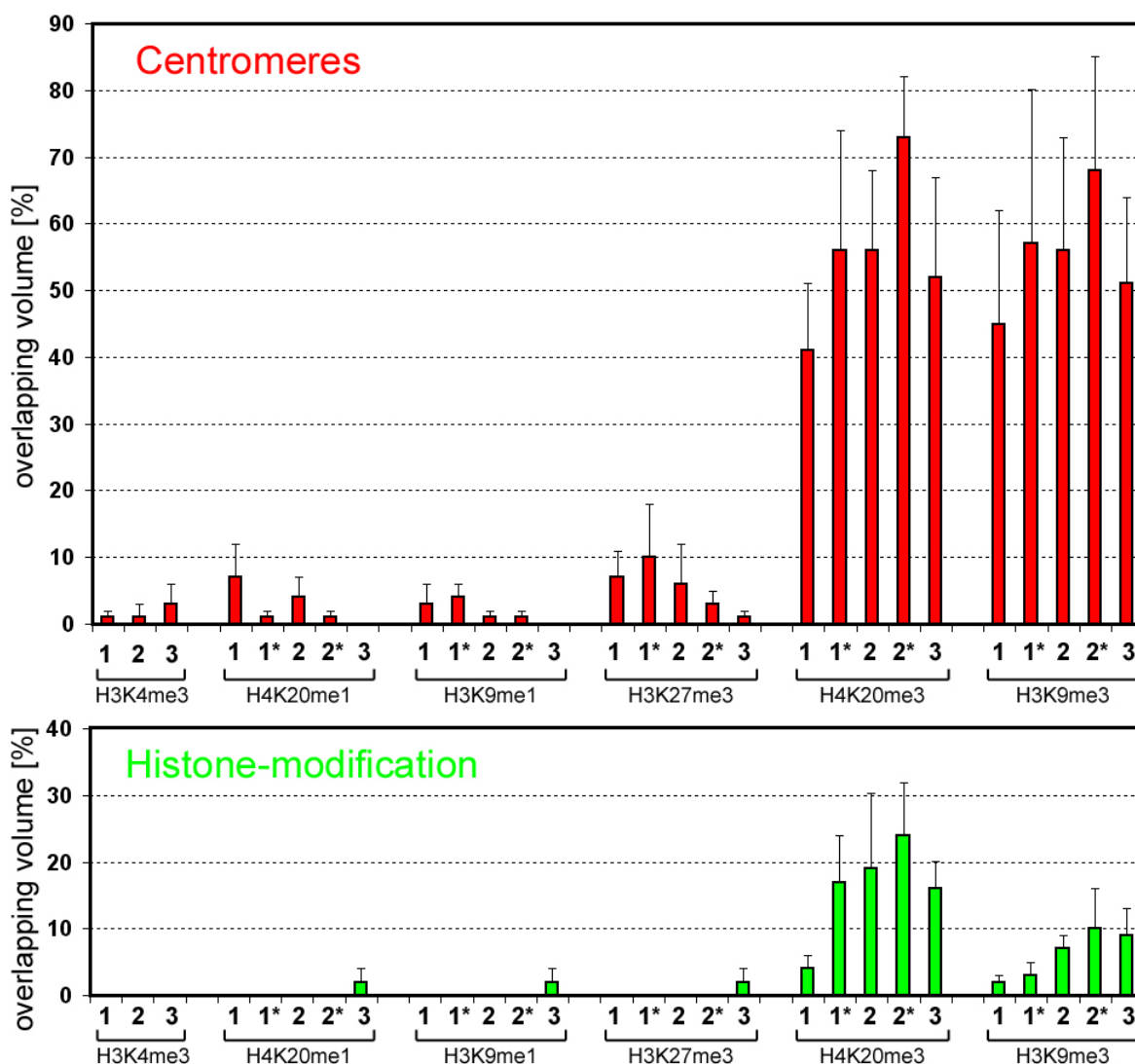


Figure 21

Quantitative assessment of overlap between centromeres (**upper graph, red**) and chromatin modified at different methylation sites (**lower graph, green**) represented as the percentage of the co-localizing volume for each color channel. Error bars show the standard deviation of ≥ 8 measured nuclei. Numbers without asterisks denote nuclei from cycling DLD-1 cells (**1**), MCF-7 cells (**2**) and human fibroblasts (**3**). Numbers with asterisks denote the overlap values for the respective cell types after exit of the cell cycle.

To quantify the spatial correlation of histone modifications and centromeres the degree of overlap between centromeres and patterns of specific histone modification sites was evaluated in 10 nuclei for each methylation site and cell type (figure 21). The Manders co-localization coefficients M1 and M2 of voxels representing centromere signals on the one hand and signals of histone modifications on the other hand were calculated (Manders et al., 1993). Both coefficients indicate the percentage of the summed up intensities of co-localizing voxels in the evaluated two color channels with regard to the summed up intensities of all voxels counted in the respective channel. The values one gets from these coefficients range between 0 and 1 (or 0-100%, respectively), thereby indicating the percentage of the summed up intensities of colocalizing voxels in the two colour channels.

The six different histone lysine modification already shown in figure 19 and 20 were investigated in DLD-1, MCF-7 and HFb (figure 21). For DLD-1 and MCF-7 cell-lines co-localization analysis was separately performed for cycling and quiescent cells.

H3K4me3 which stains actively transcribed chromatin regions and centromeres exclude each other and so consequentially the very low co-localization value is as expected. The percentage of overlap for H4K20me1 and H3K9me1 with centromeres was comparable to H3K4me3. H3K27me3 showed a minor increase in overlay.

An explicit overlap between centromeres and histone methylation sites was found for H3K9me3 as well as for H4K20me3. Between roughly 40% and 70% of all voxels assigned to centromeres co-localized with either of these histone modifications (upper panel). There are no big discrepancies between the different cell types. However the overlap of all voxels assigned to H4K20me3 ranged between 5 and 25% and for H3K9me3 between 2 and 10% (lower panel). These data argue for the idea that centromeres delineated by CREST serum are at least partially embedded in constitutive heterochromatin visualized by H4K20me3/H3K9me3 staining. Vice versa these methylation sites cannot be regarded as restricted to centromeric heterochromatin.

4.1.3 Relation between different histone modifications and nascent RNA

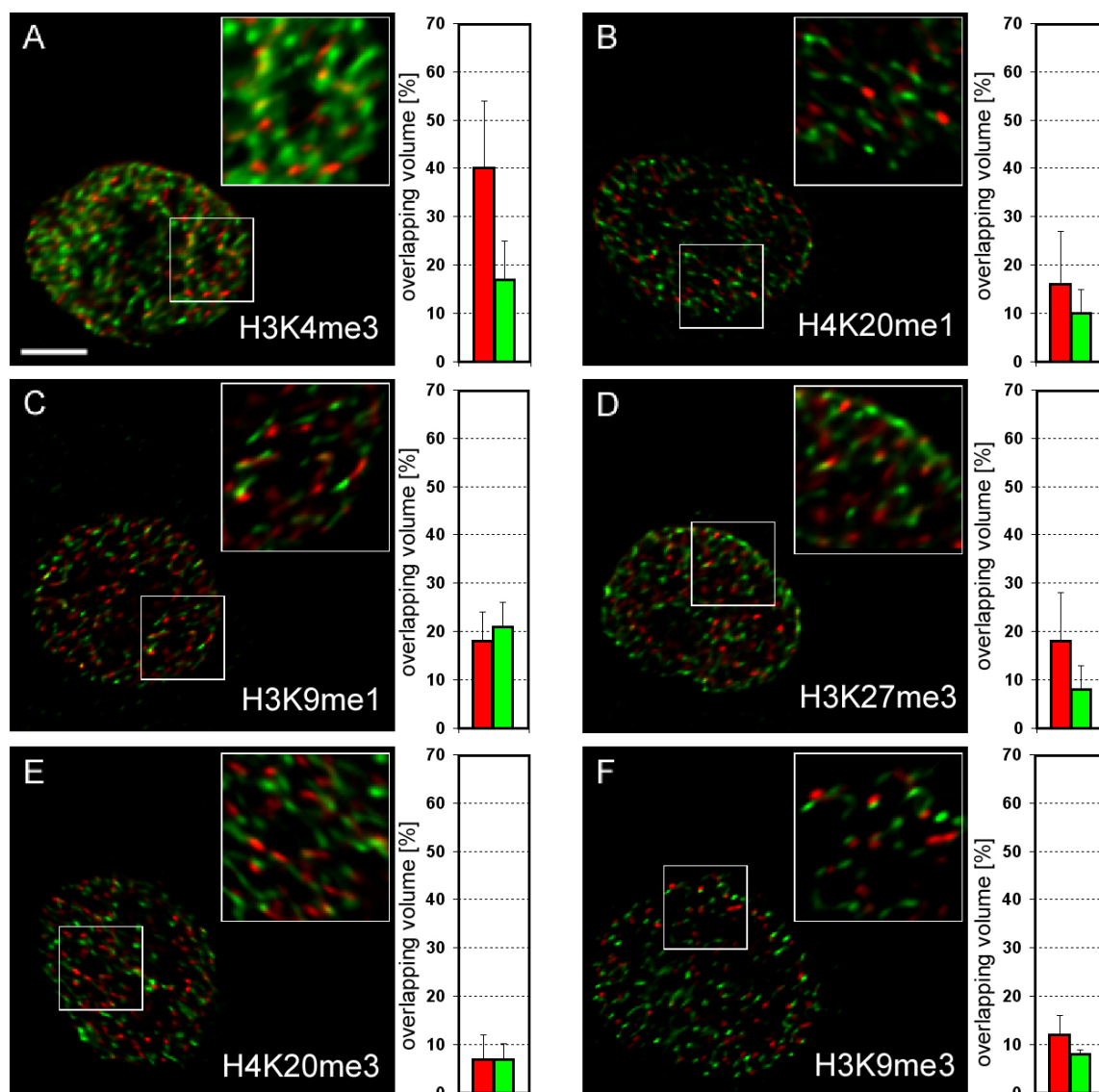


Figure 22

Spatial relation between different histone lysine methylation sites (**green**) and nascent RNA (**red**) visualized in DLD-1 cells. The graphs on the right of each image show the quantitative assessment of overlap between nascent-RNA (**red**) and each histone methylation site (**green**) as the percentage of the co-localizing volume for each color channel. All images are deconvolved. Bar indicates 5 μ m

To check whether distinct histone lysine methylation sites can be assigned to transcriptionally active sites, the spatial relationship between different methylation sites (the same six sites already investigated together with centromeres) and nascent RNA was analyzed. Cells were pulse labeled by application of Br-UTP scratch transcription labeling (Schemmelleh et al., 2001) as described in 3.3. Representative mid-sections of merged confocal images for each histone modification and nascent-RNA are shown in figure 22. Attached are their respective co-localization coefficients M1 (Br-UTP labeled nascent-RNA, red) and M2 (histone methylation, green) from 6-8 investigated nuclei. As was expected the highest co-localization coefficient with nascent-RNA was found for H3K4me3 (A) (M1=40%),

confirming its connection to actively transcribed chromatin. Nascent-RNA displayed similar overlap to H4K20me1/H3K9me1 (B, C) as well as H3K27me3 (D) (M1=17%). Very low co-localization coefficients were obtained for H3K9me3/H4K20me3 (E, F). This is as estimated because in constitutive heterochromatic regions only low transcriptional activity occurs.

4.1.4 Pattern formation in cycling and quiescent nuclei

While inspecting the histone methylation patterns in the epifluorescent microscope two different shaped pattern of H3K9me3 and H4K20me3 were eye-catching. The first idea was that the variable pattern formation depends on different cell cycle stages. MCF-7 cells providing the biggest and most distinct H4K20me3 antibody pattern were our choice for evaluation. Cycling MCF-7 cells were discriminated from quiescent cells by their positive pKi67 staining pattern. In both cycling and quiescent cells centromeres are in close contact and at least partially embedded in constitutive heterochromatin visualized by H4K20me3 staining. In quiescent cells the heterochromatic clusters appear bigger and in a more ring-like structure (23 B) compared to cycling cells (23 A). Additionally cycling cells displayed more foci throughout the nucleus and remote from centromeres. For the other antibody patterns no difference between cycling and quiescent cells was observable by visual inspection.

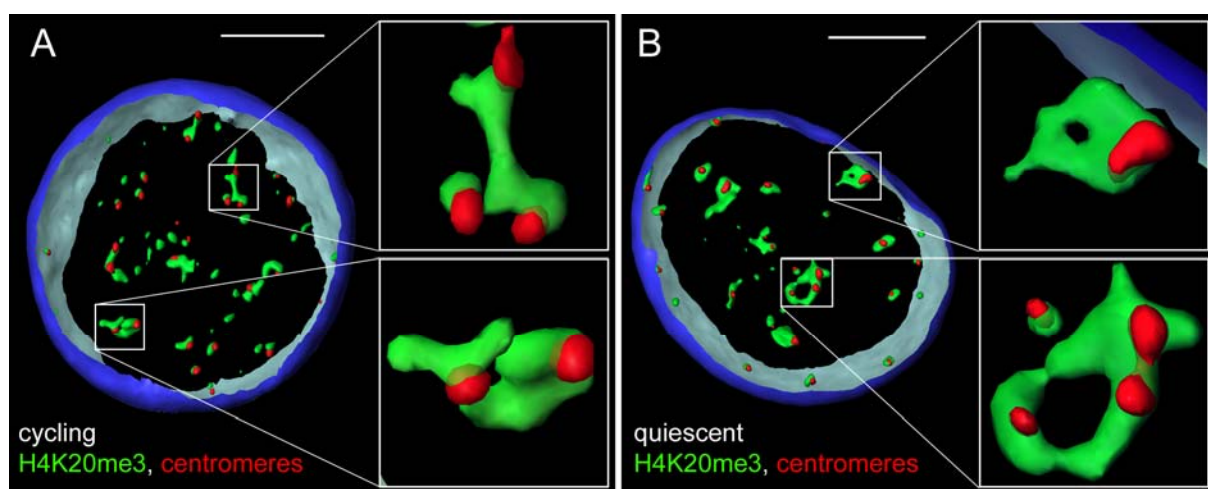


Figure 23

3D reconstructions of chromatin patterns after H4K20me3 immunostaining (green) together with centromeres (red) in a nucleus from a cycling MCF-7 cell (**A**) and from a quiescent cell (**B**). In both nuclei all centromeres are spatially associated to H4K20me3 stained chromatin clusters, but show only partial embedding. H4K20me3 clusters appear more dispersed in (**A**) compared to (**B**), where clusters frequently form ring-like structures. The inset magnifications point out in more detail the characteristic structure and spatial relation between H4K20me3 and centromeres. The 3D reconstruction was made from deconvolved images. Bars indicate 5 μ m

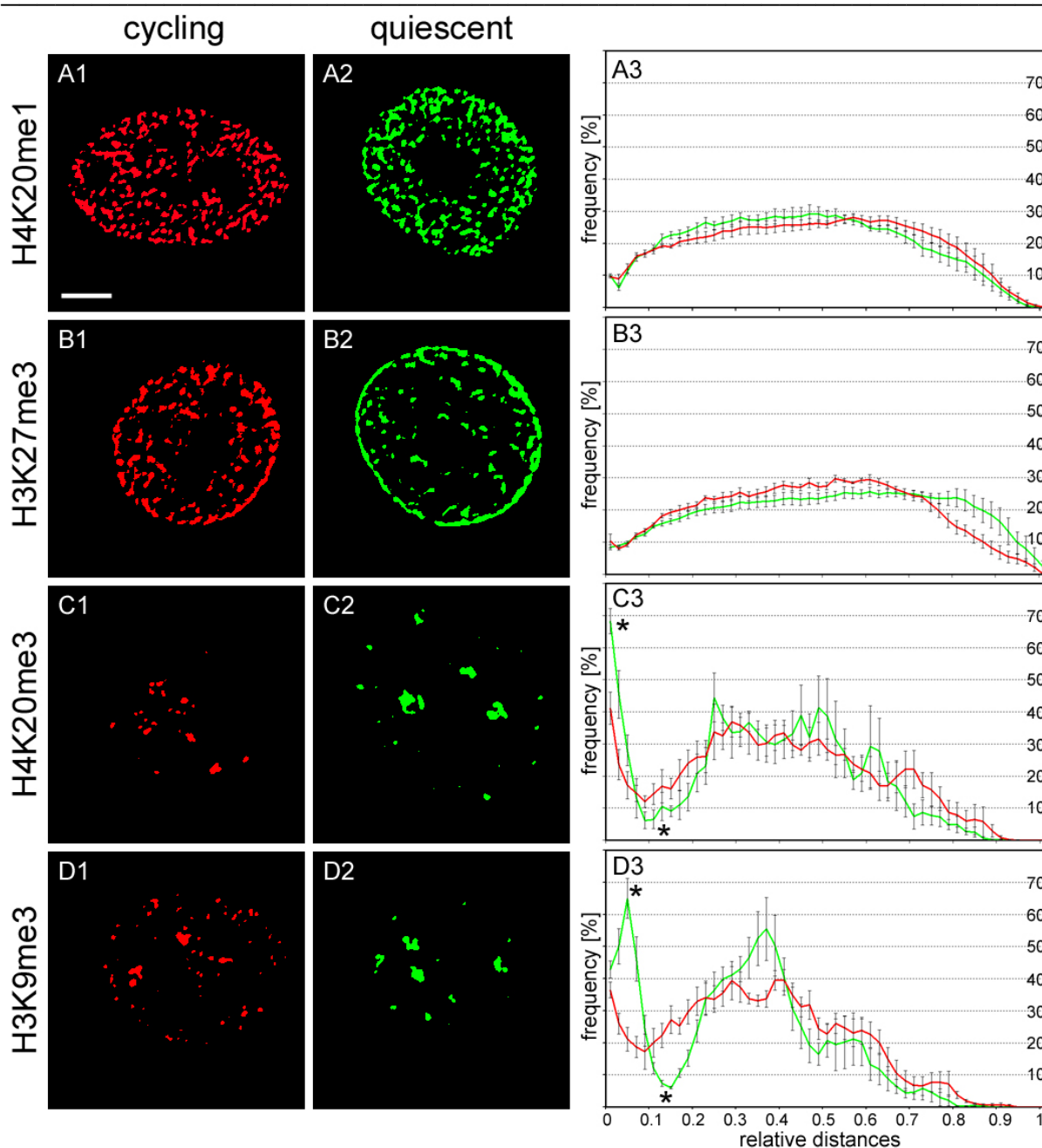


Figure 24

Comparison of pattern formation between nuclei of cycling (left panel, red) and of quiescent MCF-7 cells (mid panel, green) after immunostaining with H4K20me1 (**A**), H3K27me3 (**B**), H4K20me3 (**C**) and H3K9me3 (**D**). All pixels above threshold are shown as red or green respectively.

The graphs of the right panel illustrate the results of the applied radial autocorrelation function (RAC) summarized from ten nuclei each. The x-axis denotes relative distance intervals of the normalized nuclear length, the y-axis the percentage of pairs of pixels that fall into each relative distance interval (red curves = cycling cells, green curves = quiescent cells).

Similar pixel distribution between cycling and quiescent cells was obtained for mono-H4K20 (**A3**). The curves of the H3K27me3 signals show a slight increase of larger distances in quiescent cells (**B3**). Differences in the small distances are observed for H4K20me3 and more pronounced for H3K9me3 stained chromatin between the red and the green curves (**C3** and **D3**). The sharp peaks and consecutive drops of the green curves (**marked with asterisks in C3 and D3**) in contrast to the smoother red curves reflect the increase of small relative distances in

quiescent cells as a result of a more compact cluster formation. The shoulder within medium distance intervals together with the lack of relative distances > 0.8 indicates that the nuclear periphery is devoid of these big clusters. All images are deconvolved. Bar indicates 5 μ m.

As evaluation method to assess the difference between cycling and quiescent cells the radial autocorrelation (RAC) function analysis described by Walter et al., (Walter et al., 2003) (see methods and protocols 3.14.5) was applied. The degree of clustering was evaluated for the following histone methylation sites: H4K20me1, H3K9me3, H3K27 and H4K20 (figure 24). Each of the four modifications in nuclei from ten cycling and ten quiescent MCF-7 cells was investigated. Therefore projections were made from five subsequent optical sections representing about 1 μ m of the middle part of a given nucleus. After threshold was set manually and normalization of the size of these projections was performed, 2D distance measurements were carried out between all possible pairs of pixels representing a distinct histone modification. Distance values were grouped into 50 intervals of increasing relative distances (corresponding to approximately 200-300nm for each interval). RAC was established as a measure of the frequencies of pairs of pixels belonging to each interval. figure 24 (right panel) illustrates the results of RAC analysis summarized from ten nuclei each.

As expected already from judgement by eye, no difference between cycling (A1, red) and quiescent (A2, green) cells was detectable as reflected by the almost identical curves in the graph A3. For H3K27me3 (B1 and B2) a small shift of the staining signals towards the nuclear periphery in quiescent cells seems to occur (B3). For both H3K9me3 and H4K20me3 an increase in smaller distances was discovered. This result is mirrored in the respective graphs (C3 and D3) by the sharp peaks followed immediately by clear drops (marked by asterisks) and in contrast to the smoother curves shown for cycling cells.

4.1.5 Interrelationship of different lysine methylation sites

To test whether patterns of different histone methylation sites represent distinct nuclear zones, combinations of antibodies were performed by double immunostaining experiments (figure 25). Apart from that the following questions were addressed: share H3K9me3 and H4K20me3 which both represent constitutive heterochromatin the same 3D nuclear topology and can H4K20me1 be verified as a marker for active chromatin by co-localization with H3K4me3? Both pairs of these histone modifications displayed globally similar distribution patterns in single staining experiments (compare with figures 19 and 20). To compare histone modifications pairwise and directly in individual DLD-1 nuclei, a double immunostaining protocol had to be applied. This was necessary because all used primary

antibodies were raised in rabbit. Incubation with the second primary antibody was performed after complete blocking of the first primary antibody (see methods and protocols 4.9).

Representative histone lysine methylation staining patterns in DLD-1 cells are shown in figure 25. The respective co-localization coefficients evaluated for ten nuclei per experiment are presented at the right side of each panel. Panel A shows a nucleus with H3K9me3 (A1, red) and H4K20me3 (A2, green) staining. Signals in both channels appear distinct and show clear overlap with each other (visualized by yellow color in the overlay of red and green, A3). The overlap of these signals representing predominantly pericentromeric constitutive heterochromatin is also mirrored in the highest co-localization values of all combinations (A4). The high values, M1=31% for H4K20me3 and M2=53% for H3K9me3 reflect the high yet not complete overlap of the two modifications. However small chromatin foci stained with either H3K9me3 or H4K20me3 not associated with centromeric regions showed distinct signals for both channels.

Panel B shows a nucleus with H3K4me3 (B1, "active") and H4K20me1 (B2, "potentially active") stained chromatin foci. Numerous chromatin sites display overlap (B3, yellow color) and only few regions appear distinct. The high co-localization value for H3K4me3 of 38% with H4K20me1 (B4) indicates that a considerable sub-fraction shared the same spatial topology. In panels C-E it was investigated to which extend methylation sites with functional different assignment showed overlap or were mutually excluded from each other, thus representing distinct nuclear zones. Surprisingly for the combination of H3K27me3 and H3K9me3 co-localization values (43% for H3K27me3) were quite high regarding the fact that constitutive and facultative heterochromatic regions were compared. However this co-localization is likely due to the accumulation of H3K27 methylation at the nuclear periphery and around nucleoli. Contradictory combination of H3K4me3 with H3K27me3 on the one hand (Panel D) and H3K4me3 with H3K9me3 on the other hand (panel E) resulted as expected in little overlap of the respective modifications. These result support the existence of distinct nuclear zones for the tested histone lysine methylation sites.

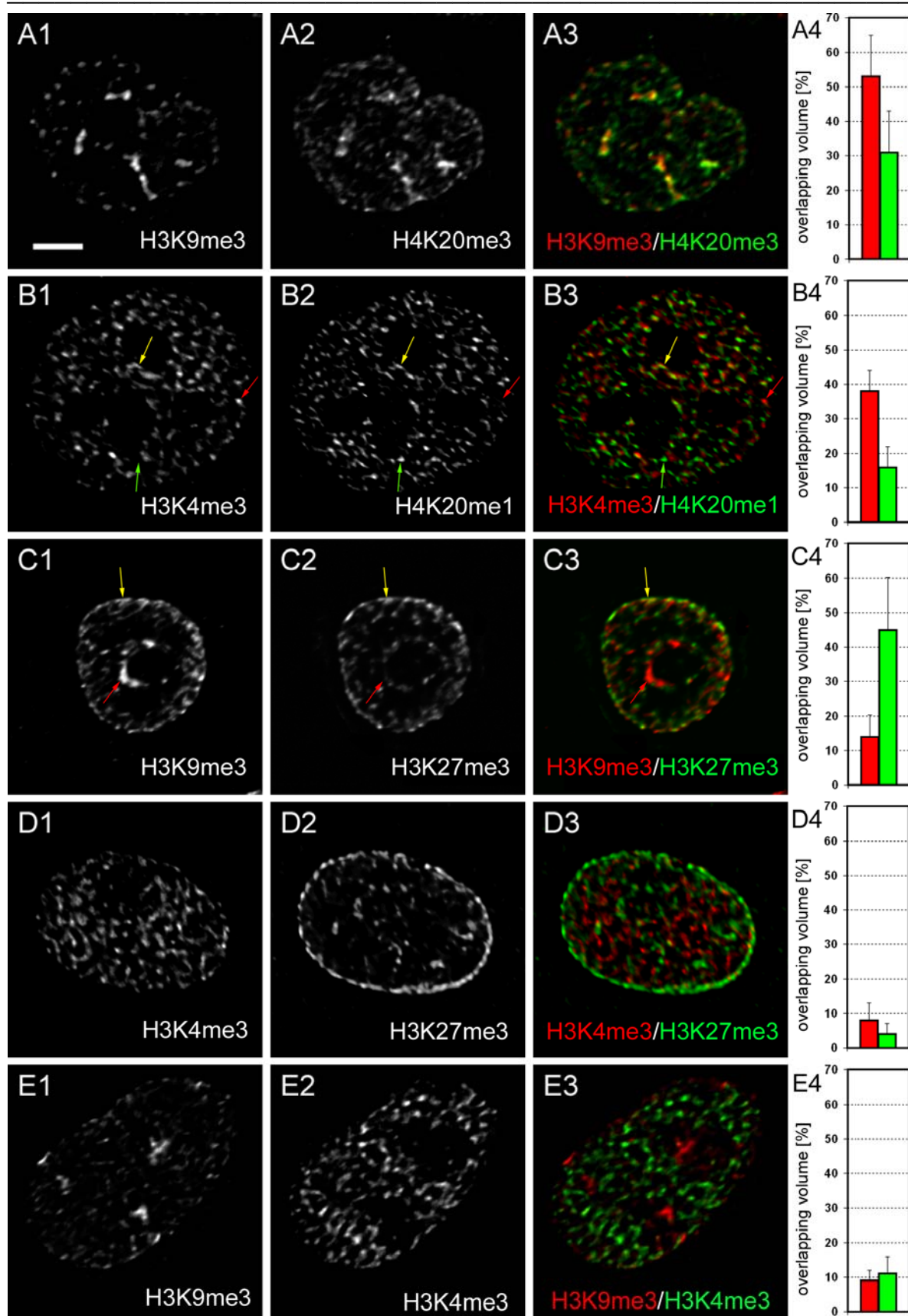


Figure 25

Comparison of differently methylated chromatin sites by double immunostaining after deconvolution in DLD-1 cells.

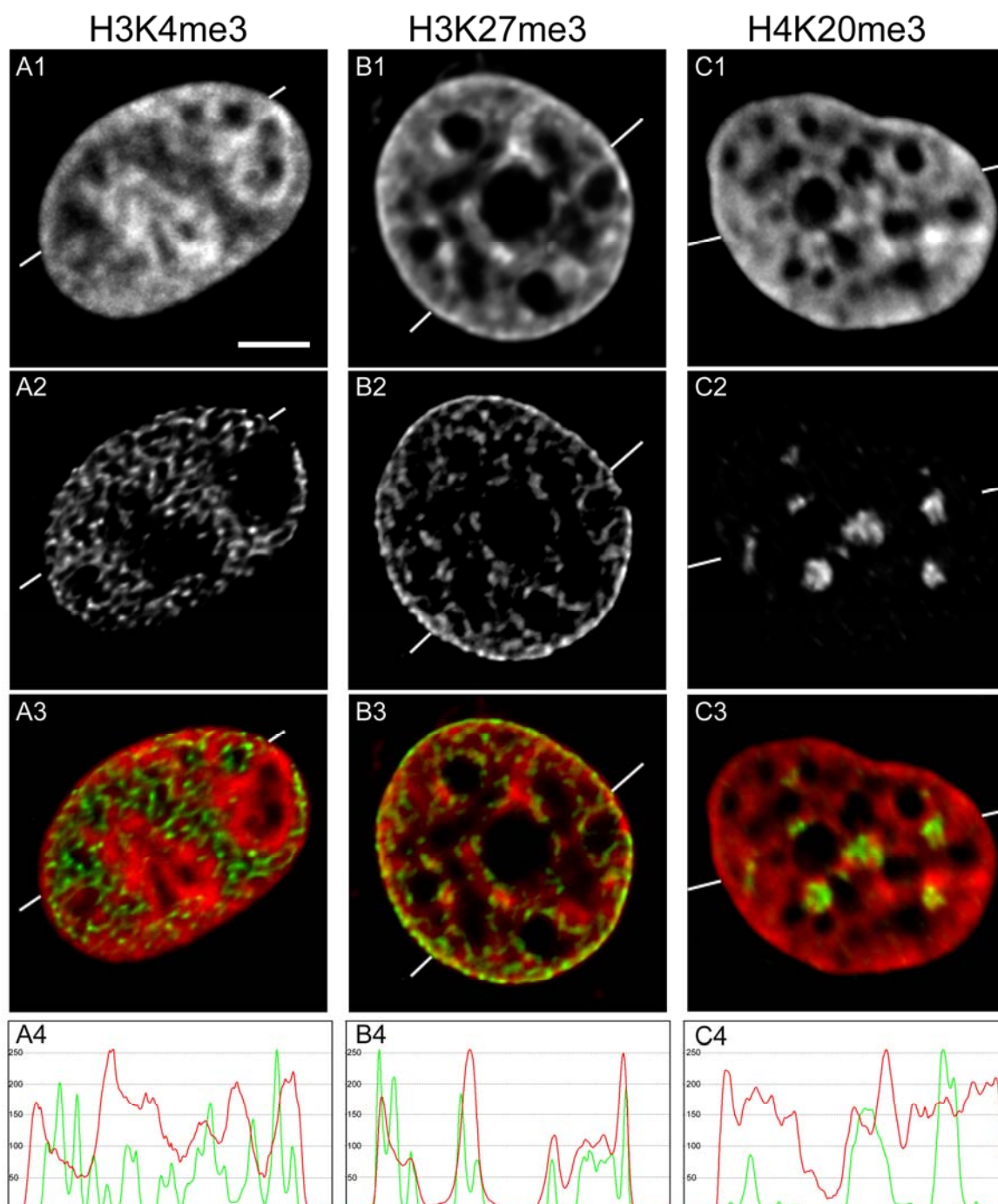
Panel A: double immunostaining of H3K9me3 (**A1**) and H4K20me3 (**A2**) shows high though not complete overlapping within the big clusters of high intensity in the merged image (**A3**). Small sites of chromatin regions stained with either H3K9me3 or H4K20me3 appear spatially associated but not strictly co-localizing. The quantitative assessment of overlap between H3K9me3 (red) and H4K20me3 (green) as the percentage of the co-localizing volume for each color channel evaluated from ten nuclei is illustrated in the graph (**A4**).

Panel B: double immunostaining of H3K4me3 (**B1**) and H4K20me1 (**B2**). Both modifications show a globally similar distribution pattern and frequent spatial associations in the merged image (**B3**). In addition to clearly co-localizing sites (example marked by yellow arrows) there are also sites that are stained only by H3K4me3 (red arrows) or by mono-H4K20me1 (green arrows). The quantitative assessment of co-localization between H3K4me3 (red) and H4K20me1 evaluated from ten nuclei is illustrated in the graph (**B4**).

Panel C: double immunostaining of H3K9me3 (**C1**) and H3K27me3 (**C2**). Intensely stained H3K9me3 clusters are not marked by H3K27me3 (see red arrows and merged image (**C3**)). However, spatial associations of chromatin marked by both modifications is seen at the nuclear periphery (yellow arrows). Considerable co-localization of H3K27me3 with H3K9me3 is confirmed by the quantitative assessment of evaluated from ten nuclei (**C4**).

Panels D and E: double immunostaining of H3K4me3 (**D1**) and H3K27me3 (**D2**) as well as H3K9me3 (**E1**) and H3K4me3 (**E2**). As shown in the merged images (**D3 and E3**) each modification is present in distinct nuclear zones. This is confirmed by the low co-localization values of quantitative assessment between H3K4me3 (red) and H3K27me3 (green) and between H3K9me3 (red) and H3K4me3 (green) evaluated from ten nuclei (**D4 and E4**). All images are deconvolved. Bar indicates 5 μ m

4.1.6 The formation of distinct nuclear zones by lysine methylation sites

**Figure 26**

Distinct nuclear zones formed by H3K4me3, H3K27me3 and H4K20me3 in quiescent MCF-7 cells.

Panel 1 shows images after TO-PRO-3 counterstaining, **Panel 2** the representative methylation patterns and **Panel 3** the merged images. **Panel 4** exhibits in line scans the intensity profiles between DNA counterstain and the respective histone methylation signals. The intensity profile of H3K4me3 reveals an anti-correlation to the nuclear counterstain intensity and a lack of signals at the utmost nuclear periphery (**A4**). In contrast line scans for H3K27me3 reveal a general consistency with DNA counterstain and an enrichment of this modification at the nuclear periphery and around nucleoli (**B4**). Clusters visualized by H4K20me3 staining are all found in TO-PRO-3 dense regions (**C4**). All images are deconvolved. Bar indicates 5 μ m

A further assessment of several different methylation sites was performed by combination of TO-PRO-3 staining with H3K4me3, H3K27me3 and H4K20me3 in MCF-7 cells, illustrated in figure 26. These representative nuclear images demonstrate the enrichment of these methylated histone sites in different nuclear zones. Line scans through the middle of the respective nuclei showing TO-PRO-3 DNA counterstain on the one hand and the particular methylation site on the other hand are plotted in figure 26 (A4-C4). Line scan for H3K4me3 and DNA counterstaining revealed a pronounced anti-correlation of both signals as well as a lack of H3K4me3 at the nuclear rim (A4). On the contrary, line scan for H3K27me3 (B4) yielded a general correlation with the intensity profile of TO-PRO-3. In this case also an enrichment at the nuclear periphery was observable (B4). The massive clusters generated by H4K20me3 staining could be attributed to very TO-PRO-3 dense regions, as reflected by the line scan (C4).

4.2 Changes in nuclear 3D topology after Chaetocin treatment

Since histone lysine methylation is associated with many epigenetic regulations and processes (see the introduction of this thesis), it was tempting to perform manipulative experiments with the SUV39h1 HMT inhibitor Chaetocin. Fortunately this drug was made available by collaborators (A. Imhof, Adolf Butenandt-Institute, Munich) in order to address possible effects of Chaetocin treatment on nuclear architecture. It was interesting to investigate how Chaetocin treatment affects nuclear architecture in general and how it changes H3K9me3 marked (peri)centromeric heterochromatin and its interactions with HP1-alpha in particular.

4.2.1 Test for the assessment of an appropriate Chaetocin dilution

A cytotoxic effect of Chaetocin dependent on cell density and incubation time was previously shown (Greiner et al., 2005). Therefore it was essential to find out a Chaetocin concentration where an effect on H3K9me3 was detectable on the one hand but on the other hand damage of cells by obvious cytotoxic effects should be avoided.

Chaetocin induced cellular oxidative stress 1000 times more potently than H₂O₂ one could proceed from the assumption that cells can bear only very low Chaetocin concentrations (Isham et al., 2006). HFbs were fixed after 24h, 48h, 4days and 7days of treatment with different incubation concentrations. Cell survival was assessed by visual inspection in the phase-contrast microscope (figure 27). Nuclear topology was assayed by IF with an antibody against H3K9me3 and DAPI-counterstaining (figure 30). As shown in figure 27, cells treated with a concentration of 0,1µM and 0,5µM started to die within 48h. HFbs survived well at a

Chaetocin concentration of $0.01\mu\text{M}$. Control cells incubated with DMSO at a concentration of $0.01\mu\text{M}$ showed no growth retardation. Hence, all subsequent experiments with Chaetocin were performed using a concentration of $0.01\mu\text{M}$. This Chaetocin concentration was determined for a initial cell density of 40-50% confluency. Media was not changed throughout the course of the experiment and Chaetocin was merely added at the beginning of the experiment

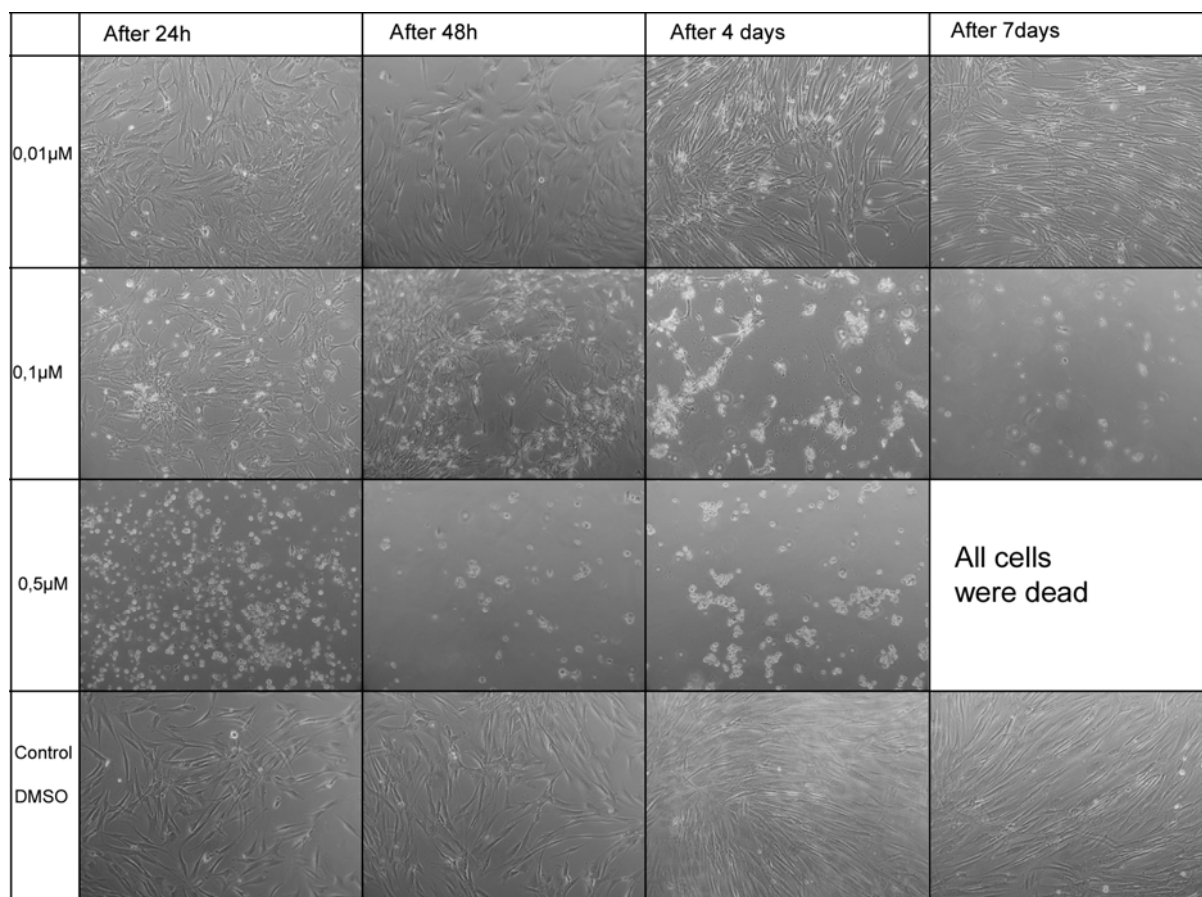


Figure 27

Cell viability in the presence of different Chaetocin concentrations was tested over a time period of one week. HFbs were fixed after 24h, 48h, 4days and 7days. As demonstrated cells treated with a concentration of $0.5\mu\text{M}$ and even $0.1\mu\text{M}$ die within 48h and are dead after a few days. Cells show morphological abnormalities and detach from the cover slip. HFbs survive drug application only at a very low Chaetocin concentration of $0.01\mu\text{M}$. Control cells incubated with DMSO show no striking changes in growth behaviour. Images were recorded at a transmission light microscope (magnification 20-fold).

4.2.2 Test for cells in S-phase

It was important to ascertain that potential changes in nuclear architecture after Chaetocin treatment were not the consequence of any cytotoxic effects of the drug. In order to test the proliferation status, cells were labeled in S-phase by a 1-hour pulse of BrdU incorporation before fixation on days 1, 3 and 7. BrdU was detected by IF (figure 28). Randomly counting

of 200 untreated and treated cells revealed no striking difference in the number of S-phase cells for HFbs as well as MEF cells (Table 7). The proportion of cells in S-phase dropped significantly from around 30% in HFbs and 15-20% in MEFs to values of about 5% after one week. Note that values for control cells and drug treated cells are similar (especially for HFbs). At all time points BrdU labeling was detectable to some extent (~5%). This result supports the earlier assumption (4.2.1) that a Chaetocin concentration of 0.01 μ M has no severe impact on cell viability.

Human fibroblasts			Mouse embryonic fibroblasts		
Time point	Control	0,01 μ M	Time point	Control	0,01 μ M
24h	35%	31%	24h	23%	13%
3 days	9%	11%	3 days	10%	5%
7 days	4%	7%	7 days	3%	6%

Table 7

In HFbs as well as in MEFs the percentage of cells in S-phase decreases, probably because of contact inhibition. At all time points, a similar proportion of cells can be detected in S-phase in control as well as in Chaetocin treated cells confirming the idea that no cytotoxic effects occur after drug application.

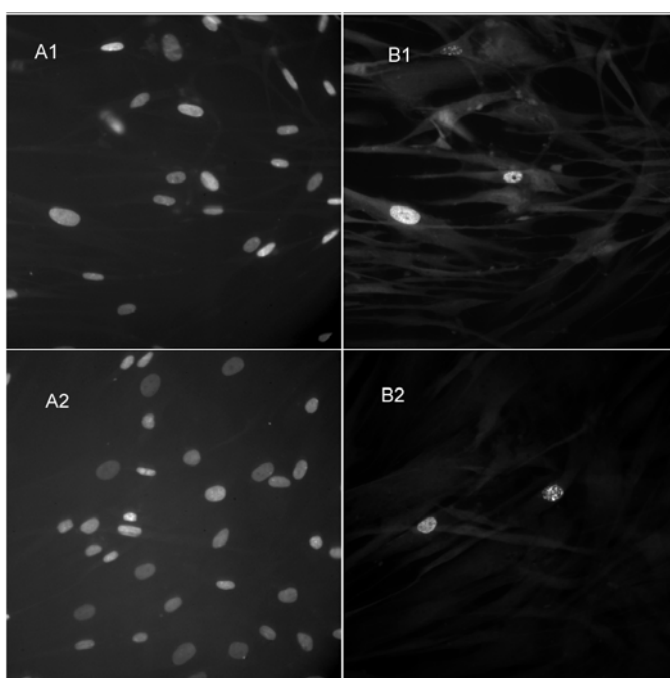


Figure 28

Replication labeling of HFbs in control cells (A1/B1) and Chaetocin treated cells (A2/B2) after seven days. **Column A** shows DAPI-pictures, **column B** cells in S-phase. Despite high confluency (contact inhibition) cells in S-phase can still be found.

All pictures are widefield images taken with a CCD camera at the epifluorescence microscope.

4.2.3 Investigation of cell morphology in a test for Chaetocin cytotoxicity

To ensure that cells were not affected by any cytotoxic effects of Chaetocin the condition of other cellular structures was investigated in a subsequent experiment. Therefore, IF was performed with antibodies against beta-tubulin, B23 and SC35. These markers were suitable to visualize the cytoskeleton, nucleoli and splicing speckles, respectively. Analysis of staining

patterns did not give any hint that changes in these cellular structures occurred after Chaetocin treatment (figure 29). In particular, the fact that patterns of SC35 staining are similar in treated and untreated cells suggests that splicing proceeded normally in the presence of Chaetocin.

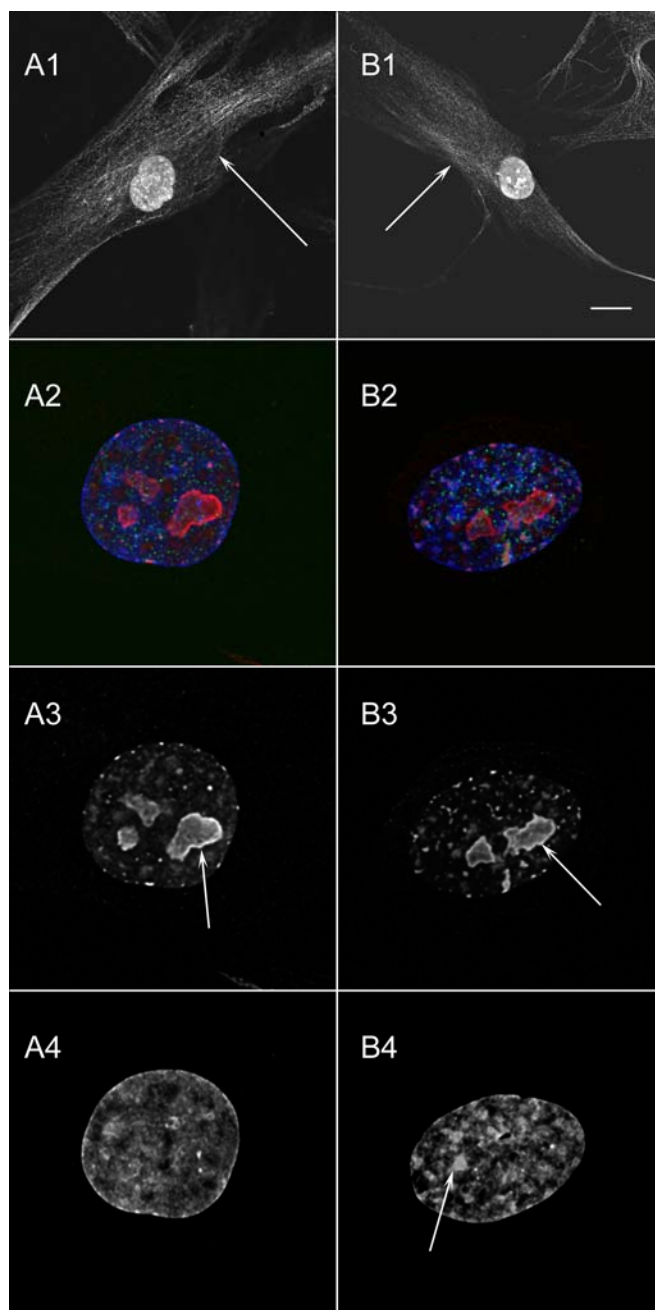


Figure 29

Comparison of different antibody stainings marking cellular compartments in control (**A1-A5**) and Chaetocin treated cells (**B1-B5**) after two days of incubation time.

Human fibroblasts are shown with staining of beta-tubulin (**A1,B1**) to visualize microtubules (microtubules are marked by white arrows), B23/nucleoplasm and SC-35 domains to display nucleoli (big, striking structures), speckles (small foci) (nucleoli are marked by white arrows) (**A3,B3**), DAPI-counterstaining (**A4,B4**) and an overlay of all channels except beta-tubulin signals respectively (**A2,B2**).

A comparison of microtubule staining in control and Chaetocin treated cells did not reveal any cytoplasmic discrepancies after drug treatment. A similar impression was obtained for staining of nucleoli and speckles. At least by visual inspection nucleoli did not display topological changes and speckles were also found in Chaetocin treated cells, thereby indicating splicing activity.

The DAPI-counterstaining pattern revealed the same chromatin reorganization as observed in all Chaetocin treated HFbs, reporting a drug specific effect at the same time. A conglomeration of DAPI-stained chromatin is marked by a white arrow (**B4**).

All images (deconvolved) show z-projections of several confocal mid-sections comprising approximately 1 μ m. Bar indicates 5 μ m

4.2.4 Changes in nuclear topology after Chaetocin treatment

Human fibroblasts were sowed at 40% confluency and incubated with Chaetocin for three days. By IF, a change in the pattern formation of H3K9me3 staining was observed in more than 90% of cells (estimated by visual inspection, data not shown). Aggregation of chromatin

marked by H3K9me3 was distinctly more pronounced compared to untreated cells (figure 30). Surprisingly a decrease in H3K9me3 fluorescence intensity was not observed.

To test whether this finding is reproducible the same experiment with HFb was repeated two times. In all cases, results were similar and revealed a rearrangement of chromatin in the majority of the cells.

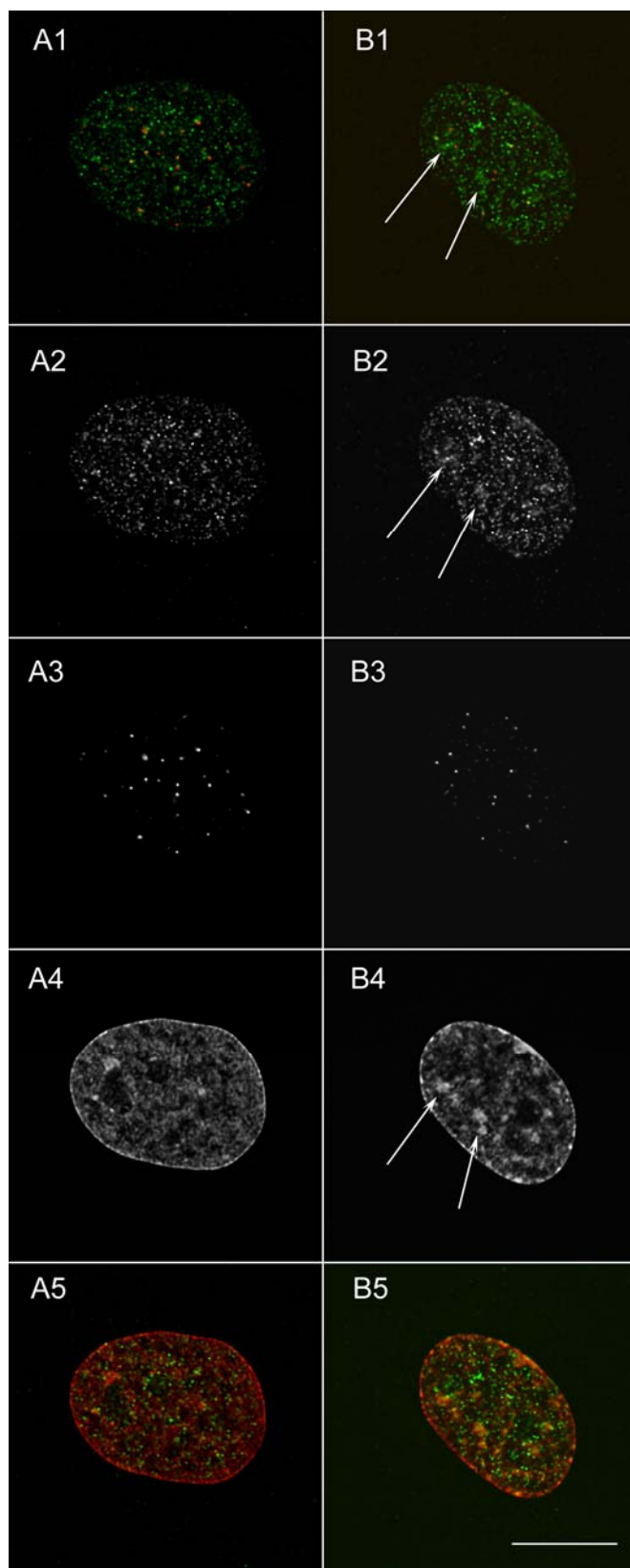


Figure 30

The figure shows single confocal mid sections of human fibroblasts in untreated control cells (**A1-A5**) and 3 days after incubation with 0,01 μ M Chaetocin (**B1-B5**).

(A1/B1) A comparison of the overlay of H3K9me3 (green) with centromere signals (CREST, red) shows that centromeres remain associated with H3K9me3 stained chromatin after drug application. H3K9me3 conglomerations (**B1**) are marked by white arrows.

(A2/B2) H3K9me3 staining in a control cell and 3 days after incubation with Chaetocin. Conglomerations of H3K9me3 (**B2**) are marked by white arrows.

(A3/B3) Centromere signals do not undergo clustering. Clustering as shown in (**B2/B4**) is probably not due to a rearrangement of centromeric heterochromatin.

(A4/B4) Changes in pattern formation are not restricted to H3K9me3 staining but are also reflected in the DAPI-counterstaining. Clusters of chromatin stained by DAPI (**B4**) are marked by white arrows.

(A5/B5) An overlay of H3K9me3 (green) and DAPI-counterstaining (red) underlines the co-localization (yellow color) of chromatin aggregates in both channels.

All images are deconvolved. Bar indicates 5 μ m

Human fibroblasts are characterized by a dot-like H3K9me3 staining pattern without prominent aggregations of constitutive heterochromatin (figure 30,31, A1) (Zinner et al., 2006). To confirm the observation made in HFbs that Chaetocin treatment leads to a reorganization of chromatin marked by H3K9me3 and DAPI (figure 31, C1 and D1), the effect of the drug was investigated in the two immortalized cancer cell-lines, MCF-7 and DLD-1 (figure 31, C2/D2 and C3/D3). DLD-1 cells are characterized by a H3K9me3 staining pattern similar to that of HFbs whereas MCF-7 cells contained big clusters of (peri)-centromeric heterochromatin (figure 31, A2,) (Cremer et al., 2004; Zinner et al., 2006).

However, after the experiments with DLD-1 and MCF-7 cells were performed with the same setup as for HFbs **no** changes in pattern formation for both, H3K9me3 chromatin clusters and AT-rich chromatin visualized by DAPI-counterstaining, were observed (figure 31, C2/D2 and C3/D3).

In HFbs all centromere signals were found associated with H3K9me3 signals indicating that (peri)-centromeric heterochromatin (H3K9me3) was not moving in relation to centromeric signals (CREST-serum). Vice versa no clustering of centromeres was observed after drug application which indicates that the observed aggregations are probably not due to clustering of centromeric heterochromatin (figure 30, A3 and B3). Similar to what was done in the case of HFbs, the experiments with Chaetocin were repeated two times for DLD-1 and MCF-7 cells, without diverging results.

To sum it up Chaetocin treatment lead to a striking reorganization of heterochromatin in normal HFbs but not in MCF-7 and DLD-1 cancer cells.

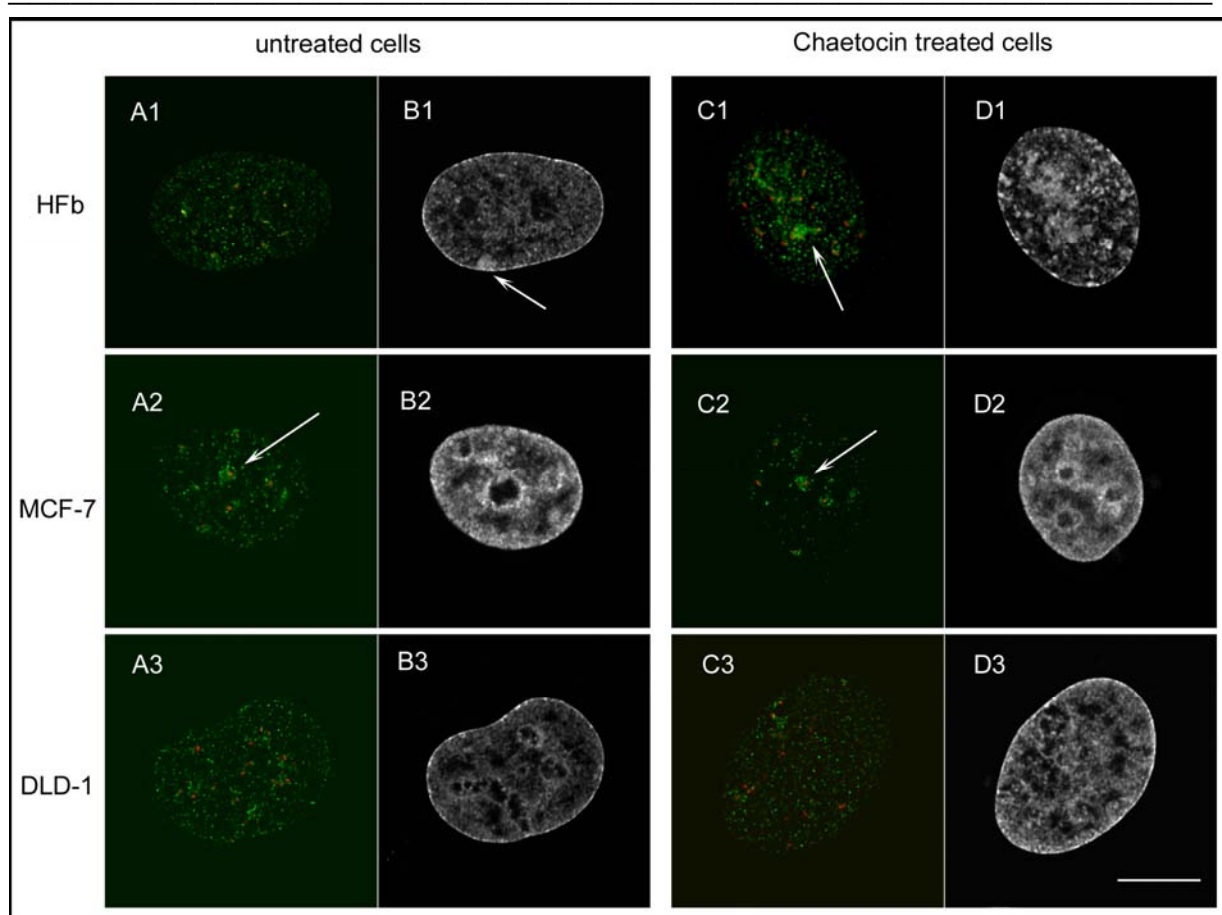


Figure 31

Changes of the H3K9me3 staining pattern occur in HFbs but not in MCF-7 and DLD-1 cancer cells.

Column **A1-A3** shows an overlay of H3K9me3 antibody staining (green) and centromere signals visualized by CREST-serum (red) in all three cell-lines not treated with Chaetocin. Centromere signals are always associated with H3K9me3 staining independent of their aggregation size. Heterochromatin clusters are unspectacular in HFbs and DLD-1 cells. However MCF-7 cells display a low number of big heterochromatic blocs. DAPI-counterstaining is shown in column **B1-B3**. In the untreated cells DAPI-counterstaining appears “normal”, in **B1** the inactive X can be identified (white arrow).

3 days after incubation with Chaetocin, an aggregation of chromatin occurs in HFbs which can not only be visualized in the H3K9me3 staining (**C1**) but also in the DAPI-counterstaining (**D1**). The cancer cell -lines MCF-7 and DLD-1 do not show changes in chromatin formation neither on the basis of H3K9me3 staining (**C2,C3**) nor DAPI-counterstaining (**D2,D3**).

All images are deconvolved and show a projection of five confocal mid-sections of a nucleus (comprising a thickness of 1 μ m). Bar indicates 5 μ m

4.2.5 Investigation of HP1-alpha distribution after Chaetocin treatment

The role of H3K9me3 as a binding site for heterochromatin protein 1 (HP1) was first shown in *Drosophila* experiments (Aagaard et al., 1999). Structure-function relationships and intercellular dynamics as well as hypothetical models suggesting how HP1 could act as a

chromatin crosslinker to organize peripheral heterochromatin have been recently described (Singh and Georgatos, 2002).

To investigate the interrelationship of HP1-alpha and H3K9me3 after Chaetocin treatment co-immunostaining was performed. Co-localization of these two targets was evaluated in 10 nuclei for each cell line. Visual inspection and co-localization analysis in untreated and Chaetocin treated cells revealed an association of H3K9me3 and HP1 in heterochromatic regions for all cell types. The images demonstrate to some extent overlay of H3K9me3 and HP1-alpha (figure 32, B1 and C1, yellow color). The increased co-localization observed after drug treatment coming along with chromatin condensation has no consequences for the overlapping volume of signals obtained for H3K9me3 and HP1-alpha staining. The evaluation of signals for DLD-1 and MCF-7 cells also revealed an association of H3K9me3 and HP1-alpha signals. DLD-1 cells, having smaller heterochromatin and HP1 clusters, give smaller co-localization values (15-25%) when compared to MCF-7 cells which display very prominent aggregations of heterochromatin (30-50%).

The observed discrepancy in co-localization of H3K9me3 and HP1-alpha in DLD-1 cells before and after Chaetocin treatment is probably due to interexperimental variability. Regarding the fact that many of the smaller foci of both signals, deriving from H3K9me3 and HP1 staining, are not overlapping, the overall co-localization values basing predominantly on overlap of pericentromeric heterochromatin can be considered as rather high. The higher volume of overlap after drug application compared to control cells in HFbs is probably due to cluster formation where most of the overlap occurs (overlap of smaller foci can be neglected).

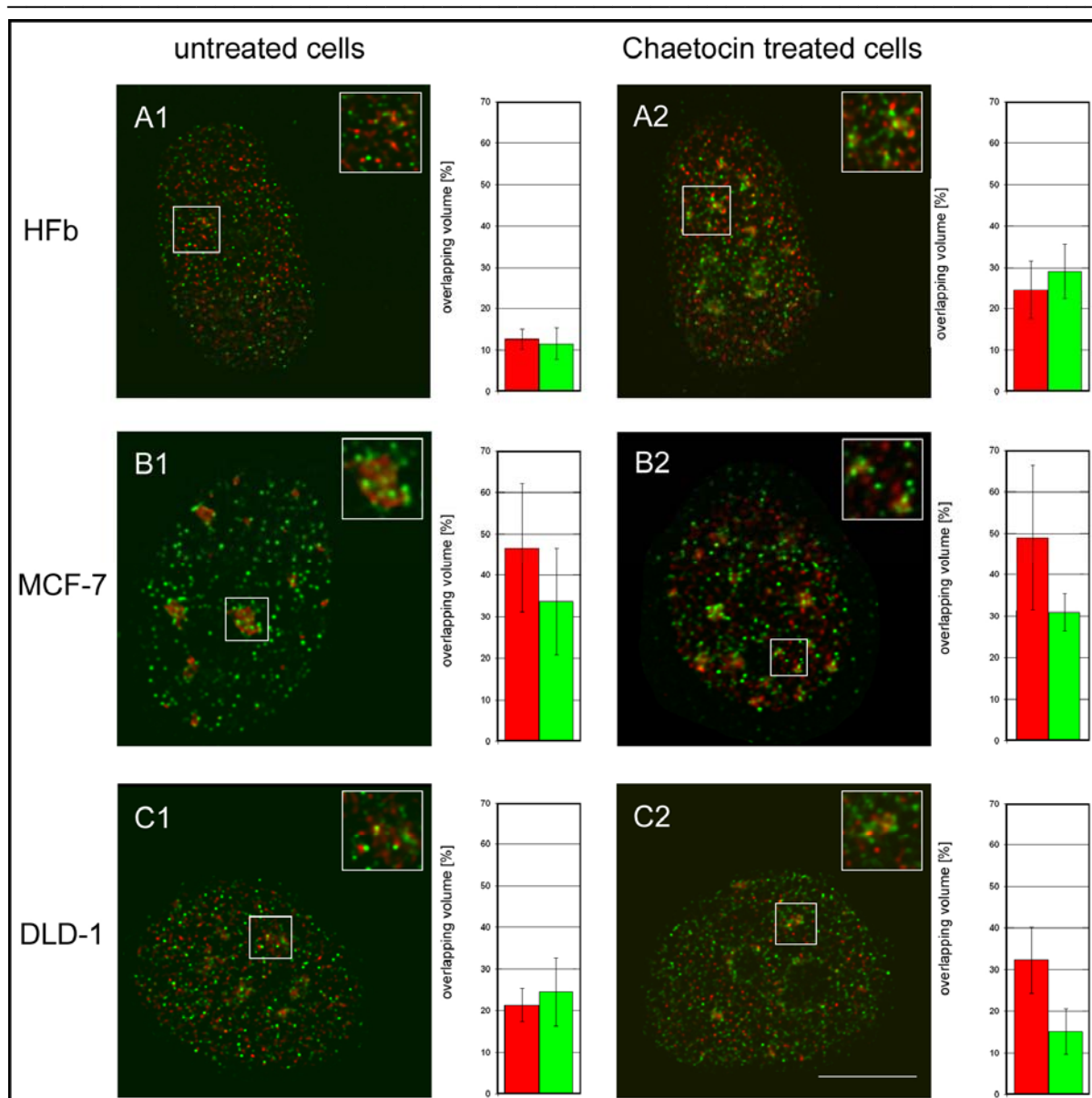


Figure 32

Antibody staining patterns of H3K9me3 and HP1 alpha in control and Chaetocin treated cells.

In all images and diagrams H3K9me3 signals are shown in green, whereas red color indicates HP1-alpha pattern formation. In all cell types HP1-alpha is associated with H3K9me3 in untreated control cells (**A1-C1**) and Chaetocin treated cells (**A2-C2**). In MCF-7 (**B1,B2**) cells the co-localizing volume appears almost identical. DLD-1 (**C1,C2**) revealed a slightly different co-localizing volume after drug application, and only in untreated HFbs differences in the overlapping volume compared to Chaetocin treated cells were observed (**A1,A2**).

All images are deconvolved and display a projection of five confocal mid-sections (comprising a thickness of 1 μ m of a nucleus). In each case 10 nuclei were used for co-localization analysis. Bar indicates 5 μ m

4.2.6 No reorganization of chromatin occurs after Chaetocin rescue

To test whether Chaetocin-induced changes of the 3D chromatin organization are reversible a rescue assay was performed. HFbs that had been treated for 2 days were washed and cultivated further for another 2 days in absence of the drug. HFbs incubated for two days with DMSO at the same concentration as the Chaetocin treated cells served as control.

Cells were incubated in the presence of Chaetocin for two days to allow the cells to complete at least one cell cycle which is in this case probably necessary for chromatin aggregation. This assumption was based on the observation that treatment for 8h did not lead to changes in overall chromatin assembly (data not shown). Indeed, changes in chromatin organization were not found until 24h after treatment (data not shown), a time interval which corresponds approximately to the cell cycle duration in HFbs (diploma thesis A.Engelhard, 2001). Staining of these cells with antibodies directed against H3K9me3 and DAPI- counterstaining did not show a reversion to the chromatin state observed in untreated cells (figure 33). The H3K9me3 staining and AT-rich chromatin phenotypical aggregations found after Chaetocin treatment were maintained.

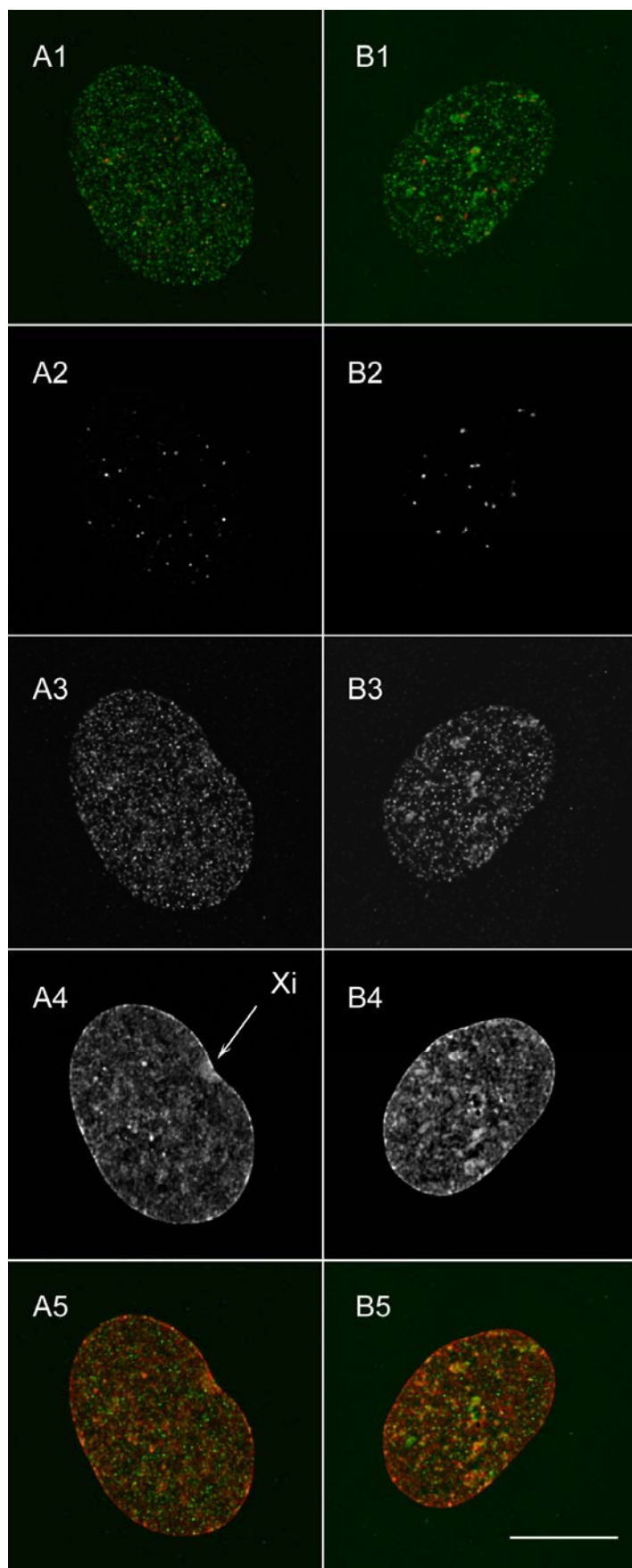


Figure 33

Rescue assay in HFbs two days after Chaetocin application.

Pattern formation of DAPI-counterstaining (**A4,B4**) and H3K9me3 staining (**A3,B3**) in control (**A1-A5**) and Chaetocin treated cells (**B1-B5**) after release.

(**A2,B2**) Centromere signals detected with CREST-antiserum, and H3K9me3 staining pattern (**A3,B3**) are shown. The formation of large heterochromatin clusters is eye-catching in nuclei incubated with Chaetocin. As exemplified in the overlay images, centromere signals (red) are associated with H3K9me3 (green) in untreated cells (**A1**) and after Chaetocin treatment (**B1**), although H3K9me3 cluster formation is much more prominent in cells incubated with the drug.

In the control nucleus, the Xi can be seen in the DAPI-counterstaining (**A4**, white arrow). Otherwise DAPI-counterstaining is inconspicuous whereas chromatin rearrangements that are similar to changes in the H3K9me3 pattern can be found in drug treated nuclei (**B4**).

An overlay of the H3K9me3 staining pattern (green) with DAPI-counterstaining (red) revealed an articulate overlap of big heterochromatin clusters after drug application (**B5**) while in control cells overlap can be found at the Xi and in some areas at the nuclear periphery (**B4**).

All images are deconvolved.

All images show z-projections of several confocal mid-sections comprising a thickness of 1 μ m. Bar indicates 5 μ m

4.2.7 Evaluation of H3K9me3 pattern size in Chaetocin experiments

Changes in H3K9me3 (and HP1) pattern formation were obvious by visual inspection but in order to quantitate these changes an evaluation method using Image J 3D object counter was applied. Therefore the number of objects was classified into objects containing >500 voxels and objects containing >1000 voxels across threshold values (THs) ranging from 15 to 60.

As an illustration of the volume occupied by objects >500 and >1000 voxels, 3D-reconstructed images of heterochromatin foci with the very voxel sizes are shown (figure 34). Therefore the THs of a centromere signal were set in a way that signals with a volume of exactly 500 and 1000 voxels remained.

Centromere signals labelled with the CREST-serum have a volume of approximately 100 voxels after deconvolution. Therefore, it seemed adequate to choose values of >500 and >1000 voxels for those adjacent blocks of constitutive heterochromatin that are visualized by H3K9me3. As shown in figure 34 these volumes reflect estimated sizes of heterochromatin clusters which seemed suitable for the investigated cell-lines. The number of objects was measured over a TH-range from 0 to 60 in a stepsize of five. Due to deconvolution the overall chosen THs had to be rather low because deconvolution reduced signal intensity significantly.

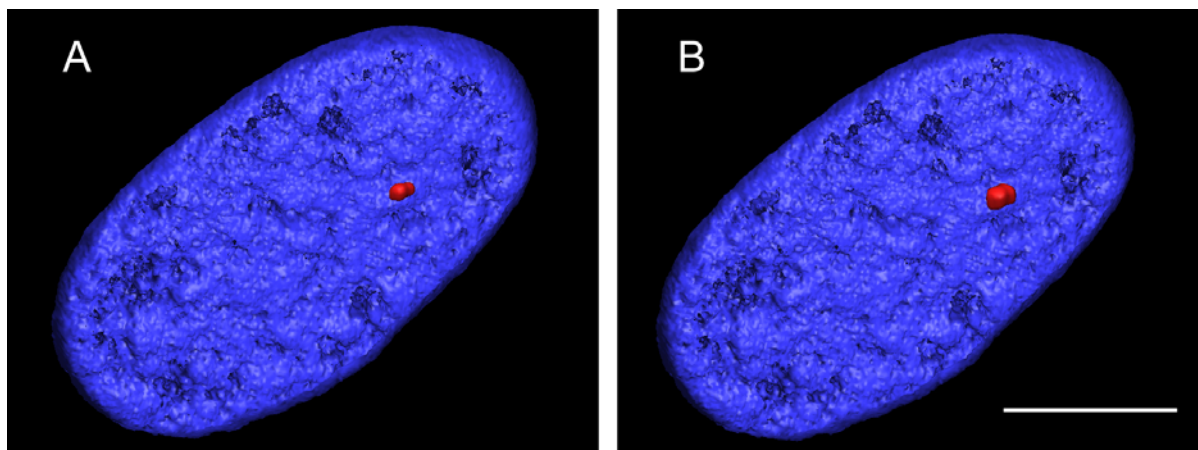


Figure 34

The images show a 3D-reconstruction of a HfB nucleus containing an object of 500 voxels (**A**) and of 1000 voxels (**B**). The objects shown correspond in size to typical H3K9me3 heterochromatin clusters. DAPI-counterstain is shown in blue. The pictures are just to illustrate the size of both objects classes used in the evaluation of H3K9me3 aggregations shown in figure 31 for control and Chaetocin treated cells. Bar indicates 5 μ m

In HfB control nuclei, distinct objects were only observed at TH < 30 for both classes (>500 and >1000 voxels). At such low THs, the impact of background blur on signals is not negligible and might lead to overestimation of the number of objects. Already at TH 20, both curves

plunge down rapidly and finally reach zero at TH 30. The small number of objects and the rapid decline indicate the absence of heterochromatin clusters visualized by H3K9me3 staining (figure 35).

The overall number of objects in HFbs is significantly higher in cells incubated with Chaetocin than in control cells. Numerous heterochromatin clusters can also be found at higher THs in treated cells, indicating that the delineated clusters after H3K9me3 staining (see respective images in figures 30 B1/B2 and 31 C1) are more intense and bigger than in control nuclei. With rising THs they decay into smaller clusters that are still above a size of >500 voxel and >1000 voxel respectively. The observation that the number of objects reaches zero at TH 60 for objects >500 voxel and at TH 50 for objects >1000 voxel supports the idea that in this case the heterochromatin clusters are not only bigger compared to control cells but persistent over a wider TH range as well.

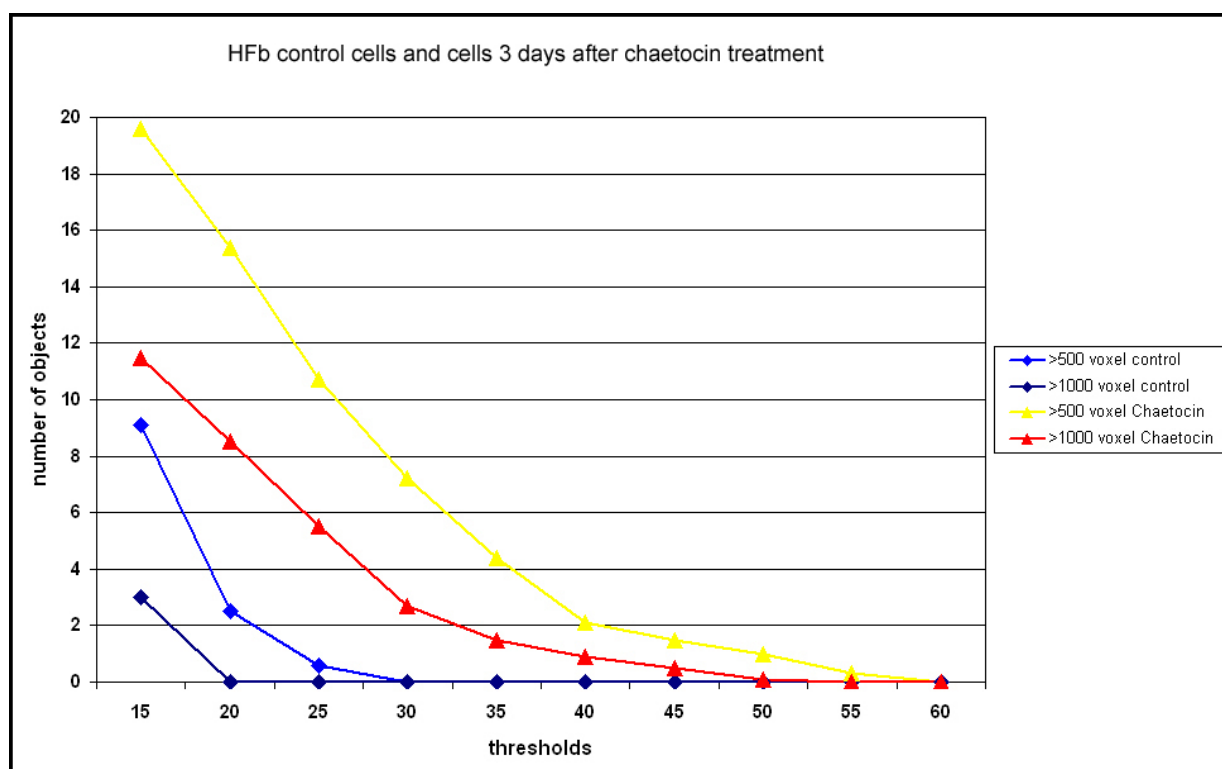


Figure 35

The figure shows the behavior of two big object classes (>500 and >1000 voxels) over thresholds ranging from 15 to 60 for control HFb cells and Chaetocin treated cells. It can be deduced from the curves that drug treated cells (yellow and red curve) show higher numbers of big objects at low thresholds than control cells (light blue and dark blue). Chaetocin treated cells show also more heterochromatin clusters with a volume bigger than 1000 voxel (red curve) compared to untreated cells with a volume of more than 500 voxel (light blue curve). The curves for the untreated cells decrease much more slowly to zero while the curves of the controls drop suddenly to zero at low thresholds indicating that the investigated heterochromatic clusters are more intense and stable. Number of objects were counted for 15 nuclei in each case.

Based on evaluation experience obtained from HFbs, in MCF-7 and DLD-1 cells object analysis was carried out only for THs 25 and 35. As shown in the figures 36 and 37, the numbers of objects are rather similar for both classes in control and Chaetocin treated cells. In MCF-7 nuclei the mean number of objects for objects >500 voxel was 17 (control) compared to 12 (Chaetocin) at threshold 25. As expected, the number of objects was smaller at TH35 but again similar in control and drug treated cells (5 versus 6 objects). In the object class >1000 voxel, the number of objects was in general lower than evaluated for smaller clusters but resulted again in very related numbers at both investigated THs for control and Chaetocin treated cells. To summarize the corresponding pointpairs delineated in the diagram after evaluation of clusters in control and Chaetocin treated cells can be found close to each other at both investigated THs, thereby demonstrating that H3K9me3 pattern size and number in MCF-7 cells remains rather similar after Chaetocin treatment (figure 36).

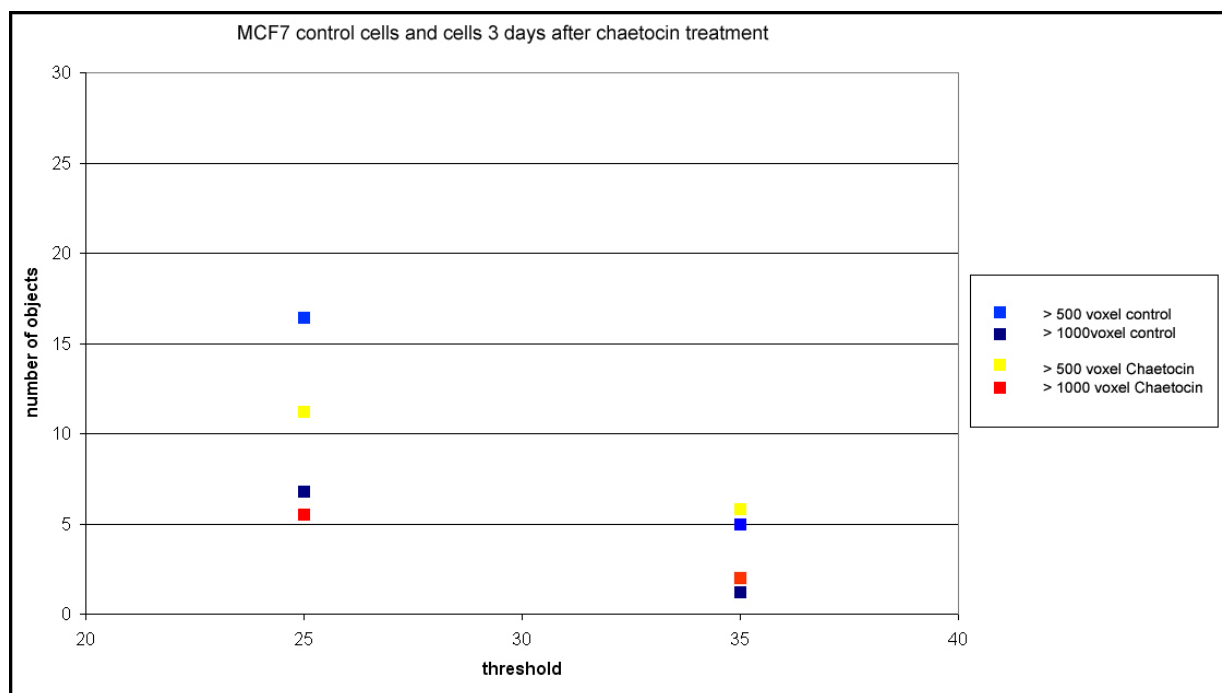


Figure 36

H3K9me3 heterochromatin clusters with an object size of > 500 and >1000 voxel in MCF-7-control and Chaetocin treated cells. Evaluation was performed exemplarily for thresholds 25 and 35 which already proved to be representative as deduced from curves of HFbs (figure 35). MCF-7 cells are well known for their big constitutive heterochromatin clusters (see figures 31 and 32). At threshold 25 many clusters with a volume >500 voxel exist and also a few with a volume of >1000. Even at threshold 35 some objects of the size assigned to both object classes can be found, reflecting the high intensity and persistence of these clusters. Furthermore the corresponding pointpairs of control and Chaetocin treated cells can be found close to each other, thereby demonstrating that H3K9me3 pattern formation remains similar after Chaetocin treatment.

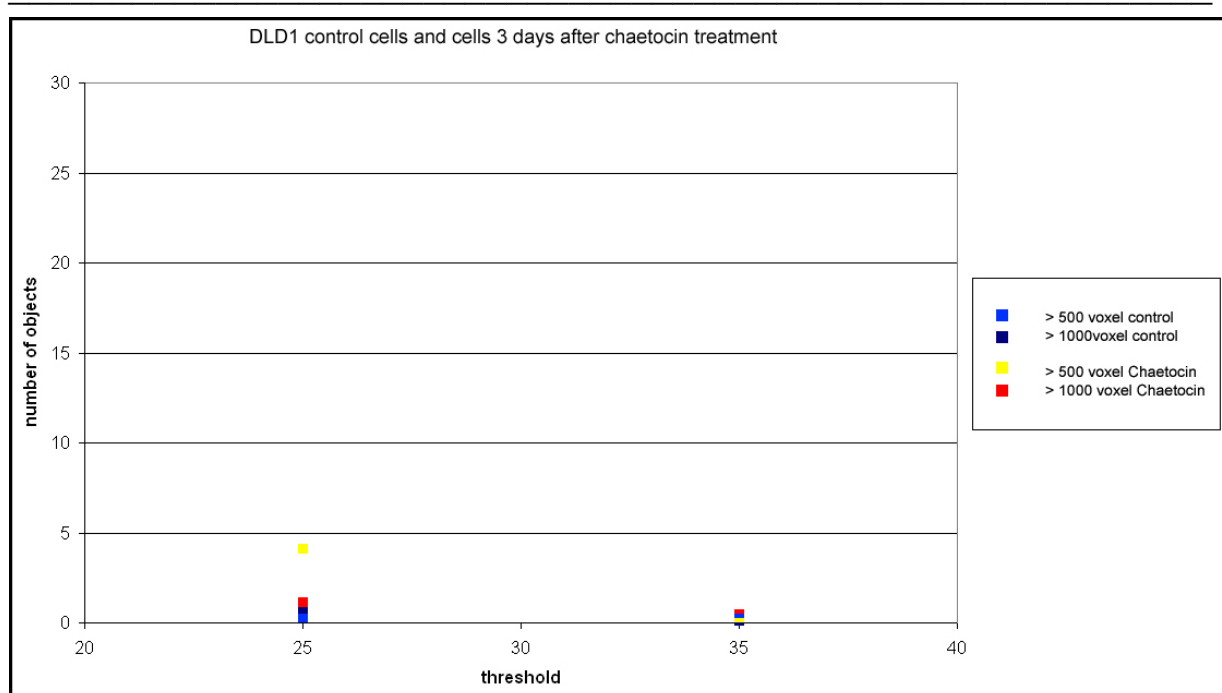


Figure 37

Behavior of objects visualized by H3K9me3 staining in DLD-1-cells. As illustrated in figures 31 and 32 DLD-1 cells display an inconspicuous heterochromatin staining pattern with small aggregations of constitutive heterochromatin. Already at threshold 25 only very few objects >500 voxel were detectable. The number of objects >1000 tends to zero. At threshold 35 in both, control and Chaetocin treated cells, the number of objects is around zero, emphasizing the impression from the deconvolved images that DLD-1 cells exhibit no formation of bigger heterochromatin clusters after drug application compared to control cells.

In DLD-1 cells 3D object counting resulted in very low amounts of objects in all investigated cases (figure 37), thereby indicating that Chaetocin treatment does not alter the chromatin pattern.

4.3 Lysine methylation sites and specific chromatin segments

After it was shown that histone lysine methylation patterns are largely arranged in distinct nuclear zones (Zinner et al., 2006), the next step was to investigate whether these clusters and foci are reflected on the one hand on a more global (chromosomal) level and if these staining patterns on the other hand can be characterized at “high resolution” down to chromosomal subdomains.

To combine immunostaining of lysine methylation sites and FISH techniques, a protocol had to be puzzled out (see methods and protocols 3.10), that allowed the simultaneous delineation of chromosome territories (CTs) in 3D preserved nuclei together with the histone methylation sites at a best preserved morphology (referred to as Immuno-FISH). For quantitative evaluation of the overlap-extent of signals in two different channels we used the

Manders coefficients M1 and M2 (first described by Manders, see 3.14.3 (Manders et al., 1993)).

4.3.1 Modifications correlate with gene density on the chromosomal level

Focus was on the investigation of spatial associations between the modified lysines H3K4me3, H3K9me3 and H3K27me3 (because they are the most stable and best characterized modifications) and the human chromosome territories (CTs) of HSA18 and HSA19 to get an impression of their topology on the chromosome level in intact cell nuclei.

HSA18 is the autosome with the lowest gene density (mean gene content 5.3 genes/Mb) and an overall low expression level. It is proportioned in predominantly equal parts of R- and G-bands, most of them intensely stained (Francke, 1994; Nusbaum et al., 2005). HSA 19 has the highest gene density in the human genome (25 genes/Mb). It is enriched in Alu sequences, contains mostly weakly stained G-bands and displays an overall high expression level (Caron et al., 2001; Grimwood et al., 2004). Genes are evenly distributed along the chromosome except for the gene-poor heteromorphous region 19p12 to 19q12 (<10 genes/Mb) that flanks the immediate pericentromeric region over approximately 6Mb. For detailed information on gene density along the chromosomes #18 and #19, see figure 38.

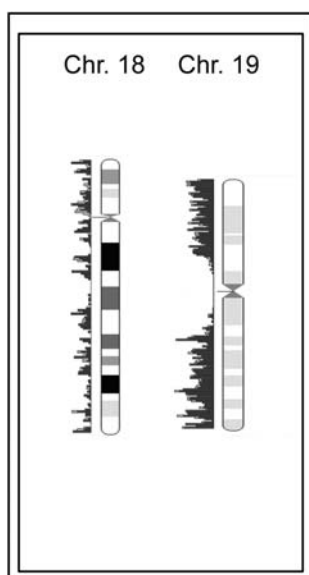


Figure 38

In courtesy of Katrin Küpper

Ideograms of human chromosomes HSA #18, 19 together with their gene-density profile (left of the ideogram).

The pattern marked by H3K9me3 staining and its spatial association with chromosomes #18 and #19 is shown in figure 39 (A1-A3). By visual inspection one could get the impression that the rather branched territory of #19 is overlapping to a higher extent with H3K9me3 than territory of #18. However co-localization values averaged from twelve nuclei were almost identical (30%, figure 39 A4). This means that for H3K9me3 no differences between chromosomes #18 and #19 were observable despite of their varying properties regarding state of “compaction”, gene content and transcriptional activity.

Striking for H3K27me3 staining in HFbs is the inactive X-chromosome (white arrow, figure 39 B1). Apart from Xi the antibody pattern consisted of many small foci throughout the nucleus with a slight pronounciation at the nuclear rim (figure 39, B1-B3) (Zinner et al., 2006). No differences in the overlapping volume of H3K27me3 and chromosomes #18 and #19 were observable as co-localization analysis for both chromosomes resulted in 10% overlap for each of them.

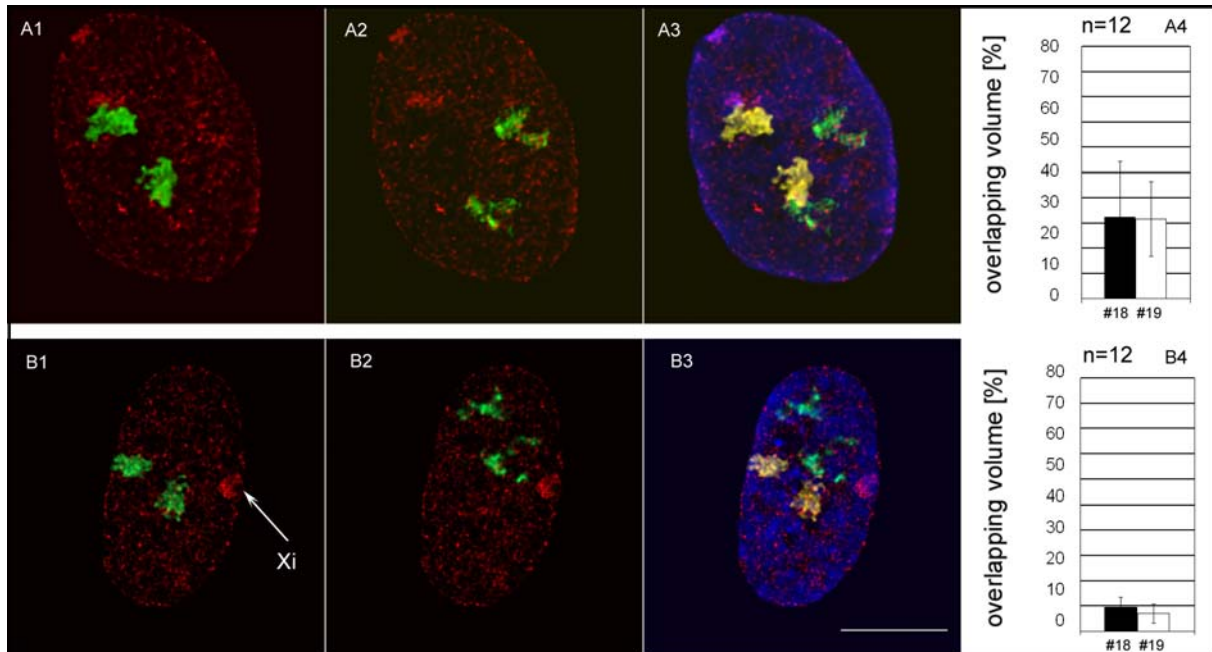


Figure 39

Immuno-FISH delineating H3K9me3 and H3K27me3 together with CTs #18 and #19. **(A1-A3)** single optical section of a HFb nucleus with H3K9me3 (red) and painted CTs #18 (green) **(A1)** and CTs #19 (green) **(A2)**. The cluster formations of H3K9me3 likely indicate pericentromeric heterochromatin. **(A3)** merged image with nuclear counterstain (blue), CTs #18 are shown here in yellow. **(A4)** Quantitative co-localization analysis of H3K9me3 with CTs #18 (black bar) and #19 (white bar). **(B1-B3)** single optical section of a HFb nucleus with H3K27me3 (red) and painted CTs #18 (green) **(B1)** and CTs #19 (green) **(B2)**. The focal cluster in **(B1)** and **(B2)** marks the region of Xi (arrow) strongly decorated by H3K27me3. **(B3)** merged image with nuclear counterstain (blue), CTs #18 are again shown in yellow. **(B4)** Quantitative co-localization analysis of H3K27me3 with CTs #18 (black bar) and #19 (white bar). All images are deconvolved. Bar indicates 10 μ m, n = number of evaluated nuclei.

As shown in figure 40 co-localization of H3K4me3 differed distinctly for CTs #18 and #19 (G,H). Gene-poor chromosome 18 is predominantly located in H3K4me3 free areas, whereas chromosome 19 co-localizes with the antibody staining to a higher extent. The nuclear periphery is almost devoid of H3K4me3 staining. Only 10% of chromatin assigned to CT #18 co-localized with H3K4me3 whereas more than 40% of CT #19 were attributed to H3K4me3 (figure 40, diagram). Thus, the approximately fourfold higher values for #19 compared to #18 after co-localization analysis matched both properties of these chromosomes, gene content and transcriptional activity.

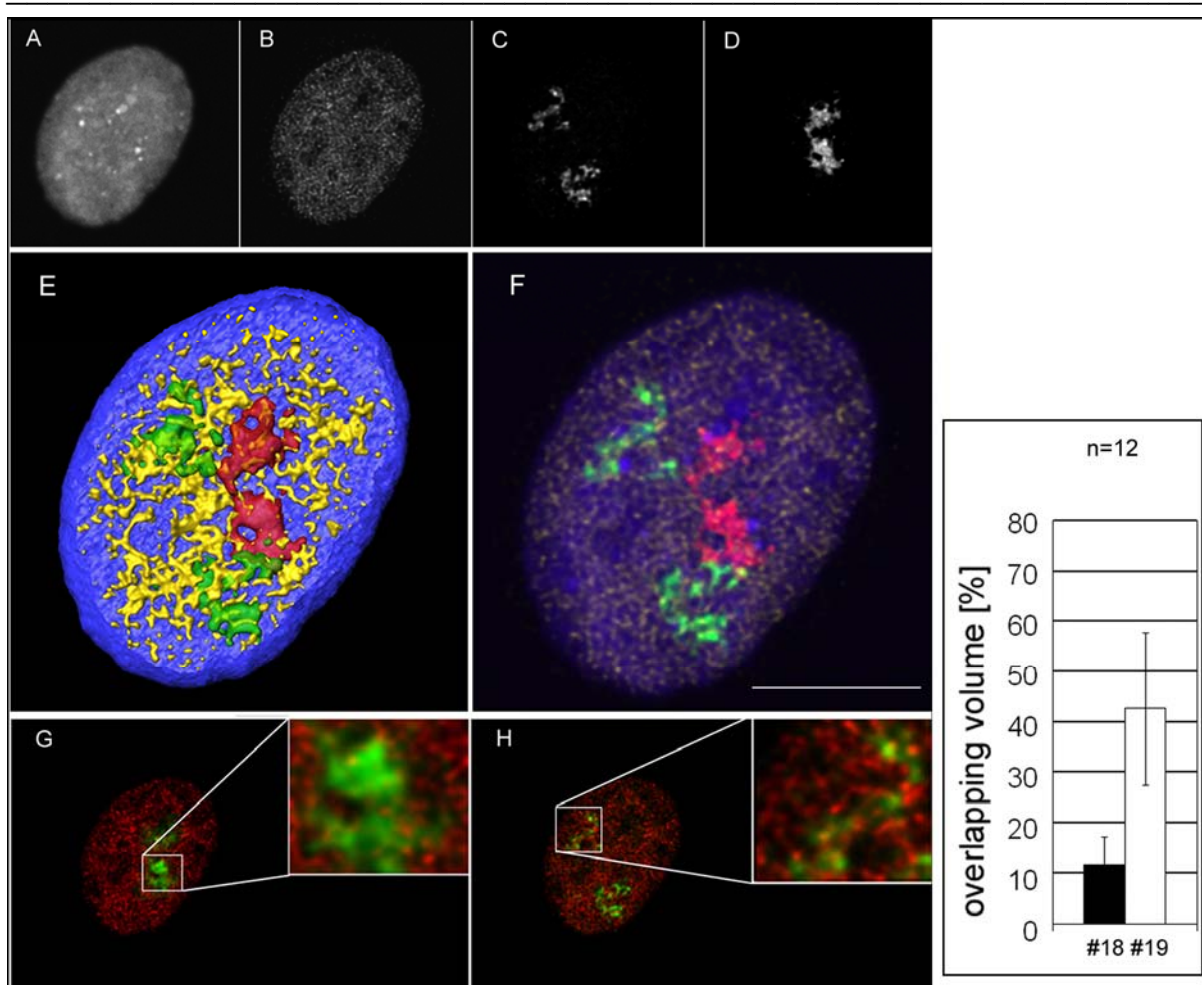


Figure 40

Immuno-FISH delineating H3K4me3 together with CTs #18 and #19. **(A-E)** single optical confocal section of a HFb nucleus. **(A)** DNA counterstain, **(B)** H3K4me3 staining, **(C)** painted CTs #19, **(D)** painted CTs #18, **(F)** overlay. **(E)** 3D image reconstruction of the whole nucleus (CT#18 red, CT#19 green), (the nuclear counterstain is slit to show the nuclear interior) using Amira 3.0 TGS software (<http://www.amiravis.com/>). H3K4me3 staining (yellow) is spared from the nuclear periphery. **(G-H)** magnifications of chromosome paints 18 **(G)** and 19 **(H)** together with H3K4me3. The territory of chromosome 18 is located in an area of low antibody staining whereas the more branched appearing chromosome 19 colocalizes at several regions with H3K4me3 **(I)** Quantitative colocalization analysis of H3K4me3 with CTs #18 (black bar) and #19 (white bar) confirm the visual observation of a different degree of overlapping for the CTs #18 and CTs #19 with H3K4me3. All images are deconvolved. Bar indicates 10 μ m, n = number of evaluated nuclei.

4.3.2 “Holes” in chromosome paints are filled with heterochromatin

After applying deconvolution on raw data sets, holes in many paint signals and Xi visualized by H3K27me3 staining were eye catching (and example is shown in figure 44 A,B and C). Since repetitive DNA-sequences are depleted from paint probes (Bolzer et al., 1999), the hypothesis that (peri)centromeric regions are embedded within these holes was tested. Therefore the approved Immuno-FISH protocol was applied. Immuno-FISH with CREST-serum (centromeres), H4K20me3 (constitutive heterochromatin) and X-paint probes, was accomplished. As can be verified by visual inspection, both centromere and H4K20me3 signals were embedded in the paint at the position of the hole (in most cases one hole per paint). This observation could be confirmed by analyzing the chromosome territory through intensity profiling. The maxima in the curve of centromere and H4K20me3 signals coincided with a minimum in the curve of the painted territory signals (figure 41).

The finding that “holes” in these type of chromosome paints always contain (peri)centromeric heterochromatin could provide additional information concerning organization of chromosome territories.

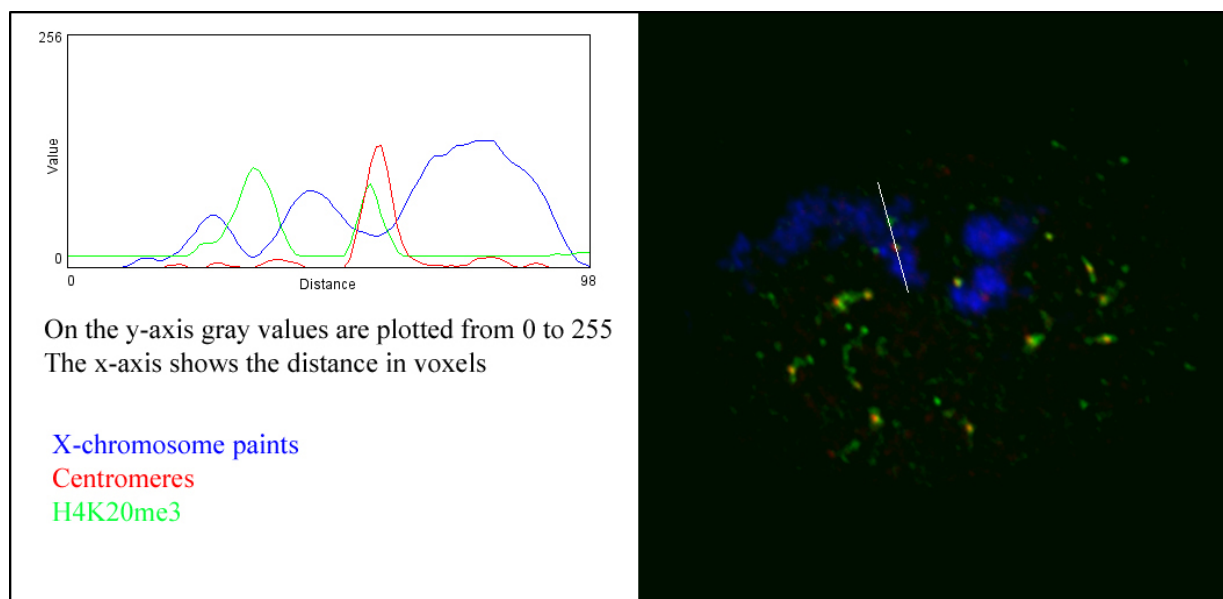


Figure 41

Linescan through a region of one of the X-chromosome territories that contains centromere and H4K20me3 signals. The white line defines start and end of the intensity profile. The curves of signal intensity for constitutive heterochromatin (H4K20me3, green) and the centromere (red) show negative correlation to the curve of the X-chromosome paint (blue). This means that in areas where the paint signal is low intensity peaks of the other two signals can be found. The second peak of the H4K20me3 signal (which is not associated with centromeres) indicates that the paint probes are really depleted of all repetitive sequences. Note that centromere signals are mostly associated with H4K20me3 staining.

Nucleus of a human fibroblast, size 10µm. The image is deconvolved and displays a single confocal mid-section.

4.3.3 Distinct lysine methylations correlate with expression levels

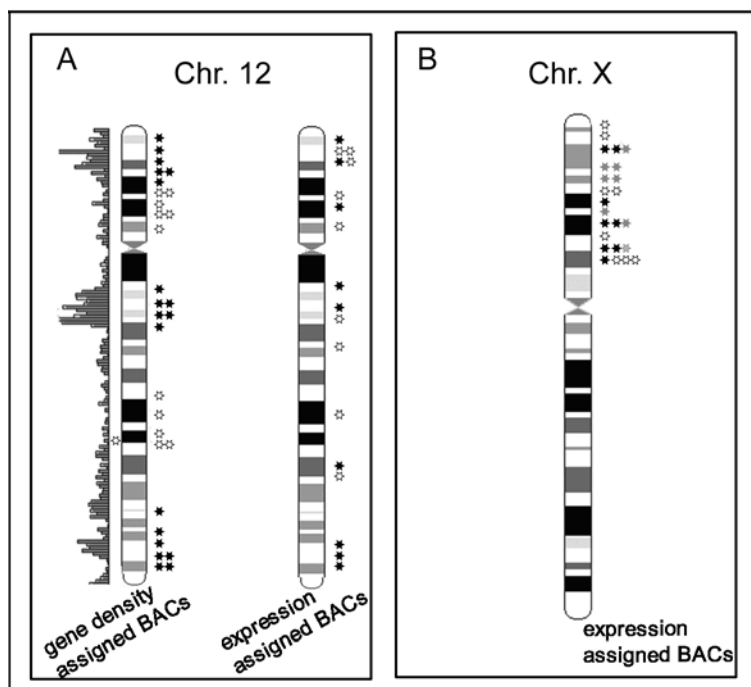


Figure 42

Ideograms of human chromosomes *HSA* #12 and X together with their gene-density profile (left of the ideogram) and chromosomal position of each BAC used in this study. For *HSA* #12 the white dots denote BACs located in a gene-dense region (left) or highly transcribed genes (right), the black dots denote BACs located in a gene-poor region (left) or repressed genes (right). For *HSA* X the white dots denote BACs with highly expressed genes, grey dots with intermediate expression levels and black dots BACs with repressed genes.

In courtesy of K. Teller and K.Küpper

HSA #12 was chosen for the investigation of gene-rich and gene-poor chromatin segments because of its property to present regions where gene densities deviate noteworthy from its overall mean gene density of ~ 13 genes/Mb within size windows of only a few Mb (see figure 42 A, left ideogram) according to the different gene-rich and gene-poor segments. The gene-rich BACs on *HSA* #12 comprised a pool of 19 BAC clones located in the three main gene-dense regions 12p12.3-12p12.32 (38 genes/Mb, ~ 10.5 Mb), 12q13.11-12q13.3 (31 genes/Mb, ~ 11 Mb) and 12q24.11-12q24.32 (16 genes/Mb, ~ 16 Mb). The gene-poor BAC pool consisted of 12 pooled BAC probes comprising the regions 12p11.22-12p12.3 (6,5 genes/Mb, ~ 15 Mb) and 12q21.2-12q21.33 (5 genes/Mb, ~ 18 Mb). BACs from *HSA* #12 containing highly expressed genes and weakly expressed genes respectively were delineated by two BAC pools each containing 9 BAC-clones irrespective of their position regarding the gene density of their environment (see figure 42 A, right ideogram). The values for expression intensity was recently investigated by an Affimetrix gene-chip for humans (U133A) (Geigl et al., 2004) and verified by TR-PCR (Kupper et al., 2007). A BAC clone was classified as highly expressed if it contained at least one gene with an expression intensity >1000 (arbitrary units on the Affimetrix chip) regardless of the expression levels of other genes on the respective BAC. The pool with weakly expressed genes consisted of BAC clones containing only genes with an expression intensity <200 units. All BACs were directly labeled by label PCR (see methods and protocols 3.4.2).

BACs containing gene poor segments or weakly expressed genes were mostly found in H3K4me3 free areas whereas gene rich segments and highly expressed genes were detected often partly overlapped or in proximity of H3K4me3 (figure 43, A,B and E,F). Quantitative co-localization analysis uncovered explicit difference of H3K4me3 overlapping values between gene poor segments (~20%) and gene rich segments (~50% figure 43 D). The same tendency was also demonstrated for weakly expressed genes (~6%) and highly expressed genes (~33% figure 43 H). The discrepancy of absolute values in both experiments, might be partly due to interexperimental variations but of course also the experimental setup, pools addressed to gene density on the one hand and pools addressed to transcriptional activity may play a more decisive part.

Quantitative co-localization analysis for H3K27me3 revealed altogether values lower than 3% for weakly and highly expressed genes (figure 43, L). These findings indicate that H3K27me3 is not associated with the addressed genes but this cannot exclude an overall involvement of H3K27me3 in transcriptional regulation.

A detailed description of the BACs used for this study is given in Küpper et al., 2007 and essential data are summarized in the appendix.

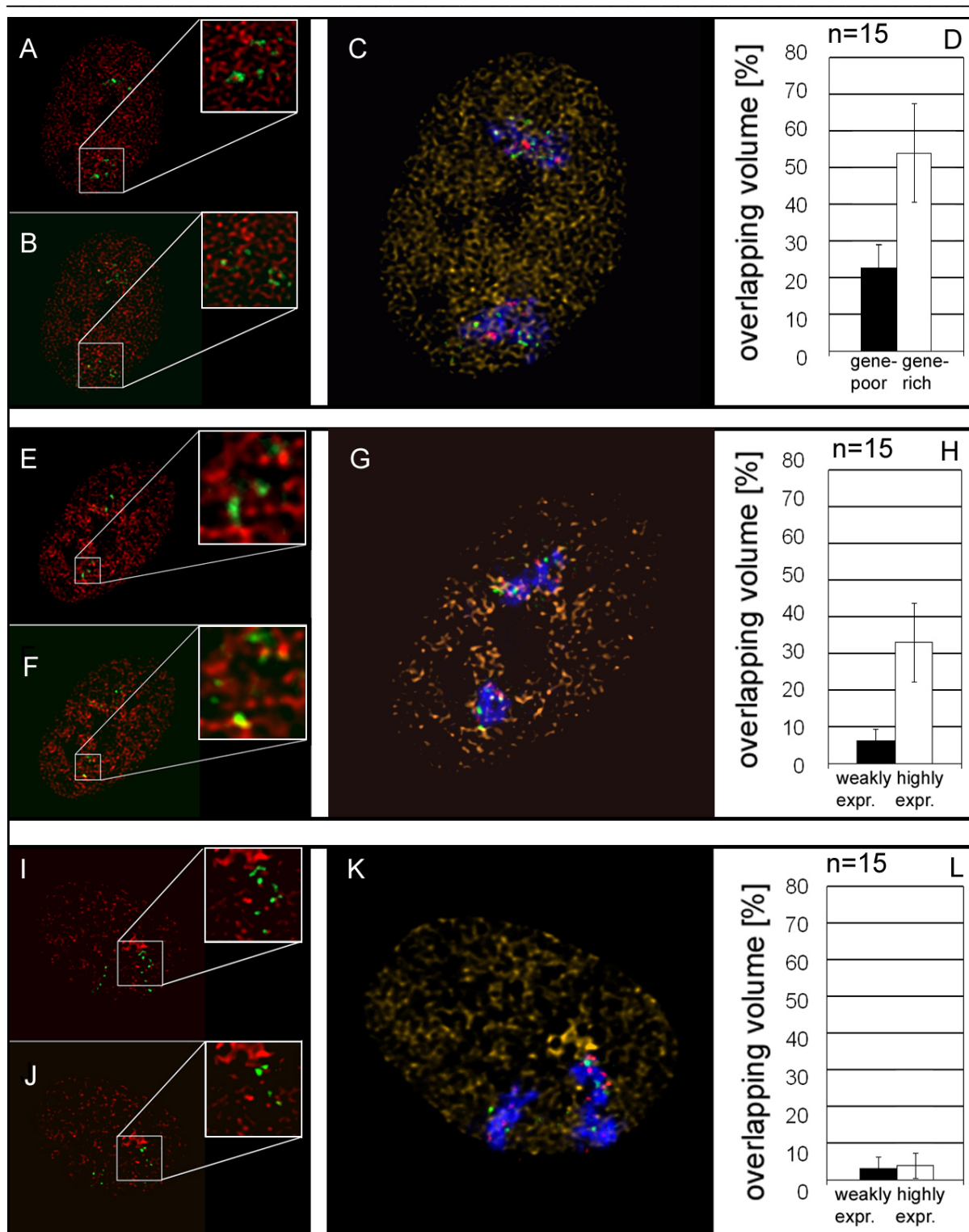


Figure 43

Immunofluorescence of gene-rich/gene-poor DNA segments of *HSA* #12 with H3K4me3 and of highly expressed/repressed genes of *HSA* #12 with H3K4me3 and H3K27me3.

All images represent single optical confocal sections of HFb nuclei after deconvolution. **(A)** pool of gene-poor BACs (green) on CT #12 combined with H3K4me3 staining (red), **(B)** pool of gene-rich BACs (green) on CT #12 combined with H3K4me3 staining (red), **(C)** overlay of H3K4me3 staining (yellow), CT #12 (blue) and gene-poor (red) / gene-rich (green) BAC pools, **(D)** quantitative co-localization analysis of gene-poor / gene-rich BAC pools on CT #12 with H3K4me3. **(E)** pool of BACs containing weakly expressed genes on CT #12 (green) combined with H3K4me3 staining (red), **(F)** pool of BACs containing highly expressed genes on CT #12 (green) combined

with H3K4me3 staining (red). The inset magnifications show BAC signals from repressed gene loci predominantly in H3K4me3 free spaces whereas BACs containing highly expressed genes are more frequently associated with H3K4me3. **(G)** overlay of H3K4me3 staining (yellow), CT #12 (blue) and BACs containing weakly expressed (red) and highly expressed (green) genes. **(H)** quantitative co-localization analysis of H3K4me3 with BACs containing highly and weakly expressed genes on CT #12. **(I)** pool of BACs containing weakly expressed genes on CT #12 (green) combined with H3K27me3 staining (red), **(J)** pool of BACs containing highly expressed genes on CT #12 (green) combined with H3K27me3 staining (red), **(K)** overlay of H3K27me3 staining (yellow), CT #12 (blue) and BACs containing weakly expressed (red) and highly expressed (green) genes **(L)** quantitative co-localization analysis of H3K27me3 with expression assigned BACs. All images are deconvolved. n = number of evaluated nuclei. Size of nuclei = 10 μ m.

To assign more precisely the relationship of H3K27me3 to chromatin segments with different expression levels on the X-chromosome, the spatial relationship of BAC pools (figure 42 B) (8 BAC clones per pool) classified into weakly, mid or highly expressed genes was compared to H3K27me3. Since X-linked gene expression is distinctly lower compared to autosomes, genes with an expression intensity >600 were declared as highly expressed while segments with at least one gene on a given BAC exhibiting a expression intensity between 300-400 were regarded as mid expressed. The BAC pool with weakly expressed genes contained genes with an expression level <200 units.

Co-localization analysis of H3K27me3 with differently expressed BAC-pools was performed separately for Xa and Xi. Chromosome territories of both X-chromosomes were marked by X chromosome specific painting probes. The co-localization coefficients between Xa and H3K27me3 and Xi and H3K27me3 provided an intra-experimental standard in each experiment. The overlapping volume between H3K27me3 and both X chromosomes was clearly different with Xa showing ~6% and Xi ~66% (figure 44, A-D). The magnification (figure 44, C) displays distinct though not total overlap between H3K27me3 and the Xi.

To answer the question to which segments the widely distributed foci could be assigned to, co-localization results of H3K27me3 with BACs containing differentially expressed genes on Xa were regarded as decisive. Analysis of H3K27me3 with highly expressed genes yielded <1% of overlap, while a co-localization value of 40% was noted for the same genes on the Xi (figure 44, E and G). This value is significantly lower as it was measured for the entire X in the same experiment (~65%). This observation is probably due to a considerable amount of genes that escape X-inactivation (~20%).

In an elaborate 5-color immuno-FISH experiment the spatial relationship of H3K27me3 with weakly and mid expressed genes on both Xa and Xi was evaluated (figure 44, H-M). Analysis of Xi revealed almost identical overlapping for mid (~62%) and weakly (~70%) expressed genes. On Xa mid expressed genes yielded a small co-localization value (~5%) comparable to highly expressed genes (~1%). However a discrepancy was found in the co-localization analysis for weakly expressed genes (~16%) with H3K27 on Xa. This value was

more than twice as high as calculated for the overall co-localization of H3K27me3 with the CT of Xa (~7%). The observation that co-localization values for weakly expressed genes on the Xa are distinctly higher than values obtained for weakly expressed genes on HSA #12 suggests a higher impact of H3K27me3 silencing effect on X-chromosomes compared to HSA #12.

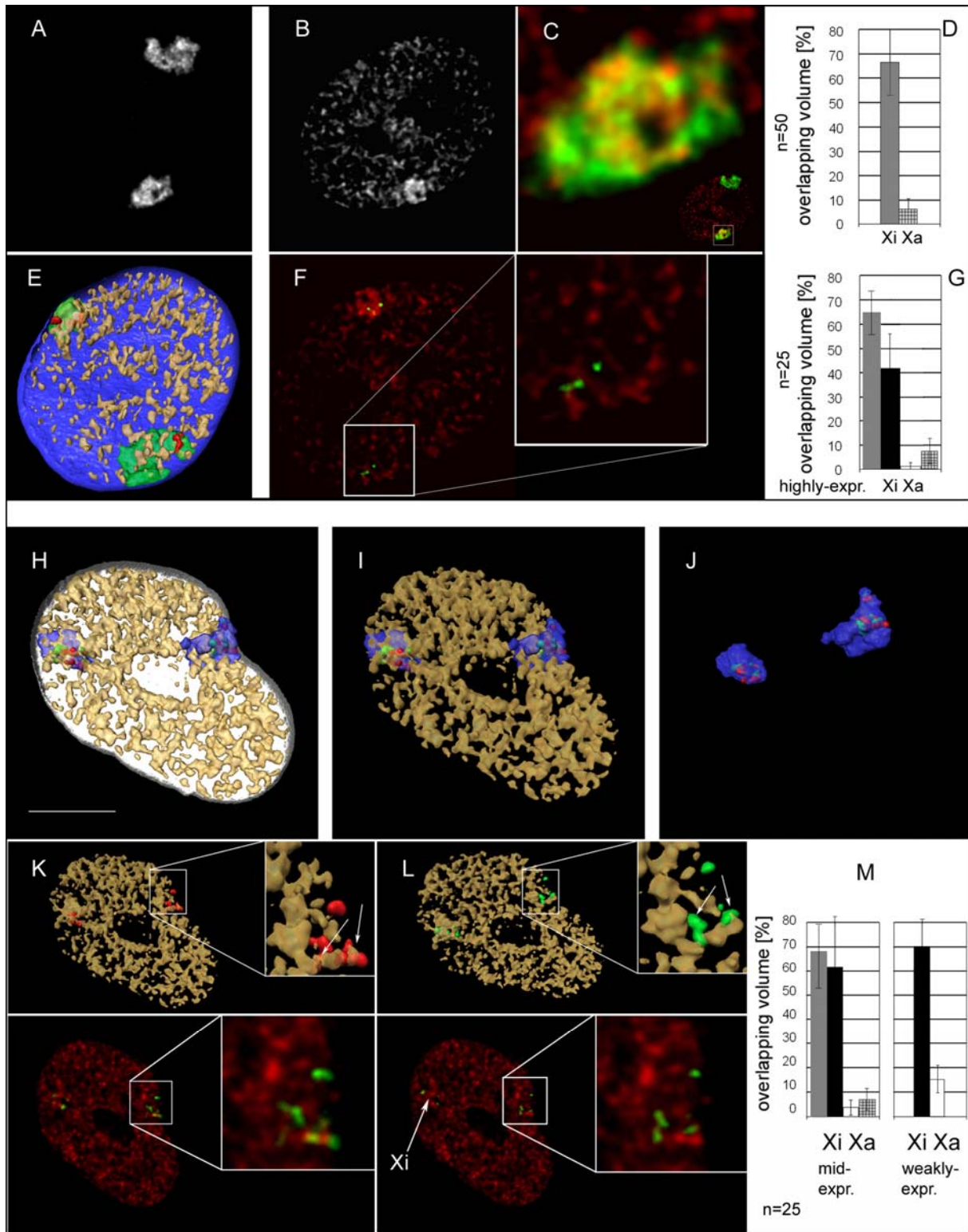


Figure 44

Immuno-FISH delineating X territories and X-specific genes together with H3K27me3. **(A)** single optical confocal section with painted territories of the X chromosomes in a female human fibroblast nucleus. **(B)** H3K27me3 staining of the same section. The insets mark the Xi. **(C)** inset magnification of the merged image of A and B shows distinct areas of intense co-localization between Xi and H3K27me3. **(D)** Quantitative co-localization analysis reflects the different level of H3K27me3 in Xi and Xa. **(E)** 3D reconstruction of an entire nucleus with painted X territories (green), BAC signals containing highly expressed genes (red) and H3K27me3 (golden). **(F)** single optical section of the same nucleus showing H3K27me3 (red) and highly expressed genes from the short arm (green), that exemplify little mutual overlapping at a higher magnification. **(G)** Quantitative co-localization analysis of H3K27me3 with Xi and Xa territories and of H3K27me3 with highly expressed gene loci **(H-I)** 3D reconstruction of a nucleus delineating DNA counterstaining (white, not shown in I) CTs of the X-chromosomes (blue), and BAC probes containing genes with intermediate expression activity (green) and weakly expressed genes (red). **(J)** magnification of the same CTs **(K)** 3D reconstruction (top) and optical section (bottom) comprising H3K27me3 immunostaining and BACs containing weakly expressed genes and **(L)** 3D reconstruction (top) and optical section (bottom) of the same nucleus comprising H3K27me3 immunostaining and BACs containing mid expressed genes. **(M)** quantitative co-localization analysis of H3K27me3 with Xi (grey) and Xa (grey checkered) territories, mid-expressed and weakly expressed gene loci. All images are deconvolved. n = number of evaluated nuclei.

5 Discussion

The present thesis can be subdivided into three main topics. In the first part the 3D architecture and spatial relationships of different histone lysine methylation sites (H3K4me3, H3K9me1, H4K20me1, H3K9me3, H3K27me3 and H4K20me3) with defined nuclear targets like centromeres, nascent RNA and with each other was investigated in various cell types.

The second part comprised experiments that were performed with the SUV39H1 inhibitor Chaetocin.

Concerning the final part a complex immuno-FISH protocol was established first and consecutively an investigation of spatial associations of histone methylation sites (H3K4, H3K9 and H3K27) with distinct chromatin targets on the chromosomal and subchromosomal level was performed.

5.1 Lysine methylation patterns are arranged in nuclear zones

In this work emphasis is put on the nuclear topology and spatial interrelationships of chromatin methylated at several different histone lysine sites. Therefore the use of highly specific antibodies was compulsory. The antibody specificity was tested on MCF-7 cells as they showed the most distinct patterns of all cell types investigated so far (Zinner et al., 2006). All antibodies preincubated with their specific peptide revealed a weak diffuse background without any pattern formation reflecting high affinity to their respective peptide. Even tests for H3K9 and H3K27 which are embedded within the same amino acid sequence "ARKS", did not reveal cross reaction, so subsequent experiments could be performed proceeding from the assumption that all antibodies are highly specific for the epitopes they should recognize.

Despite the fact that all core histones are evolutionary highly conserved in length and amino acid sequence (Baxevanis and Landsman, 1996) methylation sites show plasticity (Peters et al., 2003). This caveat should be kept in mind comparing findings on a certain modification in different cell types of one species to the same cell type in a different species (Martens et al., 2005; Spada et al., 2005).

The data obtained for H3K4me3 in this work is in consistency with what was already known from the literature where it was considered predominantly as a marker for active chromatin. This modification lacked almost any overlap with centromeric regions and the outermost (transcriptionally inactive) nuclear periphery, while co-localization analysis with nascent RNA generated clearly higher values. Apart from that H3K4me3 was predominantly restricted to nuclear zones of low TO-PRO-3 staining intensity supporting the idea that this modification can be regarded as a marker for actively transcribed chromatin. But against this widely

accepted assignment of H3K4me3 to active chromatin a role also in active gene repression has recently been reported (Shi et al., 2006). The authors showed that members of the inhibitor of growth family (ING) of tumor suppressor proteins bind to H3K4me3 via a PHD-domain and thus stabilize a HDAC-complex at the promoters of proliferation genes.

The DNA dye TO-PRO-3 has been shown to be a specific and sensitive nuclear counterstaining dye in human cells (Matsuzaki 1997) and in *Xenopus laevis* (de Maziere et al., 1996) embryos as well as on frozen sections of rat (Suzuki et al., 1997). Its affinity to ds DNA makes it comparable to DAPI (Bink et al., 2001). The latter however has an affinity to AT-rich sequences which was not reported for TO-PRO-3 (Petty 2000). Areas of low TO-PRO-3 staining intensity represent less compacted or decondensed DNA, a chromatin state indicative for high gene density and genetic activity (Gilbert et al., 2004). On the light microscopic level both dyes stained similar areas namely regions containing dense chromatin.

It was shown recently that H4K20me1 is involved in cell cycle regulation (Karachentsev et al., 2005). The observation during the present thesis that two “populations” of antibody staining signals exist supports the idea of a connection of H4K20me1 to cell cycle progression. Other processes where H4K20me1 was reported to play a role are chromosome segregation during mitosis in *Drosophila* (Julien and Herr, 2004), DNA repair mechanisms in yeast (Nakamura et al., 2004; Sanders et al., 2004) and the initiation of X-inactivation (Kohlmaier et al., 2004). Controversial data have been published assigning H4K20me1 to promotor regions on the one hand (Talasz et al., 2005) and to silent chromatin on the other hand (Karachentsev et al., 2005; Nishioka et al., 2002). The striking similarity in the nuclear arrangement and the dot like appearance of both antibody signals H3K4me3 and H4K20me1 suggests that the latter modification is also associated with active gene loci or at least chromatin with a transcriptional permissive state. The still large fraction of separate signals of the two antibodies after co-immunostaining indicates that chromatin segments exist which were spatially excluded from each other and therefore mark distinct types of chromatin.

A connection of H4K20me1 to repetitive sequences was shown in the mouse model, where in ChIP experiments H4K20me1 was merely found to be enriched in SINEB1 (correspond to the human Alu family) repeats (Martens et al., 2005). However this modification could not be assigned to centromeres as evaluated by co-localization analysis. The observation that H4K20me1 is apparently only to a minor extent associated with nascent RNA leads to the conclusion that the detected pattern mirrors a very special type of chromatin that cannot simply be assigned to either actively transcribed or repressed chromatin regions.

Assessment of H3K9me1 in human led to the suggestion that this modification reflects temporarily silent chromatin domains (Rice et al., 2003). Tests by ChIP analysis in mouse revealed low H3K9me1 enrichment at repetitive sequences as well as in transcriptionally active regions (Martens et al., 2005). Comparable to H4K20me1 also H3K9me1 is characterized by a punctual pattern. Both modifications showing staining foci distributed throughout the nucleus (except nucleoli and the nuclear rim) are alike regarding their low level of co-localization with centromeres and nascent RNA. The immunostaining experiments produced often signals in TO-PRO-3 rich areas which favors the idea of H3K9me1 reflecting rather silent domains. The discrepancy of information about this modification is probably due to varieties between the species human and mouse (Martens et al., 2005; Rice et al., 2003).

H3K27me3 is predominantly mentioned in the context of imprinted facultative heterochromatin formation and initiation of X-chromosome inactivation (Okamoto et al., 2004; Plath et al., 2003). Additionally a function in maintaining X inactivation has recently been described (Kohlmaier et al., 2004). The presence of H3K27me3 at unexpressed autosomal genes suggests that this mark is an ubiquitary label for heterochromatin rather than a X-specific marker (Brinkman et al., 2006). The staining pattern of H3K27me3 in DLD-1 and MCF-7 cells resembles the pattern for mid (to-late) replicating chromatin in a very striking manner. This pattern is found around the nucleoli and at the nuclear periphery thereby sustaining the idea of an association with gene repressing chromatin. Mid-replicating chromatin and facultative heterochromatin (Craig and Bickmore, 1993) corresponds to a large extent to G-dark bands which contain tissue-specific genes that are transcribed only in selected cell types (Manuelidis, 1990). These genes have a high content of LINE elements but no enrichment of H3K27me3 with LINE elements could be uncovered in mouse (Martens et al., 2005). The question if such an association is also existent in humans remains unanswered at the moment.

In neither cell type an association of H3K27me3 with centromeres was observed and also co-localization analysis with nascent RNA revealed low overlapping volume. Taken into account that H3K27me3 was never brought into connection with actively transcribed genes and the co-localization data of this modification with centromeres and nascent RNA obtained in this work, chromatin visualized by H3K27me3 seems to represent a discrete type of heterochromatin.

H3K9me3 is the probably best known and characterized epigenetic marker for constitutive heterochromatin in a variety of species (Lehnertz et al., 2003; Martin and Zhang, 2005; Rea et al., 2000; Rice et al., 2003). After it was shown that this epitope serves as a binding site for HP1-alpha it became evident that H3K9me3 plays a key role in nuclear formation of

constitutive heterochromatin via these interaction (Bannister et al., 2001; Lachner et al., 2001). In mouse a high overlap of H3K9me3 with chromocenters (visualized by DAPI-counterstaining) was observed linking it to (peri-) centromeric heterochromatin (Peters et al., 2003; Rice et al., 2003). CHIP analysis of the bulk of repetitive sequences in mouse confirmed a strong and stable enrichment of H3K9me3 in the major and minor tandem satellite repeats in all investigated cell types (Martens et al., 2005) whereas enrichment for different subsets of interspersed repetitive elements with H3K9me3 was found to be rather cell cycle dependent. The observation in this thesis that H3K9me3 exists either in smaller and more dispersed clusters or in big intense clusters posed the question if there is a dynamic movement of constitutive heterochromatin dependent on cell cycle stage. Changes in pattern formation after exit of the cell cycle and also during the cell cycle were already observed in the past (Cremer et al., 2004). These results are to align with the claim that dynamic properties of heterochromatin are required for its nuclear function (Baxter et al., 2004; Manuelidis, 1990). Recently the absence of several histone methylation sites in resting B and T lymphocytes was described which were remarkably increased after mitotic stimulation (Baxter et al., 2004). The discrepancy of this observation with data obtained in this work is probably due to the fact that lymphocytes represent a very special case and exit of the cell cycle as investigated for tumor cells may differ fundamentally from mechanisms in senescent cells or during terminal differentiation.

RAC analysis could confirm the observation made by visual inspection, that H3K9me3 pattern changes its conformation and compaction during the cell cycle. To say more precisely, the dispersed H3K9me3 pattern could be assigned to cycling cells while in quiescent cells bigger clusters were dominating. However RAC analysis could not reveal differences in the pattern formation during cell cycle progression for H3K27me3 and H4K20me1. But this does not exclude the possibility of cell cycle dependent changes of these histone modifications because the RAC-method depends highly on the 3-dimensional shape of the evaluated objects. It is also possible and very likely that smaller foci do move but in relative to each other not forming bigger aggregates. This could not be detected by RAC because this program is only suitable to uncover changes in pattern size. The observed changes of H3K9me3 marked (peri-)centromeric heterochromatin pattern probably comes along with a silencing of genes as it was recently described for the beta globin locus (Litt et al., 2001).

H3K9me3 was found associated with centromere signals visualized by CREST-serum throughout all cell types. The histone methylation signal was found to a different extent around or partly overlapping with centromeres and probably represents rather pericentromeric heterochromatin than the centromere itself. The abundance of much smaller foci distributed all over the nucleus but remote from centromeres and nucleoli varied a little bit between cell types. These foci not associated with constitutive heterochromatin might

represent interspersed elements that are enriched within these modification. Surprisingly the appearance of H3K9me3 also in coding regions of active genes was recently reported for the X-chromosomes (Brinkman et al., 2006). If an association with active genes also exists for other chromosomes has to be elucidated.

However this could explain the existence of many smaller foci distributed all over the nucleus. Co-localization analysis of H3K9me3 with nascent RNA yielded low values and perhaps this reflects rather overlap of nascent RNA with smaller foci than with big heterochromatic regions. Since overlap of constitutive heterochromatin marked by H3K9me3 with nascent RNA is negligible the observed co-localization might be due to overlapping volume of smaller foci addressed to coding regions with nascent RNA.

Related to H3K9me3, the potential function of H4K20me3 as a label for constitutive heterochromatin and its involvement in gene repression are shown in model organisms like mouse and *Drosophila* (Gonzalo et al., 2005; Kourmouli et al., 2004; Schotta et al., 2004b). The 3D nuclear topology of both modification is also very similar (Zinner et al., 2006). The relationship of these modifications is not surprising taking into account the close interrelationship involving H3K9me3 and H4K20me3 as described in a new publication (Sims et al., 2006). In all investigated cell types centromeres were to a related extent embedded in signals deriving from H4K20me3 staining. CREST antiserum, which is directed against centromeric proteins CENP-A, CENP-B and CENP-C gives reliable information about the spatial disposition of the central domain of the centromere-kinetochore complex (Earnshaw and Rothfield, 1985). Centromeric chromatin is distinct from that of both euchromatin and flanking heterochromatin (Sullivan and Karpen, 2004). The partial embedding of centromeres in heterochromatin clusters contributes to the unique domain organization and three-dimensional structure of centromeric regions. Furthermore the antibody pattern appeared more dispersed in cycling cells than in quiescent cells with the latter coming up with a striking ring like structure of pericentromeric chromatin. This cell cycle dependent reorganization observed for heterochromatin clusters is in accordance with the highly dynamic properties of condensed chromatin (Cheutin et al., 2003; Grigoryev et al., 2004).

Co-localization analysis of distinct histone methylation sites with nascent RNA was made under the assumption that a statement about the involvement of distinct methylation sites in transcriptional activity can be made by the judgement of overlap. However all investigated methylation sites revealed low overlapping volume with nascent RNA. H3K4me3 and H3K9me1 yielded the highest co-localization values at about 20%. This observation can be partly explained by new data that assigns basic gene transcription mainly to H3K4me2 whereas H3K4me3 is associated with cell type specific transcription (Bernstein et al., 2005).

Another aspect is that RNA-transcription occurs to a certain extent on non-coding intergenic DNA-sequences (Cheng et al., 2005; Mattick, 2003) which are probably not marked by H3K4me3. One should also keep in mind that RNA has the potential of a very dynamic behavior (Pederson, 1999; Politz et al., 1999) which makes it difficult to spot the current situation. This might also explain the low overlapping volume with constitutive heterochromatin visualized by H3K9me3 and H4K20me3. Therefore co-localization analysis with nascent RNA as a parameter for present gene activity should be treated with caution.

To investigate 3D lysine methylation patterns with regard to each other the specific antibodies were combined in various combinations. The problem deriving from the fact that all antibodies were raised within the same species made a protocol for sequential antibody labeling (Spada et al., 2005) mandatory. Combination of antibodies revealed that the investigated histone methylation sites can be assigned to distinct nuclear zones (Zinner et al., 2006). H3K9me3 and H4K20me3 which are supposed to stain similar types of chromatin showed high overlapping volume with each other. H3K4me3 is clearly separated of both H3K9me3 and H3K27me3 which means that it is not associated with neither constitutive heterochromatin nor facultative heterochromatin. It is presently open to what dimension constitutive heterochromatin in the human genome is also marked by H3K27me3 or facultative heterochromatin by H3K9me3 and to what extent these two functionally distinct chromatin segments share in parts the same topology. But the idea that distinct modifications can be addressed to a specific type of chromatin was challenged lately (Brinkman et al., 2006; Chadwick, 2006). Combination of H3K4me3 with H4K20me1 does not yield clear information about the latter modification and also H3K9me3 combined with H3K27me3 did not give an explicit result because intermingling was observed to a certain degree. Co-localization analysis gave clear results only for signals representing either similar types of chromatin like H3K9me3 and H4K20me3 which share overlapping volume to a certain extent or totally different types of chromatin, e.g. H3K4me3 and H3K9me3 where a negative correlation was evaluated.

The organization of nuclear zones visualized by distinct histone methylation sites seems to follow basic principles as well as the spatial arrangement of early vs mid-to-late replicating chromatin (Dimitrova and Berezney, 2002). H3K4me3 pattern looks similar to early replicating chromatin, H3K27me3 is correspondent to the mid replication pattern and H4K20me3 mirrors gene poor, big, late replicating heterochromatin clusters. The impelling forces underlying these non-random topological arrangements of chromatin have not yet been uncovered but their evolutionary high conservation underline their outstanding functional relevance (Alexandrova et al., 2003; Postberg et al., 2005; Tanabe et al., 2002a; Tanabe et al., 2002b).

5.2 Changes in nuclear 3D topology after Chaetocin treatment

Chaetocin is a member of the epipolythiodioxopiperazine (ETP) class of toxins. Properties of these secondary fungal metabolites were recently reviewed by Gardiner et al. (Gardiner et al., 2005). The cytotoxic effect of the given concentration of a drug can vary somewhat between cell types. Hence, it was essential to define the appropriate Chaetocin dilution for the cells that were used in this work. This step was also necessary because Chaetocin toxicity is highly dependent on the initial cell density when the inhibitor is added to the cells seeded on coverslips (Greiner et al., 2005). Therefore it was important to start all experiments with the same initial cell density. After the appropriate Chaetocin concentration for the used cell types was established the next aim was to check whether cytotoxicity was involved in the observed chromatin rearrangements. Visual analysis and BrdU incorporation after several days revealed that a similar proportion of drug-treated and control cells were in S-phase. These findings argue against an involvement of cytotoxic effects at the applied Chaetocin concentration.

In subsequent experiments the topology of nucleoli, speckles and microtubules was investigated to gain information about a potentially impact of Chaetocin application on cellular morphology. Nuclei harbor pre-mRNA splicing factors in about 25-50 nuclear speckles (Spector, 2001). These speckles are highly dynamic and serve as reservoir of splicing factors to neighboring sites of transcription. Nuclear speckles and their surrounding regions were shown to be major sites of RNA-polymerase II mediated transcription (Wei et al., 1999a). Transcription sites are observed throughout the nucleoplasm including the periphery of speckles (Spector, 2001). It was recently shown that speckles also serve as storage sites for RNA-polymerase II although not for its active form (Xie et al., 2006). Taken together, these findings support the notion that the existence of speckles can provide an indirect tool for ongoing transcriptional activity.

Since rRNA synthesis, rRNA processing and assembly of ribosomal subunits occurs in the nucleolus, this compartment can be regarded as an indicator of nuclear activity (Spector, 1993). The cellular location of B23 serving as a nucleolar marker was extensively described in the early 90's (Chan, 1992).

Microtubules are crucial for cytoplasmic organization and were thus taken as a marker for general cellular structure (Malikov et al., 2005).

IF experiments with antibodies against these cellular structures were also performed because changes in the morphology of the investigated compartments after drug treatment have been reported. It was shown that the nucleolar phosphoprotein B23 dissociates from nucleoli of cells after treatments with various drugs (Chan et al., 1999). Inhibition of transcription resulted in prominent round clusters of SC-35 domains (Xing et al., 1995). DRB

and alpha-amanitin application changed the nuclear poly (A)-RNA organization from the typical speckled localization pattern into fewer and larger clusters of splicing compartments (Huang et al., 1994). Microtubules were selectively destructed by inhibitors of phosphatases (Merrick et al., 1997) and tubulin disruption was recently shown as a mechanism by which inhibitors of HDACs reduce the secretion of interleukin-1 (Carta et al., 2006).

An overall impact of the drug as would have been expected in the case of cytotoxicity would have certainly led to changes in the morphology of the investigated cellular structures. However immunofluorescence with antibodies against nucleoli, speckles and microtubules did not reveal variations in the appearance of the stained compartments after chaetocin treatment on the light-microscopic level.

Despite lacking morphological changes and positive tests for S-phase in drug treated cells, (hetero)chromatin condensation as observed after Chaetocin treatment in HFbs is not inconsistent with cytotoxicity.

Cells committing apoptosis also display chromatin aggregated into dense compact masses (Fadeel and Orrenius, 2005; Lawen, 2003). However it was shown that *de novo* chromatin condensation normally seen during mitosis does not occur when cells undergo apoptosis. Instead, the noticed condensed chromatin results from aggregation of the typical constitutive heterochromatin (Hendzel et al., 1998).

Mitotic cell death (MCD) also known as “mitotic catastrophe” is another form of cell death to eliminate damaged cells and is mainly described in morphological terms (Blank et al., 2006). To date, evidence of premature mitosis in damaged cells relies primarily on the appearance of uneven chromatin condensation (UCC), which is the formation of hypercondensed chromatin aggregates (Roninson et al., 2001). Since MCD was identified as a prominent response of cells to different anticancer drugs (Lock and Stribinskiene, 1996; Tounekti et al., 1993) (Torres and Horwitz, 1998), this process might be an explanation for the observed effects after Chaetocin treatment.

Surprisingly, an overall decrease in H3K9me3 staining intensity, at least by visual inspection, was not observed after drug application, suggesting that SUV39H1 activity and therefore H3K9me3 levels are not altered in Chaetocin-treated cells. This is at least partly in consistency with *in vivo* inhibition of SU(VAR)3-9 in *Drosophila* SL-2 cells which show mainly a reduction of H3K9me2 rather than H3K9me3 in mass spectrometry (MS) (Greiner et al., 2005). However in another experiment the authors could also observe a substantial drop in H3K9me3.

In HFbs Chaetocin treatment led to a rearrangement of chromatin that could be highlighted by changes in the patterns after H3K9me3 staining **and** DAPI-counterstaining. The relocated chromatin is characterized by very large clusters, of what is mostly but not exclusively (peri)-centromeric heterochromatin. However, keeping in mind the amount of chromatin that seems

to be rearranged, it is very likely that heterochromatic as well as euchromatic regions are affected by drug treatment.

Taking into account the fact that Chaetocin treatment induces changes in chromatin formation in general it is reasonable to suppose that the appearance of H3K9me3 clusters is a consequence of this overall chromatin alteration rather than a direct effect of SUV39H1 inhibition. However information about SUV39H1 enzyme activity remains to be obtained by enzyme activity assays.

Western blot analysis of SUV39H, H3K9me3 and H3 (as a control) could provide a much better resolution compared to simple visual inspection and is essential for any final conclusions on this topic.

The mechanisms leading to the rearrangement of heterochromatin that are described here remain unclear. Taken all observations together it seems rather unlikely that the observed chromatin rearrangements in HFbs were simply based on cytotoxicity.

Another important question to be answered is why a similar impact of Chaetocin was only observed in HFbs but not in the cancer cell-lines DLD-1 and MCF-7.

An explanation might be the development of several mechanisms for drug resistance in cancer cells. Each cancer cell has specific genetic and epigenetic alterations (Ballestar and Esteller, 2005). Hence tumor cells express different arrays of drug-resistance genes conferring simultaneous resistance to many different drugs, a phenomenon called multidrug resistance (Gottesman et al., 1994). Much data is provided about mechanisms that alter accumulation of drugs within cells (Ambudkar et al., 1999; Borst et al., 2000). There are two ways for drug resistance of cancer cells that should be also taken into account for the discussed observations. A first mechanism can increase drug efflux from cancer cells and a second mechanism leads to reduced uptake of drugs. The latter argument does not fit the finding that all cells from all cell-lines died at 0,1 μ M Chaetocin.

Most tumor cells show ABC-transporter (ATP-binding cassette)-mediated multidrug resistance (Higgins, 1992). This type of resistance was already discovered in 1976 (Juliano and Ling, 1976). The major mechanism of multidrug resistance in cultured cancer cells was the expression of an energy-dependent drug efflux pump, known alternatively as P-glycoprotein (Pgp) (Ueda et al., 1987). It is the product of the MDR1 gene in humans and highly expressed in cancer cells (Chen et al., 1986). Although big efforts have been made recently for overcoming this feature of tumor cells (Borowski et al., 2005) it is still a major cause of failure in anti-tumor therapy. The resistance is due to the expression of ABC transporter glycoproteins which participate actively in effluxing the drug out of the cell thus preventing the accumulation of substances. These general findings in tumor cells would

provide an explanation why no changes in higher chromatin organization were found in nuclei of DLD-1 and MCF-7 cells.

An explanation why chromatin condensation in HFbs occurs already at a Chaetocin concentration of only 0,01 μ M could be a redox-uptake mechanism that has recently been described for a ETP-toxin (Bernardo et al., 2003). The concentration of the substance within a cell can be several orders of magnitude greater (up to 1500-fold) than the applied concentration. This accumulation appears to enhance the toxicity of ETPs.

It is much more difficult to uncover a mechanism in the context of regulating histone lysine methylation than histone acetylation (Turner, 2000). This is because the latter mainly depends on repulsion of charges whereas lysine methylation effector functions depend on the recruitment and interaction of many proteins (Bernstein et al., 2007; Li et al., 2007). Furthermore epigenetic “cross-talk” can occur, making research and interpretations even more complicated (Fischle et al., 2003b; Kouzarides, 2007). This means that all possible interaction partners of H3K9me3, HP1-alpha and SUV39H1 have to be taken into account when it comes to a discussion about the underlying mechanisms of these changes observed after Chaetocin treatment.

Another question that has to be addressed is whether the enzyme activity after Chaetocin application is as high as in control cells. To investigate enzymatic activity directly several types of enzyme assays have been developed over the decades (Lottspeich, 1998). Enzyme assays can be split into two groups according to their sampling method: continuous assays, where the assay gives a continuous reading of activity, and discontinuous assays, where samples are taken, the reaction stopped and then the concentration of substrates/products determined. To test the hypothesis if the changes of H3K9me3 after drug application are due to altered enzyme activity an enzyme activity assay against the HMT SUV39H1 should be executed in subsequent experiments as was applied for HATs (Brownell et al., 1999).

Since cancer cells obviously have mechanisms to escape the effects of drug treatment at least at low concentrations it seems necessary to investigate the effect of Chaetocin application in other “normal” cell-strains.

HP1-alpha, which, binds to H3K9me3 (Bannister et al., 2001; Lachner et al., 2001), can still be found co-localizing after Chaetocin treatment. In all three cell types HP1-alpha was found to be overlapping with H3K9me3 to some extent in untreated control cells and in Chaetocin treated cells, indicating that H3K9me3 as a binding site for HP1-alpha is not affected by the drug. In MCF-7 and DLD-1 cells the overlapping volume of HP1-alpha appears similar before and after drug treatment; only in untreated HFbs different overlapping volume compared to Chaetocin treated cells was observed. The observation that HP1-alpha remains overlapping

at least partly with H3K9me3 in HFbs raises again the question whether the HP1/H3K9me3-system involved in heterochromatin formation is affected at all or if other pathways are altered by Chaetocin treatment.

An important finding was that a rearrangement of chromatin was not observed after an incubation time of 8h. Together with the observation that changes in chromatin occur after 24h this finding argues for a cell cycle dependence of the described effect because the time window where changes can be detected correspond approximately to the duration of one cell cycle in HFbs (diploma thesis A. Engelhard, 2001). The described changes are more likely due to a process where the passing of S-phase is required.

In a rescue assay where Chaetocin was “washed out” two days after application no re-establishment of chromatin occurred. Cells were not capable to rearrange their chromatin to the original state as observed in control cells. This would on the one hand argue for cytotoxicity or on the other hand confirm that the process initiated by Chaetocin application is irreversible, thereby suggesting a long term epigenetic alteration (Lachner et al., 2004; Reinberg et al., 2004).

The performed experiments to uncover the role of this drug on the level of nuclear architecture were a necessary completion to the exclusively biochemical experiments made when Chaetocin was found and proofed to be a specific inhibitor of SU(VAR)3-9.

5.3 Analysis of lysine sites with regard to chromatin segments

In this chapter the spatial relationship of histone modifications H3K4me3, H3K9me3 and H3K27me3 with whole chromosome territories (CT), chromosomal subdomains and selected gene loci is discussed.

The gene poor chromosome 18 and the gene rich chromosome 19 differ in their enrichment for H3K4me3 staining but not for H3K9me3 and H3K27me3. Co-localization analysis for H3K9me3 and the CTs of chromosomes 18 and 19 respectively yielded almost identical values despite their different “compaction” state, gene content and overall transcriptional activity. The bulk of H3K9me3 can be assigned to blocs of pericentromeric heterochromatin containing tandem repeats (Peters et al., 2003; Rice et al., 2003; Zinner et al., 2006). Since chromosome specific painting probes do not represent these large heterochromatin blocs due to Cot-1 DNA suppression in FISH-experiments or depletion of repetitive sequences in probe generation (Bolzer et al., 1999) it is not surprising that overlap occurs merely to a minor extent. This observation was confirmed by experiments where signals of centromeres and constitutive heterochromatin marked by H4K20me3 were found in “holes” of chromosome paints. Therefore co-localization data are mainly obtained by overlapping regions not associated with pericentromeric heterochromatin. A large number of small foci

distributed all over the nucleus, not associated with pericentric heterochromatin, was recently observed (Zinner et al., 2006). In humans a selective enrichment of H3K9me3 in interspersed sequences (LINEs and SINEs) has not been described so far. The finding that H3K9me3 is present in coding regions of genes makes an interpretation more complicated but might explain the existence of these small foci (Brinkman et al., 2006). CT #19 is higher enriched in Alu sequences compared to CT #18 (Grimwood et al., 2004). Our evaluations do not confirm an association of H3K9me3 with Alu sequences because if so, co-localization analysis should have revealed a clear discrepancy between both chromosomes. Data reporting HSA #18 not generally enriched in repetitive sequences, despite being gene poor (Nusbaum et al., 2005), are supportive to the identical co-localization results.

H3K27me3 can be assigned to the Xi both topologically and functionally (Kohlmaier et al., 2004; Plath et al., 2003). Similar to H3K9me3, the H3K27me3 staining pattern appears as a conglomeration of small dots throughout the nucleus with a slight enhancement at the nuclear periphery. The low amount of overlapping volume that was calculated for CTs #18 and #19 is consistent with findings that H3K27me3 participates in the repression of only a sparsely described subset of autosomal genes such as HOX clusters (Cao et al., 2005; Cao et al., 2002) or genes subject to imprinting in humans and mouse (Delaval and Feil, 2004; Mager et al., 2003).

Co-localization analysis of H3K4me3 with CTs #18 and #19 respectively produced clearly different results. The ratio of H3K4me3 overlapping with #19 was fourfold higher compared to overlapping with #18. These findings were confirmed and partly explained by publications that either report H3K4me3 associated with promoter regions (Schubeler et al., 2004), or data that attribute H3K4me3 to active genes since SET1 the HMT for this modification is in contact with RNA polymerase II during elongation (Ng et al., 2003). However Brinkman et al. (2006) found H3K4me3 not necessarily as a marker for ongoing transcription (Brinkman et al., 2006). But this is not a discrepancy with the data described in this thesis because a chromosome territory comprises a rather large area concerning the whole nuclear volume and is therefore not decisive for co-localization analysis if transcription just started or ended. Probably the higher H3K4me3 co-localization values with HSA #19 simply mirrored the exalted gene content and a higher overall transcriptional activity of HSA #19 (Caron et al., 2001).

To get deeper insight into histone lysine methylation on a higher resolution, H3K4me3 and H3K27me3 were addressed to chromosomal subdomains and selected genes on HSA #12 defined by a distinct regional gene density or transcriptional activity. For overlap with H3K4me3 similar and high co-localization values were found for both, gene dense DNA segments and highly expressed genes on HSA #12. BACs containing gene poor segments or weakly expressed genes are predominantly found in H3K4me3 free spaces while BACs

containing gene rich segments or highly expressed genes are to a higher extent associated with this modification. The results support the idea that H3K4me3 is not exclusively connected to transcription but represents a rather competent chromatin state for transcription. Co-localization analysis of H3K27 with BACs containing highly and weakly expressed genes gave overall low values, suggesting no impacts of H3K27me3 for a regulation of the investigated genes.

Given that H3K27me3 covers almost the entire Xi a possible association with differential expressed genes (weakly, mid and highly) on both, the Xi and Xa was investigated. After co-localization analysis low values were calculated for the Xa with H3K27me3 while Xi revealed very high values. This confirmed the impression from images of interphase nuclei after immuno-FISH with X-paints and H3K27me3 where signals of both structures seemed to occupy the same spatial area. In metaphases a variable distribution of H3K27me3 on the Xi was reported (Chadwick, 2006; Chadwick and Willard, 2004). Co-localization analysis of H3K27me3 with highly expressed genes on Xa almost tended to zero, while co-localization of 40% was evaluated for the same genes on the Xi. An even higher value of 65% was measured for the entire X-chromosome in the same experiment. The discrepancy can be explained by the fact that 19% of all genes on the Xi escape inactivation and another 10% show variable patterns of inactivation between individuals (Carrel and Willard, 2005; Distèche, 1995; Distèche, 1999). These genes are not restricted to the pseudoautosomal regions on both chromosomal arms but are found over the whole chromosome with a pronouncement on the short arm (Carrel and Willard, 1999).

In an elaborate five-color immuno-FISH experiment was performed to investigate the co-localization of mid and weakly expressed X-linked genes with H3K27me3 were investigated on both X chromosomes. Similar high values of overlap were found for the Xi, while for mid and weakly expressed genes a discrepancy on the Xa was observed. Mid expressed genes showed an overlapping volume of 5% with H3K27me3 whereas weakly expressed genes an increased level of 16%. The latter was also distinctly higher to the overall co-localization of H3K27me3 with the painted Xa territory compared to co-localization values for the repressed genes on chromosome #12 (3%). These data are supported by the observation that two X-linked genes are associated with H3K27me3 in lymphoblastoid cell where these genes are inactive (Brinkman et al., 2006). These findings taken together would support the idea that H3K27me3 has a higher affinity to the X-chromosomes than to autosomes.

5.4 The methodological approach

Confocal image stacks were used for a quantitative evaluation of:

1. the degree of clustering by RAC analysis
2. the degree of overlap between histone methylation sites with each other, centromeres and nascent RNA
3. Cluster-size in Chaetocin experiments
4. overlap of chromosome-territories and DNA segments with lysine methylation sites

Among several publications that describe approaches for an analysis of co-localization of two different objects (Kreft et al., 2004; Landmann and Marbet, 2004; Manders et al., 1992; Manders et al., 1993), the co-localization coefficients M1 and M2 first described by Manders et al. (1993) were chosen. An important advantage of these coefficients was the implication of an intensity weighted calculation. The evaluation method is suitable in cases of little or no overlap and also in cases where voxel numbers differ significantly in one of two channels which mirrors exactly situations that were found in nuclei evaluated in this work (Manders et al., 1993).

However co-localization analysis is afflicted with several problems. What is the correct way of describing and interpreting data resulting from Manders coefficients M1 and M2. It is very difficult to judge if a given value (say 0.2) is important and meaningful or not. Therefore it is required to compare always two data sets within one experiment, e.g. highly **and** weakly expressed genes visualized on a chromosome within the same experiment and judgement of co-localization values relative to each other. Another problem emerges from the statistical point of view. How to deal with data by statistics when single voxels can not be regarded as "independent events".

As was shown in the method chapter for thresholds in a certain range co-localization coefficients differ significantly for both, big objects (chromosome paints) as well as for smaller objects (BAC signals). From one step to the next the overlapping values change only a few %-points which does not lead the user astray if the TH is somewhat set properly. But for a person which is familiar with the shape and structure of histone methylation patterns it should not be a problem to set an appropriate threshold within a range of few gray values TH (plus/minus 5). In principle threshold independent evaluation tools are highly desirable and have recently been implemented in our evaluation spectrum (Cremer et al., 2004; Stadler et al., 2004).

The immuno-FISH protocol turned out to be a proper tool to visualize histone modifications and DNA targets simultaneously. Since two fundamentally different goals are pursued in this approach, on the one hand to maintain methylated lysine epitopes as best as possible and

on the other hand gain accessibility for complex DNA probes to their nuclear target sequences, it is clear that 3D-immuno-FISH is a rather critical procedure. DNA-FISH typically requires HCl treatment and heat denaturation which is harmful to protein structure. With regard to the structural and morphological preservation of the nucleus, especially lysine methylations, best results were achieved by binding the histone epitope with the highly specific primary antibody followed by a Biotin-conjugated secondary antibody and stabilizing this complex in a post fixation step. This step turned out to be of fundamental importance, since biotin is rather heat resistant (Gonzalez et al., 1999; Wei and Wright, 1964) and thus not prone to destruction by the subsequent heat denaturation before hybridization (Solovei et al., 2002a). The effect of FISH on chromatin formations was assessed in nuclei with histone H2B-GFP-tagged chromatin. Accordingly light microscopy could not reveal any changes down to a level of 1Mb chromatin domains (Solovei et al., 2002b). However these investigations revealed alterations in the ultrastructure of the nucleus probably caused by heat denaturation. Therefore a risk for misinterpretation at high resolution in nanometer scales exists questioning the usefulness of these investigations in the nm range. The experimental procedure benefits from the high affinity and specificity of the biotin-avidin complex (Korpela, 1984). Shifting the antibody detection of Biotin to the end of the protocol prevents the fluorochrome to be destroyed by heat.

Depending on the protein of interest many different approaches to combine immunofluorescence and FISH have been suggested (Brown, 2002; Grimaud, 2005; Lavrov et al., 2004). The immuno-FISH protocol successfully established in this work copes with these problems, as far as can be judged by confocal light microscopy, and can reveal interactions between nuclear components, like DNA and RNA on the one hand and proteins on the other hand.

Another aspect that can affect a qualitative and a quantitative evaluation of immunofluorescence is the inter-experimental difference in antibody staining intensity. As was shown by co-localization analysis of DAPI and different histone methylation patterns in several experiments the amount of antibody signal varies to a certain extent (figure 45) even within one series of experiments. This phenomenon might also lead to discrepancies in the evaluation and interpretation of data. But as illustrated in figure 45 the interexperimental discrepancies that came along with the immuno-FISH approach used in this work were not as drastic that conclusions were not to draw out of these data.

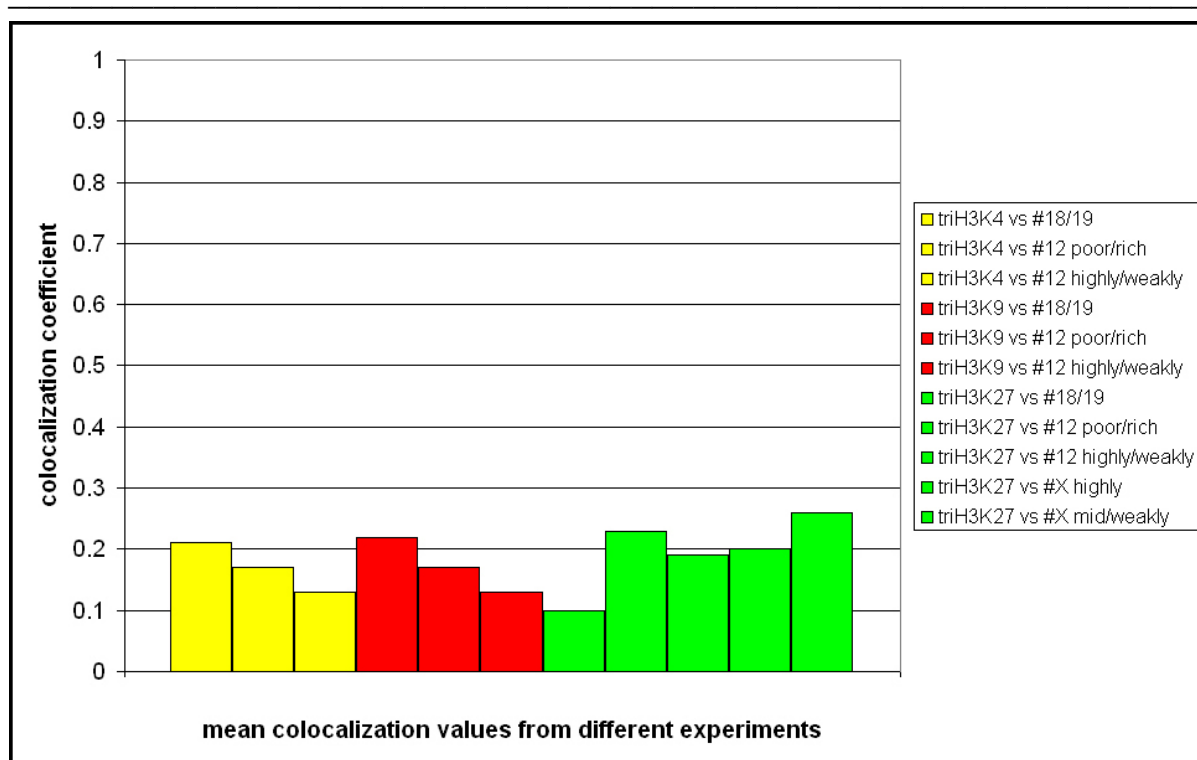


Figure 45

The figure describes the inter-experimental differences of several histone methylation sites (H3K4me3, H3K9me3 and H3K27me3) that were investigated in multi-color immuno-FISH experiments. The legend refers to the type of experiment that was performed. Co-localization of antibody staining was measured against DAPI-counterstaining in all evaluated nuclei. The evaluation comprised 25 nuclei for each experiment.

Deconvolution which was applied to all raw images prior to evaluation is not without controversy. There are several adjustable parameters for the deconvolution setting which might be a source of error. The question if the appearance of images after deconvolution represent “reality” is justified and raised as an issue in recent publications (Conchello and Lichtman, 2005; Walter et al., 2006). Moreover instead of improving image quality new artifacts might be generated by deconvolution (Wallace et al., 2001). Also the immanent problem of subjectivity applying a threshold can not be solved by deconvolution.

But otherwise deconvolution reduces background blur significantly and yields superior results in contrast to conventional judgement of images (Landmann, 2002; Landmann and Marbet, 2004). If applied properly deconvolution facilitates the manual threshold setting and provides a tool to separate artefacts from the “true” signal (Pawley, 2006). The improvement in image quality after deconvolution clearly facilitates the choice of an optimal TH to segment complex morphological structures like signals deriving from histone methylation sites, and it helps to quantitate data more easily (Albiez et al. in prep.). Despite these advantages of deconvolution one should always attempt to compare only different labelled targets to the same reference structure within a given nucleus. Following this guideline does not help to

make a clear statements about absolute values but makes an interpretation of the relative difference between two signals compared to a reference structure more reasonable.

Deconvolution has also been shown to deliver better results for co-localization analyses when compared to other techniques like filtering (Landmann, 2002; Sedarat et al., 2004).

Interestingly deconvolution of raw images has lately been commonly accepted as an indispensable tool for quantitative evaluation of 3D reconstructed image stacks (Pawley, 2006).

Image stacks taken from a confocal microscope with signals in several channels have to cope with lateral and axial shifting which yields a source of errors especially for co-localization analysis. Despite the performed axial shift-correction an impact of shifting as a source of error still remains because of the small lateral shift that was uncorrected and the axial shift that changed during intervalls of measurements (several weeks). All investigations should be always considered with the awareness of the limits of optical resolution of the used confocal microscope. A lateral resolution of >200nm and an axial resolution of >500nm have to be considered for a careful interpretation of confocal microscopic data.

Nonetheless of many debatable issues in the described approaches the data described in this thesis provided clear results for many questions that were addressed in the carried out experiments. Many of the data obtained in this work are consistant with molecular approaches like ChiP, array and blotting techniques. To conclude the applied evaluation methods and protocols were adequate to contribute new data to the still puzzling field of epigenetics and to the role of histone lysine methylation in the context of nuclear architecture.

6 References

- Aagaard, L., G. Laible, P. Selenko, M. Schmid, R. Dorn, G. Schotta, S. Kuhfittig, A. Wolf, A. Lebersorger, P.B. Singh, G. Reuter, and T. Jenuwein. 1999. Functional mammalian homologues of the *Drosophila* PEV-modifier Su(var)3-9 encode centromere-associated proteins which complex with the heterochromatin component M31. *Embo J.* 18:1923-38.
- Alberts, B., Johnson, A., Lewis, J., Raff, M., Roberts, K., and Walter, P. 2002. *Molecular Biology of the Cell.* Garland Science, New York.
- Alexandrova, O., I. Solovei, T. Cremer, and C.N. David. 2003. Replication labeling patterns and chromosome territories typical of mammalian nuclei are conserved in the early metazoan Hydra. *Chromosoma.* 112:190-200.
- Allfrey, V.G.F.a.M.A.E. 1964. Acetylation and methylation of histones and their possible role in the regulation of RNA synthesis. *Proc.Natl.Acad.Sci USA.* 51:786-94.
- Allis, C.D., Jenuwein, T., Reinberg, D. 2007. *Epigenetics.* Cold Spring Harbor Laboratory Press.
- Ambudkar, S.V., S. Dey, C.A. Hrycyna, M. Ramachandra, I. Pastan, and M.M. Gottesman. 1999. Biochemical, cellular, and pharmacological aspects of the multidrug transporter. *Annu Rev Pharmacol Toxicol.* 39:361-98.
- Arents, G., R.W. Burlingame, B.C. Wang, W.E. Love, and E.N. Moudrianakis. 1991. The nucleosomal core histone octamer at 3.1 Å resolution: a tripartite protein assembly and a left-handed superhelix. *Proc Natl Acad Sci U S A.* 88:10148-52.
- Avner, P., and E. Heard. 2001. X-chromosome inactivation: counting, choice and initiation. *Nat Rev Genet.* 2:59-67.
- Ballestar, E., and M. Esteller. 2005. The epigenetic breakdown of cancer cells: from DNA methylation to histone modifications. *Prog Mol Subcell Biol.* 38:169-81.
- Bannister, A.J., and T. Kouzarides. 2004. Histone methylation: recognizing the methyl mark. *Methods Enzymol.* 376:269-88.
- Bannister, A.J., R. Schneider, and T. Kouzarides. 2002. Histone methylation: dynamic or static? *Cell.* 109:801-6.
- Bannister, A.J., P. Zegerman, J.F. Partridge, E.A. Miska, J.O. Thomas, R.C. Allshire, and T. Kouzarides. 2001. Selective recognition of methylated lysine 9 on histone H3 by the HP1 chromo domain. *Nature.* 410:120-4.
- Barr, M.L., and E.G. Bertram. 1949. A morphological distinction between neurons of the male and female, and the behavior of the nucleolar satellite during accelerated nucleoprotein synthesis. *Nature.* 163:676-677.
- Bauer, U.M., S. Daujat, S.J. Nielsen, K. Nightingale, and T. Kouzarides. 2002. Methylation at arginine 17 of histone H3 is linked to gene activation. *EMBO Rep.* 3:39-44.
- Baxeavanis, A.D., and D. Landsman. 1996. Histone Sequence Database: a compilation of highly-conserved nucleoprotein sequences. *Nucleic Acids Res.* 24:245-7.
- Baxter, J., S. Sauer, A. Peters, R. John, R. Williams, M.L. Caparros, K. Arney, A. Otte, T. Jenuwein, M. Merkenschlager, and A.G. Fisher. 2004. Histone hypomethylation is an indicator of epigenetic plasticity in quiescent lymphocytes. *Embo J.* 23:4462-72.
- Bedford, M.T., and S. Richard. 2005. Arginine methylation an emerging regulator of protein function. *Mol Cell.* 18:263-72.
- Bell, P.A., and C.N. Jones. 1982. Cytotoxic effects of butyrate and other 'differentiation inducers' on immature lymphoid cells. *Biochem Biophys Res Commun.* 104:1202-8.
- Belmont, A.S., and K. Bruce. 1994. Visualization of G1 chromosomes: a folded, twisted, supercoiled chromonema model of interphase chromatid structure. *J Cell Biol.* 127:287-302.
- Belmont, A.S., S. Dietzel, A.C. Nye, Y.G. Strukov, and T. Tumber. 1999. Large-scale chromatin structure and function. *Curr Opin Cell Biol.* 11:307-11.
- Bender, J. 2004. DNA methylation and epigenetics. *Annu Rev Plant Biol.* 55:41-68.
- Bernardo, P.H., N. Brasch, C.L. Chai, and P. Waring. 2003. A novel redox mechanism for the glutathione-dependent reversible uptake of a fungal toxin in cells. *J Biol Chem.* 278:46549-55.
- Bernstein, B.E., E.L. Humphrey, R.L. Erlich, R. Schneider, P. Bouman, J.S. Liu, T. Kouzarides, and S.L. Schreiber. 2002. Methylation of histone H3 Lys 4 in coding regions of active genes. *Proc Natl Acad Sci U S A.* 99:8695-700.
- Bernstein, B.E., E.L. Humphrey, C.L. Liu, and S.L. Schreiber. 2004. The use of chromatin immunoprecipitation assays in genome-wide analyses of histone modifications. *Methods Enzymol.* 376:349-60.
- Bernstein, B.E., M. Kamal, K. Lindblad-Toh, S. Bekiranov, D.K. Bailey, D.J. Huebert, S. McMahon, E.K. Karlsson, E.J. Kulbokas, 3rd, T.R. Gingeras, S.L. Schreiber, and E.S. Lander. 2005. Genomic maps and comparative analysis of histone modifications in human and mouse. *Cell.* 120:169-81.
- Bernstein, B.E., A. Meissner, and E.S. Lander. 2007. The Mammalian epigenome. *Cell.* 128:669-81.
- Bink, K., A. Waich, A. Feuchtinger, H. Eisenmann, P. Hutzler, H. Hofler, and M. Werner. 2001. TO-PRO-3 is an optimal fluorescent dye for nuclear counterstaining in dual-colour FISH on paraffin sections. *Histochem Cell Biol.* 115:293-9.
- Bird, A. 2002. DNA methylation patterns and epigenetic memory. *Genes Dev.* 16:6-21.
- Blais, A., and B.D. Dynlacht. 2005. Constructing transcriptional regulatory networks. *Genes Dev.* 19:1499-511.

- Blank, M., Y. Lerenthal, L. Mittelman, and Y. Shiloh. 2006. Condensin I recruitment and uneven chromatin condensation precede mitotic cell death in response to DNA damage. *J Cell Biol.* 174:195-206.
- Boggs, B.A., P. Cheung, E. Heard, D.L. Spector, A.C. Chinault, and C.D. Allis. 2002. Differentially methylated forms of histone H3 show unique association patterns with inactive human X chromosomes. *Nat Genet.* 30:73-6.
- Bolzer, A., J.M. Craig, T. Cremer, and M.R. Speicher. 1999. A complete set of repeat-depleted, PCR-amplifiable, human chromosome-specific painting probes. *Cytogenet Cell Genet.* 84:233-40.
- Borowski, E., M.M. Bontemps-Gracz, and A. Piwkowska. 2005. Strategies for overcoming ABC-transporters-mediated multidrug resistance (MDR) of tumor cells. *Acta Biochim Pol.* 52:609-27.
- Borst, P., R. Evers, M. Kool, and J. Wijnholds. 2000. A family of drug transporters: the multidrug resistance-associated proteins. *J Natl Cancer Inst.* 92:1295-302.
- Boyer, L.A., K. Plath, J. Zeitlinger, T. Brambrink, L.A. Medeiros, T.I. Lee, S.S. Levine, M. Wernig, A. Tajonar, M.K. Ray, G.W. Bell, A.P. Otte, M. Vidal, D.K. Gifford, R.A. Young, and R. Jaenisch. 2006. Polycomb complexes repress developmental regulators in murine embryonic stem cells. *Nature.* 441:349-53.
- Boyle, S., S. Gilchrist, J.M. Bridger, N.L. Mahy, J.A. Ellis, and W.A. Bickmore. 2001. The spatial organization of human chromosomes within the nuclei of normal and emerin-mutant cells. *Hum Mol Genet.* 10:211-9.
- Briggs, S.D., M. Bryk, B.D. Strahl, W.L. Cheung, J.K. Davie, S.Y. Dent, F. Winston, and C.D. Allis. 2001. Histone H3 lysine 4 methylation is mediated by Set1 and required for cell growth and rDNA silencing in *Saccharomyces cerevisiae*. *Genes Dev.* 15:3286-95.
- Brinkman, A.B., T. Roelofsen, S.W. Pennings, J.H. Martens, T. Jenuwein, and H.G. Stunnenberg. 2006. Histone modification patterns associated with the human X chromosome. *EMBO Rep.*
- Brown, K. 2002. Visualizing nuclear proteins together with transcribed and inactive genes in structurally preserved cells. *Methods.* 26:10-8.
- Brown, K.E., S.S. Guest, S.T. Smale, K. Hahm, M. Merkenschlager, and A.G. Fisher. 1997. Association of transcriptionally silent genes with Ikaros complexes at centromeric heterochromatin. *Cell.* 91:845-54.
- Brown, S.W. 1966. Heterochromatin. *Science.* 151:417-25.
- Brownell, J.E., C.A. Mizzen, and C.D. Allis. 1999. An SDS-PAGE-based enzyme activity assay for the detection and identification of histone acetyltransferases. *Methods Mol Biol.* 119:343-53.
- Brownell, J.E., J. Zhou, T. Ranalli, R. Kobayashi, D.G. Edmondson, S.Y. Roth, and C.D. Allis. 1996. Tetrahymena histone acetyltransferase A: a homolog to yeast Gcn5p linking histone acetylation to gene activation. *Cell.* 84:843-51.
- Buchon, N., and C. Vaury. 2006. RNAi: a defensive RNA-silencing against viruses and transposable elements. *Heredity.* 96:195-202.
- Cam, H.P., T. Sugiyama, E.S. Chen, X. Chen, P.C. FitzGerald, and S.I. Grewal. 2005. Comprehensive analysis of heterochromatin- and RNAi-mediated epigenetic control of the fission yeast genome. *Nat Genet.* 37:809-19.
- Cao, R., Y. Tsukada, and Y. Zhang. 2005. Role of Bmi-1 and Ring1A in H2A ubiquitylation and Hox gene silencing. *Mol Cell.* 20:845-54.
- Cao, R., L. Wang, H. Wang, L. Xia, H. Erdjument-Bromage, P. Tempst, R.S. Jones, and Y. Zhang. 2002. Role of histone H3 lysine 27 methylation in Polycomb-group silencing. *Science.* 298:1039-43.
- Caron, H., B. van Schaik, M. van der Mee, F. Baas, G. Riggins, P. van Sluis, M.C. Hermus, R. van Asperen, K. Boon, P.A. Voute, S. Heisterkamp, A. van Kampen, and R. Versteeg. 2001. The human transcriptome map: clustering of highly expressed genes in chromosomal domains. *Science.* 291:1289-92.
- Carrel, L., and H.F. Willard. 1999. Heterogeneous gene expression from the inactive X chromosome: an X-linked gene that escapes X inactivation in some human cell lines but is inactivated in others. *Proc Natl Acad Sci U S A.* 96:7364-9.
- Carrel, L., and H.F. Willard. 2005. X-inactivation profile reveals extensive variability in X-linked gene expression in females. *Nature.* 434:400-4.
- Carta, S., S. Tassi, C. Semino, G. Fossati, P. Mascagni, C.A. Dinarello, and A. Rubartelli. 2006. Histone deacetylase inhibitors prevent exocytosis of interleukin-1beta-containing secretory lysosomes: role of microtubules. *Blood.* 108:1618-26.
- Chadwick, B.P. 2006. Variation in Xi chromatin organization and correlation of the H3K27me3 chromatin territories to transcribed sequences by microarray analysis. *Chromosoma.*
- Chadwick, B.P., and H.F. Willard. 2004. Multiple spatially distinct types of facultative heterochromatin on the human inactive X chromosome. *Proc Natl Acad Sci U S A.* 101:17450-5.
- Chan, P.K. 1992. Characterization and cellular localization of nucleophosmin/B23 in HeLa cells treated with selected cytotoxic agents (studies of B23-translocation mechanism). *Exp Cell Res.* 203:174-81.
- Chan, P.K., D.A. Bloom, and T.T. Hoang. 1999. The N-terminal half of NPM dissociates from nucleoli of HeLa cells after anticancer drug treatments. *Biochem Biophys Res Commun.* 264:305-9.
- Chaumeil, J., I. Okamoto, M. Guggiari, and E. Heard. 2002. Integrated kinetics of X chromosome inactivation in differentiating embryonic stem cells. *Cytogenet Genome Res.* 99:75-84.
- Chen, C.J., J.E. Chin, K. Ueda, D.P. Clark, I. Pastan, M.M. Gottesman, and I.B. Roninson. 1986. Internal duplication and homology with bacterial transport proteins in the *mdr1* (P-glycoprotein) gene from multidrug-resistant human cells. *Cell.* 47:381-9.
- Cheng, J., P. Kapranov, J. Drenkow, S. Dike, S. Brubaker, S. Patel, J. Long, D. Stern, H. Tammana, G. Helt, V. Sementchenko, A. Piccolboni, S. Bekiranov, D.K. Bailey, M. Ganesh, S. Ghosh, I. Bell, D.S. Gerhard, and T.R. Gingeras. 2005. Transcriptional maps of 10 human chromosomes at 5-nucleotide resolution. *Science.* 308:1149-54.

- Cheung, P., K.G. Tanner, W.L. Cheung, P. Sassone-Corsi, J.M. Denu, and C.D. Allis. 2000. Synergistic coupling of histone H3 phosphorylation and acetylation in response to epidermal growth factor stimulation. *Mol Cell*. 5:905-15.
- Cheutin, T., A.J. McNairn, T. Jenuwein, D.M. Gilbert, P.B. Singh, and T. Misteli. 2003. Maintenance of stable heterochromatin domains by dynamic HP1 binding. *Science*. 299:721-5.
- Clarke, A.S., J.E. Lowell, S.J. Jacobson, and L. Pillus. 1999. Esa1p is an essential histone acetyltransferase required for cell cycle progression. *Mol Cell Biol*. 19:2515-26.
- Clayton, A.L., S. Rose, M.J. Barratt, and L.C. Mahadevan. 2000. Phosphoacetylation of histone H3 on c-fos- and c-jun-associated nucleosomes upon gene activation. *Embo J*. 19:3714-26.
- Clement, J.Q., and M.F. Wilkinson. 2000. Rapid induction of nuclear transcripts and inhibition of intron decay in response to the polymerase II inhibitor DRB. *J Mol Biol*. 299:1179-91.
- Cocklin, R.R., and M. Wang. 2003. Identification of methylation and acetylation sites on mouse histone H3 using matrix-assisted laser desorption/ionization time-of-flight and nanoelectrospray ionization tandem mass spectrometry. *J Protein Chem*. 22:327-34.
- Conchello, J.A., and J.W. Lichtman. 2005. Optical sectioning microscopy. *Nat Methods*. 2:920-31.
- Cosgrove, M.S., J.D. Boeke, and C. Wolberger. 2004. Regulated nucleosome mobility and the histone code. *Nat Struct Mol Biol*. 11:1037-43.
- Craig, J.M., and W.A. Bickmore. 1993. Chromosome bands--flavours to savour. *Bioessays*. 15:349-54.
- Cremer, M., J. von Hase, T. Volm, A. Brero, G. Kreth, J. Walter, C. Fischer, I. Solovei, C. Cremer, and T. Cremer. 2001. Non-random radial higher-order chromatin arrangements in nuclei of diploid human cells. *Chromosome Res*. 9:541-67.
- Cremer, M., R. Zinner, S. Stein, H. Albiez, B. Wagler, C. Cremer, and T. Cremer. 2004. Three dimensional analysis of histone methylation patterns in normal and tumor cell nuclei. *Eur J Histochem*. 48:15-28.
- Cremer, T., and C. Cremer. 2001. Chromosome territories, nuclear architecture and gene regulation in mammalian cells. *Nat Rev Genet*. 2:292-301.
- Cremer, T., A. Kurz, R. Zirbel, S. Dietzel, B. Rinke, E. Schrock, M.R. Speicher, U. Mathieu, A. Jauch, P. Emmerich, H. Scherthan, T. Ried, C. Cremer, and P. Lichter. 1993. Role of chromosome territories in the functional compartmentalization of the cell nucleus. *Cold Spring Harb Symp Quant Biol*. 58:777-92.
- Czernin, B., R. Melfi, D. McCabe, V. Seitz, A. Imhof, and V. Pirrotta. 2002. Drosophila enhancer of Zeste/ESC complexes have a histone H3 methyltransferase activity that marks chromosomal Polycomb sites. *Cell*. 111:185-96.
- Daujat, S., U.M. Bauer, V. Shah, B. Turner, S. Berger, and T. Kouzarides. 2002. Crosstalk between CARM1 methylation and CBP acetylation on histone H3. *Curr Biol*. 12:2090-7.
- de Maziere, A.M., W.J. Hage, and G.A. Ubbels. 1996. A method for staining of cell nuclei in *Xenopus laevis* embryos with cyanine dyes for whole-mount confocal laser scanning microscopy. *J Histochem Cytochem*. 44:399-402.
- Dehe, P.M., and V. Geli. 2006. The multiple faces of Set1. *Biochem Cell Biol*. 84:536-48.
- DeLange, R.J., Fambrough, D.M., Smith, E., Bonner, J. 1969a. Calf and pea histone IV.II. The complete amino acid sequence of calf thymus histone IV; presence of epsilon-N-aceyllysine. *J. Biol. Chem*. 244:319-334.
- DeLange, R.J., Fambrough, D.M., Smith, E., Bonner, J. 1969b. Calf and pea histone IV.III. Complete amino acid sequence of pea seedling histone IV; comparison with the homologous calf thymus histone. *J. Biol. Chem*. 244:5669-5679.
- Delaval, K., and R. Feil. 2004. Epigenetic regulation of mammalian genomic imprinting. *Curr Opin Genet Dev*. 14:188-95.
- Deng, W., S.W. Tsao, J.N. Lucas, C.S. Leung, and A.L. Cheung. 2003. A new method for improving metaphase chromosome spreading. *Cytometry A*. 51:46-51.
- Dhalluin, C., J.E. Carlson, L. Zeng, C. He, A.K. Aggarwal, and M.M. Zhou. 1999. Structure and ligand of a histone acetyltransferase bromodomain. *Nature*. 399:491-6.
- Dijk, v. 2005. Monomethyl histone H3 lysine 4 as an epigenetic mark for silenced euchromatin in *Chlamydomonas*. *Plant Cell*. 17:2439-2453.
- Dillon, N. 2004. Heterochromatin structure and function. *Biol Cell*. 96:631-7.
- Dillon, N., and R. Festenstein. 2002. Unravelling heterochromatin: competition between positive and negative factors regulates accessibility. *Trends Genet*. 18:252-8.
- Dimitrov, S., M.C. Dasso, and A.P. Wolffe. 1994. Remodeling sperm chromatin in *Xenopus laevis* egg extracts: the role of core histone phosphorylation and linker histone B4 in chromatin assembly. *J Cell Biol*. 126:591-601.
- Dimitrova, D.S., and R. Berezney. 2002. The spatio-temporal organization of DNA replication sites is identical in primary, immortalized and transformed mammalian cells. *J Cell Sci*. 115:4037-51.
- Disteche, C.M. 1995. Escape from X inactivation in human and mouse. *Trends Genet*. 11:17-22.
- Disteche, C.M. 1999. Escapees on the X chromosome. *Proc Natl Acad Sci U S A*. 96:14180-2.
- Doiron, K.M., J. Lavigne-Nicolas, and C.G. Cupples. 1999. Effect of interaction between 5-azacytidine and DNA (cytosine-5) methyltransferase on C-to-G and C-to-T mutations in *Escherichia coli*. *Mutat Res*. 429:37-44.
- Dundr, M., and T. Misteli. 2001. Functional architecture in the cell nucleus. *Biochem J*. 356:297-310.
- Earnshaw, W.C., and R.L. Bernat. 1991. Chromosomal passengers: toward an integrated view of mitosis. *Chromosoma*. 100:139-46.
- Earnshaw, W.C., and N. Rothfield. 1985. Identification of a family of human centromere proteins using autoimmune sera from patients with scleroderma. *Chromosoma*. 91:313-21.

- Edmondson, D.G., M.M. Smith, and S.Y. Roth. 1996. Repression domain of the yeast global repressor Tup1 interacts directly with histones H3 and H4. *Genes Dev.* 10:1247-59.
- Eissenberg, J.C., T.C. James, D.M. Foster-Hartnett, T. Hartnett, V. Ngan, and S.C. Elgin. 1990. Mutation in a heterochromatin-specific chromosomal protein is associated with suppression of position-effect variegation in *Drosophila melanogaster*. *Proc Natl Acad Sci U S A.* 87:9923-7.
- Espino, P.S., B. Drobic, K.L. Dunn, and J.R. Davie. 2005. Histone modifications as a platform for cancer therapy. *J Cell Biochem.* 94:1088-102.
- Fadeel, B., and S. Orrenius. 2005. Apoptosis: a basic biological phenomenon with wide-ranging implications in human disease. *J Intern Med.* 258:479-517.
- Fang, J., Q. Feng, C.S. Ketel, H. Wang, R. Cao, L. Xia, H. Erdjument-Bromage, P. Tempst, J.A. Simon, and Y. Zhang. 2002. Purification and functional characterization of SET8, a nucleosomal histone H4-lysine 20-specific methyltransferase. *Curr Biol.* 12:1086-99.
- Felsenfeld, G., and M. Groudine. 2003. Controlling the double helix. *Nature.* 421:448-53.
- Festenstein, R., S.N. Pagakis, K. Hiragami, D. Lyon, A. Verreault, B. Sekkali, and D. Kioussis. 2003. Modulation of heterochromatin protein 1 dynamics in primary Mammalian cells. *Science.* 299:719-21.
- Fiegler, H., P. Carr, E.J. Douglas, D.C. Burford, S. Hunt, C.E. Scott, J. Smith, D. Vetrie, P. Gorman, I.P. Tomlinson, and N.P. Carter. 2003. DNA microarrays for comparative genomic hybridization based on DOP-PCR amplification of BAC and PAC clones. *Genes Chromosomes Cancer.* 36:361-74.
- Firestein, R., X. Cui, P. Huie, and M.L. Cleary. 2000. Set domain-dependent regulation of transcriptional silencing and growth control by SUV39H1, a mammalian ortholog of *Drosophila* Su(var)3-9. *Mol Cell Biol.* 20:4900-9.
- Fischer, A., I. Hofmann, K. Naumann, and G. Reuter. 2006. Heterochromatin proteins and the control of heterochromatic gene silencing in *Arabidopsis*. *J Plant Physiol.* 163:358-68.
- Fischle, W., Y. Wang, and C.D. Allis. 2003a. Binary switches and modification cassettes in histone biology and beyond. *Nature.* 425:475-9.
- Fischle, W., Y. Wang, and C.D. Allis. 2003b. Histone and chromatin cross-talk. *Curr Opin Cell Biol.* 15:172-83.
- Flemming, W. 1882. Beiträge zur Kenntnis der Zelle und ihrer Lebenserscheinungen. In *Archiv für Mikroskopische Anatomie*. v. la valette St. George and W. Waldeyer, editors. Verlag von Max hen & Sohn, Bonn. 1-87.
- Fodor, B.D., S. Kubicek, M. Yonezawa, J. O'Sullivan R, R. Sengupta, L. Perez-Burgos, S. Opravil, K. Mechtler, G. Schotta, and T. Jenuwein. 2006. Jmjd2b antagonizes H3K9 trimethylation at pericentric heterochromatin in mammalian cells. *Genes Dev.*
- Fraga, M.F., E. Ballestar, A. Villar-Garea, M. Boix-Chornet, J. Espada, G. Schotta, T. Bonaldi, C. Haydon, S. Ropero, K. Petrie, N.G. Iyer, A. Perez-Rosado, E. Calvo, J.A. Lopez, A. Cano, M.J. Calasanz, D. Colomer, M.A. Piris, N. Ahn, A. Imhof, C. Caldas, T. Jenuwein, and M. Esteller. 2005. Loss of acetylation at Lys16 and trimethylation at Lys20 of histone H4 is a common hallmark of human cancer. *Nat Genet.* 37:391-400.
- Francke, U. 1994. Digitized and differentially shaded human chromosome ideograms for genomic applications. *Cytogenet Cell Genet.* 65:206-18.
- Freitag, M., and E.U. Selker. 2005. Controlling DNA methylation: many roads to one modification. *Curr Opin Genet Dev.* 15:191-9.
- Freitas, M.A., A.R. Sklenar, and M.R. Parthun. 2004. Application of mass spectrometry to the identification and quantification of histone post-translational modifications. *J Cell Biochem.* 92:691-700.
- Frey, U., S. Frey, F. Schollmeier, and M. Krug. 1996. Influence of actinomycin D, a RNA synthesis inhibitor, on long-term potentiation in rat hippocampal neurons in vivo and in vitro. *J Physiol.* 490 (Pt 3):703-11.
- Fuks, F. 2005. DNA methylation and histone modifications: teaming up to silence genes. *Curr Opin Genet Dev.* 15:490-5.
- Fuks, F., P.J. Hurd, D. Wolf, X. Nan, A.P. Bird, and T. Kouzarides. 2003. The methyl-CpG-binding protein MeCP2 links DNA methylation to histone methylation. *J Biol Chem.* 278:4035-40.
- Galun, E., J. Gressel, and A. Keynan. 1964. Suppression of Floral Induction of Actinomycin D - an Inhibitor of 'Messenger' Rna Synthesis. *Life Sci.* 3:911-5.
- Ganesan, S., D.P. Silver, R.A. Greenberg, D. Avni, R. Drapkin, A. Miron, S.C. Mok, V. Randrianarison, S. Brodie, J. Salstrom, T.P. Rasmussen, A. Klimke, C. Marrese, Y. Marahrens, C.X. Deng, J. Feunteun, and D.M. Livingston. 2002. BRCA1 supports XIST RNA concentration on the inactive X chromosome. *Cell.* 111:393-405.
- Garcia-Cao, M., R. O'Sullivan, A.H. Peters, T. Jenuwein, and M.A. Blasco. 2004. Epigenetic regulation of telomere length in mammalian cells by the Suv39h1 and Suv39h2 histone methyltransferases. *Nat Genet.* 36:94-9.
- Gardiner, D.M., P. Waring, and B.J. Howlett. 2005. The epipolythiodioxopiperazine (ETP) class of fungal toxins: distribution, mode of action, functions and biosynthesis. *Microbiology.* 151:1021-32.
- Gasser, S.M., and U.K. Laemmli. 1986. The organisation of chromatin loops: characterization of a scaffold attachment site. *Embo J.* 5:511-518.
- Geigl, J.B., S. Langer, S. Barwisch, K. Pflieger, G. Lederer, and M.R. Speicher. 2004. Analysis of gene expression patterns and chromosomal changes associated with aging. *Cancer Res.* 64:8550-7.
- Gilbert, N., S. Boyle, H. Fiegler, K. Woodfine, N.P. Carter, and W.A. Bickmore. 2004. Chromatin architecture of the human genome: gene-rich domains are enriched in open chromatin fibers. *Cell.* 118:555-66.
- Gilbert, N., S. Boyle, H. Sutherland, J. de Las Heras, J. Allan, T. Jenuwein, and W.A. Bickmore. 2003. Formation of facultative heterochromatin in the absence of HP1. *Embo J.* 22:5540-50.
- Gong, X.Q., Y.A. Nedialkov, and Z.F. Burton. 2004. Alpha-amanitin blocks translocation by human RNA polymerase II. *J Biol Chem.* 279:27422-7.

- Gonzalez, M., C.E. Argarana, and G.D. Fidelio. 1999. Extremely high thermal stability of streptavidin and avidin upon biotin binding. *Biomol Eng.* 16:67-72.
- Gonzalo, S., M. Garcia-Cao, M.F. Fraga, G. Schotta, A.H. Peters, S.E. Cotter, R. Eguia, D.C. Dean, M. Esteller, T. Jenuwein, and M.A. Blasco. 2005. Role of the RB1 family in stabilizing histone methylation at constitutive heterochromatin. *Nat Cell Biol.* 7:420-8.
- Gorisch, S.M., M. Wachsmuth, K.F. Toth, P. Lichter, and K. Rippe. 2005. Histone acetylation increases chromatin accessibility. *J Cell Sci.* 118:5825-34.
- Gottesman, M.M., S.V. Ambudkar, B. Ni, J.M. Aran, Y. Sugimoto, C.O. Cardarelli, and I. Pastan. 1994. Exploiting multidrug resistance to treat cancer. *Cold Spring Harb Symp Quant Biol.* 59:677-83.
- Grady, D.L., R.L. Ratliff, D.L. Robinson, E.C. McCanlies, J. Meyne, and R.K. Moyzis. 1992. Highly conserved repetitive DNA sequences are present at human centromeres. *Proc Natl Acad Sci U S A.* 89:1695-9.
- Grant, P.A., A. Eberharter, S. John, R.G. Cook, B.M. Turner, and J.L. Workman. 1999. Expanded lysine acetylation specificity of Gcn5 in native complexes. *J Biol Chem.* 274:5895-900.
- Gratzner, H.G. 1982. Monoclonal antibody to 5-bromo- and 5-iododeoxyuridine: A new reagent for detection of DNA replication. *Science.* 218:474-5.
- Greiner, D., T. Bonaldi, R. Eskeland, E. Roemer, and A. Imhof. 2005. Identification of a specific inhibitor of the histone methyltransferase SU(VAR)3-9. *Nat Chem Biol.* 1:143-5.
- Grigoryev, S.A., T. Nikitina, J.R. Pehrson, P.B. Singh, and C.L. Woodcock. 2004. Dynamic relocation of epigenetic chromatin markers reveals an active role of constitutive heterochromatin in the transition from proliferation to quiescence. *J Cell Sci.* 117:6153-62.
- Grimaud, B.F., Cavalli G. 2005. Fluorescent in situ Hybridization Combined with Immunostaining on Polytene Chromosomes. *Epigenome network of excellence: Research tools-protocols.*
- Grimwood, J., L.A. Gordon, A. Olsen, A. Terry, J. Schmutz, J. Lamerdin, U. Hellsten, D. Goodstein, O. Couronne, M. Tran-Gyamfi, A. Aerts, M. Altherr, L. Ashworth, E. Bajorek, S. Black, E. Branscomb, S. Caenepeel, A. Carrano, C. Caoile, Y.M. Chan, M. Christensen, C.A. Cleland, A. Copeland, E. Dalin, P. Dehal, M. Denys, J.C. Detter, J. Escobar, D. Flowers, D. Fotopulos, C. Garcia, A.M. Georgescu, T. Glavina, M. Gomez, E. Gonzales, M. Groza, N. Hammon, T. Hawkins, L. Haydu, I. Ho, W. Huang, S. Israni, J. Jett, K. Kadner, H. Kimball, A. Kobayashi, V. Larionov, S.H. Leem, F. Lopez, Y. Lou, S. Lowry, S. Malfatti, D. Martinez, P. McCready, C. Medina, J. Morgan, K. Nelson, M. Nolan, I. Ovcharenko, S. Pitluck, M. Pollard, A.P. Popkie, P. Predki, G. Quan, L. Ramirez, S. Rash, J. Retterer, A. Rodriguez, S. Rogers, A. Salamov, A. Salazar, X. She, D. Smith, T. Slezak, V. Solovyev, N. Thayer, H. Tice, M. Tsai, A. Ustaszewska, N. Vo, M. Wagner, J. Wheeler, K. Wu, G. Xie, J. Yang, I. Dubchak, T.S. Furey, P. DeJong, M. Dickson, D. Gordon, E.E. Eichler, L.A. Pennacchio, P. Richardson, L. Stubbs, D.S. Rokhsar, R.M. Myers, E.M. Rubin, and S.M. Lucas. 2004. The DNA sequence and biology of human chromosome 19. *Nature.* 428:529-35.
- Hague, A., A.M. Manning, K.A. Hanlon, L.I. Huschtscha, D. Hart, and C. Paraskeva. 1993. Sodium butyrate induces apoptosis in human colonic tumour cell lines in a p53-independent pathway: implications for the possible role of dietary fibre in the prevention of large-bowel cancer. *Int J Cancer.* 55:498-505.
- Heard, E. 2005. Delving into the diversity of facultative heterochromatin: the epigenetics of the inactive X chromosome. *Curr Opin Genet Dev.* 15:482-9.
- Heard, E., C. Rougeulle, D. Arnaud, P. Avner, C.D. Allis, and D.L. Spector. 2001. Methylation of histone H3 at Lys-9 is an early mark on the X chromosome during X inactivation. *Cell.* 107:727-38.
- Hecht, A., T. Laroche, S. Strahl-Bolsinger, S.M. Gasser, and M. Grunstein. 1995. Histone H3 and H4 N-termini interact with SIR3 and SIR4 proteins: a molecular model for the formation of heterochromatin in yeast. *Cell.* 80:583-92.
- Heitz, E. 1928. Das Heterochromatin der Moose. *Jahrb. Wiss. Botanik.* 1:762-818.
- Hendrich, B., and A. Bird. 1998. Identification and characterization of a family of mammalian methyl-CpG binding proteins. *Mol Cell Biol.* 18:6538-47.
- Hendrich, B., and S. Tweedie. 2003. The methyl-CpG binding domain and the evolving role of DNA methylation in animals. *Trends Genet.* 19:269-77.
- Henzel, M.J., W.K. Nishioka, Y. Raymond, C.D. Allis, D.P. Bazett-Jones, and J.P. Th'ng. 1998. Chromatin condensation is not associated with apoptosis. *J Biol Chem.* 273:24470-8.
- Hensold, J.O., D. Barth, and C.A. Stratton. 1996. RNA polymerase II inhibitor, 5,6-dichloro-1-beta-D-ribofuranosylbenzimidazole (DRB) causes erythroleukemic differentiation and transcriptional activation of erythroid genes. *J Cell Physiol.* 168:105-13.
- Hermann, A., S. Schmitt, and A. Jeltsch. 2003. The human Dnmt2 has residual DNA-(cytosine-C5) methyltransferase activity. *J Biol Chem.* 278:31717-21.
- Higgins, C.F. 1992. ABC transporters: from microorganisms to man. *Annu Rev Cell Biol.* 8:67-113.
- Huang, S., T.J. Deerinck, M.H. Ellisman, and D.L. Spector. 1994. In vivo analysis of the stability and transport of nuclear poly(A)+ RNA. *J Cell Biol.* 126:877-99.
- Huisinga, K.L., B. Brower-Toland, and S.C. Elgin. 2006. The contradictory definitions of heterochromatin: transcription and silencing. *Chromosoma.* 115:110-22.
- Imai, S., C.M. Armstrong, M. Kaeberlein, and L. Guarente. 2000. Transcriptional silencing and longevity protein Sir2 is an NAD-dependent histone deacetylase. *Nature.* 403:795-800.
- Isham, C.R., J.D. Tibodeau, W. Jin, R. Xu, M.M. Timm, and K.C. Bible. 2006. Chaetocin, a promising new anti-melanoma agent with in vitro and in vivo activity mediated via imposition of oxidative stress. *Blood.*
- James, T.C., and S.C. Elgin. 1986. Identification of a nonhistone chromosomal protein associated with heterochromatin in *Drosophila melanogaster* and its gene. *Mol Cell Biol.* 6:3862-72.

- Janicki, S.M., T. Tsukamoto, S.E. Salghetti, W.P. Tansey, R. Sachidanandam, K.V. Prasanth, T. Ried, Y. Shav-Tal, E. Bertrand, R.H. Singer, and D.L. Spector. 2004. From silencing to gene expression: real-time analysis in single cells. *Cell*. 116:683-98.
- Jenuwein, T., and C.D. Allis. 2001. Translating the histone code. *Science*. 293:1074-80.
- Jones, D.O., I.G. Cowell, and P.B. Singh. 2000. Mammalian chromodomain proteins: their role in genome organisation and expression. *Bioessays*. 22:124-37.
- Jones, P.A., and S.B. Baylin. 2002. The fundamental role of epigenetic events in cancer. *Nat Rev Genet*. 3:415-28.
- Juliano, R.L., and V. Ling. 1976. A surface glycoprotein modulating drug permeability in Chinese hamster ovary cell mutants. *Biochim Biophys Acta*. 455:152-62.
- Julien, E., and W. Herr. 2004. A switch in mitotic histone H4 lysine 20 methylation status is linked to M phase defects upon loss of HCF-1. *Mol Cell*. 14:713-25.
- Karachentsev, D., K. Sarma, D. Reinberg, and R. Steward. 2005. PR-Set7-dependent methylation of histone H4 Lys 20 functions in repression of gene expression and is essential for mitosis. *Genes Dev*. 19:431-5.
- Katan-Khaykovich, Y., and K. Struhl. 2005. Heterochromatin formation involves changes in histone modifications over multiple cell generations. *Embo J*. 24:2138-49.
- Keohane, A.M., P. O'Neill, N.D. Belyaev, J.S. Lavender, and B.M. Turner. 1996. X-Inactivation and histone H4 acetylation in embryonic stem cells. *Dev Biol*. 180:618-30.
- Khorasanizadeh, S. 2004. The nucleosome: from genomic organization to genomic regulation. *Cell*. 116:259-72.
- Kim, S., and W.K. Paik. 1965. Studies on the origin of epsilon-N-methyl-L-lysine in protein. *J Biol Chem*. 240:4629-34.
- Kim, S.M., D.D. Dubey, and J.A. Huberman. 2003. Early-replicating heterochromatin. *Genes Dev*. 17:330-5.
- Klose, R.J., and A.P. Bird. 2006. Genomic DNA methylation: the mark and its mediators. *Trends Biochem Sci*. 31:89-97.
- Kohlmaier, A., F. Savarese, M. Lachner, J. Martens, T. Jenuwein, and A. Wutz. 2004. A chromosomal memory triggered by Xist regulates histone methylation in X inactivation. *PLoS Biol*. 2:E171.
- Kornberg, R.D. 1974. Chromatin structure: a repeating unit of histones and DNA. *Science*. 184:868-71.
- Korpela, J. 1984. Avidin, a high affinity biotin-binding protein, as a tool and subject of biological research. *Med Biol*. 62:5-26.
- Kourmouli, N., P. Jeppesen, S. Mahadevhaiah, P. Burgoyne, R. Wu, D.M. Gilbert, S. Bongiorno, G. Prantera, L. Fanti, S. Pimpinelli, W. Shi, R. Fundele, and P.B. Singh. 2004. Heterochromatin and tri-methylated lysine 20 of histone H4 in animals. *J Cell Sci*. 117:2491-501.
- Kouzarides, T. 2002. Histone methylation in transcriptional control. *Curr Opin Genet Dev*. 12:198-209.
- Kouzarides, T. 2007. Chromatin modifications and their function. *Cell*. 128:693-705.
- Kreft, M., I. Milisav, M. Potokar, and R. Zorec. 2004. Automated high through-put colocalization analysis of multichannel confocal images. *Comput Methods Programs Biomed*. 74:63-7.
- Krogan, N.J., J. Dover, S. Khorrami, J.F. Greenblatt, J. Schneider, M. Johnston, and A. Shilatifard. 2002. COMPASS, a histone H3 (Lysine 4) methyltransferase required for telomeric silencing of gene expression. *J Biol Chem*. 277:10753-5.
- Kruger, W., C.L. Peterson, A. Sil, C. Coburn, G. Arents, E.N. Moudrianakis, and I. Herskowitz. 1995. Amino acid substitutions in the structured domains of histones H3 and H4 partially relieve the requirement of the yeast SWI/SNF complex for transcription. *Genes Dev*. 9:2770-9.
- Kupper, K., A. Kolbl, D. Biener, S. Dittrich, J. von Hase, T. Thormeyer, H. Fiegler, N.P. Carter, M.R. Speicher, T. Cremer, and M. Cremer. 2007. Radial chromatin positioning is shaped by local gene density, not by gene expression. *Chromosoma*.
- Kurdistani, S.K., and M. Grunstein. 2003. Histone acetylation and deacetylation in yeast. *Nat Rev Mol Cell Biol*. 4:276-84.
- Kurdistani, S.K., S. Tavazoie, and M. Grunstein. 2004. Mapping global histone acetylation patterns to gene expression. *Cell*. 117:721-33.
- Kuzmichev, A., K. Nishioka, H. Erdjument-Bromage, P. Tempst, and D. Reinberg. 2002. Histone methyltransferase activity associated with a human multiprotein complex containing the Enhancer of Zeste protein. *Genes Dev*. 16:2893-905.
- Lachmanovich, E., D.E. Shvartsman, Y. Malka, C. Botvin, Y.I. Henis, and A.M. Weiss. 2003. Co-localization analysis of complex formation among membrane proteins by computerized fluorescence microscopy: application to immunofluorescence co-patching studies. *J Microsc*. 212:122-31.
- Lachner, M., and T. Jenuwein. 2002. The many faces of histone lysine methylation. *Curr Opin Cell Biol*. 14:286-98.
- Lachner, M., D. O'Carroll, S. Rea, K. Mechtler, and T. Jenuwein. 2001. Methylation of histone H3 lysine 9 creates a binding site for HP1 proteins. *Nature*. 410:116-20.
- Lachner, M., R.J. O'Sullivan, and T. Jenuwein. 2003. An epigenetic road map for histone lysine methylation. *J Cell Sci*. 116:2117-24.
- Lachner, M., R. Sengupta, G. Schotta, and T. Jenuwein. 2004. Trilogies of histone lysine methylation as epigenetic landmarks of the eukaryotic genome. *Cold Spring Harb Symp Quant Biol*. 69:209-18.
- Lander, E.S., L.M. Linton, B. Birren, C. Nusbaum, M.C. Zody, J. Baldwin, K. Devon, K. Dewar, M. Doyle, W. FitzHugh, R. Funke, D. Gage, K. Harris, A. Heaford, J. Howland, L. Kann, J. Lehoczy, R. LeVine, P. McEwan, K. McKernan, J. Meldrim, J.P. Mesirov, C. Miranda, W. Morris, J. Naylor, C. Raymond, M. Rosetti, R. Santos, A. Sheridan, C. Sougnez, N. Stange-Thomann, N. Stojanovic, A. Subramanian, D. Wyman, J. Rogers, J. Sulston, R. Ainscough, S. Beck, D. Bentley, J. Burton, C. Clee, N. Carter, A. Coulson, R. Deadman, P. Deloukas, A. Dunham, I. Dunham, R. Durbin, L. French, D. Grafham, S.

- Gregory, T. Hubbard, S. Humphray, A. Hunt, M. Jones, C. Lloyd, A. McMurray, L. Matthews, S. Mercer, S. Milne, J.C. Mullikin, A. Mungall, R. Plumb, M. Ross, R. Showkeen, S. Sims, R.H. Waterston, R.K. Wilson, L.W. Hillier, J.D. McPherson, M.A. Marra, E.R. Mardis, L.A. Fulton, A.T. Chinwalla, K.H. Pepin, W.R. Gish, S.L. Chissoe, M.C. Wendl, K.D. Delehaunty, T.L. Miner, A. Delehaunty, J.B. Kramer, L.L. Cook, R.S. Fulton, D.L. Johnson, P.J. Minx, S.W. Clifton, T. Hawkins, E. Branscomb, P. Predki, P. Richardson, S. Wenning, T. Slezak, N. Doggett, J.F. Cheng, A. Olsen, S. Lucas, C. Elkin, E. Uberbacher, M. Frazier, et al. 2001. Initial sequencing and analysis of the human genome. *Nature*. 409:860-921.
- Landmann, L. 2002. Deconvolution improves colocalization analysis of multiple fluorochromes in 3D confocal data sets more than filtering techniques. *J Microsc.* 208:134-47.
- Landmann, L., and P. Marbet. 2004. Colocalization analysis yields superior results after image restoration. *Microsc Res Tech.* 64:103-12.
- Langst, G., and P.B. Becker. 2004. Nucleosome remodeling: one mechanism, many phenomena? *Biochim Biophys Acta.* 1677:58-63.
- Lavrov, S., J. DeJardin, and G. Cavalli. 2004. Combined immunostaining and FISH analysis of polytene chromosomes. *Methods Mol Biol.* 247:289-303.
- Lawen, A. 2003. Apoptosis-an introduction. *Bioessays.* 25:888-96.
- Lehnertz, B., Y. Ueda, A.A. Derijck, U. Braunschweig, L. Perez-Burgos, S. Kubicek, T. Chen, E. Li, T. Jenuwein, and A.H. Peters. 2003. Suv39h-mediated histone H3 lysine 9 methylation directs DNA methylation to major satellite repeats at pericentric heterochromatin. *Curr Biol.* 13:1192-200.
- Lesne, A. 2006. The chromatin regulatory code: Beyond a histone code. *Eur Phys J E Soft Matter.* 19:375-7.
- Lesne, A., and J.M. Victor. 2006. Chromatin fiber functional organization: Some plausible models. *Eur Phys J E Soft Matter.* 19:279-90.
- Lewis, J.D., R.R. Meehan, W.J. Henzel, I. Maurer-Fogy, P. Jeppesen, F. Klein, and A. Bird. 1992. Purification, sequence, and cellular localization of a novel chromosomal protein that binds to methylated DNA. *Cell.* 69:905-14.
- Li, B., M. Carey, and J.L. Workman. 2007. The Role of Chromatin during Transcription. *Cell.* 128:707-19.
- Li, E. 2002. Chromatin modification and epigenetic reprogramming in mammalian development. *Nat Rev Genet.* 3:662-73.
- Li, E., T.H. Bestor, and R. Jaenisch. 1992. Targeted mutation of the DNA methyltransferase gene results in embryonic lethality. *Cell.* 69:915-26.
- Lichtman, J.W., and J.A. Conchello. 2005. Fluorescence microscopy. *Nat Methods.* 2:910-9.
- Litt, M.D., M. Simpson, M. Gaszner, C.D. Allis, and G. Felsenfeld. 2001. Correlation between histone lysine methylation and developmental changes at the chicken beta-globin locus. *Science.* 293:2453-5.
- Lock, R.B., and L. Stribinskiene. 1996. Dual modes of death induced by etoposide in human epithelial tumor cells allow Bcl-2 to inhibit apoptosis without affecting clonogenic survival. *Cancer Res.* 56:4006-12.
- Lomberk, G., D. Bensi, M.E. Fernandez-Zapico, and R. Urrutia. 2006. Evidence for the existence of an HP1-mediated subcode within the histone code. *Nat Cell Biol.* 8:407-15.
- Lottspeich, F.Z., H. 1998. Bioanalytik. *Spektrum.*
- Lu, L.J., and K. Randerath. 1980. Mechanism of 5-azacytidine-induced transfer RNA cytosine-5-methyltransferase deficiency. *Cancer Res.* 40:2701-5.
- Lyon, M.F. 1999. X-chromosome inactivation. *Curr Biol.* 9:R235-7.
- Mager, J., N.D. Montgomery, F.P. de Villena, and T. Magnuson. 2003. Genome imprinting regulated by the mouse Polycomb group protein Eed. *Nat Genet.* 33:502-7.
- Mahadevan, L.C., A.C. Willis, and M.J. Barratt. 1991. Rapid histone H3 phosphorylation in response to growth factors, phorbol esters, okadaic acid, and protein synthesis inhibitors. *Cell.* 65:775-83.
- Maison, C., and G. Almouzni. 2004. HP1 and the dynamics of heterochromatin maintenance. *Nat Rev Mol Cell Biol.* 5:296-304.
- Maison, C., D. Bailly, A.H. Peters, J.P. Quivy, D. Roche, A. Taddei, M. Lachner, T. Jenuwein, and G. Almouzni. 2002. Higher-order structure in pericentric heterochromatin involves a distinct pattern of histone modification and an RNA component. *Nat Genet.* 30:329-34.
- Malikov, V., E.N. Cytrynbaum, A. Kashina, A. Mogilner, and V. Rodionov. 2005. Centering of a radial microtubule array by translocation along microtubules spontaneously nucleated in the cytoplasm. *Nat Cell Biol.* 7:1213-8.
- Manders, E.M., J. Stap, G.J. Brakenhoff, R. van Driel, and J.A. Aten. 1992. Dynamics of three-dimensional replication patterns during the S-phase, analysed by double labelling of DNA and confocal microscopy. *J Cell Sci.* 103 (Pt 3):857-62.
- Manders, E.M.M., F.J. Verbeek, and J.A. Aten. 1993. Measurement of co-localization of objects in dual-colour confocal images. *Journal of Microscopy.* 169:375-382.
- Mann, M., and O.N. Jensen. 2003. Proteomic analysis of post-translational modifications. *Nat Biotechnol.* 21:255-61.
- Manuelidis, L. 1990. A view of interphase chromosomes. *Science.* 250:1533-40.
- Markham, J., and J.A. Conchello. 2001. Artefacts in restored images due to intensity loss in three-dimensional fluorescence microscopy. *J Microsc.* 204:93-8.
- Martens, J.H., R.J. O'Sullivan, U. Braunschweig, S. Opravil, M. Radolf, P. Steinlein, and T. Jenuwein. 2005. The profile of repeat-associated histone lysine methylation states in the mouse epigenome. *Embo J.* 24:800-12.
- Martin, C., and Y. Zhang. 2005. The diverse functions of histone lysine methylation. *Nat Rev Mol Cell Biol.* 6:838-49.

- Martin, S., and A. Pombo. 2003. Transcription factories: quantitative studies of nanostructures in the mammalian nucleus. *Chromosome Res.* 11:461-70.
- Mateescu, B., P. England, F. Halgand, M. Yaniv, and C. Muchardt. 2004. Tethering of HP1 proteins to chromatin is relieved by phosphoacetylation of histone H3. *EMBO Rep.* 5:490-6.
- Mathis, G., and F.R. Althaus. 1990. Uncoupling of DNA excision repair and nucleosomal unfolding in poly(ADP-ribose)-depleted mammalian cells. *Carcinogenesis.* 11:1237-9.
- Matsuzaki, S.M., Fujikura K, Takata K. 1997. Nuclear staining for laser confocal microscopy. *Acta Histochem Cytochem.* 30:309-314.
- Mattick, J.S. 2003. Challenging the dogma: the hidden layer of non-protein-coding RNAs in complex organisms. *Bioessays.* 25:930-9.
- Matzke, M.A., and J.A. Birchler. 2005. RNAi-mediated pathways in the nucleus. *Nat Rev Genet.* 6:24-35.
- McNally, J.G., T. Karpova, J. Cooper, and J.A. Conchello. 1999. Three-dimensional imaging by deconvolution microscopy. *Methods.* 19:373-85.
- Meehan, R.R., J.D. Lewis, S. McKay, E.L. Kleiner, and A.P. Bird. 1989. Identification of a mammalian protein that binds specifically to DNA containing methylated CpGs. *Cell.* 58:499-507.
- Melcher, M., M. Schmid, L. Aagaard, P. Selenko, G. Laible, and T. Jenuwein. 2000. Structure-function analysis of SUV39H1 reveals a dominant role in heterochromatin organization, chromosome segregation, and mitotic progression. *Mol Cell Biol.* 20:3728-41.
- Mellor, J. 2005. The dynamics of chromatin remodeling at promoters. *Mol Cell.* 19:147-57.
- Mermoud, J.E., B. Popova, A.H. Peters, T. Jenuwein, and N. Brockdorff. 2002. Histone H3 lysine 9 methylation occurs rapidly at the onset of random X chromosome inactivation. *Curr Biol.* 12:247-51.
- Merrick, S.E., J.Q. Trojanowski, and V.M. Lee. 1997. Selective destruction of stable microtubules and axons by inhibitors of protein serine/threonine phosphatases in cultured human neurons. *J Neurosci.* 17:5726-37.
- Misteli, T. 2004. Spatial positioning; a new dimension in genome function. *Cell.* 119:153-6.
- Misteli, T. 2005. Concepts in nuclear architecture. *Bioessays.* 27:477-87.
- Misteli, T. 2007. Beyond the sequence: cellular organization of genome function. *Cell.* 128:787-800.
- Muller, H.J. 1930. Types of visible variations produced by X-rays in *Drosophila melanogaster*. *J.Genet.* 22:299-334.
- Murray, K. 1964. The occurrence of e-N-methyllysine in histones. *Biochemistry.* 3:10-15.
- Myster, S.H., F. Wang, R. Cavallo, W. Christian, S. Bhotika, C.T. Anderson, and M. Peifer. 2004. Genetic and bioinformatic analysis of 41C and the 2R heterochromatin of *Drosophila melanogaster*: a window on the heterochromatin-euchromatin junction. *Genetics.* 166:807-22.
- Nakamura, T.M., L.L. Du, C. Redon, and P. Russell. 2004. Histone H2A phosphorylation controls Crb2 recruitment at DNA breaks, maintains checkpoint arrest, and influences DNA repair in fission yeast. *Mol Cell Biol.* 24:6215-30.
- Nakayama, J., J.C. Rice, B.D. Strahl, C.D. Allis, and S.I. Grewal. 2001. Role of histone H3 lysine 9 methylation in epigenetic control of heterochromatin assembly. *Science.* 292:110-3.
- Nan, X., H.H. Ng, C.A. Johnson, C.D. Laherty, B.M. Turner, R.N. Eisenman, and A. Bird. 1998. Transcriptional repression by the methyl-CpG-binding protein MeCP2 involves a histone deacetylase complex. *Nature.* 393:386-9.
- Narita, M., S. Nunez, E. Heard, A.W. Lin, S.A. Hearn, D.L. Spector, G.J. Hannon, and S.W. Lowe. 2003. Rb-mediated heterochromatin formation and silencing of E2F target genes during cellular senescence. *Cell.* 113:703-16.
- Ng, H.H., F. Robert, R.A. Young, and K. Struhl. 2003. Targeted recruitment of Set1 histone methylase by elongating Pol II provides a localized mark and memory of recent transcriptional activity. *Mol Cell.* 11:709-19.
- Nicolas, E., C. Roumillac, and D. Trouche. 2003. Balance between acetylation and methylation of histone H3 lysine 9 on the E2F-responsive dihydrofolate reductase promoter. *Mol Cell Biol.* 23:1614-22.
- Nielsen, S.J., R. Schneider, U.M. Bauer, A.J. Bannister, A. Morrison, D. O'Carroll, R. Firestein, M. Cleary, T. Jenuwein, R.E. Herrera, and T. Kouzarides. 2001. Rb targets histone H3 methylation and HP1 to promoters. *Nature.* 412:561-5.
- Nightingale, K.P., L.P. O'Neill, and B.M. Turner. 2006. Histone modifications: signalling receptors and potential elements of a heritable epigenetic code. *Curr Opin Genet Dev.* 16:125-36.
- Nishioka, K., J.C. Rice, K. Sarma, H. Erdjument-Bromage, J. Werner, Y. Wang, S. Chuikov, P. Valenzuela, P. Tempst, R. Steward, J.T. Lis, C.D. Allis, and D. Reinberg. 2002. PR-Set7 is a nucleosome-specific methyltransferase that modifies lysine 20 of histone H4 and is associated with silent chromatin. *Mol Cell.* 9:1201-13.
- Nusbaum, C., M.C. Zody, M.L. Borowsky, M. Kamal, C.D. Kodira, T.D. Taylor, C.A. Whittaker, J.L. Chang, C.A. Cuomo, K. Dewar, M.G. FitzGerald, X. Yang, A. Abouelleil, N.R. Allen, S. Anderson, T. Bloom, B. Bugalter, J. Butler, A. Cook, D. DeCaprio, R. Engels, M. Garber, A. Gnirke, N. Hafez, J.L. Hall, C.H. Norman, T. Itoh, D.B. Jaffe, Y. Kuroki, J. Lehoczy, A. Lui, P. Macdonald, E. Mauceli, T.S. Mikkelsen, J.W. Naylor, R. Nicol, C. Nguyen, H. Noguchi, S.B. O'Leary, K. O'Neill, B. Piqani, C.L. Smith, J.A. Talamas, K. Topham, Y. Totoki, A. Toyoda, H.M. Wain, S.K. Young, Q. Zeng, A.R. Zimmer, A. Fujiyama, M. Hattori, B.W. Birren, Y. Sakaki, and E.S. Lander. 2005. DNA sequence and analysis of human chromosome 18. *Nature.* 437:551-5.
- O'Carroll, D., S. Erhardt, M. Pagani, S.C. Barton, M.A. Surani, and T. Jenuwein. 2001. The polycomb-group gene *Ezh2* is required for early mouse development. *Mol Cell Biol.* 21:4330-6.
- Okamoto, I., A.P. Otte, C.D. Allis, D. Reinberg, and E. Heard. 2004. Epigenetic dynamics of imprinted X inactivation during early mouse development. *Science.* 303:644-9.

- Okano, M., D.W. Bell, D.A. Haber, and E. Li. 1999. DNA methyltransferases Dnmt3a and Dnmt3b are essential for de novo methylation and mammalian development. *Cell*. 99:247-57.
- Olins, A.L., and D.E. Olins. 1974. Spheroid chromatin units (v bodies). *Science*. 183:330-2.
- Paik, W.K., and S. Kim. 1971. Protein methylation. *Science*. 174:114-9.
- Panning, B., J. Dausman, and R. Jaenisch. 1997. X chromosome inactivation is mediated by Xist RNA stabilization. *Cell*. 90:907-16.
- Parada, L.A., S. Sotiriou, and T. Misteli. 2004. Spatial genome organization. *Exp Cell Res*. 296:64-70.
- Park, J.H., M.S. Cosgrove, E. Youngman, C. Wolberger, and J.D. Boeke. 2002. A core nucleosome surface crucial for transcriptional silencing. *Nat Genet*. 32:273-9.
- Paro, R., and D.S. Hogness. 1991. The Polycomb protein shares a homologous domain with a heterochromatin-associated protein of *Drosophila*. *Proc Natl Acad Sci U S A*. 88:263-7.
- Parthun, M.R., J. Widom, and D.E. Gottschling. 1996. The major cytoplasmic histone acetyltransferase in yeast: links to chromatin replication and histone metabolism. *Cell*. 87:85-94.
- Paulson, J.R., and U.K. Laemmli. 1977. The structure of histone-depleted metaphase chromosomes. *Cell*. 12:817-28.
- Pawley, J.B. 2006. Handbook of biological confocal microscopy. *Springer (Science and business media)*.
- Pederson, T. 1999. Movement and localization of RNA in the cell nucleus. *Faseb J*. 13 Suppl 2:S238-42.
- Perez-Burgos, L., A.H. Peters, S. Opravil, M. Kauer, K. Mechtler, and T. Jenuwein. 2004. Generation and characterization of methyl-lysine histone antibodies. *Methods Enzymol*. 376:234-54.
- Peters, A.H., S. Kubicek, K. Mechtler, R.J. O'Sullivan, A.A. Derijck, L. Perez-Burgos, A. Kohlmaier, S. Opravil, M. Tachibana, Y. Shinkai, J.H. Martens, and T. Jenuwein. 2003. Partitioning and plasticity of repressive histone methylation states in mammalian chromatin. *Mol Cell*. 12:1577-89.
- Peters, A.H., D. O'Carroll, H. Scherthan, K. Mechtler, S. Sauer, C. Schofer, K. Weipoltshammer, M. Pagani, M. Lachner, A. Kohlmaier, S. Opravil, M. Doyle, M. Sibilia, and T. Jenuwein. 2001. Loss of the Suv39h histone methyltransferases impairs mammalian heterochromatin and genome stability. *Cell*. 107:323-37.
- Petty, B.J., Robertson ME. 2000. Thermodynamic characterization of the association of cyanine dyes with DNA. *J Phys Chem. B* 104:7221-7227.
- Pickersgill, H., B. Kalverda, E. de Wit, W. Talhout, M. Fornerod, and B. van Steensel. 2006. Characterization of the *Drosophila melanogaster* genome at the nuclear lamina. *Nat Genet*. 38:1005-14.
- Plath, K., J. Fang, S.K. Mlynarczyk-Evans, R. Cao, K.A. Worringer, H. Wang, C.C. de la Cruz, A.P. Otte, B. Panning, and Y. Zhang. 2003. Role of histone H3 lysine 27 methylation in X inactivation. *Science*. 300:131-5.
- Pokholok, D.K., C.T. Harbison, S. Levine, M. Cole, N.M. Hannett, T.I. Lee, G.W. Bell, K. Walker, P.A. Rolfe, E. Herbolzheimer, J. Zeitlinger, F. Lwitter, D.K. Gifford, and R.A. Young. 2005. Genome-wide map of nucleosome acetylation and methylation in yeast. *Cell*. 122:517-27.
- Politz, J.C., R.A. Tuft, T. Pederson, and R.H. Singer. 1999. Movement of nuclear poly(A) RNA throughout the interchromatin space in living cells. *Curr Biol*. 9:285-91.
- Postberg, J., O. Alexandrova, T. Cremer, and H.J. Lipps. 2005. Exploiting nuclear duality of ciliates to analyse topological requirements for DNA replication and transcription. *J Cell Sci*. 118:3973-83.
- Raska, I., K. Koberna, J. Malinsky, H. Fidlerova, and M. Masata. 2004. The nucleolus and transcription of ribosomal genes. *Biol Cell*. 96:579-94.
- Rea, S., F. Eisenhaber, D. O'Carroll, B.D. Strahl, Z.W. Sun, M. Schmid, S. Opravil, K. Mechtler, C.P. Ponting, C.D. Allis, and T. Jenuwein. 2000. Regulation of chromatin structure by site-specific histone H3 methyltransferases. *Nature*. 406:593-9.
- Reik, W., W. Dean, and J. Walter. 2001. Epigenetic reprogramming in mammalian development. *Science*. 293:1089-93.
- Reinberg, D., S. Chuikov, P. Farnham, D. Karachentsev, A. Kirmizis, A. Kuzmichev, R. Margueron, K. Nishioka, T.S. Preissner, K. Sarma, C. Abate-Shen, R. Steward, and A. Vaquero. 2004. Steps toward understanding the inheritance of repressive methyl-lysine marks in histones. *Cold Spring Harb Symp Quant Biol*. 69:171-82.
- Rice, J.C., S.D. Briggs, B. Ueberheide, C.M. Barber, J. Shabanowitz, D.F. Hunt, Y. Shinkai, and C.D. Allis. 2003. Histone methyltransferases direct different degrees of methylation to define distinct chromatin domains. *Mol Cell*. 12:1591-8.
- Riggs, A.D. 1975. X inactivation, differentiation, and DNA methylation. *Cytogenet Cell Genet*. 14:9-25.
- Ringrose, L., and R. Paro. 2004. Epigenetic regulation of cellular memory by the Polycomb and Trithorax group proteins. *Annu Rev Genet*. 38:413-43.
- Robertson, K.D. 2005. DNA methylation and human disease. *Nat Rev Genet*. 6:597-610.
- Robertson, K.D., S. Ait-Si-Ali, T. Yokochi, P.A. Wade, P.L. Jones, and A.P. Wolffe. 2000. DNMT1 forms a complex with Rb, E2F1 and HDAC1 and represses transcription from E2F-responsive promoters. *Nat Genet*. 25:338-42.
- Roninson, I.B., E.V. Broude, and B.D. Chang. 2001. If not apoptosis, then what? Treatment-induced senescence and mitotic catastrophe in tumor cells. *Drug Resist Updat*. 4:303-13.
- Rougeulle, C., J. Chaumeil, K. Sarma, C.D. Allis, D. Reinberg, P. Avner, and E. Heard. 2004. Differential histone H3 Lys-9 and Lys-27 methylation profiles on the X chromosome. *Mol Cell Biol*. 24:5475-84.
- Ruthenburg, A.J., C.D. Allis, and J. Wysocka. 2007. Methylation of lysine 4 on histone H3: intricacy of writing and reading a single epigenetic mark. *Mol Cell*. 25:15-30.
- Sanders, S.L., M. Portoso, J. Mata, J. Bahler, R.C. Allshire, and T. Kouzarides. 2004. Methylation of histone H4 lysine 20 controls recruitment of Crb2 to sites of DNA damage. *Cell*. 119:603-14.

- Santos-Rosa, H., R. Schneider, A.J. Bannister, J. Sherriff, B.E. Bernstein, N.C. Emre, S.L. Schreiber, J. Mellor, and T. Kouzarides. 2002. Active genes are tri-methylated at K4 of histone H3. *Nature*. 419:407-11.
- Sarraf, S.A., and I. Stancheva. 2004. Methyl-CpG binding protein MBD1 couples histone H3 methylation at lysine 9 by SETDB1 to DNA replication and chromatin assembly. *Mol Cell*. 15:595-605.
- Schermelleh, L., I. Solovei, D. Zink, and T. Cremer. 2001. Two-color fluorescence labeling of early and mid-to-late replicating chromatin in living cells. *Chromosome Res*. 9:77-80.
- Schiltz, R.L., C.A. Mizzen, A. Vassilev, R.G. Cook, C.D. Allis, and Y. Nakatani. 1999. Overlapping but distinct patterns of histone acetylation by the human coactivators p300 and PCAF within nucleosomal substrates. *J Biol Chem*. 274:1189-92.
- Schneider, R., A.J. Bannister, F.A. Myers, A.W. Thorne, C. Crane-Robinson, and T. Kouzarides. 2004. Histone H3 lysine 4 methylation patterns in higher eukaryotic genes. *Nat Cell Biol*. 6:73-7.
- Schotta, G., A. Ebert, V. Krauss, A. Fischer, J. Hoffmann, S. Rea, T. Jenuwein, R. Dorn, and G. Reuter. 2002. Central role of Drosophila SU(VAR)3-9 in histone H3-K9 methylation and heterochromatic gene silencing. *Embo J*. 21:1121-31.
- Schotta, G., M. Lachner, A.H. Peters, and T. Jenuwein. 2004a. The indexing potential of histone lysine methylation. *Novartis Found Symp*. 259:22-37; discussion 37-47, 163-9.
- Schotta, G., M. Lachner, K. Sarma, A. Ebert, R. Sengupta, G. Reuter, D. Reinberg, and T. Jenuwein. 2004b. A silencing pathway to induce H3-K9 and H4-K20 trimethylation at constitutive heterochromatin. *Genes Dev*. 18:1251-62.
- Schubeler, D., D.M. MacAlpine, D. Scalzo, C. Wirbelauer, C. Kooperberg, F. van Leeuwen, D.E. Gottschling, L.P. O'Neill, B.M. Turner, J. Delrow, S.P. Bell, and M. Groudine. 2004. The histone modification pattern of active genes revealed through genome-wide chromatin analysis of a higher eukaryote. *Genes Dev*. 18:1263-71.
- Schultz, J. 1939. The function of heterochromatin. *Proc VII Int. Congr. Genet.*:257-262.
- Schwabish, M.A., and K. Struhl. 2004. Evidence for eviction and rapid deposition of histones upon transcriptional elongation by RNA polymerase II. *Mol Cell Biol*. 24:10111-7.
- Schwartz, B.E., and K. Ahmad. 2005. Transcriptional activation triggers deposition and removal of the histone variant H3.3. *Genes Dev*. 19:804-14.
- Sedarat, F., E. Lin, E.D. Moore, and G.F. Tibbits. 2004. Deconvolution of confocal images of dihydropyridine and ryanodine receptors in developing cardiomyocytes. *J Appl Physiol*. 97:1098-103.
- Sedat, J., and L. Manuelidis. 1978. A direct approach to the structure of eukaryotic chromosomes. *Cold Spring Harb Symp Quant Biol*. 42 Pt 1:331-50.
- Seligson, D.B., S. Horvath, T. Shi, H. Yu, S. Tze, M. Grunstein, and S.K. Kurdastani. 2005. Global histone modification patterns predict risk of prostate cancer recurrence. *Nature*. 435:1262-6.
- Sewalt, R.G., M. Lachner, M. Vargas, K.M. Hamer, J.L. den Blaauwen, T. Hendrix, M. Melcher, D. Schweizer, T. Jenuwein, and A.P. Otte. 2002. Selective interactions between vertebrate polycomb homologs and the SUV39H1 histone lysine methyltransferase suggest that histone H3-K9 methylation contributes to chromosomal targeting of Polycomb group proteins. *Mol Cell Biol*. 22:5539-53.
- Shaw, P.J., and D.J. Rawlins. 1991. Three-dimensional fluorescence microscopy. *Prog Biophys Mol Biol*. 56:187-213.
- Sheardown, S.A., S.M. Duthie, C.M. Johnston, A.E. Newall, E.J. Formstone, R.M. Arkell, T.B. Nesterova, G.C. Alghisi, S. Rastan, and N. Brockdorff. 1997. Stabilization of Xist RNA mediates initiation of X chromosome inactivation. *Cell*. 91:99-107.
- Sheppard, C.J.R., and P. Török. 1997. Effects of specimen refractive index on confocal imaging. *Journal of Microscopy*. 185:366-374.
- Shi, X., T. Hong, K.L. Walter, M. Ewalt, E. Michishita, T. Hung, D. Carney, P. Pena, F. Lan, M.R. Kaadige, N. Lacoste, C. Cayrou, F. Davrazou, A. Saha, B.R. Cairns, D.E. Ayer, T.G. Kutateladze, Y. Shi, J. Cote, K.F. Chua, and O. Gozani. 2006. ING2 PHD domain links histone H3 lysine 4 methylation to active gene repression. *Nature*. 442:96-9.
- Shi, Y., F. Lan, C. Matson, P. Mulligan, J.R. Whetstine, P.A. Cole, and R.A. Casero. 2004. Histone demethylation mediated by the nuclear amine oxidase homolog LSD1. *Cell*. 119:941-53.
- Shi, Y., and J.R. Whetstine. 2007. Dynamic regulation of histone lysine methylation by demethylases. *Mol Cell*. 25:1-14.
- Shumaker, D.K., T. Dechat, A. Kohlmaier, S.A. Adam, M.R. Bozovsky, M.R. Erdos, M. Eriksson, A.E. Goldman, S. Khun, F.S. Collins, T. Jenuwein, and R.D. Goldman. 2006. Mutant nuclear lamin A leads to progressive alterations of epigenetic control in premature aging. *Proc Natl Acad Sci U S A*. 103:8703-8.
- Sickmann, A., M. Mreyen, and H.E. Meyer. 2002. Identification of modified proteins by mass spectrometry. *IUBMB Life*. 54:51-7.
- Siddiqui, H., S.R. Fox, R.W. Gunawardena, and E.S. Knudsen. 2007. Loss of RB compromises specific heterochromatin modifications and modulates HP1alpha dynamics. *J Cell Physiol*. 211:131-7.
- Silva, J., W. Mak, I. Zvetkova, R. Appanah, T.B. Nesterova, Z. Webster, A.H. Peters, T. Jenuwein, A.P. Otte, and N. Brockdorff. 2003. Establishment of histone h3 methylation on the inactive X chromosome requires transient recruitment of Eed-Enx1 polycomb group complexes. *Dev Cell*. 4:481-95.
- Simpson, R.T. 1978. Structure of the chromatosome, a chromatin particle containing 160 base pairs of DNA and all the histones. *Biochemistry*. 17:5524-31.
- Sims, J.K., S.I. Houston, T. Magazinnik, and J.C. Rice. 2006. A Trans-tail Histone Code Defined by Monomethylated H4 Lys-20 and H3 Lys-9 Demarcates Distinct Regions of Silent Chromatin. *J Biol Chem*. 281:12760-6.

- Sims, R.J., 3rd, K. Nishioka, and D. Reinberg. 2003. Histone lysine methylation: a signature for chromatin function. *Trends Genet.* 19:629-39.
- Singh, P.B., and S.D. Georgatos. 2002. HP1: facts, open questions, and speculation. *J Struct Biol.* 140:10-6.
- Singh, P.B., J.R. Miller, J. Pearce, R. Kothary, R.D. Burton, R. Paro, T.C. James, and S.J. Gaunt. 1991. A sequence motif found in a Drosophila heterochromatin protein is conserved in animals and plants. *Nucleic Acids Res.* 19:789-94.
- Smith, E.R., C. Cayrou, R. Huang, W.S. Lane, J. Cote, and J.C. Lucchesi. 2005. A human protein complex homologous to the Drosophila MSL complex is responsible for the majority of histone H4 acetylation at lysine 16. *Mol Cell Biol.* 25:9175-88.
- Solovei, I., A. Cavallo, L. Schermelleh, F. Jaunin, C. Scasselati, D. Cmarko, C. Cremer, S. Fakan, and T. Cremer. 2002a. Spatial preservation of nuclear chromatin architecture during three-dimensional fluorescence in situ hybridization (3D-FISH). *Exp Cell Res.* 276:10-23.
- Solovei, I., J. Walter, M. Cremer, F. Habermann, L. Schermelleh, and T. Cremer. 2002b. FISH on three-dimensionally preserved nuclei. In *FISH: a practical approach*, chapter 7. B. Beatty, S. Mai, and J. Squire, editors. Oxford University Press, Oxford. 119-157.
- Spada, F., M. Vincent, and E.M. Thompson. 2005. Plasticity of histone modifications across the invertebrate to vertebrate transition: histone H3 lysine 4 trimethylation in heterochromatin. *Chromosome Res.* 13:57-72.
- Spector, D.L. 1993. Macromolecular domains within the cell nucleus. *Annu Rev Cell Biol.* 9:265-315.
- Spector, D.L. 2001. Nuclear domains. *J Cell Sci.* 114:2891-3.
- Srinivasan, P.R.a.B., E. 1964. Enzymatic alteration of nucleic acid structure. *Science.* 145:548-53.
- Stadler, S., V. Schnapp, R. Mayer, S. Stein, C. Cremer, C. Bonifer, T. Cremer, and S. Dietzel. 2004. The architecture of chicken chromosome territories changes during differentiation. *BMC Cell Biol.* 5:44.
- Stewart, M.D., J. Li, and J. Wong. 2005. Relationship between histone H3 lysine 9 methylation, transcription repression, and heterochromatin protein 1 recruitment. *Mol Cell Biol.* 25:2525-38.
- Strahl, B.D., and C.D. Allis. 2000. The language of covalent histone modifications. *Nature.* 403:41-5.
- Strahl, B.D., S.D. Briggs, C.J. Brame, J.A. Caldwell, S.S. Koh, H. Ma, R.G. Cook, J. Shabanowitz, D.F. Hunt, M.R. Stallcup, and C.D. Allis. 2001. Methylation of histone H4 at arginine 3 occurs in vivo and is mediated by the nuclear receptor coactivator PRMT1. *Curr Biol.* 11:996-1000.
- Strahl, B.D., R. Ohba, R.G. Cook, and C.D. Allis. 1999. Methylation of histone H3 at lysine 4 is highly conserved and correlates with transcriptionally active nuclei in Tetrahymena. *Proc Natl Acad Sci U S A.* 96:14967-72.
- Su, R.C., K.E. Brown, S. Saaber, A.G. Fisher, M. Merckenschlager, and S.T. Smale. 2004. Dynamic assembly of silent chromatin during thymocyte maturation. *Nat Genet.* 36:502-6.
- Sullivan, B.A., and G.H. Karpen. 2004. Centromeric chromatin exhibits a histone modification pattern that is distinct from both euchromatin and heterochromatin. *Nat Struct Mol Biol.* 11:1076-83.
- Sun, Z.W., and C.D. Allis. 2002. Ubiquitination of histone H2B regulates H3 methylation and gene silencing in yeast. *Nature.* 418:104-8.
- Suzuki, T., K. Fujikura, T. Higashiyama, and K. Takata. 1997. DNA staining for fluorescence and laser confocal microscopy. *J Histochem Cytochem.* 45:49-53.
- Talasz, H., H.H. Lindner, B. Sarg, and W. Helliger. 2005. Histone H4-lysine 20 monomethylation is increased in promoter and coding regions of active genes and correlates with hyperacetylation. *J Biol Chem.* 280:38814-22.
- Tanabe, H., F.A. Habermann, I. Solovei, M. Cremer, and T. Cremer. 2002a. Non-random radial arrangements of interphase chromosome territories: evolutionary considerations and functional implications. *Mutat Res.* 504:37-45.
- Tanabe, H., S. Muller, M. Neusser, J. von Hase, E. Calcagno, M. Cremer, I. Solovei, C. Cremer, and T. Cremer. 2002b. Evolutionary conservation of chromosome territory arrangements in cell nuclei from higher primates. *Proc Natl Acad Sci U S A.* 99:4424-9.
- Taunton, J., C.A. Hassig, and S.L. Schreiber. 1996. A mammalian histone deacetylase related to the yeast transcriptional regulator Rpd3p. *Science.* 272:408-11.
- Telenius, H., N.P. Carter, C.E. Bebb, M. Nordenskjold, B.A. Ponder, and A. Tunnacliffe. 1992. Degenerate oligonucleotide-primed PCR: general amplification of target DNA by a single degenerate primer. *Genomics.* 13:718-25.
- Therkelsen, A.J., A. Nielsen, and S. Kolvraa. 1997. Localisation of the classical DNA satellites on human chromosomes as determined by primed in situ labelling (PRINS). *Hum Genet.* 100:322-6.
- Torres, K., and S.B. Horwitz. 1998. Mechanisms of Taxol-induced cell death are concentration dependent. *Cancer Res.* 58:3620-6.
- Tounekti, O., G. Pron, J. Belehradek, Jr., and L.M. Mir. 1993. Bleomycin, an apoptosis-mimetic drug that induces two types of cell death depending on the number of molecules internalized. *Cancer Res.* 53:5462-9.
- Trewick, S.C., P.J. McLaughlin, and R.C. Allshire. 2005. Methylation: lost in hydroxylation? *EMBO Rep.* 6:315-20.
- Tsukada, Y., J. Fang, H. Erdjument-Bromage, M.E. Warren, C.H. Borchers, P. Tempst, and Y. Zhang. 2006. Histone demethylation by a family of JmjC domain-containing proteins. *Nature.* 439:811-6.
- Turner, B.M. 2000. Histone acetylation and an epigenetic code. *Bioessays.* 22:836-45.
- Turner, B.M. 2005. Reading signals on the nucleosome with a new nomenclature for modified histones. *Nat Struct Mol Biol.* 12:110-2.
- Ueda, K., C. Cardarelli, M.M. Gottesman, and I. Pastan. 1987. Expression of a full-length cDNA for the human "MDR1" gene confers resistance to colchicine, doxorubicin, and vinblastine. *Proc Natl Acad Sci U S A.* 84:3004-8.

- van Leeuwen, F., P.R. Gafken, and D.E. Gottschling. 2002. Dot1p modulates silencing in yeast by methylation of the nucleosome core. *Cell*. 109:745-56.
- van Steensel, B., J. Delrow, and S. Henikoff. 2001. Chromatin profiling using targeted DNA adenine methyltransferase. *Nat Genet*. 27:304-8.
- Vaquero, A., M. Scher, D. Lee, H. Erdjument-Bromage, P. Tempst, and D. Reinberg. 2004. Human SirT1 interacts with histone H1 and promotes formation of facultative heterochromatin. *Mol Cell*. 16:93-105.
- Varga-Weisz, P.D., and P.B. Becker. 2006. Regulation of higher-order chromatin structures by nucleosome-remodelling factors. *Curr Opin Genet Dev*. 16:151-6.
- Vertino, P.M., J.A. Sekowski, J.M. Coll, N. Applegren, S. Han, R.J. Hickey, and L.H. Malkas. 2002. DNMT1 is a component of a multiprotein DNA replication complex. *Cell Cycle*. 1:416-23.
- Volkel, P., and P.O. Angrand. 2006. The control of histone lysine methylation in epigenetic regulation. *Biochimie*.
- Volpi, E.V., E. Chevret, T. Jones, R. Vatcheva, J. Williamson, S. Beck, R.D. Campbell, M. Goldsworthy, S.H. Powis, J. Ragoussis, J. Trowsdale, and D. Sheer. 2000. Large-scale chromatin organization of the major histocompatibility complex and other regions of human chromosome 6 and its response to interferon in interphase nuclei. *J Cell Sci*. 113 (Pt 9):1565-76.
- Wade, P.A., A. Geggion, P.L. Jones, E. Ballestar, F. Aubry, and A.P. Wolffe. 1999. Mi-2 complex couples DNA methylation to chromatin remodelling and histone deacetylation. *Nat Genet*. 23:62-6.
- Wallace, J.A., and T.L. Orr-Weaver. 2005. Replication of heterochromatin: insights into mechanisms of epigenetic inheritance. *Chromosoma*. 114:389-402.
- Wallace, W., L.H. Schaefer, and J.R. Swedlow. 2001. A workingperson's guide to deconvolution in light microscopy. *Biotechniques*. 31:1076-8, 1080, 1082 passim.
- Walter, J., B. Joffe, A. Bolzer, H. Albiez, P.A. Benedetti, S. Muller, M.R. Speicher, T. Cremer, M. Cremer, and I. Solovei. 2006. Towards many colors in FISH on 3D-preserved interphase nuclei. *Cytogenet Genome Res*. 114:367-78.
- Walter, J., L. Schermelleh, M. Cremer, S. Tashiro, and T. Cremer. 2003. Chromosome order in HeLa cells changes during mitosis and early G1, but is stably maintained during subsequent interphase stages. *J Cell Biol*. 160:685-97.
- Wang, H., Z.Q. Huang, L. Xia, Q. Feng, H. Erdjument-Bromage, B.D. Strahl, S.D. Briggs, C.D. Allis, J. Wong, P. Tempst, and Y. Zhang. 2001. Methylation of histone H4 at arginine 3 facilitating transcriptional activation by nuclear hormone receptor. *Science*. 293:853-7.
- Wassenegger, M. 2005. The role of the RNAi machinery in heterochromatin formation. *Cell*. 122:13-6.
- Waterborg, J.H., S.R. Fried, and H.R. Matthews. 1983. Acetylation and methylation sites in histone H4 from *Physarum polycephalum*. *Eur J Biochem*. 136:245-52.
- Waterston, R.H., K. Lindblad-Toh, E. Birney, J. Rogers, J.F. Abril, P. Agarwal, R. Agarwala, R. Ainscough, M. Alexandersson, P. An, S.E. Antonarakis, J. Attwood, R. Baertsch, J. Bailey, K. Barlow, S. Beck, E. Berry, B. Birren, T. Bloom, P. Bork, M. Botcherby, N. Bray, M.R. Brent, D.G. Brown, S.D. Brown, C. Bult, J. Burton, J. Butler, R.D. Campbell, P. Carninci, S. Cawley, F. Chiaromonte, A.T. Chinwalla, D.M. Church, M. Clamp, C. Clee, F.S. Collins, L.L. Cook, R.R. Copley, A. Coulson, O. Couronne, J. Cuff, V. Curwen, T. Cutts, M. Daly, R. David, J. Davies, K.D. Delehaunty, J. Deri, E.T. Dermitzakis, C. Dewey, N.J. Dickens, M. Diekhans, S. Dodge, I. Dubchak, D.M. Dunn, S.R. Eddy, L. Elnitski, R.D. Emes, P. Eswara, E. Eyas, A. Felsenfeld, G.A. Fewell, P. Flicek, K. Foley, W.N. Frankel, L.A. Fulton, R.S. Fulton, T.S. Furey, D. Gage, R.A. Gibbs, G. Glusman, S. Gnerre, N. Goldman, L. Goodstadt, D. Grafham, T.A. Graves, E.D. Green, S. Gregory, R. Guigo, M. Guyer, R.C. Hardison, D. Haussler, Y. Hayashizaki, L.W. Hillier, A. Hinrichs, W. Hlavina, T. Holzer, F. Hsu, A. Hua, T. Hubbard, A. Hunt, I. Jackson, D.B. Jaffe, L.S. Johnson, M. Jones, T.A. Jones, A. Joy, M. Kamal, E.K. Karlsson, et al. 2002. Initial sequencing and comparative analysis of the mouse genome. *Nature*. 420:520-62.
- Watson, J.D. 2003. Celebrating the genetic jubilee: a conversation with James D. Watson. Interviewed by John Rennie. *Sci Am*. 288:66-9.
- Watt, F.a.M., P.L. 1988. Cytosine methylation prevents binding to DNA of a HeLa cell transcription factor required for optimal expression of the adenovirus major late promoter. *Genes and Dev*. 2:1136-1143.
- Waye, J.S., and H.F. Willard. 1989. Human beta satellite DNA: genomic organization and sequence definition of a class of highly repetitive tandem DNA. *Proc Natl Acad Sci U S A*. 86:6250-4.
- Wei, R.D., and L.D. Wright. 1964. Heat Stability of Avidin and Avidin-Biotin Complex and Influence of Ionic Strength on Affinity of Avidin for Biotin. *Proc Soc Exp Biol Med*. 117:341-4.
- Wei, X., S. Somanathan, J. Samarabandu, and R. Berezney. 1999a. Three-dimensional visualization of transcription sites and their association with splicing factor-rich nuclear speckles. *J Cell Biol*. 146:543-58.
- Wei, Y., L. Yu, J. Bowen, M.A. Gorovsky, and C.D. Allis. 1999b. Phosphorylation of histone H3 is required for proper chromosome condensation and segregation. *Cell*. 97:99-109.
- Whetstine, J.R., A. Nottke, F. Lan, M. Huarte, S. Smolikov, Z. Chen, E. Spooner, E. Li, G. Zhang, M. Colaiacovo, and Y. Shi. 2006. Reversal of histone lysine trimethylation by the JMJD2 family of histone demethylases. *Cell*. 125:467-81.
- Williams, R.R., S. Broad, D. Sheer, and J. Ragoussis. 2002. Subchromosomal positioning of the epidermal differentiation complex (EDC) in keratinocyte and lymphoblast interphase nuclei. *Exp Cell Res*. 272:163-75.
- Wolffe, A.P. 1996. Histone deacetylase: a regulator of transcription. *Science*. 272:371-2.
- Wu, R., A.V. Terry, P.B. Singh, and D.M. Gilbert. 2005. Differential subnuclear localization and replication timing of histone H3 lysine 9 methylation states. *Mol Biol Cell*. 16:2872-81.

-
- Xiao, B., C. Jing, G. Kelly, P.A. Walker, F.W. Muskett, T.A. Frenkiel, S.R. Martin, K. Sarma, D. Reinberg, S.J. Gamblin, and J.R. Wilson. 2005. Specificity and mechanism of the histone methyltransferase Pr-Set7. *Genes Dev.* 19:1444-54.
- Xie, S.Q., S. Martin, P.V. Guillot, D.L. Bentley, and A. Pombo. 2006. Splicing speckles are not reservoirs of RNA polymerase II, but contain an inactive form, phosphorylated on serine2 residues of the C-terminal domain. *Mol Biol Cell.* 17:1723-33.
- Xing, Y., C.V. Johnson, P.T. Moen, Jr., J.A. McNeil, and J. Lawrence. 1995. Nonrandom gene organization: structural arrangements of specific pre-mRNA transcription and splicing with SC-35 domains. *J Cell Biol.* 131:1635-47.
- Xiong, Z., W. Tsark, J. Singer-Sam, and A.D. Riggs. 1998. Differential replication timing of X-linked genes measured by a novel method using single-nucleotide primer extension. *Nucleic Acids Res.* 26:684-6.
- Yoshida, M., Y. Hoshikawa, K. Koseki, K. Mori, and T. Beppu. 1990. Structural specificity for biological activity of trichostatin A, a specific inhibitor of mammalian cell cycle with potent differentiation-inducing activity in Friend leukemia cells. *J Antibiot (Tokyo).* 43:1101-6.
- Zaratiegui, M., D.V. Irvine, and R.A. Martienssen. 2007. Noncoding RNAs and Gene Silencing. *Cell.* 128:763-76.
- Zhang, K., W. Lin, J.A. Latham, G.M. Riefler, J.M. Schumacher, C. Chan, K. Tatchell, D.H. Hawke, R. Kobayashi, and S.Y. Dent. 2005. The Set1 methyltransferase opposes Ipl1 aurora kinase functions in chromosome segregation. *Cell.* 122:723-34.
- Zhang, L., E.E. Eugeni, M.R. Parthun, and M.A. Freitas. 2003. Identification of novel histone post-translational modifications by peptide mass fingerprinting. *Chromosoma.* 112:77-86.
- Zinner, R., H. Albiez, J. Walter, A.H. Peters, T. Cremer, and M. Cremer. 2006. Histone lysine methylation patterns in human cell types are arranged in distinct three-dimensional nuclear zones. *Histochem Cell Biol.* 125:3-19.

7 Appendix

7.1 Material and technical equipment

7.1.1 Cells

Cell type	Medium	Source
Primary human fibroblasts, XX	DMEM 10% FCS+ P/S	Kindly provided by S.Götze from a healthy patient hospital Amsterdam
DLD-1	McCoy 5A+ 10% FCS+ P/S	Kindly provided by Dr.C.Lengauer
MCF-7	RPMI 10% FCS+ P/S	Kindly provided by Dr. P.Meltzer (NIH) Bethesda
MEF-W9	DMEM 10% FCS+ P/S	Kindly provided by Dr.T.Jenuwein IMP Vienna

7.1.2 Chemicals, enzymes and reagents

Chemicals

Acetic acid (100%)	Merck, Darmstadt
Antifade-Medium (Vectashield)	Vector, Burlingame
BSA	Roche, Mannheim
Cetus II buffer	Roche, Mannheim
Colcemide (10µg/ml)	Seromed Biochrom, Berlin
DAPI	Serva
Dimethyl-sulfoxid (DMSO)	Merck, Darmstadt
Dextranulphate	Amersham Biosciences, Freiburg
DMEM	Gibco Invitrogen, Karlsruhe
Ethanol	Merck, Darmstadt
Fetal calf serum (FCS)	Seromed Biochrom, Berlin
Formaldehyde (37%)	Sigma-Aldrich, Deisenhofen
Formamide	Merck, Darmstadt
Glycerol	Sigma-Aldrich, Taufkirchen
HCl 1N	Merck, Darmstadt

Isopropanol	Merck, Darmstadt
Methanol	Merck, Darmstadt
MgCl ₂	Merck, Darmstadt
NaCl	Merck, Darmstadt
Na-citrate dihydrate	Merck, Darmstadt
Nick-translation buffer (10x)	Roche, Mannheim
Penicillin/Streptomycin (10000 I.E./10000 µg/ml)	Seromed Biochrom, Berlin
RPMI 1640 media	Seromed Biochrom, Berlin
Sodiumchloride	Merck, Darmstadt
Solution 3	Roche, Mannheim
TO-PRO-3	Molecular Probes, Leiden NL
Triton X-100	Merck, Darmstadt
Tween 20	Merck, Darmstadt

Enzymes

DNase I	Roche, Mannheim
Pepsin (10% in H ₂ O)	Sigma Aldrich, Taufkirchen
Proteinase K	Roche, Mannheim
10xTrypsin/EDTA	Biochrom AG, Berlin
Taq-Polymerase	Invitrogen GmbH, Karlsruhe

Nucleotides

5-Bromo-2'-deoxyuridine	Sigma-Aldrich, Taufkirchen
Biotin-16-dUTP	Roche, Mannheim
BrUTP	Sigma-Aldrich, Deisenhofen
Cot1-DNA	Invitrogen GmbH, Karlsruhe
DOP2/DOP3-primer	MWG Biotech
dATP, dCTP, dGTP, dTTP	Amersham Biosciences, Freiburg
Digoxigenin-11-dUTP	Roche, Mannheim
6MW -primer	MWG-Biotech, Ebersberg
Tamra-dUTP, TR-dUTP	Molecular Probes

Antibodies

Primary antibodies

Goat anti-DNP	Sigma-Aldrich, Deisenhofen
Human anti-CREST serum	Euroimmun, Lübeck
Mouse anti-B23	Sigma-Aldrich, Deisenhofen
Mouse anti-BrdU	Roche, Mannheim
Mouse anti-β-tubulin	Sigma-Aldrich, Deisenhofen

Mouse anti-CI/Br	Caltag, Hamburg
Mouse anti-Digoxigenin	Sigma-Aldrich, Deisenhofen
Mouse anti-HP1 alpha	Euromedex, Souffelweyersheim
Mouse anti-SC35	Sigma-Aldrich Deisenhofen
Rabbit anti-Ki67	Roche, Mannheim
Rabbit anti- H3K4me3	Abcam, Cambridge
Rabbit anti- H3K9me1	All following antibodies are kindly provided by T.Jenuwein MIP and A.Peters FMI, Basel
Rabbit anti- H3K9me3	
Rabbit anti- H3K27me3	
Rabbit anti- monomethylated H4K20	
Rabbit anti- trimethylated H4K20	
Rat anti-BrdU	Serotec, Oxford

Secondary antibodies

Avidin-Cy5	Sigma-Aldrich, Deisenhofen
Avidin-FITC	Vector, Burlingame CA, USA
Avidin-alexa488	Molecular Probes, Leiden NL
Donkey anti-human-Cy3	Jackson Immunoresearch, Baltimore
Donkey anti-rat-Cy3	Jackson Immunoresearch, Baltimore
Donkey anti-goat-alexa488	Molecular Probes, Leiden NL
Goat anti-Avidin-Biotin	Vector, Burlingame CA, USA
Goat anti-Avidin-FITC	Vector, Burlingame CA, USA
Goat anti-mouse-Biotin	Vector, Burlingame CA, USA
Goat anti-mouse-Cy5	Jackson Immunoresearch, Baltimore
Goat anti-mouse-AMCA	Molecular Probes, Leiden NL
Goat anti-mouse-alexa488 h.c.a.	Molecular Probes, Leiden NL
Goat anti-rabbit-alexa488 h.c.a.	Molecular Probes, Leiden NL
Goat anti-rabbit-Biotin	Biosource, Camarillo
Goat anti-rabbit-Cy3	Amersham Biosciences, Freiburg
Goat anti-rabbit-Cy3-Fab	Jackson Immunoresearch, Baltimore
Goat anti-rabbit-Fab non conjugated	Jackson Immunoresearch, Baltimore
Goat anti-rabbit-FITC	Biosource, Camarillo
Goat anti-rat-Cy3	Amersham Biosciences, Freiburg
Goat anti-Streptavidin-Biotin	Vector, Burlingame CA, USA
Horse anti-goat-Biotin	Vector, Burlingame CA, USA
Rabbit anti-human-Cy3	Jackson Immunoresearch, Baltimore
Sheep anti-Digoxigenin-FITC	Roche, Penzberg
Sheep anti-mouse-Cy3	Jackson Immunoresearch, Baltimore
Sheep anti-mouse-FITC	Sigma-Aldrich, Deisenhofen
Streptavidin-Cy5	Jackson Immunoresearch, Baltimore
Streptavidin-Cy3	Jackson Immunoresearch, Baltimore

7.1.3 Media, buffers and solutions

Buffers/Solutions	Constituent	Notes
ACG-Mix for label DOP-PCR	2mM dATP, dCTP and dGTP	10µl of dATP, dCTP and dGTP (100mM) each + 470µl H ₂ O bidest store at -20°C
Blocking solution	2% BSA in PBST	PBST 0.01% Tween + 0.04% Na-Azid store at 4°C 2g BSA → ad 100ml PBST
DAPI stock solution	2mg/ml dd H ₂ O	steril filtered
DAPI working solution	0,02µg/ml in PBST	dilute stock solution 1:4000 in PBST
DNase I stock solution	2 U/µl DNase I 0,03 M NaCl	1mg/ml DNase I (2000 U/mg)
	50% Glycerin	
DMEM full media	450ml DMEM	Constituents DMEM:
	50ml FCS (10%)	3,7g/l NaHCO ₃
	5ml Penicillin/Streptomycin (100 I.E./100 µg/ml)	4,5g/l D-Glucose
		Stable Glutamine, Na-pyruvate
dTTP for label DOP-PCR	1mM dTTP	10µl dTTP+990µl H ₂ O bidest store at -20°C
Ethanol (30%, 50%, 70% and 90%)	Ethanol (type 642)	30, 50,70,90ml EtOH→ad 100ml Using H ₂ O bidest
Fixative (for chromosomes)	Methanol/acetic acid 3:1	cool to -20°C before use
Fixative for post-fixation	1% Formaldehyde in PBST	dilute Formaldehyde 37% about 1:40 in PBST
Fixative (for 3D preserved cells)	3,7% Formaldehyde in PBST	dilute Formaldehyde 37% 1:10 in PBST
Formamide/2xSSC (storing and denaturation solution)	50% formamide in 2xSSC	50ml 20xSSC + 350ml formamide + 100ml H ₂ O bidest. Adjust to pH 7.0 with 1M HCl, store at -20°C
Freezing medium	20% FCS 10% DMSO (appropriate medium)	
Glycerol (20%)	20% glycerol in 1xPBS	100ml glycerol + 400ml 1xPBS
HCl (0,1M)		50ml HCl (1M)
Hybridization mastermix	20% Dextran sulphate in 2xSSC	Dissolve 8g Dextran sulphate in 40ml 2xSSC, vortex, filter using 0,45µm filter, aliquot, store at -20°C
KCl solution, hypotone	75mM KCl	0,56g/100ml H ₂ O
McCoy's 5A modified media	450ml McCoy's 50ml FCS (10%) 5ml Penicillin/Streptomycin (100 I.E./100 µg/ml)	6,5g/l NaCl 2,0g NaHCO ₃ , 5mg/IPhenolred Prewarm to 37°C before use

NaCl solution (4)	4 M NaCl in H ₂ O	23,4g/100ml H ₂ O
PBS (pH 7,4)	137 mM NaCl 2,7 mM KCl 8,0 mM Na ₂ HPO ₄ 1,5 mM KH ₂ PO ₄	10xPBS: 80g NaCl 2g KCl 11,5 Na ₂ HPO ₄ 11,5 Na ₂ HPO ₄ ad 1l dd H ₂ O
PBST	0,02% Tween 20 in 1xPBS	200µl Tween 20 in 1l PBS
Pepsinization solution	0,005% pepsin in 0,01 M HCl	10µl (20%) pepsin + 0,5ml 1N HCl →ad 49,5ml H ₂ O bidest
RPMI 1640 full media	450ml RPMI 1640 50ml FCS (10%) 5ml Penicillin/Streptomycin (100 I.E./100 µg/ml)	Constituents RPMI 1640: 25mM HEPES, 5,5g/l NaCl, 2,0g NaHCO ₃ , 5mg/l Phenolred, 0,5g/l N-Acetyl-L-alanyl-L-glutamin Prewarm to 37°C before use
20xSSC (Standard Saline Citrate)	NaCl, Na-citrate dihydrate and H ₂ O	173,3g NaCl 88,2g Na-citrate →add 1l H ₂ O bidest Adjust to pH 7 with NaOH
Triton X-100 (0,5%) permeabilization solution	0,5% Triton X-100 in PBST	500µl in 100ml PBST
Trypsin-EDTA	0,05% 0,02% EDTA	Trypsin Prepare from 10x concentrated solution

7.1.4 Equipment and instrumentation

Glass, plastic ware and other implements

Items	Company
6 well plates	Greiner bio-one, Frickenhausen
12 well plates	Greiner bio-one, Frickenhausen
Automatic pipette	Gilson, Inc., Middleton
Canula	Braun, Melsungen
Cell culture flasks (75cm ² , 25cm ²)	Falcon/Becton Dickinson, S. Jose Greiner bio-one, Frickenhausen
Coverslips 12×12mm	Hecht Assistant, Sondheim
Coverslips 15×15mm	Menzel-Gläser
Coverslips 18×18mm	Marienfeld, Lauda-Königshofen
Coverslips 20×20mm	Marienfeld, Lauda-Königshofen
Coverslips 24×24mm	Marienfeld, Lauda-Königshofen
Coverslips 24×60mm	Menzel-Gläser, Braunschweig
Culture dishes	Falcon/Becton Dickinson, S. Jose
Cryo-tubes 2ml	Greinerbio-one, Frickenhausen
Fixogum	Marabu, Tamm

Glass marker diamond	Kraus & Winter, Hamburg
Glass bottles 100ml, 250ml, 500ml	Schott, Stafford UK
Gloves Nitril	Ansell, Richmond Meditrade, Kiefersfelden
Gloves Latex	Ansell, Richmond Meditrade, Kiefersfelden
Isopropanol box	Nalgene, Rochester
Immersion oil	Zeiss, Jena
Immersion oil	Leica, Wetzlar
Kim wipes	Kimberly-Clark
Liquid nitrogen tank with racks	Messer, Griesheim
Metal box with lid	Schubert Medizinprodukte GmbH
Mikro-Pipette tips	Greiner bio-one, Frickenhausen
Mikro-Pipettes (2µl, 10µl, 200µl, 1000µl)	Gilson, Inc., Middleton
Nail polish	Manhattan, Müller GmbH & Co. KG, Ulm- v Jungingen
Parafilm-M®	Pechiney Plastic Packaging, Inc., Neenah
PCR tubes 0.5 ml	Molecular probes, San Diego
Pipette tips white	Molecular Bio Products
Pipette tips yellow and blue	Greiner Labortechnik
Pipette tips for PCR	Molecular Bio Products
Plastic dishes, different sizes, round and square	Falcon/Becton, Greiner bio-one
Quadriperms (4 well plates)	VivaScience AG, Hannover
Rubber cement	Marabu, Tamm
Reaction tubes 1,5ml	Eppendorf, Hamburg
Safety pipette filler	Deutsch und Neumann
Slides	Langenbrinck, Teningen
Slide briefcases and boxes	Schubert Medizinprodukte GmbH
Staining Jars acc. to Coplin Staining Jars acc. to Hellendahl	Hecht Assistant, Sondheim
Serological pipettes 2ml, 5ml, 10ml, 25ml	Sarstedt, Nümbrecht
Sterile plastic pipettes 1ml, 2ml, 5ml, 10ml, 25ml	Falcon/Becton Dickinson, S. Jose
Sterile tubes 50ml/15ml	Falcon/Becton Dickinson, S. Jose
Test tubes 1.5ml/2ml	Eppendorf, Hamburg
Tweezers	Dumont, Montignez
Waste container	Biochrom, Berlin

Technical equipment

Items	Company
Centrifuge/Biofuge pico	Kendro, Langenselbold
Centrifuge/Rotana/S	Hettich, Tuttlingen
CO2 incubator/BB6220 CU	Kendro, Langenselbold
CO2 incubator/Hera Cell	Kendro, Langenselbold
Freezer (-80°C)/6485	GFL, Burgwedel

Freezers/various types (-20°C)	Privileg/Quelle, Fürth AEG, Frankfurt a. M.
Fridge (+4°C)	Bosch, Gerlingen-Schillerhöhe
Heating block/DB 2-D	Techne, Cambridge
Ice machine/AF-10	Scotsman, Bettolino di Pogliano
Incubator/Certomat HK	B.Braun Biotech international, Melsungen
Laminar air flow cabinet	Biohit Helsinki
Magnetic stirrer/IkaMag RH	Ika Labortechnik, Staufen
Magnetic stirrer/RCT basic	Ika Labortechnik, Staufen
Minicentrifuge	National Labnet, Woodbridge
pH-meter/pH538	WTW, Weilheim
PS-speck microscope point-source-kit	Molecular probes, San Diego
Test tube rotator/34528	Snijders, Tilburg
Thermocycler/Techne Progene	Techne, Cambridge
Vacuum centrifuge/BaVaco-M Mini-30	Bachhofer, Reutlingen
Vortexing machine	Ika Labortechnik, Staufen
Water baths/1004	GFL, Burgwedel
Water baths/5	Julabo, Seelbach
Water baths/M12	Lauda, Lauda-Königshofen
Weighing machine/ 2254	Sartorius, Göttingen

Miscellaneous

<ul style="list-style-type: none"> • Bunsen burner • Table-centrifuge • Immersion oil • Tweezers • Filter paper 	<ul style="list-style-type: none"> • Ice machine • pH-meter • UV-lamp (air flow cabinet) • Preparation folders • Overhead marker
--	---

Software

Programs	Company
Imaging	
Adobe Photoshop® 7.0	Adobe Systems, Inc., S. Jose
Cytovision	Applied Imaging International Ltd, Newcastle Upon Tyne
Image J (v1.29)	National Institute of Health, USA
Irfan View version 3.8	Irfan Skiljan, Wiener Neustadt
Leica-TCS-SP2 software	Leica, Heidelberg
LSM 410 software version 3.95	Zeiss, Jena
Zeiss Image Browser	Zeiss, Jena
Other	
Adobe Acrobat version 5.0	Adobe Systems, Inc., S. Jose
Amira version 4.0	TGS Europe, Merignac Cedex
Endnote version 6.0	Thomson/ISI Researchsoft, Carlsbad
Microsoft Office XP	Microsoft, USA

Optics

Microscopes and accessories	Specifications
Phase contrast microscope Objectives Digital camera	Axiovert 25 C (Carl Zeiss, Jena) CP Achromat, 5x/0,12 CP Achromat, 10x/0,25 Ph1 LD Achrostat, 20x/0,3 Ph1 Achrostat, 40x/0,55 Ph2 Canon G5 (5 Mpixel resolution)
Fluorescence microscope objectives dichroic filter sets CCD-Kamera	Axiophot 2 (Carl Zeiss, Jena) Plan-Neofluar 16x/0,5 Fluar 40x/1,3 Oil, Ph 3 Plan- Neofluar 40x/1,3 Oil Plan-Apochromat 63x/1,4 Oil Plan-Neofluar 100x/1,3 Oil DAPI (BP 365; FT 395; LP 450-490) FITC (BP 450-490; FT 510; LP 515-565) TRITC/Cy3 (BP 546; FT 580; LP 590) Cy5 (BP 575-625; FT 645; BP 660-710) Triple Filter (TBP400/495/570;FT410/505/585; TBP460/530/610)
Leica Confocal Laser Scanning Microscope objectives Laser Beam splitters Emission filters	SP 2 (Leica, Heidelberg) Plan-Apochromat 63x/1,4 Oil Argon: 458nm(5mW)/476nm(5mW)/488nm(20mW) / 496nm (5mW)/514nm(20mW) laser lines Helium/Neon 594 nm laser line, 2,5mW 633 nm laser line, 10mW DPSS: 561nm laser line, 10mW UV-laser: 405nm laser line, 50mW RSP 525: emission spectrum red RSP 650: emission spectrum infrared TD 488/568/647: for emission spectrum green and for green red combinations AOTF: A cousto O ptical T unable F ilter
Software	TCS-SP2 software
Zeiss Confocal Laser Scanning Microscope objectives Laser Beam splitters Emission filters	LSM 410 (Carl Zeiss, Jena) Plan-Neofluar 10x/0.3 Ph1 Plan-Apochromat 63x/1.4 Oil Argon: 488nm, 15mW Helium/Neon1: 543nm laser line, 0,5mW Helium/Neon2: 633nm laser line, 5mW FT 488/543 BP 502-542: emission spectrum green LP 570: emission spectrum red

	BP 575-640: emission spectrum red LP 650: for emission spectrum infrared
Software	LSM 410 software, Version 3.95

7.1.5 BACs used in the experiments

Overview of the R-/G-band assigned BAC pool and the gene-density assigned BAC pool of chromosome 12 for human fibroblasts

Clone ID	Internal ID	Band assignment	Position	G/R band	Gene density 2Mb	Gene density 10Mb	Transcriptional activity	Genes	Pool assignments	Replication Index	Reference Clone
RP11-283I3	12/1	12p13.33	155K – 330K	R	9	16.5	HLy: low HFb: median	4	R -	1.605 median	---
RP11-359B12	12/2	12p13.33	860K – 1085K	R	9	16.5	HLy: median HFb: median	3	R -	1.717 early	---
RP11-388F6	12/3	12p13.32	4315K – 4485K	G (1)	12.5	16.5	HLy: low HFb: median	4	G gene-rich	1.667 early	---
RP11-433J6	12/4	12p13.31	6580K-6750K	R	28	19.7	HLy: median HFb: high	10	R gene-rich	1.736 early	---
RP11-13C13	12/5	12p13.2	10125K-10290K	G (2)	28	19.5	HLy: low HFb: high	6	G gene-rich	1.645 early	---
RP11-4N23	12/6	12p13.1	13505K-13640K	R	9	13	HLy: low HFb: low	1	R gene-rich	1.461 median	---
RP11-502N13	12/7	12p13.1	14520K-14700K	R	9	11.4	HLy: low HFb: median	3	R gene-rich	1.565 median	RP11-109N5
RP11-489N6	12/8	12p12.3	15980K-16170K	G (3)	7.5	7	HLy: low HFb: median	1	G gene-rich	1.433 median	---
RP11-69C13	12/9	12p12.3	16640K-16785K	G (3)	6	7.3	HLy: low HFb: low	1	G gene-poor	1.373 late	---
RP11-871F6	12/10	12p12.3	17425K-17640K	G (3)	4	7.2	HLy: ??? HFb: ???	2	G gene-poor	1.292 late	RP11-161L1
RP11-729I10	12/11	12p12.1	21775K-21960K	G (3)	9	4.8	HLy: low HFb: low	2	G gene-poor	1.357 late	RP11-59N23
RP11-12D15	12/12	12p12.1	22210K-22370K	G (3)	7	5.4	HLy: low HFb: low	1	G gene-poor	1.455 median	---
RP11-877E17	12/13	12p12.1	25985K-26165K	G (3)	8	5.9	HLy: low HFb: low	1	G gene-poor	1.625 median	RP11-16A24
RP11-485K18	12/14	12p11.22	28290K-28465K	G (2)	5.5	6.2	HLy: low HFb: median	1	G gene-poor	1.352 late	RP11-425D17
RP11-498B21	12/15	12q12	39750K-39940K	G (3)	3.5	4.4	HLy: low HFb: low	0	G -	1.311 late	---
RP11-490D11	12/16	12q12	40110K-40280K	G (3)	5.5	4.5	HLy: low HFb: low	1	G -	1.333 late	RP11-184I5
RP11-510P12	12/17	12q12	41500K-41670K	G (3)	9	5.6	HLy: low HFb: low	0	G -	1.388 late	---
RP11-624G19	12/18	12q12	42530K-42690K	G (3)	6	9.1	HLy: ??? HFb: ???	2	G -	1.500 median	RP11-329A19
RP11-559C10	12/19	12q12	43180K-43370K	G (3)	6	10	HLy: low HFb: low	1	G -	1.459 median	---
RP11-	12/20	12q12	43510K-	G (3)	4.5	10.5	HLy: low	1	G	1.431	---

Appendix

176J16			43650K				HFb: low		-	median	
RP11-480H15	12/21	12q13.11	47235K-47425K	R	28.5	18.7	HLy: low HFb: median	6	R gene-rich	1.569 median	---
RP11-1100L3	12/22	12q13.13	50550K-50765K	R	29	27.5	HLy: low HFb: high	6	R gene-rich	1.591 median	RP11-324C17
RP11-624J6	12/23	12q13.13	51750K-51955K	R	38	30.2	HLy: low HFb: high	10	R gene-rich	1.610 median	RP11-323I9
RP11-681G7	12/24	12q13.2	53145K-53355K	G (1)	27	26	HLy: median HFb: low	6	G gene-rich	1.660 early	RP11-192J19
RP11-973D8	12/25	12q13.2	54580K-54795K	G (1)	38.5	23.8	HLy: high HFb: high	10	G gene-rich	1.784 early	RP11-152L9
RP11-799O6	12/26	12q13.3	55625K-55825K	R	37.5	21.8	HLy: low HFb: high	10	R gene-rich	1.772 early	RP11-545N8
RP11-557F20	12/27	12q14.1	57605K-57765K	G (2)	2.5	16.2	HLy: low HFb: low	0	G -	1.283 late	---
RP11-1143G9	12/28	12q15	67910K-68060K	R	10	6.4	HLy: low HFb: median	3	R -	1.670 early	RP11-324P9
RP11-1022D13	12/29	12q15	68180K-68370K	R	11	6.3	HLy: high HFb: high	5	R -	1.665 early	RP11-15L3
RP11-148D15	12/30	12q21.2	76670K-76845K	R	2	3.6	HLy: low HFb: median	1	R gene-poor	1.363 late	---
RP11-362A1	12/31	12q21.31	80805K-80950K	G (3)	2.5	3	HLy: low HFb: low	0	G gene-poor	1.304 late	---
RP11-900F13	12/32	12q21.32	87350K-87525K	R	5	3.9	HLy: low HFb: low	1	R gene-poor	1.391 late	RP11-464G3
RP11-81H17	12/33	12q21.33	88300K-88485K	G (3)	4	4.9	HLy: low HFb: low	3	G gene-poor	1.563 median	---
RP11-40P18	12/34	12q21.33	89170K-89360K	G (3)	6	4.9	HLy: low HFb: low	0	G gene-poor	1.515 median	---
RP11-917O5	12/35	12q21.33	89910K-90090K	G (3)	3.5	5	HLy: low HFb: high	3	G gene-poor	1.462 median	RP11-424L2
RP11-18B24	12/36	12q22	92275K-92430K	R	6.5	5.4	HLy: median HFb: high	3	R -	1.688 early	---
RP11-690J15	12/37	12q23.1	96845K-97030K	G (2)	4	7.1	HLy: low HFb: low	0	G -	1.331 late	RP11-552H16
RP11-482D24	12/38	12q23.3	105550K-105730K	G (2)	8	10.2	HLy: low HFb: low	2	G -	1.556 median	---
RP11-90N16	12/39	12q23.3	106080K-106245K	G (2)	8	10.5	HLy: ??? HFb: ???	1	G -	1.501 median	RP11-561I21
RP11-608E13	12/40	12q24.11	108465K-108625K	R	17.5	11.4	HLy: median HFb: high	2	R gene-rich	1.656 early	RP1-7G5
RP11-25E2	12/41	12q24.21	113915K-114105K	G (2)	3.5	8.5	HLy: low HFb: low	0	G gene-rich	1.293 late	---
RP11-131H7	12/42	12q24.23	117565K-117755K	G (2)	7.5	11	HLy: low HFb: low	0	G gene-rich	1.356 late	---
RP11-87C12	12/43	12q24.31	120770K-120960K	R	18.5	11.9	HLy: low HFb: high	3	R gene-rich	1.780 early	---
RP11-512M8	12/44	12q24.31	121150K-121340K	R	18.5	11.9	HLy: low HFb: high	5	R gene-rich	1.811 early	---
RP11-486O12	12/45	12q24.31	122415K-122615K	R	16	11.6	HLy: median HFb: high	6	R gene-rich	1.654 early	---
RP11-380L11	12/46	12q24.31	122825K-123025K	R	13	11.9	HLy: median HFb: high	3	R gene-rich	1.720 early	---
RP11-205M16	12/47	12q24.32	125875K-126030K	G (2)	5	8.6	HLy: ??? HFb: ???	1	G -	1.276 late	RP11-111F6
RP11-394D10	12/48	12q24.33	132135K-132315K	R	17.5	8.2	HLy: low HFb: median	5	R -	1.520 median	RP11-46H11

For the experiments gene-rich and gene-poor BACs respectively were pooled. All BACs used in this work were marked by color, **gene rich** BACs in **green** and **gene-poor** BACs in **red**.

Overview of the transcriptional activity assigned BAC pool of chromosome 12 for human fibroblasts

Clone ID	Internal ID	Band assignment	Position	G/R band	Gene density 2Mb	Gene density 10Mb	Transcriptional activity (=pool assignment)	Genes	Replication Index	Reference Clone
RP11-150J21	12FbEx-3	12p13.31	6742K-6893K	R	30.5	19.6	high	8	1.776 early	RP11-8J11
RP11-157G21	12FbEx-4	12p13.31	7460K-7637K	R	31	19.6	low	1	1.509 median	---
RP11-69M1	12FbEx-5	12p13.1	7988K-8174K	R	20.5	20.1	low	4	1.701 early	---
RP11-20D14	12FbEx-6	12p12.31	8690K-8864K	R	21.5	19.8	high	1	1.645 early	---
RP11-118B22	12FbEx-7	12p13.1	9190K-9317K	R	23	19.4	low	2	1.599 median	---
RP11-80N2	12FbEx-8	12p12.2	20833K-21009K	R	8	4.9	low	1	1.289 late	---
RP11-92H16	12FbEx-9	12p12.1	21633K-21784K	G(3)	9.5	4.8	high	2	1.363 late	---
RP11-993B23	12FbEx-12	12p11.22	27882K-28040K	G(2)	8	6.2	low	1	1.71 early	RP11-299E2
RP11-76H15	12FbEx-13	12q13.11	45001K-45162K	R	5.5	12.7	high	1	1.638 early	RP11-474P2
RP11-1136G11	12FbEx-15	12q13.13	51745K-51903K	R	38	30.5	high	5	1.61 median	RP11-323I9
RP11-616L12	12FbEx-17	12q13.2	53665K-53867K	G(1)	31.5	24.9	low	1	1.475 median	RP11-101M22
RP11-715H19	12FbEx-19	12q14.2	61745K-61896K	R	7	4.6	low	1	1.391 late	RP11-263K23
RP11-18J9	12FbEx-21	12q21.31	84703K-84875K	G(3)	4.5	3.2	low	2	1.293 late	---
RP11-481K9	12FbEx-22	12q23.1	97449K-97545K	G(2)	3.5	6.8	high	2	1.678 early	---
RP11-210L7	12FbEx-23	12q23.2	101290K-101460K	R	8	6.9	low	1	1.632 median	---
RP11-144B2	12FbEx-24	12q24.23	119040K-119225K	G	18	11.8	high	6	1.678 early	---
RP11-282O18	12FbEx-25	12q24.31	122244K-122332K	R	17	11.5	high	3	1.699 early	---
RP11-592O2	12FbEx-26	12q24.31	123817K-123939K	R	6	11.3	high	2	1.789 early	RP11-22H15

For the experiments BACs containing weakly- and highly expressed genes respectively were pooled. All BACs used in this work were marked by color, BACs containing **weakly-expressed genes** in **red** and **highly-expressed genes** in **green**.

Overview of the transcriptional activity assigned BAC pool of the X-chromosome for human fibroblasts

BAC	begin	end	band	R-or G- band	Genes	expression level	genes/1Mb (2Mb)	genes/1Mb (10Mb)
RP11-155F12	2449600	2605375	p22.33	R	LOC401577	high	2	3,8
RP11-428I5	3231922	3407677	p22.33	R	CD99 DKFZp564I1922 ASSP4	high	1	4,4
RP11-196N16	10041748	10137830	p22.2	G2	CLCN4	low	2,5	5,2
RP11-66H17	11211051	11361474	p22.2	G2	ARHGAP6	low	3,5	6,6
RP11-30I2	11691588	11844380	p22.2	G2	PDZK10	mid	6,5	6,9
RP11-347D6	16180299	16347878	p22.2	G2	LOC392429 CTPS2 CALB3	mid	11	7,1
RP11-160F21	16267255	16432260	p22.2	G2	LOC392429 CTPS2 CALB3 SYAP1	mid	10	7,1
RP11-75D20	18074131	18266588	p22.13	R	SCML2 CDKL5	mid	7	7
RP11-317L16	19317804	19487786	p22.12	G2	FLJ16518 SH3KBP1	mid	8	7,4
RP11-16H4	21227780	21397725	p22.12	G2	CNKSR2	low	4	6,5
RP11-147O5	21659073	21823564	p22.11	R	MBTPS2 SMS PHEX	high	5	6
RP11-359I12	23304119	23461397	p22.11	R	PRDX4	high	9	6,5
RP11-326D20	23523356	23731243	p22.11	R	SAT MGC4825 LOC317771 FLJ25444	mid	9,5	6,4
RP11-241G16	29834432	30026614	p21.2	R	MAGEB2 MAGEB3 MAGEB4 MAGEB1	mid	5	3,7
RP11-242C19	30468985	30634237	p21.2	R	GK TAB3	low	6	3,7
RP11-46A23	30874687	31028427	p21.2	R	DMD	low	5,5	3,9
RP11-562E1	37007363	37179999	p21.1	G3	PRRG1 LOC389844 LOC139249	mid	11,5	6
RP11-495K15	37239134	37425983	p21.1- p11.4	G3/R	FLJ42925 XK CYBB	low	12	6
RP11-245M13	37686362	37831467	p11.4	R	SYTL5 SRPX	high	13	6,1

RP11-64H6	38029097	38197598	p11.4	R	OTC LOC392442 LOC392443 LOC442446 TM4SF2	low	10	6,3
RP11-429N5	39524948	39730119	p11.4	R	LOC392445 BCOR	low	5,5	7,1
RP11-126D17	40108591	40246636	p11.4	R	ATP6AP2 LOC347411 MGC39350	high	8,5	7,1
RP11-185O17	40472057	40655592	p11.4	R	LOC401584 LOC392447 LOC286444 LOC442447	high	10,5	7,3
RP11-360E17	40860674	41053405	p11.4	R	DDX3X	high	9	7,5

For the experiments BACs containing weakly-, mid- and highly expressed genes respectively were pooled. All BACs used in this work were marked by color, BACs containing **weakly-expressed genes** in red, **mid-expressed genes** in yellow and **highly-expressed genes** in green.

All BACs were kindly provided by Rogier Versteeg (Amsterdam) and originally generated in the Sanger Institute.

8 Abbreviations

2D	2-dimensional
3D	3-dimensional
Ab	Antibody
BAC	Bacterial Artificial Chromosome
Bp	Base pair
BrdU	5-bromo-2'-deoxyuridine
BSA	Bovine Serum Albumine
CCD	Charge-Coupled Device
CENP-A,-B,-C	Centromeric Proteins -A,-B,-C
ChIP	Chromatin Immunoprecipitation
cm	centimeter
CT	Chromosome Territory
DAPI	4',6-diamidino-2-phenylindole
Dig	Digoxigenine
DNMT	DNA Methyl Transferase
d H ₂ O	de-ionized water
dd H ₂ O	ultrapure water
DMEM	Dulbecco's Modified Eagle Medium
DNA	Deoxyribo-Nucleic Acid
Dnase	Deoxyribo-nuclease
DOP-PCR	Degenerate Oligonucleotid Primer-Polymerase Chain Reaction
dUTP	deoxyuridine-triphosphate
EDTA	Ethylendiamintetraacetat
EtOH	Ethanol
EZH	Enhancer of Zeste
FA	Formaldehyde
FCS	Fetal Calf Serum
FISH	Fluorescence In Situ Hybridization
FITC	Fluorescein-isothiocyanat
HAT	Histone Acetyl Transferase
HDAC	Histone Deacetylase
h.c.a.	highly cross adsorbed
HEPES	N-2-hydroxyethylpiperazin-N'-2-ethanesulfonic acid
HFb	Human Fibroblasts
HMT	Histone Methyl-Transferase
HSA	Homo Sapiens Autosome
HOX	Homeobox genes
HP-1	Heterochromatin Protein-1
IF	Immunofluorescence
kb	kilobase
LINE/SINE	Long/Short Interspersed Nuclear Element
MCF-7	Mammary Carcinoma Fibroblasts
MEF	Mouse Embryonic Fibroblasts
Mb	Megabase
ON	Over Night
PBS	Phosphate-Buffered Saline
PEV	Position Effect Variegation
PcG	Polycomb Group
PSF	Point Spread Function
RAC	Radial Autocorrelation Function
RNA	Ribonucleic Acid
RPMI	cell culture medium (Roswell Park Memorial Institute)
Rpm	Rotations per minute
RT	Room Temperature
SAM	S-Adenosyl-Methionine
SET1/SET2	Proteins containing a SET-domain
SSC	Sodium chloride Sodium Citrate
SUV 39	Suppressor of Variegation
Tris	Tri(hydroxymethyl)aminomethane
Triton X-100	Octylphenoldecaethylenglycolether
Tween 20	Polyoxyethylensorbitanmonolaurat
Xa/Xi	active X-chromosome/inactivated X-chromosome
wt	wildtype
Xic	X inactivation centre
XIST	X Inactive Specific Transcript RNA

9 Table of Figures

Figures

Fig. 1	Structural features of the IC-CT model	-4-
Fig. 2	The packing of DNA and nucleosomes to higher chromatin folding levels	-6-
Fig. 3	Lysine methylation sites on histones H3 and H4	-13-
Fig. 4	Histone methyltransferases and their substrates	-13-
Fig. 5	Partitioning of chromatin by histone lysine methylation	-14-
Fig. 6	A schematic representation of the HP1 protein	-17-
Fig. 7	Transmission images of DLD-1 cells	-31-
Fig. 8	BACs and paints of HSA #12 tested on metaphase spreads	-41-
Fig. 9	Peptide competition assay: “normal” antibody pattern	-44-
Fig. 10	Peptide competition assay: incubation with specific peptides	-44-
Fig. 11	Peptide competition assay: incubation with similar peptides	-45-
Fig. 12	Point spread function measured on the Leica SP2	-56-
Fig. 13	The impact of deconvolution on image restoration	-59-
Fig. 14	H3K27me3 staining before and after deconvolution (magnification)	-60-
Fig. 15	Deconvolution facilitates threshold-setting	-61-
Fig. 16	Test for the consistency of co-localization analysis over a range of thresholds	-62-
Fig. 17	Results of co-localization analysis delineated in a scatterplot	-65-
Fig. 18	Path in Image J to calculate Manders coefficients out of two channels	-66-
Fig. 19	Histone lysine methylation patterns of H3K4me3, H3K9me1 and H4K20me1 together with centromeres	-70-
Fig. 20	Histone lysine methylation patterns of H3K9me3, H3K27me3 and H4K20me3 together with centromeres	-72-
Fig. 21	Quantitative overlap-assessment of centromeres and different histone lysine methylation sites	-73-
Fig. 22	Spatial relation between different histone lysine methylation sites and nascent RNA	-75-
Fig. 23	3D reconstructions of H4K20me3 staining patterns in cycling and quiescent cells	-76-
Fig. 24	Comparison of different lysine methylation sites in cycling and quiescent cells by RAC analysis	-77-
Fig. 25	Comparison of differently methylated histone sites by double immunostaining	-80-
Fig. 26	Distinct nuclear zones formed by histone methylation sites	-82-
Fig. 27	Cell viability in the presence of different Chaetocin concentrations	-84-
Fig. 28	Replication labeling in control and Chaetocin treated cells	-85-

Fig. 29	Comparison of tubulin, B23, SC-35 and H3K9me3 antibody staining in untreated cells and three days after Chaetocin incubation	-86-
Fig. 30	Confocal mid-sections of a HFb nucleus three days after Chaetocin treatment and in control cells	-87-
Fig. 31	H3K9me3 and DAPI pattern formation changes in HFbs but not in the cancer cell-lines MCF-7 and DLD-1	-89-
Fig. 32	Distribution of HP1-alpha in HFbs, DLD-1 and MCF-7 cells before and after Chaetocin treatment	-91-
Fig. 33	No reorganization of chromatin occurs after Chaetocin rescue	-93-
Fig. 34	3D-reconstruction of objects with a size of 500 and 1000 voxel	-94-
Fig. 35	Evaluation of H3K9me3 pattern size in HFbs before and after Chaetocin application	-95-
Fig. 36	Evaluation of H3K9me3 pattern size in MCF-7 cells before and after Chaetocin application	-96-
Fig. 37	Evaluation of H3K9me3 pattern size in DLD-1 cells before and after Chaetocin application	-97-
Fig. 38	Ideogramms of human chromosomes HSA #18, 19	-98-
Fig. 39	Immuno-FISH delineating H3K27me3 and H3K9me3 together with HSA #18 and 19	-99-
Fig. 40	Immuno-FISH delineating H3K4me3 together with HSA #18 and 19	-100-
Fig. 41	Linescan through a X-chromosome territory	-101-
Fig. 42	Ideogramms of human chromosomes HSA #12 and X	-102-
Fig. 43	Immuno-FISH of gene-rich/poor DNA segments of HSA #12 with H3K4me3 and of highly expressed/repressed genes of HSA #12 with H3K4me3 and H3K27me3	-104-
Fig. 44	Immuno-FISH delineating X-territories and X-specific genes together with H3K27me3	-106-
Fig. 45	The interexperimental differences of histone methylation sites	-123-

Tables

Table 1	Properties of different types of chromatin	-7/8-
Table 2	Flow chart of different approaches for a new immuno-FISH protocol	-48-
Table 3	Parameters for Zeiss LSM 410	-53/54-
Table 4	Parameters for Leica SP2	-54-
Table 5	General parameters for Huygens deconvolution program	-57/58-
Table 6	Flow chart of the evaluation procedure after Chaetocin treatment	-69-
Table 7	Cells in S-phase after incubation with Chaetocin	-85-

10 Publications

Nuclear architecture of heterochromatin in normal and tumor cell nuclei visualized by immunostaining of methylated histone 3

R. Zinner, H. Albiez, S. Stein, A. Peters, T. Jenuwein, C. Cremer and T. Cremer
European Journal of Cell Biology, 83 Suppl. 54 (2004 March)

Three dimensional analysis of histone methylation patterns in normal and tumor cell nuclei

M. Cremer, R. Zinner, S. Stein, H. Albiez, B. Wagler, C. Cremer, T. Cremer
European Journal of Histochemistry Vol.48(1)15-28 (2004)

Histone lysine methylation patterns in human cell types are arranged in distinct three-dimensional nuclear zones.

Zinner R, Albiez H, Walter J, Peters AH, Cremer T, Cremer M
Histochem Cell Biol. 2006

Biochemistry meets nuclear architecture: Multicolor immuno-FISH for co-localization analysis of chromosome segments and differentially expressed gene loci with various histone methylations.

Zinner R, Teller K, Versteeg R, Cremer T, Cremer M
Advances in enzyme regulation 2007 DOI: 10.1016

Multicolor 3D-FISH for imaging interphase chromosomes

M.Cremer, T.Cremer, F.Grasser, C.Lanctot, S.Müller, M.Neusser, I.Solovei, **R.Zinner**
In press

Deconvolution of 3D confocal microscope data sets improves image quality

H. Albiez, **R. Zinner**, C. Tiberi, L. Vecchio, C. Weierich, L. Schermelleh, H. Strickfaden, I. Solovei, S. Fakan and T. Cremer
In prep.

The NHEJ factor artemis locates to sites of DSB after single ion microirradiation and forms discrete foci

*Drexler, Hable, Hauptner, Greubel, Krücken, Strickfaden, Dietzel, Cremer, **Zinner**, Dollinger, Friedl*

In prep.

Chaetocin, an inhibitor of the HMT SUV39H1 results in global changes of chromatin arrangement in normal but not in malignant cells

Zinner R., Lanctot C., Imhof A., Cremer C., Cremer M.

J. Biol.Chem. In prep.

Poster presentation

Spatial analysis of histone modification sites in nuclei of different cell types for the characterization of euchromatic and heterochromatic nuclear zones

R. Zinner, M. Cremer, H. Albiez, A. Peters, T. Jenuwein, R. Brack-Werner, K. Pflieger, M. Speicher, T. Cremer

Jahrestagung der Deutschen Gesellschaft für Zellbiologie 24.03-27.03. 2004 Berlin

11 Curriculum Vitae

Name: Roman Michael Zinner

Date of birth: 11.11.1976

Place of birth: Weilheim (Germany)

Marital status: Unmarried

Education:

Elementary school 1983-1986 (Elementary school "am Hardt")

Grammar school: 1986-1997 (Grammar school Weilheim)

Finished with a general qualification for university entrance

Final grade: 2,3

Military service (from 07.1997- 04.1998)

Studies: Studies of biology at the Ludwig-Maximilians-University Munich (LMU-Munich)

From 11.1998-09.2003

Special subjects: Human genetics, biochemistry, immunology and zoology

Diploma thesis: In the Lab of Prof. Dr. T.Cremer in Munich

Title: Correlation of the localization of nascent RNA in the cell nucleus and the distribution of eu-and heterochromatin

Final grade: 1.0

Since 01.2004 graduation in the working group of Prof. Dr. T.Cremer

Topic of the thesis:

Histone lysine methylation in the context of nuclear architecture

Methods:

Cell culture

Fluorescence In Situ Hybridisation (FISH)

DNA/RNA isolation

PCR techniques

Metaphase spreading

Immunofluorescence techniques

Microscopy (confocal, widefield, transmitted light)

Computer applications: Microsoft Office Photoshop, Image J, Amira, Deconvolution, etc.

Hobbies: Music(piano/guitar), mountaineering, tennis, photography (Course of studies in photography (from 01.2004-03.2005 final grade:1.3)), traveling, reading

Languages:

Spanish: basic knowledge

English: fluent in written and spoken

12 Acknowledgement

Zuerst möchte ich mich bei meinem Doktorvater **Thomas Cremer** ganz herzlich dafür bedanken dass ich in seiner Arbeitsgruppe promovieren durfte. Auch möchte ich ihm dafür danken dass er keine starren Richtlinien vorgegeben hat, was die Durchführung der Experimente anbelangt, sondern jedem Doktoranden die Möglichkeit gibt eigene Gedanken bzw. Ideen einzubringen und umzusetzen.

Ein großes Dankeschön geht an **Angelika Böttger** für die Übernahme der Zweitkorrektur.

Marion Cremer möchte ich für ihre nette Art, meine Betreuung, das Korrekturlesen meiner Arbeit, für ihre Ruhe während der entbehrungsreichen Zeit der Paper-Produktion sowie für die vielen netten Gespräche über die Wissenschaft als auch über Themen fernab davon danken.

Meinen Kollegen möchte ich danken das sie zu einem tollen Arbeitsklima beigetragen haben: auf ihre Hilfe war immer Verlass, der Zusammenhalt stets groß, in ihrer Gesellschaft war es nie langweilig und man konnte mit ihnen über fast alles lachen (wenn ich mich recht entsinne gab es jeden Tag was zu lachen und das ist gut so). Der „harte Kern“ sei hier erwähnt aber auch die vielen anderen Leute die meinen Weg gekreuzt haben sollen sich nicht vergessen fühlen. Auch ihnen möchte ich herzlich danken, jedoch ist ihre Zahl zu groß und unübersichtlich um sie namentlich zu erwähnen.

Um keiner Persons' Gefühle zu verletzen, hier die Regeln der Auflistung: Ladies first, than men, both in alphabetical order.

Carolin Bleese (Photoshop Expertin), **Claudia Heppberger** (ist immer gut gelaunt und schafft es mit zwei Hasen unter ihrem Bett zu leben), **Heidi Jahn-Henninger** (Unser Labor Django, harte Schale weicher Kern), **Dani Köhler** (einer der größten Red Hot Chili Peppers-Fans die ich kenne, kann ausgezeichnet kochen und betätigt sich gern in Männersportarten (hat mir eine der übelsten Blutgrätschen verpasst die ich je einstecken musste)), **Alexandra Kölbl** (stets hilfsbereit wenn man etwas von ihr braucht), **Katrin Küpper** (man sollte sich nicht von ihrem Outfit täuschen lassen, sie kann richtig fröhlich sein), **Michaela Neusser** (macht immer schöne Seminarpläne), **Irina Solovei** (thanks for your shashlik parties and the organization of the lab), **Kathrin Teller** (kann immer über alle Albernheiten lachen und dabei ihre Gesichtsfarbe wechseln, bleib so wie du bist), **Radka Symanova** (immer freundlich), **Claudia Weierich** (Küchenchefin und Organisationstalent, in Geschwindigkeit und Menge beim Biertrinken auch für Männer schwer zu schlagen, aber das Problem dabei ist.....;-),

Ming Zhao (die netteste Chinesin die ich kenne), **Heiner Albiez** (danke für die lustigen aber auch lehrreichen Espressodiskussionen und dass du mir Computerdeppen so oft bei der Bewältigung der Probleme mit diesem rätselhaften Gerät geholfen hast), **Sandro Brero** (Wenns ihn nicht schon gäbe müsste man ihn glatt erfinden, immer gut drauf, immer hilfsbereit und immer zu begeistern, schade das er nicht Prof. werden will, ich würde glatt in jede Vorlesung gehen, mein persönlicher Lieblings-Postdoc), **Steffen Dietzel** (danke für die Hilfe bei Computerproblemen), **Florian Grasser** (bei seinem Elan wird er es weit bringen), **Roy Hessing** (danke für die netten Gespräche über Fotografie), **Christian Lanctot** (danke für die nette gemeinsame Zeit im Büro and dafür das du mich an deinem reichen Wissen (+philosophischen Diskussionen) teilhaben hast lassen), **Robert Mayer** (Chefzyniker, könnte perfekt den Bruder Barnabas am Nockherberg spielen), **Stefan Müller** (hat einen ausgezeichneten Biergeschmack), **Jens Nagel** (nicht nur das er Snooker-Fan ist macht ihn sympathisch), **Hilmar Strickfaden** (Danke für die Gitarren Tips, ich hoffe du lernst irgendwann noch Noten lesen, wäre echt schade drum, wenn nicht), **Andreas „Zuni“ Zunhammer** (das beste Beispiel dafür, das es doch gut ist, aus Bayern zu kommen)

Ich möchte auch meiner Ex-Freundin **Steffi** ganz herzlich danken dass sie immer für mich da war und mir durch ihr tolle Art über viele Stolpersteine des Lebens hinweggeholfen hat.

Meiner Freundin **Dani** möchte ich für ihre Liebe, Fröhlichkeit und Unterstützung danken, you're the best I know.....;-)

Meinen **Eltern** möchte ich sehr herzlich für ihre Unterstützung in jeglicher Hinsicht danken.

„It's better to live 1 year like a tiger than 1000 years like a sheep “

Tibetan Saying

Ehrenwörtliche Versicherung

Hiermit bestätige ich, dass ich die vorliegende Dissertation selbständig und nur mit den angegebenen Materialien und Quellen durchgeführt habe.

München, den 21.03.2007

Roman Zinner

Erklärung über frühere Promotionsversuche

Hiermit bestätige ich, dass ich vor dieser Arbeit keine anderen Promotionsversuche unternommen habe. Dies ist meine erste und einzige Dissertation.

München, den 21.03.2007

Roman Zinner